The background of the entire page is a scanning electron micrograph (SEM) showing a dense field of synthetic bone graft substitutes. These substitutes are characterized by their elongated, hexagonal or rectangular prismatic shapes, which are randomly oriented and packed together. The image is rendered in a monochromatic teal or cyan color, highlighting the intricate surface textures and sharp edges of the individual particles.

# **ENHANCING BONE REGENERATION BY CALCIUM PHOSPHATES WITH SURFACE TOPOGRAPHY**

**A translational evaluation  
of synthetic bone graft substitutes**

**LUUK VAN DIJK**



# **Enhancing bone regeneration by calcium phosphates with surface topography**

A translational evaluation of synthetic bone graft substitutes

ISBN 9789464238815

Layout: Marian Sloot || [www.proefschriftmaken.nl](http://www.proefschriftmaken.nl)

Printing: ProefschriftMaken || [www.proefschriftmaken.nl](http://www.proefschriftmaken.nl)

© copyright Luuk van Dijk, 2022

All rights reserved. No part of this publication may be reproduced, stored in a retrieval system or transmitted, in any form or by any means, electronic, mechanical, photocopying, recording or otherwise, without prior permission of the author or the copyright-owning journals for previous published chapters.

Financial support for the printing of the thesis was kindly provided by the 'Utrechtse Stichting tot Bevordering der Mondziekten, Kaak- en Aangezichtschirurgie', Kuros Biosciences BV, and the Dutch society for Biomaterials and Tissue Engineering (NBTE).

# **Enhancing bone regeneration by calcium phosphates with surface topography**

A translational evaluation of synthetic bone graft substitutes

**Verbeteren van botregeneratie door gebruik van calciumfosfaten met oppervlaktetopografie**

Een translationele evaluatie van synthetische botvervangers

(met een samenvatting in het Nederlands)

## **Proefschrift**

ter verkrijging van de graad van doctor aan de  
Universiteit Utrecht  
op gezag van de  
rector magnificus, prof.dr. H.R.B.M. Kummeling,  
ingevolge het besluit van het college voor promoties  
in het openbaar te verdedigen op

woensdag 6 juli 2022 des ochtends te 10.15 uur

door

**Lukas Alexander van Dijk**

geboren op 21 september 1989  
te Woerden

**Promotoren:**

Prof. dr. A.J.W.P. Rosenberg

Prof. dr. J.D. de Bruijn

**Copromotoren:**

Dr. ir. D. Gawlitta

Dr. F. de Groot

**Beoordelingscommissie:**

Prof. dr. F.C. Öner

Prof. dr. R. Goldschmeding

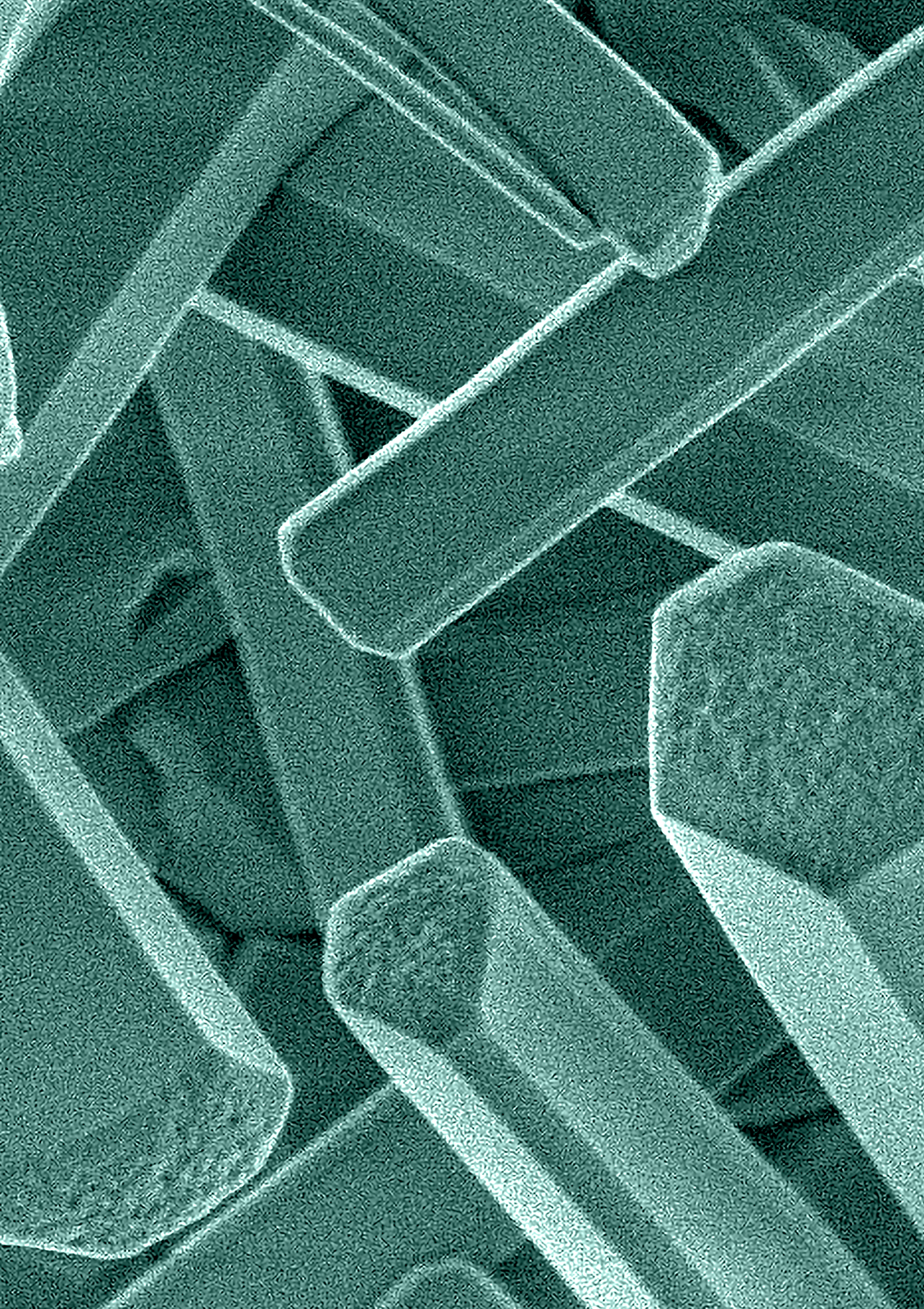
Prof. dr. ir. H.H. Weinans

Prof. dr. R.J. Stokroos

Prof. dr. ir. S.C.G. Leeuwenburgh

# Table of Contents

<b>CHAPTER 1</b>	General introduction & thesis outline	7
<b>PART I</b>	Improving the surface topography of calcium phosphates to enhance their osteoinductive potential	43
<b>CHAPTER 2</b>	Accelerated bone formation by biphasic calcium phosphate with a novel sub-micron surface topography	45
<b>PART II</b>	Efficacy of osteoinductive calcium phosphate as bone graft material in spinal fusion	69
<b>CHAPTER 3</b>	Efficacy of a synthetic calcium phosphate with submicron surface topography as autograft extender in lapine posterolateral spinal fusion	71
<b>CHAPTER 4</b>	Biphasic calcium phosphate with submicron surface topography in an Ovine model of instrumented posterolateral spinal fusion	95
<b>CHAPTER 5</b>	MagnetOs, Vitoss, and Novabone in a multi-endpoint study of posterolateral fusion: A true fusion or not?	115
<b>PART III</b>	Efficacy of osteoinductive calcium phosphate in maxillary sinus floor augmentation	141
<b>CHAPTER 6</b>	Osteoinductive calcium phosphate with submicron topography as bone graft substitute for maxillary sinus floor augmentation: A translational study	143
<b>PART IV</b>	Evaluation of the macrophage response to osteoinductive calcium phosphate	179
<b>CHAPTER 7</b>	Calcium phosphate with submicron topography induces M2 macrophage phenotype in primary human macrophages, enhancing downstream angiogenesis and osteogenesis in vitro	181
<b>CHAPTER 8</b>	From benchtop to clinic: a translational analysis of the immune response to submicron topography and its relevance to bone healing	217
<b>CHAPTER 9</b>	Summary, general discussion and future perspectives	243





# **C H A P T E R 1**



## **GENERAL INTRODUCTION & THISIS OUTLINE**

## **WE HAVE COME A LONG WAY**

---

Around 300,000 years ago, the earliest known populations of our species, *Homo Sapiens* (Latin: “wise man”), inhabited the African continent[1]. In the period between 120,000 – 12,000 years ago, our early ancestors dispersed to regions all over the planet. First along the southern coast of Asia and in Oceania, then settling in Europe and eventually The Americas[2]. Although at least nine other human species have lived on our planet, some even alongside us, we have survived as the only species of the *Homo* genus[3]. The reason for this has been an ongoing topic of debate. For instance, we were not larger or stronger in anatomy compared to other hominins, nor the first or only species to use tools, clothes, or fire[4–6]. *Homo Sapiens* also did not have the largest brain of all human species, nor were we significantly more intelligent[7–9]. One proposed explanation of why our species has thrived is because of an exceptional ability to innovate and adapt under the stress of changing environments[10]. This may be a consequence of our tendency to socialize and share information amongst ourselves, not only in the spatial domain, *i.e.* between geographical regions, but also in the temporal domain, *i.e.* across generations. As knowledge was passed down generations by our early ancestors, this formed the foundation of a cultural and intellectual revolution that is still ongoing today.

Ever since agriculture encouraged humans to settle in a permanent habitat, the surplus production of food has allowed a portion of the population to focus on non-agricultural professions. This created free time for contemplative, creative and abstract thinking, which led to the emergence of the disciplines of script, mathematics, astronomy, philosophy, medicine and many more. Whereas ancient medical practice was largely based on magical or spiritual rituals and beliefs, over centuries it evolved to become a physical and rational science. Early treatments that aimed to relieve pain and restore rudimental function using tools available at hand, developed into advanced molecules, biomaterials, and surgical techniques of modern medicine, which are successfully used to treat a wide range of injuries and diseases each day.

Recent advances in the field of biomedical science are considered a hallmark of human civilization. For example, the discovery of anesthesia and antiseptic and aseptic methods during the 19<sup>th</sup> century, which revolutionized the field of surgery [11,12]. Likewise, the first vaccines were developed in the 1880s, a technology that is still in use today for protection against numerous diseases[11,12]. At the turn of the 19<sup>th</sup> century, Röntgen discovered X-rays which formed the foundation for the field of noninvasive medical imaging [11,12]. Another great milestone is the discovery of the double helix structure of deoxyribonucleic acid (DNA) by Franklin, Watson and Crick in 1953, which gave rise to modern molecular biology and genetics [11,12]. In line with these great discoveries, the second half of the



20<sup>th</sup> century continued to see an exponential increase in scientific knowledge on human biology, pharmacology and biomaterials. Among the latest developments is the emergence of the field of regenerative medicine, which aims to 'replace or regenerate human cells, tissue or organs, to restore or establish normal function'[13]. The restoration of bone tissue is a topic that is extensively studied in current times, as bone tissue gives our body its essential structure, facilitates movement and protects our vital organs such as the heart and the brain. Interestingly, the origins of bone restoration go back hundreds, even thousands of years.

### **A history of bone surgery and the first use of graft materials**

Considering the recent revolutionary developments in medicine and surgery, it is striking to realize that the first surgeries on humans were already performed in prehistoric times. The oldest surgical procedure that we know of is trepanation – the creation of a full-thickness defect in the intact skull by surgically excising a piece of the cranial vault. Substantial evidence in the form of thousands of trepanned human skulls from various geographical regions, with the oldest examples over 7,000 years old, indicates that the practice of trepanation was widespread in many different civilizations since prehistory[14]. While the exact reasons for trepanation in these early times remain mysterious, it possibly included treatment of mental illness, epilepsy, headaches, or the release of evil spirits. Surprisingly, estimated survival rates of the procedure were relatively high (40-90%)[15], especially when considering the lack of modern surgical tools and aseptic techniques. The ancient practice of trepanation also records the earliest use of medical implants for cranioplasty. Evidence from roughly 2,000 BC in the ancient Americas indicates that cranioplasty after trepanation, using plates of gold, silver or even nutshells was not uncommon [16]. This qualifies as the first documented use of biomaterials for restoration of bodily function. Further testimony of the prehistoric use of medical implants was found in a female skull from 2,000 BC Armenia, in which a small traumatic cranial defect was treated with a plug of animal bone [17], a treatment that we now call xenografting. Another ancient example of the use of medical implants is from around 800-700 AD in the Maya civilization. A mandible fragment of a 20-year-old woman was discovered, which contained three dental implants crafted from Nacre shell in place of the three lower incisors. Radiographic assessment of the mandible fragment revealed that the shell implants were solidly integrated in the alveolar bone[18,19]. Recent assessment of nacre shell indeed confirmed that this material has good biocompatibility with bone tissue and can enhance osteogenic activity of bone cells *in vitro* and *in vivo*[20,21].

While the disciplines of medicine and surgery underwent great developments during the Classical and Middle ages, there are limited records on the use of implant materials from this period, besides literature on tooth replacements using cadaver teeth or animal bone fragments[22]. In the early 16<sup>th</sup> century (1505 AD), an Ottoman surgeon named Ibrahim



**Figure 1. Evidence of trepanation and cranioplasty in ancient times.**

The image on the left shows a bronze age skull from 2,200 BC that was excavated in Jericho, Israel which has several trepanation holes (Science Museum, London). The holes show evidence of healing, which indicates the patient survived the surgery. The image on the right shows the result of a frontal cranioplasty on a Peruvian skull using a gold plate, with signs of osteointegration (National Museum of Archeology, Anthropology and History of Peru, Lima).

bin Abdullah described in a surgical textbook how bone graft from goats or dogs could be used to repair traumatic skull defects. Similarly, in the beginning of the modern age (1,668 AD), a Dutch surgeon named Job van Meekeren described a story of a Russian nobleman who had a traumatic defect in his cranium following a sword fight, which was repaired using bone graft from the skull of a dog (*i.e.* xenograft). However, the nobleman was then excommunicated because the Church forbid that tissue of an animal would reside inside the body of a Christian. Upon return to the surgeon for removal of the graft, it was found impossible to remove the bone graft since it had healed well and was fully integrated with the patient's cranial bone[23]. Roughly 150 years later in 1821, the German surgeon Philipp von Walther performed the first surgery with autograft bone, again on a cranial trepanation defect, which reportedly healed well despite a wound infection [24]. In the following years, research into bone graft surgery gained more and more traction. In 1867, the term 'bone graft ("greffe osseuse") was first used by the Frenchman Leopold Ollier, who avidly studied autografts and xenografts in various animal models [25]. Another great milestone was the first successful human allograft in 1879, transplanted to the humeral shaft of a 3-year-old boy who had lost it due to osteomyelitis. The Scottish surgeon William MacEwan removed over two thirds of the afflicted humeral shaft and subsequently replaced it with three consecutive tibial grafts from a child with rickets[26]. From here on, the bone grafting field developed rapidly, with influential works on principles and criteria of bone grafting published by Vittori Putti and F.H. Albee in the 1910s[27,28]. Developments in the use of



autologous bone grafts were also fueled by the need for treatments of the many casualties of during World War I[29]. Not long after, by now over a century ago, the use of autograft would become adopted as the 'gold standard' in bone graft surgery.

### **Bone grafts in the 21<sup>st</sup> century: Reasons and requirements of bone graft substitutes**

Bone graft surgeries are a common procedure in today's clinical practice, being second only to blood transfusion in the list of most frequently transplanted tissues in the world[30]. It has been estimated that an annual 1.3-1.5 million bone graft procedures are performed in bone and joint surgery in the United States alone, and that bone grafts are used in over 2.5 million dental implant procedures worldwide each year [31,32]. The use of bone grafts is expected to continue to rise in the coming decades due to aging of the population in modern Western societies. Spinal fusion surgery and maxillary sinus floor augmentations are common procedures in which bone grafts are used in orthopedic and maxillofacial surgery, respectively. Due to ease of accessibility and large quantities of available cancellous bone, the iliac crest is often used as donor site for autograft harvesting. Alternatively, autograft bone can be obtained from local sites, such as the lamina in spine surgery, or intra-oral sites in maxillofacial surgery. Autograft is traditionally considered the 'gold standard' treatment in bone graft surgery in terms of efficacy, due to being osteoconductive, osteoinductive and osteogenic[33] (**Table 1**). Nevertheless, certain disadvantages to the use of autograft have been recognized. First of all, the available quantity of autograft may not be sufficient for certain procedures, especially when only locally obtained bone is used [34–36]. Secondly, there are extended operating time and costs related to the harvesting procedure, in particular when a secondary harvesting site is required [37,38]. Furthermore, the quality of autograft bone is donor dependent and may be compromised in diseased or aged patients[39]. Lastly, autograft harvesting has been associated with risks of complications and donor site morbidity, including wound complications, persistent donor site pain, sensory disturbances and even functional limitations[40–42].

**Table 1. Definitions of bone graft properties**

Graft property	Definition*
Osteoconductive	When bone is promoted to appose and grow along the surface and into the pores of a graft (or implant) when placed into a bony site, by virtue of its composition, macro- and microstructure.
Osteoinductive	When a stimulus is provided for recruitment, stimulation and induction of differentiation of osteoprogenitors cells and/or multipotent stem cells into functional osteoblasts or preosteoblasts; the initial cellular phase of a bone-forming lineage, which may result in <i>de novo</i> bone formation even in ectopic, non-bony sites.
Osteogenic	When viable osteogenic cells are provided that can form bone or are capable of differentiating into bone-forming cells, <i>i.e.</i> osteoblasts, preosteoblasts, osteoprogenitors and mesenchymal stem cells.

\*Adapted from Di Silvio and Jayakumar (2009)[43]

Anatomically, bone tissue consists of a dense, shell-like outer layer called cortical bone and an inner porous core called cancellous or spongy bone[44]. The function of cortical bone is to provide strength and structure, whereas cancellous bone allows the absorption of loads by deformation due to its high porosity (75-85%)[45,46]. Cancellous bone has a higher metabolic activity and harbors the bone marrow, which is the stem cell niche of hematopoietic and mesenchymal stem cells[47]. In overall composition, bone tissue consists of 90% matrix with a cellular component of 10%[44,48]. The matrix consists of 60-70% inorganic calcium phosphate, 20-30% organic matrix and 10-15% lipids and water, where the organic part is pre-dominantly type I collagen (90%) and the remainder consists of non-collagenous proteins[44,48]. Among these proteins are the transforming growth factor  $\beta$  superfamily members, including the osteoinductive bone morphogenetic proteins (BMPs) and many others[44]. As for the cellular component, besides the earlier mentioned bone marrow niche, bone is home to osteoblasts, the 'bone-makers', osteoclasts, the 'bone-resorbers', and osteocytes, the 'bone-regulators'[45]. These three cell types are in continuous communication with each other to control the formation, remodeling and maintenance of the bone matrix.

To overcome the drawbacks of the use of autograft for orthopedic and maxillofacial surgery, various alternative bone graft materials have been developed during the past century. These 'orthobiologics', or bone graft substitutes, are graft materials made from or based on biological components and can be used as extenders or substitutes of autograft in bone surgery. In the design and evaluation of these orthobiologics, the 'triad' of bone graft properties is considered (**Table 1**). In theory, the ideal bone graft substitute is osteoconductive, osteoinductive and osteogenic, like autograft bone. Different categories of orthobiologics based on the origin of the substitute, include allogeneic bone grafts (allografts), bone grafts from another species (xenografts), synthetic graft materials, growth factors (BMPs) and cell-based matrices. While each of these orthobiologic solutions have an underlying scientific rationale and meet at least one of the essential properties of autograft, none of them provides a perfect alternative to autograft bone in terms of efficacy.

Bone graft substitutes based on growth factors and cell-based matrices are the most recent solutions that have become available in the clinic[49,50]. Growth factor-based bone substitutes consist of the earlier described BMPs, which are osteoinductive and can induce bone formation by upregulating osteogenic differentiation of cells. While BMPs were initially widely used in spinal fusion in the 2000s after their introduction to the market and they demonstrated high efficacy, their use has more recently strongly reduced due to reports of serious complications in certain indications[50]. As for cell-based matrices, these are allografts processed to contain viable (stem) cells from the donor, which are thought to contribute to bone formation after implantation. Although their adoption has grown in recent years, the evidence for their efficacy is mixed and does not justify their



use over conventional allografts[51,52]. Both BMPs and cell-based allograft are a costly solution compared to other orthobiologics, and both have a frozen supply chain, which reduces their ease of use.

Synthetic graft materials have received increasing interest because of their relatively simple manufacturing method, low cost, unlimited availability and 'off-the-shelf' supply. Moreover, because of their synthetic nature, the material properties can be controlled during the manufacturing process, which allows for ongoing optimization of these materials to improve their efficacy. Of the available synthetic bone grafts, calcium phosphate ceramics and cements have been traditionally the most well-known and studied.

### **Calcium Phosphate Bone Graft Materials**

In parallel with the historical developments in medical science and surgery, significant progress was made in the field of biology and chemistry. By the end of the 18<sup>th</sup> century, research into composition of bone resulted in the discovery of calcium (ortho)phosphates and their basic chemical characterization. In 1769, the two renowned Swedish chemists Gahn and Scheele were the first to discover that phosphate of lime, also known as tricalcium phosphate (TCP), could be extracted from bones [53]. This discovery laid the groundworks for a vast body of research focusing on calcium phosphates, including their characterization, manufacturing and their utility as biomaterials.

Calcium (ortho)phosphates are minerals that consist of the three chemical elements: Calcium, Phosphorus and Oxygen, established in an atomic crystal arrangement around a network of orthophosphate groups ( $\text{PO}_4$ )[54]. By this definition, more than 10 different forms of calcium phosphates have been identified[55,56]. Pure calcium phosphate crystals have a white color and are the main component of all biological calcified tissues, including bones, teeth, shells and antlers[54]. It is due to their chemical similarity to native bone mineral that both natural and synthetically manufactured calcium phosphates have good biocompatibility and inherent osteoconductive capacity, making them suitable as bone graft materials[54]. Calcium phosphate materials can be derived from natural sources by isolating the inorganic phase of animal bone or coral, or can be synthetically produced. Synthetic calcium phosphate bone grafts exist as ceramics, manufactured by sintering of calcium phosphate at high temperatures, or cements, that harden *in situ* when combined with an aqueous solution.

### **The emergence of calcium phosphate ceramics as bone graft substitutes**

In 1920, F.H. Albee was the first to evaluate TCP as bone graft material in the repair of bone defects in an animal model. He reported faster bone healing in rabbit bone defects that were grafted with TCP compared to an untreated control[57]. Around the 1950s, the first clinical use of animal- and coral-derived bone graft materials was reported and the first

'bone banks' were established to supply them. Clinical use of synthetic calcium phosphates began around 1975 in maxillofacial surgery, with reports on the use of TCP ceramics as fillers of periodontal defects and use of HA cylinders as dental root replacements[58,59]. Soon after, wide-scale commercialization of calcium phosphate bone graft materials took off during the 1980s[60]. Following the initial use of calcium phosphates in maxillofacial surgery, their use in orthopedic surgery for treatment of bone defects and as bone grafts for spinal fusion emerged at the end of the decade[61–65]. From that time on, the use of calcium phosphates as bone graft materials for maxillofacial and orthopedic surgery was increasingly adopted. While the early calcium phosphate materials were merely osteoconductive, the later discovery of osteoinductive calcium phosphates significantly increased the potential of these materials as bone graft substitutes.

## **Relevant physicochemical properties of calcium phosphate bone graft materials**

### ***Composition***

The various types of calcium phosphates have different molecular structure and associated properties, such as Ca/P molar ratio, crystal structure, crystallinity and density[56]. The difference in these chemical properties leads to different behavior *in vivo*, including their behavior as bone graft materials[66]. Overall, HA and TCP are the most common phases used in calcium phosphate bone graft materials. While HA has a relatively high Ca/P ratio ( $\text{Ca}_{10}(\text{PO}_4)_6(\text{OH})_2$ ) and low solubility, TCP has a lower Ca/P ratio ( $\text{Ca}_3(\text{PO}_4)_2$ ) and higher solubility[56]. The solubility of calcium phosphates affects their behavior after implantation, as a higher solubility will lead to increased *in vivo* degradation through phagocytosis by multinucleated giant cells and resorption by osteoclasts [66,67]. A balanced degradation rate is deemed to be ideal, as a lack of degradation of HA as well as expedited degradation of TCP may lead to suboptimal healing outcomes[68–70]. For this reason, HA and TCP phases are commonly mixed to obtain a biphasic calcium phosphate (BCP) that has a controllable resorption rate, depending on the mixing ratio[71,72].

### ***Macrostructure***

The macrostructure of calcium phosphates comprises their macroscopic form (e.g. block vs particulate) geometry (e.g. flat/smooth vs uneven/rough structure) and macroporosity (i.e. porous volume, pore size and interconnectivity). These macrostructural features control material-tissue interactions as they affect surface area and the extent of tissue ingrowth, including capillaries that are essential for exchange of oxygen, nutrients, cells and metabolic waste[73–75]. Porosity is arguably the most important macrostructural feature of calcium phosphates, as overly dense materials allow limited circulation of body fluids and tissue ingrowth required for integration and regeneration[76]. A macropore size of between 100-500  $\mu\text{m}$  has been reported to be optimal for ingrowth of bone tissue[77]. It should be noted that for particulate materials, the interparticle space can also be considered a form





of porosity, so a particulate of a dense material may still provide sufficient porosity. Besides having influence on the biological response, macrostructural features affect mechanical strength. Indeed, particulate materials and materials with higher porous volume have been shown to have lower compressive strengths compared to blocks and denser materials, respectively[78,79]. Lastly, another aspect related to macrostructure are the handling properties. While pre-formed calcium phosphate blocks are ideal for filling of defects with predefined shape and size (e.g. burr hole, periodontal socket), particulate materials allow for filling of defects of variable dimensions, albeit with poorer handling properties in larger defects. To improve handling of calcium phosphate bone grafts, various carriers have been developed to provide putties/pastes that can be manually shaped or extruded from a syringe to accommodate implantation into a defect[80,81].

### **Microstructure**

Microstructural properties of calcium phosphate bone grafts include microporosity, surface topography and their associated specific surface area. For calcium phosphates, microporosity implicates the presence of micropores of  $<10\ \mu\text{m}$  in diameter, which can be created by sintering the material[82]. Research outcomes suggested that despite their small diameter, cells may invade micropores to form bone inside them, although this is controversial[83,84]. Various studies have demonstrated that calcium phosphates with microporosity exhibit enhanced bone healing characteristics *in vivo*, corresponding with the formation of greater volumes of bone after implantation in bone defects. [84–90]. It has been shown that even in absence of macroporosity, some microporous calcium phosphates can be resorbed and replaced by new bone[91].

The shape, size and distribution of features on the surface of a material is defined as its surface topography. The type of surface topography has been shown to influence the biological response against a biomaterial. For example, submicron needle-like pillared surface topographies have been shown to influence adhesion, mechanics and osteogenic differentiation of murine and human stem cells, as well as evoke a favorable pro-healing response from immune cells (i.e. macrophages)[92–94]. Calcium phosphates materials with a surface topography of microcrystals of plate-like, net-like, needle-like or grain-like morphology have been described in literature [95]. Alternatively, by means of fabrication, calcium phosphates with defined surface patterns, such as micro-grooves, -pillars and -holes have been manufactured[95]. Lastly, surface roughness has been used as a parameter of calcium phosphate topography. A large variety of *in vitro* and *in vivo* studies have determined a relation between surface topography, biological response and ultimately bone healing capacity of calcium phosphate materials[96–99]. Besides structure, the size of surface features has been shown to affect healing outcomes. In general, both the presence of microporosity and surface topography increase the surface area of a material, leading

to enhanced surface reactivity, including dissolution/reprecipitation events and protein adsorption[100].

### **Osteoinductive calcium phosphate**

Although all calcium phosphate bone grafts are generally osteoconductive, a subset of calcium phosphates has been found to be capable of osteoinduction. The first reports describing osteoinduction by calcium phosphate-based materials were published during the early 90s[86–90]. These studies demonstrated that selected calcium phosphate materials were able to induce *de novo* bone formation in ectopic sites, without the addition of cells or growth factors.

Decades earlier, Marshall Urist had described the process of osteoinduction and had defined Bone Morphogenetic Proteins (BMPs) as the sole trigger[101,102]. However, later discoveries that synthetic materials, such as polyhydroxyethyl methacrylate (poly-HEMA) sponges, titanium and different ceramics could also be osteoinductive challenged this view of Urist[103]. In all cases, osteoinduction by these materials was preceded by precipitation of a calcium phosphate surface layer, which hinted at a role of calcium phosphate.

Osteoinduction by calcium phosphates has been demonstrated numerous times by means of ectopic implantation (intramuscular or subcutaneous) in different animal models, including dogs, goats, sheep, pigs, monkeys, baboons, rabbits, rats and mice[103–107]. Various types of calcium phosphate ceramics have been found to be osteoinductive, including HAs, TCPs, BCPs, as well as calcium phosphate cements and coatings[108–111]. Being both osteoconductive and osteoinductive, osteoinductive calcium phosphates meet 2 of the 3 characteristic properties of autograft (**Table 1**). Not surprisingly, osteoinductive calcium phosphates have demonstrated enhanced performance compared to their merely osteoconductive counterparts as bone graft materials in pre-clinical bone graft models[96,106,112–114]. Osteoinductive calcium phosphates are therefore considered promising bone graft materials.

### **Physicochemical properties associated with osteoinductive calcium phosphates**

Research on osteoinductive calcium phosphates has been aimed at identifying the specific material properties responsible for osteoinductive capacity, including chemical composition, macrostructure and microstructure.

Chemical composition has been shown to play a role in osteoinduction by calcium phosphates, with a general tendency of enhanced osteoinduction by more resorbable materials [103,115]. However, not all resorbable calcium phosphates have inherent osteoinductive capacity, while also non-resorbable HA and even insoluble materials such

as titanium have been shown to be osteoinductive, indicating that chemistry is not the only factor critical for osteoinduction.

The influence of macrostructural properties such as the presence of pores and specific geometries such as concavities or channels that create “protected” spaces for bone formation, have been suggested to be prerequisites for osteoinduction[103,116–119]. However, osteoinductive bone formation has also been reported on the surface of completely flat and dense (i.e. non-porous) calcium phosphate [120], suggesting that macrostructure may be an important, but not an essential factor for osteoinduction.

Considerably stronger links have been established between osteoinductive capacity and microstructural surface features of calcium phosphate materials. Indeed, calcium phosphates ceramics that were manufactured to have surface micropores and/or submicron surface topography, i.e. surface structures smaller than 1  $\mu\text{m}$  in size, have been repeatedly demonstrated to have osteoinductive capacity, while experimental controls without such surface features did not, or only to a lesser extent [90,113,114]. Even though the physicochemical properties of materials are intertwined and difficult to evaluate in isolation, mounting evidence suggests that microstructural surface features are the dominant factor that dictates the osteoinductive potential of calcium phosphates.

### **Mechanism of osteoinduction by calcium phosphates**

Although the phenomenon of osteoinduction by calcium phosphate (and other) materials has been abundantly reported in literature, the biological mechanism that underlies it is not entirely understood. It is clear that cells in the ectopic intramuscular or subcutaneous environment close to the surface of the material eventually undergo osteogenic differentiation, leading to *de novo* bone formation. A study by Song et al. demonstrated that bone marrow stromal cells can migrate from the bone marrow, through the vascular network, to intramuscular calcium phosphate implants, and contribute to ectopic bone formation there[121]. Other studies have suggested that stem-like cells present in the local vascular niche, such as pericytes and myoendothelial cells, may play a role in osteoinductive bone formation by calcium phosphates[122]. However, while the origin of these stem cells may be understood, an unanswered question is how they are induced to undergo osteogenic differentiation into bone-forming osteoblasts. During the past decades, various theories have been proposed on the mechanism by which osteoinductive calcium phosphates with their specific material features can induce ectopic bone formation (**Table 2**).



**Table 2. Theories of osteoinduction by calcium phosphate materials**

Theory	Explanation
Surface mineralization[123]	Surface mineralization in the form of a biological apatite layer on the surface of osteoinductive materials may be an osteoinductive stimulus for mesenchymal stem cells.
Endogenous BMPs[124]	Accumulation of endogenous BMPs on the surface of osteoinductive calcium phosphates through adsorption or co-precipitation induces osteogenic differentiation.
Physical surface cues to MSCs[95]	Osteogenic differentiation of stem cells is triggered through direct physical cues from the microstructural surface features (e.g. micropores, submicron topography) of osteoinductive materials.
Osteoclastogenesis[120]	Osteoinductive ceramics promote the formation of osteoclast-like multinucleated giant cells on their surface, which communicate towards MSCs to undergo osteogenic differentiation.
M2 macrophage polarization[115,125]	Submicron surface topography on osteoinductive materials induces the polarization of macrophages towards the pro-regenerative M2 phenotype, which promotes angiogenesis and osteogenic differentiation of stem cells.

Calcium phosphates and other materials have been demonstrated to undergo surface mineralization after implantation *in vivo* and in *in vitro* assays using simulated body fluid [126–128]. This mineralization consists of the formation of a biological carbonated apatite layer on a material's surface, and is influenced by the composition and structure of materials[126,127]. For calcium phosphates, release of  $\text{Ca}^{2+}$ ,  $\text{PO}_4^{3-}$  and  $\text{HPO}_4^{2-}$  from the material surface has been thought to cause local supersaturated concentrations of ions, resulting in the precipitation of the apatite layer [103]. However, a recent theory by Böhner and Miron (2019) [129] proposes that biological apatite formation in implants does not result from local supersaturation due to ion release, but instead the opposite occurs: apatite precipitation consumes physiological  $\text{Ca}^{2+}$  and  $\text{PO}_4^{3-}$  and thereby depletes local ion concentrations. Nevertheless, the ability to form an apatite layer has been used to determine the 'bioactivity' of materials, and has been correlated with their bone healing potential *in vivo* [130,131]. Calcium phosphates that have a rougher surface and therefore a larger surface area, as is the case with osteoinductive ceramics, were shown to enhance the formation of an apatite layer[127]. For these reasons, together with the fact that osteoinductive polymers and titanium have also demonstrated mineralization, it has been speculated that the formation of an apatite layer, which preferentially occurs on osteoinductive materials, may play a role in inducing osteogenic differentiation[103]. Indeed, it is thought that the bone-like biological apatite may function as a physicochemical trigger for the osteogenic differentiation of cells, since it mimics the matrix of bone tissue[123].

Because osteoinduction by BMPs and calcium phosphates have a similar biological outcome, i.e. ectopic bone formation, another theory suggests that endogenous BMPs and other growth factors accumulate on the structured surface of ceramics through adsorption

or co-precipitation in the carbonated apatite surface layer. These growth factors are held responsible for the induction of osteogenic differentiation of (stem) cells on osteoinductive ceramics. Materials with specific structure, such as microstructural surface features that increase the surface area, or 'protective concavities', are believed to accumulate higher concentrations of endogenous growth factors, which may trigger the osteoinductive response once they cross a certain threshold concentration (**Figure 2**)[123,124].

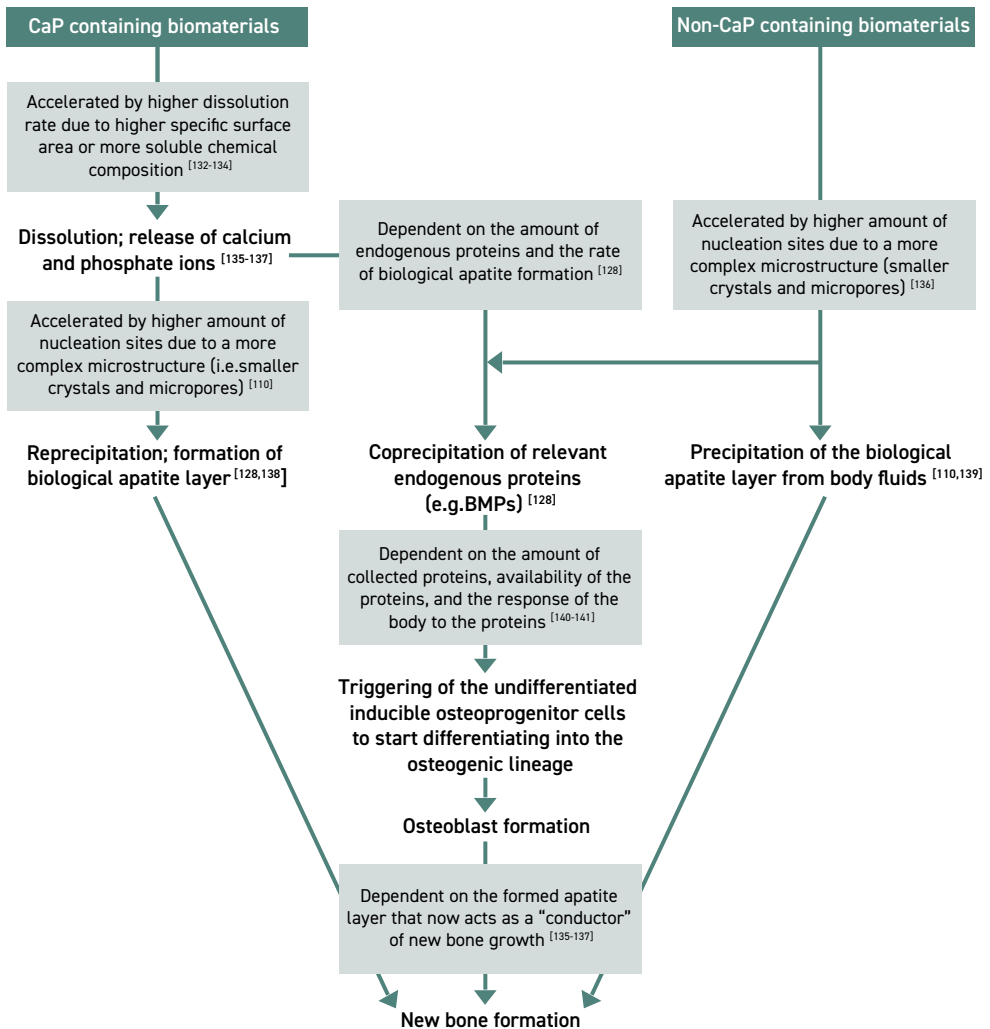


**Figure 2.** Flow chart of the proposed mechanism of osteoinduction by biomaterials through biological apatite formation and coprecipitation of BMPs. Adapted from Habibovic et al. [123]

Another view is that osteoinduction is triggered by the direct effect of surface features on cells that interact with them. Many studies have shown that surface features of biomaterials can influence behavioral responses in cells, such as promoting osteogenic differentiation of adherent stem cells[98]. Therefore, an alternative theory of osteoinduction is that instead of apatite layers or growth factors, the physical, microstructural surface features of osteoinductive materials give direct cues to cells and instruct them to undergo differentiation towards the osteogenic lineage. This can be achieved through morphological and adhesion changes in cells in contact with surface structured materials, which are translated to a functional response through mechanotransduction pathways[142,143]. Indeed, several studies have demonstrated enhanced osteogenic differentiation in cells cultured on the surface of osteoinductive calcium phosphates with submicron surface features [144–147].

An alternative perspective poses that prior to osteogenic differentiation of MSCs into bone-forming osteoblasts, osteoclasts first arise on the surface of osteoinductive materials and form a trigger for bone formation. Indeed, large multinucleated giant cells have been consistently associated with osteoinductive calcium phosphates after implantation *in vivo*. Although these cells are similar in phenotype to inflammatory foreign body giant cells, they have a different function and exhibit osteoclast-like properties[148]. Osteoclasts have been shown to promote osteogenic differentiation of MSCs[149], and therefore it has been theorized that early osteoclast formation on structured calcium phosphates (osteoclastogenesis) is a trigger for osteoinduction. Several studies have supported this hypothesis. For example, Davison et al. associated tartrate-resistant acid phosphatase (TRAP)-positive osteoclasts with osteoinductive calcium phosphate with a microstructured surface *in vivo*, whereas osteoclast depletion using liposomal clodronate could inhibit osteoinduction[150,151]. Furthermore, *in vitro*, microstructured calcium phosphate was demonstrated to upregulate osteoclast formation, proliferation, survival and size, as well as the secretion of factors that could induce osteogenic differentiation of human mesenchymal stem cells[120,151,152].

Interestingly, foreign body giant cells and osteoclasts are known to form through the fusion of immune cells, called macrophages. In recent years, the biomaterials field has recognized that besides osteogenic cells, the response of the immune system to materials is another relevant target of investigation. The relatively new field of osteoimmunology, which studies the relationship between the immune system and bone tissue, has provided new insights on bone formation by osteoinductive materials. Indeed, a pro-regenerative immune cell called the M2 macrophage has been associated with bone formation, and recent evidence has pointed towards a role of these cells in the mechanism of material-induced bone formation[115,125,153].



## Osteoimmunology and its relevance to bone graft materials

While developments in the fields of bone biology and immunology were independently well underway during the 19<sup>th</sup> and 20<sup>th</sup> century, it was only at the turn of the 21<sup>st</sup> century that these fields converged into a novel scientific area: osteoimmunology. The field of osteoimmunology studies the cross-talk between our bone and immune systems [154]. Research performed in the last 20 years has established that there exists an intricate relationship between these two systems, which is very important in the context of bone homeostasis and healing. For example, the healing of a bone fracture occurs through a tightly regulated cascade of events, with defined steps and phases that involve various types of immune cells, including neutrophils, monocytes, macrophages, T cells and B cells, which secrete a plethora of different biochemical factors throughout the process [155]. This relationship is so essential, that bone healing is delayed in situations where the immune function is compromised, such as during administration of immunosuppressant medication or in HIV-positive patients [156–158].

During the healing of tissue injury and following biomaterial implantation, the innate immune response plays an essential role. After tissue injury, initial blood coagulation and haemostasis is followed by an influx of neutrophils that elicit an acute inflammatory response. Next, circulating monocytes are recruited to the wound bed where they differentiate into macrophages, which are the key regulators during the various phases of the healing cascade [159,160]. Macrophages are a heterogeneous population of immune cells that perform a plethora of functions, including clearance of invading pathogens and cellular debris, promoting and resolving inflammation, and communicating with local cells for tissue repair and remodeling [161,162]. Macrophages can be derived from monocytes, but also reside permanently in local tissues as so-called tissue-resident macrophages [163]. As first described in a groundbreaking work by Charles Mills et al. in the year 2000, macrophages have the unique ability to adopt distinct functional phenotypes in response to their microenvironment [164]. The phenotypes are categorized into those with a pro-inflammatory role and those with an anti-inflammatory role. The pro-inflammatory phenotype, also known as the 'classically' activated or 'M1' phenotype, promotes inflammation by release of pro-inflammatory cytokines and produces reactive oxygen species to clear pathogens, debris and foreign materials. The anti-inflammatory phenotype, known as the 'alternatively' activated, 'M2' or pro-healing phenotype, resolves inflammation through release of anti-inflammatory factors and promotes regeneration and remodeling by signaling to local stem- or progenitor cells that are involved in tissue repair [165,166]. During normal tissue healing, an early phase of M1 macrophage dominance is generally followed by upregulation of pro-healing M2 macrophages [153]. Macrophages can shift between the M1 and M2 phenotypes in response to environmental cues, in a process called macrophage "polarization" [165,167].

## Macrophages and bone metabolism

Macrophages have an essential role in bone regeneration and homeostasis. For example, tissue-resident osteal macrophages, termed OsteoMacs, were shown to directly regulate osteoblast survival and bone matrix deposition *in vivo* [168,169]. Macrophages have also been demonstrated to exhibit crosstalk with mesenchymal stem cells (MSCs) that leads to osteogenic differentiation [170,171]. Furthermore, in a mouse tibial fracture model, depletion of macrophages using liposomal clodronate resulted in delayed union and impaired callus mineralization as compared to healthy controls [172]. Although both M1 and M2 macrophage subtypes are important in bone healing, the M2 phenotype has been associated with the regenerative phase in bone healing. Some studies have suggested that a high M1/M2 macrophage ratio is associated with bone catabolism, i.e. bone resorption, while higher M2/M1 ratios is bone-anabolic, leading to regeneration and healing. For example, M1-dominant macrophage populations have been associated with bone resorption in different situations, including osteoporosis [173], orthodontic tooth movement [174,175], periodontitis [176] and bisphosphonate-related osteonecrosis of the jaw [177–179]. In contrast, M2 macrophages have been associated with bone regeneration. A recent study by Zhang et al. reported a correlation between accelerated fracture healing and higher M2/M1 ratios in human fracture calluses [38]. Similarly, impaired bone fracture healing in aged rats has been associated with impaired M2 macrophage function [180]. Furthermore, various strategies to upregulate M2 macrophages during bone repair resulted in enhanced healing outcomes, associated with higher M2/M1 ratios [181–186].

## Potential role of M2 macrophages in osteoinduction by calcium phosphates

Besides the ample evidence of macrophage involvement in bone metabolism and regeneration, studies have also demonstrated a clear role for macrophages in pathologic ectopic bone formation, also known as heterotopic ossification [187–189]. This phenomenon describes the formation of bone in soft tissues following trauma (nerve injury, blast/burn injury) or due to disorders such as fibrodysplasia ossificans progressiva (FOP), and shares similarities with ectopic bone formation by osteoinductive materials. Recently, a sub-population of M2 macrophage-like cells have been associated with early heterotopic ossification [190]. Due to the clear association between M2 macrophages and bone regeneration, and the apparent involvement of M2 macrophage-like cells in heterotopic ossification, it is probable that M2 macrophages also play a role in the process of bone formation by osteoinductive calcium phosphates (Table 2). In fact, previous studies have already demonstrated an important role for macrophages in ectopic bone formation by materials. In an earlier mentioned study, Davison et al. implanted osteoinductive TCP in subcutaneous pockets of mice and proceeded to give local, weekly injections of liposome-encapsulated clodronate, which is known to deplete macrophages [150]. The authors reported that clodronate treatment attenuated ectopic bone formation by osteoinductive calcium phosphate, indicating the importance of macrophages in material-induced





bone formation. Although macrophage phenotypes were not assessed in the study by Davison et al., it was demonstrated that clodronate treatment more selectively depletes M2 macrophages than M1 macrophages, resulting in a shift towards an M1 dominant macrophage population [191–193]. The latter may suggest that downregulation of M2 macrophages may have had a role in the attenuation of ectopic bone formation observed by Davison et al. In fact, two recent studies have demonstrated that murine M2 macrophages are upregulated by calcium phosphate materials with osteoinductive capacity *in vitro* and *in vivo*, prior to ectopic bone formation[115,125].

## **RESEARCH AIM AND THESIS OUTLINE**

---

Osteoinductive calcium phosphates are promising bone graft substitutes because of their ability to induce bone formation in sites distant from host bone tissue. Microstructural surface features, including topography, have been shown to be the dominant material factor that dictates this osteoinductive potential.

*The overall objective of this thesis is to determine if and how topography of calcium phosphates can be improved for increased efficacy as bone graft materials for maxillofacial and orthopedic surgery.*

To achieve this goal, the following research questions will be answered in this work:

- Can the osteoinductive potential of calcium phosphate bone graft substitutes be improved by optimizing their topographical features?
- Does an optimized surface topography translate to enhanced efficacy with regard to bone formation compared to conventional non-osteoinductive synthetic bone graft materials?
- Is osteoinductive calcium phosphate an effective alternative to autograft and other synthetic bone graft substitutes for common orthopedic and maxillofacial bone grafting indications?
- Does osteoinductive calcium phosphate affect the innate immune response (*i.e.* macrophage polarization) and could this response play a role in bone formation by these materials?

The work presented in this thesis is divided in four parts:

## **Part I: Improving the surface topography of calcium phosphates to enhance their osteoinductive potential**

*The aim of part I is to determine how size and morphology of topographical features on calcium phosphates affect their osteoinductive potential, and to identify which surface topography correlates with the highest osteoinductive capacity.*

Topographical features of calcium phosphates have been shown to affect osteoinductive potential and their ability to regenerate orthotopic defects. **Chapter 2** presents an investigation of the role of specific surface properties on the osteoinductive potential of calcium phosphates at a more challenging ectopic location. The osteoinductive potential of four calcium phosphate bone graft substitutes with different surface topographies are compared using a canine intramuscular implantation model. The material with the highest osteoinductive potential, *i.e.* with a needle-shaped submicron surface topography, was selected for further evaluation in the following parts of this thesis.

## **Part II: Efficacy of osteoinductive calcium phosphate as bone graft material in spinal fusion**

*The aim of part II is to evaluate whether osteoinductive calcium phosphate is an effective alternative to autograft and other bone graft substitutes for spinal fusion.*

Spinal arthrodesis, or spinal fusion, is one of the most frequently performed bone grafting procedures in orthopedic surgery. In this section, a calcium phosphate with needle-shaped submicron topography is evaluated in different animal models of posterolateral spinal fusion. In **chapter 3**, its use as an autograft extender is compared with autograft in a validated rabbit model of posterolateral fusion. In **chapters 4** and **5**, the material, as standalone bone graft substitute, is evaluated in a clinically-relevant sheep model of instrumented posterolateral fusion. In more detail, in **chapter 4**, the efficacy of this material is compared with autograft at various timepoints, while **chapter 5** describes a comparison with two other bone graft materials that are clinically used in spinal fusion. Additionally, **chapters 3** and **4** investigate the effect of a polymeric carrier designed to improve handling properties on the efficacy of osteoinductive calcium phosphate.

## **Part III: Efficacy of osteoinductive calcium phosphate in maxillary sinus floor augmentation**

*The aim of part III is to evaluate the efficacy of osteoinductive calcium phosphate compared with autograft and other bone graft substitutes in maxillary sinus floor augmentation.*

Maxillary sinus floor augmentation (MSFA) is a procedure in maxillofacial surgery that involves the use of bone grafts to facilitate dental implant placement. In **chapter 6**, calcium phosphate with needle-shaped submicron topography is evaluated as a bone grafting



material for this procedure. Firstly, the material is evaluated in a pre-clinical sheep model of sinus floor augmentation, compared to autograft and a calcium phosphate bone graft with different surface features. Secondly, this chapter includes results of a randomized controlled clinical study of maxillary sinus floor augmentation, in which osteoinductive calcium phosphate was evaluated *versus* autograft.

#### **Part IV: The response of macrophages to osteoinductive calcium phosphate**

*The aim of part IV is to explore the potential relation of the macrophage response to calcium phosphates, to their osteoinductive and bone healing capacity*

Macrophages are key regulators of the healing response and have an intricate relation with bone tissue. In particular, upregulation of the M2 macrophage phenotype during bone healing has been associated with enhanced healing outcomes. **Chapter 7** describes an *in vitro* investigation of the polarization response of primary human macrophages to different calcium phosphate bone graft substitutes, including osteoinductive calcium phosphate with submicron needle-shaped topography. This chapter also assesses downstream regenerative effects of macrophages using *in vitro* angiogenic and osteogenic assays. **Chapter 8** is a translational analysis of the relevance of the innate immune response to calcium phosphate bone substitutes and other biomaterials to bone healing. It describes original results from studies from the benchtop to the clinic, which are placed in perspective of the recent literature on macrophage response to biomaterials with specific structural and topographical properties.

## REFERENCES

---

- [1] J.J. Hublin, A. Ben-Ncer, S.E. Bailey, S.E. Freidline, S. Neubauer, M.M. Skinner, I. Bergmann, A. Le Cabec, S. Benazzi, K. Harvati, P. Gunz, New fossils from Jebel Irhoud, Morocco and the pan-African origin of *Homo sapiens*, *Nature*. 546 (2017) 289–292. <https://doi.org/10.1038/nature22336>.
- [2] C.J. Bae, K. Douka, M.D. Petraglia, On the origin of modern humans: Asian perspectives, *Science* (80-.). 358 (2017). [https://doi.org/10.1126/SCIENCE.AAI9067/ASSET/46F553EA-DF06-4ED0-805B-916D3F587F29/ASSETS/GRAPHIC/358\\_AAI9067\\_F2.JPEG](https://doi.org/10.1126/SCIENCE.AAI9067/ASSET/46F553EA-DF06-4ED0-805B-916D3F587F29/ASSETS/GRAPHIC/358_AAI9067_F2.JPEG).
- [3] N. Longrich, There used to be nine species of human. What happened to them? | National Post, (n.d.). <https://nationalpost.com/news/world/there-used-to-be-nine-species-of-human-what-happened-to-them> (accessed December 6, 2021).
- [4] S.P. McPherron, Z. Alemseged, C.W. Marean, J.G. Wynn, D. Reed, D. Geraads, R. Bobe, H.A. Béarat, Evidence for stone-tool-assisted consumption of animal tissues before 3.39 million years ago at Dikika, Ethiopia, *Nature*. 466 (2010) 857–860. <https://doi.org/10.1038/NATURE09248>.
- [5] S.R. James, R.W. Dennell, A.S. Gilbert, H.T. Lewis, J.A.J. Gowlett, T.F. Lynch, W.C. McGrew, C.R. Peters, G.G. Pope, A.B. Stahl, S.R. James, Hominid Use of Fire in the Lower and Middle Pleistocene: A Review of the Evidence [and Comments and Replies], <https://doi-org.proxy.library.uu.nl/10.1086/203705>. 30 (2015) 1–26. <https://doi.org/10.1086/203705>.
- [6] B.L. Hardy, M.H. Moncel, C. Kerfant, M. Lebon, L. Bellot-Gurlet, N. Mélard, Direct evidence of Neanderthal fibre technology and its cognitive and behavioral implications, *Sci. Rep.* 10 (2020). <https://doi.org/10.1038/S41598-020-61839-W>.
- [7] R.L. Holloway, D.C. Broadfield, M.S. (Michael S.-T. Yuan, The human fossil record. Volume three, Brain endocasts, the paleoneurological evidence, (2004). <https://www.wiley.com/en-us/The+Human+Fossil+Record%2C+Volume+3%2C+Brain+Endocasts+The+Paleoneurological+Evidence-p-9780471663577> (accessed December 6, 2021).
- [8] S. Peeters, H. Zwart, Neanderthals as familiar strangers and the human spark: How the “golden years” of Neanderthal research reopen the question of human uniqueness, *Hist. Philos. Life Sci.* 42 (2020). <https://doi.org/10.1007/S40656-020-00327-W>.
- [9] M. Breyll, Triangulating Neanderthal cognition: A tale of not seeing the forest for the trees, *Wiley Interdiscip. Rev. Cogn. Sci.* 12 (2021). <https://doi.org/10.1002/WCS.1545>.
- [10] P. Roberts, B.A. Stewart, Defining the ‘generalist specialist’ niche for Pleistocene *Homo sapiens*, *Nat. Hum. Behav.* 2 (2018) 542–550. <https://doi.org/10.1038/S41562-018-0394-4>.
- [11] R. Hajar, History of Medicine Timeline, *Heart Views*. 16 (2015) 43. <https://doi.org/10.4103/1995-705X.153008>.
- [12] R. Porter, *The Cambridge illustrated history of medicine*, Cambridge University Press, New York, 2001.
- [13] C. Mason, P. Dunnill, A brief definition of regenerative medicine, <http://dx.doi.org/10.2217/17460751.3.1.1.3> (2007) 1–5. <https://doi.org/10.2217/17460751.3.1.1>.

- [14] E. De Divitiis, The prehistoric practice of trepanation, *World Neurosurg.* (2013). <https://doi.org/10.1016/j.wneu.2013.01.069>.
- [15] D.S. Kushner, J.W. Verano, A.R. Titelbaum, Trepanation Procedures/Outcomes: Comparison of Prehistoric Peru with Other Ancient, Medieval, and American Civil War Cranial Surgery, *World Neurosurg.* (2018). <https://doi.org/10.1016/j.wneu.2018.03.143>.
- [16] A. Sanan, S.J. Haines, Repairing holes in the head: A history of cranioplasty, *Neurosurgery.* (1997). <https://doi.org/10.1097/00006123-199703000-00033>.
- [17] G. Flati, C. Di Stanislao, Chirurgica nella preistoria. Part-I., *Prov Med Aquil.* 2 (2004) 8–11.
- [18] A. Bobbio, The first endosseous alloplastic implant in the history of man., *Bull. Hist. Dent.* (1972).
- [19] A. Bobbio, Maia o primeiro autêntico implante dentário aloplástico endo-ósseo. Uui aprimoramento e uma prioridade., *Rev. Assoc. Paul. Cir. Dent.* (1973).
- [20] M.E. Pasqualini, Un impianto alloplastico in una mandibola di 1300 anni. *Ricerca istologica., Dent Cadmos.* 11 (2000) 57–62.
- [21] M. Lamghari, M.J. Almeida, S. Berland, H. Huet, A. Laurent, C. Milet, E. Lopez, Stimulation of bone marrow cells and bone formation by nacre: in vivo and in vitro studies, *Bone.* 25 (1999). [https://doi.org/10.1016/S8756-3282\(99\)00141-6](https://doi.org/10.1016/S8756-3282(99)00141-6).
- [22] U. Pasqualini, M.E. Pasqualini, *Treatise of Implant Dentistry*, 2009.
- [23] J. van Meekeren, *Heel en geneeskonstige aanmerkingen*, Casparus Commelijn, Amsterdam, 1668.
- [24] P. von Walther, Wiedereinheilung der bei der Trepanation ausgebohrten Knochenscheibe, *J Chir Augenheilkd.* 2 (1821) 571–583.
- [25] L. Ollier, *Traité Expérimental et Clinique de la Régénération des Os et de la Production Artificielle du Tissu Osseux.*, Victor Masson Et Fils, Paris, 1867. <https://doi.org/10.1097/00000441-186801000-00029>.
- [26] W. MacEwan, Observations concerning transplantation of bone. Illustrated by a case of inter-human osseous transplantation, whereby over two-thirds of the shaft of a humerus was restored, *Proc. R. Soc. London.* 32 (1881) 232–247. <https://doi.org/10.1098/rspl.1881.0025>.
- [27] F.H. Albee, *Bone Graft Surgery*, Saunders, Philadelphia, 1915.
- [28] V. Putti, I trapianti ossei, *Arch Ortop.* 29 (1912) 294–334.
- [29] P.P. Brunner, Die Entwicklung der Knochenplastik am Unterkiefer im Ersten Weltkrieg, (1996) 125. [https://books.google.com/books/about/Die\\_Entwicklung\\_der\\_Knochenplastik\\_am\\_Un.html?id=RpseAQAIAAJ](https://books.google.com/books/about/Die_Entwicklung_der_Knochenplastik_am_Un.html?id=RpseAQAIAAJ) (accessed December 7, 2021).
- [30] O. Faour, R. Dimitriou, C.A. Cousins, P. V. Giannoudis, The use of bone graft substitutes in large cancellous voids: Any specific needs?, *Injury.* (2011). <https://doi.org/10.1016/j.injury.2011.06.020>.
- [31] R. V. Deev, A.Y. Drobyshev, I.Y. Bozo, A.A. Isaev, Ordinary and Activated Bone Grafts: Applied Classification and the Main Features, *Biomed Res. Int.* (2015). <https://doi.org/10.1155/2015/365050>.




- [32] G. Hannink, J.J.C. Arts, Bioresorbability, porosity and mechanical strength of bone substitutes: What is optimal for bone regeneration?, *Injury*. (2011). <https://doi.org/10.1016/j.injury.2011.06.008>.
- [33] T.T. Roberts, A.J. Rosenbaum, Bone grafts, bone substitutes and orthobiologics the bridge between basic science and clinical advancements in fracture healing, *Organogenesis*. 8 (2012) 114–124. <https://doi.org/10.4161/org.23306>.
- [34] R.J. Klijn, G.J. Meijer, E.M. Bronkhorst, J.A. Jansen, Sinus floor augmentation surgery using autologous bone grafts from various donor sites: A meta-analysis of the total bone volume, *Tissue Eng.-Part B Rev*. 16 (2010) 295–303. <https://doi.org/10.1089/ten.teb.2009.0558>.
- [35] K. Inage, S. Ohtori, T. Koshi, M. Suzuki, M. Takaso, M. Yamashita, K. Yamauchi, G. Inoue, S. Orita, Y. Eguchi, N. Ochiai, S. Kishida, K. Kuniyoshi, Y. Aoki, J. Nakamura, T. Ishikawa, G. Arai, M. Miyagi, H. Kamoda, T. Suzuki, T. Toyone, K. Takahashi, One, two-, and three-level instrumented posterolateral fusion of the lumbar spine with a local bone graft: a prospective study with a 2-year follow-up., *Spine (Phila. Pa. 1976)*. 36 (2011) 1392–1396. <https://doi.org/10.1097/BRS.0b013e3181f40e69>.
- [36] D.K. Park, R. Roberts, P. Arnold, D.H. Kim, R. Sasso, K.C. Baker, J.S. Fischgrund, Lumbar Spine Fusion Rates With Local Bone in Posterolateral and Combined Posterolateral and Interbody Approaches, *JAAOS Glob. Res. Rev*. 3 (2019) e018. <https://doi.org/10.5435/jaaosglobal-d-18-00018>.
- [37] A. Truedsson, K. Hjalte, B. Sunzel, G. Warfvinge, Maxillary sinus augmentation with iliac autograft—A health-economic analysis, *Clin. Oral Implants Res*. 24 (2013) 1088–1093. <https://doi.org/10.1111/j.1600-0501.2012.02515.x>.
- [38] C.G. Gjerde, S. Shanbhag, E. Neppelberg, K. Mustafa, H. Gjengedal, Patient experience following iliac crest-derived alveolar bone grafting and implant placement, *Int. J. Implant Dent*. 6 (2020) 4. <https://doi.org/10.1186/s40729-019-0200-8>.
- [39] G.C. Berlet, J.F. Baumhauer, M. Glazebrook, S.L. Haddad, A. Younger, J.D. Quiton, D.A. Fitch, T.R. Daniels, C.W. DiGiovanni, The Impact of Patient Age on Foot and Ankle Arthrodesis Supplemented with Autograft or an Autograft Alternative (rhPDGF-BB/ $\beta$ -TCP), *JB JS Open Access*. 5 (2020) e20.00056–e20.00056. <https://doi.org/10.2106/JBJS.OA.20.00056>.
- [40] D.H. Kim, R. Rhim, L. Li, J. Martha, B.H. Swaim, R.J. Banco, L.G. Jenis, S.G. Tromanhauser, Prospective study of iliac crest bone graft harvest site pain and morbidity, *Spine J*. (2009). <https://doi.org/10.1016/j.spinee.2009.05.006>.
- [41] J.A. Rihn, K. Kirkpatrick, T.J. Albert, Graft options in posterolateral and posterior interbody lumbar fusion, *Spine (Phila. Pa. 1976)*. (2010). <https://doi.org/10.1097/BRS.0b013e3181d25803>.
- [42] R. Dimitriou, G.I. Mataliotakis, A.G. Angoules, N.K. Kanakaris, P. V. Giannoudis, Complications following autologous bone graft harvesting from the iliac crest and using the RIA: A systematic review, *Injury*. 42 (2011). <https://doi.org/10.1016/j.injury.2011.06.015>.
- [43] L. Di Silvio, P. Jayakumar, Cellular response to osteoinductive materials in orthopaedic surgery, *Cell. Response to Biomater*. (2009) 313–343. <https://doi.org/10.1533/9781845695477.2.313>.
- [44] B. Clarke, Normal bone anatomy and physiology, *Clin. J. Am. Soc. Nephrol*. (2008).

- [45] D.W. Buck, G.A. Dumanian, Bone biology and physiology: Part I. the fundamentals, *Plast. Reconstr. Surg.* 129 (2012) 1314–1320. <https://doi.org/10.1097/PRS.0B013E31824ECA94>.
- [46] S. Lee, M. Porter, S. Wasko, G. Lau, P.-Y. Chen, E.E. Novitskaya, A.P. Tomsia, A. Almutairi, M.A. Meyers, J. Mckittrick, Potential Bone Replacement Materials Prepared by Two Methods, (n.d.).
- [47] R. Hoffman, B.K. Marcellino, Bone Marrow Microenvironment in Health and Disease, *Encycl. Bone Biol.* (2020) 1–11. <https://doi.org/10.1016/B978-0-12-801238-3.11195-X>.
- [48] J.A. Buckwalter, M.J. Glimcher, R.R. Cooper, R. Recker, Bone biology. I: Structure, blood supply, cells, matrix, and mineralization., *Instr. Course Lect.* 45 (1996).
- [49] B. Skovrtlj, J.Z. Guzman, M. Al Maaieh, S.K. Cho, J.C. Iatridis, S.A. Qureshi, Cellular bone matrices: viable stem cell-containing bone graft substitutes, *Spine J.* 14 (2014) 2763. <https://doi.org/10.1016/J.SPINEE.2014.05.024>.
- [50] J.W. Hustedt, D.J. Blizzard, The Controversy Surrounding Bone Morphogenetic Proteins in the Spine: A Review of Current Research, *Yale J. Biol. Med.* 87 (2014) 549. [/pmc/articles/PMC4257039/](https://pubmed.ncbi.nlm.nih.gov/24257039/) (accessed December 22, 2021).
- [51] B. SM, W. TY, P. C, R. S, G. CR, K. IO, A.-E.-B. MM, S. CI, Y. CK, T. KD, Pseudarthrosis rate following anterior cervical discectomy with fusion using an allograft cellular bone matrix: a multi-institutional analysis, *Neurosurg. Focus.* 50 (2021) 1–8. <https://doi.org/10.3171/2021.3.FOCUS2166>.
- [52] A. Abedi, B. Formanek, N. Russell, F. Vizesi, S.D. Boden, J.C. Wang, Z. Buser, Examination of the Role of Cells in Commercially Available Cellular Allografts in Spine Fusion: An in Vivo Animal Study, *J. Bone Joint Surg. Am.* 102 (2020) e135. <https://doi.org/10.2106/JBJS.20.00330>.
- [53] H. Roscoe, C. Schorlemmer, *A Treatise on Chemistry. Volume I: The Non-metallic Elements*, Macmillan and Co., London, 1881.
- [54] S. V. Dorozhkin, Calcium Orthophosphates in Nature, Biology and Medicine, *Materials (Basel)*. 2 (2009) 399. <https://doi.org/10.3390/MA2020399>.
- [55] S. V. Dorozhkin, A history of calcium orthophosphates (CaPO<sub>4</sub>) and their biomedical applications, *Morphologie.* 101 (2017) 143–153. <https://doi.org/10.1016/J.MORPHO.2017.05.001>.
- [56] N. Eliaz, N. Metoki, Calcium phosphate bioceramics: A review of their history, structure, properties, coating technologies and biomedical applications, *Materials (Basel)*. (2017). <https://doi.org/10.3390/ma10040334>.
- [57] F.H. Albee, Studies in Bone Growth: Triple Calcium Phosphate As a Stimulus To Osteogenesis., *Ann. Surg.* 71 (1920) 32–9. <https://doi.org/10.1097/00000658-192001000-00006>.
- [58] M.O. Ludlow, Apical closure after nonsurgical apical curettage, *J. Endod.* (1979). [https://doi.org/10.1016/S0099-2399\(79\)80036-9](https://doi.org/10.1016/S0099-2399(79)80036-9).
- [59] H.W. Denissen, K. de Groot, Immediate dental root implants from synthetic dense calcium hydroxylapatite, *J. Prosthet. Dent.* 42 (1979) 551–556. [https://doi.org/10.1016/0022-3913\(79\)90253-1](https://doi.org/10.1016/0022-3913(79)90253-1).
- [60] S. V. Dorozhkin, A detailed history of calcium orthophosphates from 1770s till 1950, *Mater. Sci. Eng. C.* (2013). <https://doi.org/10.1016/j.msec.2013.04.002>.



- [61] N. Passuti, G. Daculsi, J.M. Rogez, S. Martin, J. V. Bainvel, Macroporous calcium phosphate ceramic performance in human spine fusion, *Clin. Orthop. Relat. Res.* (1989). <https://doi.org/10.1097/00003086-198911000-00027>.
- [62] H. Tsuji, N. Hirano, Y. Katoh, H. Ohsima, H. Ishihara, H. Matsui, Y. Hayashi, Ceramic interspinous block (CISB) assisted anterior interbody fusion, *J. Spinal Disord.* (1990). <https://doi.org/10.1097/00002517-199003000-00013>.
- [63] H. Waisbrod, H.U. Gerbershagen, A pilot study of the value of ceramics for bone replacement, *Arch. Orthop. Trauma. Surg.* (1986). <https://doi.org/10.1007/BF00449930>.
- [64] R.W. Bucholz, Clinical experience with bone graft substitutes, *J. Orthop. Trauma.* 1 (1987) 260–262. <https://doi.org/10.1097/00005131-198701030-00013>.
- [65] R.W. Bucholz, A. Carlton, R. Holmes, Interporous hydroxyapatite as a bone graft substitute in tibial plateau fractures, *Clin. Orthop. Relat. Res.* (1989). <https://doi.org/10.1097/00003086-198903000-00008>.
- [66] S. Ghanaati, M. Barbeck, R. Detsch, U. Deisinger, U. Hilbig, V. Rausch, R. Sader, R.E. Unger, G. Ziegler, C.J. Kirkpatrick, The chemical composition of synthetic bone substitutes influences tissue reactions in vivo: Histological and histomorphometrical analysis of the cellular inflammatory response to hydroxyapatite, beta-tricalcium phosphate and biphasic calcium phosphate cer, *Biomed. Mater.* 7 (2012) 15005. <https://doi.org/10.1088/1748-6041/7/1/015005>.
- [67] J.Y. Hong, J.S. Lee, E.K. Pang, U.W. Jung, S.H. Choi, C.K. Kim, Impact of different synthetic bone fillers on healing of extraction sockets: an experimental study in dogs, *Clin. Oral Implants Res.* 25 (2014). <https://doi.org/10.1111/CLR.12041>.
- [68] W.R. Walsh, R.A. Oliver, C. Christou, V. Lovric, E.R. Walsh, G.R. Prado, T. Haider, Critical size bone defect healing using collagen-calcium phosphate bone graft materials, *PLoS One.* 12 (2017). <https://doi.org/10.1371/journal.pone.0168883>.
- [69] K.A. Hing, L.F. Wilson, T. Buckland, Comparative performance of three ceramic bone graft substitutes, *Spine J.* 7 (2007) 475–490. <https://doi.org/10.1016/j.spinee.2006.07.017>.
- [70] H.G. Baramki, T. Steffen, P. Lander, M. Chang, D. Marchesi, The efficacy of interconnected porous hydroxyapatite in achieving posterolateral lumbar fusion in sheep, *Spine (Phila. Pa. 1976).* 25 (2000) 1053–1060. <https://doi.org/10.1097/00007632-200005010-00003>.
- [71] S.S. Jensen, M.M. Bornstein, M. Dard, D.D. Bosshardt, D. Buser, Comparative study of biphasic calcium phosphates with different HA/TCP ratios in mandibular bone defects. A long-term histomorphometric study in minipigs, *J. Biomed. Mater. Res.–Part B Appl. Biomater.* 90 B (2009) 171–181. <https://doi.org/10.1002/jbm.b.31271>.
- [72] H.-C. Lim, M.-L. Zhang, J.-S. Lee, U.-W. Jung, S.-H. Choi, Effect of different hydroxyapatite:β-tricalcium phosphate ratios on the osteoconductivity of biphasic calcium phosphate in the rabbit sinus model, *Int. J. Oral Maxillofac. Implants.* 30 (2015) 65–72. <https://doi.org/10.11607/JOMI.3709>.
- [73] C.M. Murphy, M.G. Haugh, F.J. O'Brien, The effect of mean pore size on cell attachment, proliferation and migration in collagen–glycosaminoglycan scaffolds for bone tissue engineering, *Biomaterials.* 31 (2010) 461–466. <https://doi.org/10.1016/J.BIOMATERIALS.2009.09.063>.



- 
- [74] P.S. Eggli, W. Muller, R.K. Schenk, Porous hydroxyapatite and tricalcium phosphate cylinders with two different pore size ranges implanted in the cancellous bone of rabbits. A comparative histomorphometric and histologic study of bone ingrowth and implant substitution, *Clin. Orthop. Relat. Res.* (1988) 127–138. <https://doi.org/10.1097/00003086-198807000-00017>.
- [75] F.M. Klenke, Y. Liu, H. Yuan, E.B. Hunziker, K.A. Siebenrock, W. Hofstetter, Impact of pore size on the vascularization and osseointegration of ceramic bone substitutes in vivo, *J. Biomed. Mater. Res.–Part A*. 85 (2008) 777–786. <https://doi.org/10.1002/jbm.a.31559>.
- [76] N. Abbasi, S. Hamlet, R.M. Love, N.T. Nguyen, Porous scaffolds for bone regeneration, *J. Sci. Adv. Mater. Devices*. 5 (2020) 1–9. <https://doi.org/10.1016/J.JSAMD.2020.01.007>.
- [77] A. Nouri, P.D. Hodgson, C. Wen, Biomimetic Porous Titanium Scaffolds for Orthopedic and Dental Applications, *Biomimetics Learn. from Nat.* (2010). <https://doi.org/10.5772/8787>.
- [78] V.R. Salvini, V.C. Pandolfelli, D. Spinelli, Mechanical Properties of Porous Ceramics, *Recent Adv. Porous Ceram.* (2018). <https://doi.org/10.5772/INTECHOPEN.71612>.
- [79] J. Seuba, S. Deville, C. Guizard, A.J. Stevenson, Mechanical properties and failure behavior of unidirectional porous ceramics, *Sci. Rep.* 6 (2016). <https://doi.org/10.1038/SREP24326>.
- [80] D. Barbieri, H. Yuan, A.S. Ismailo lu, J.D. De Bruijn, Comparison of two moldable calcium phosphate-based bone graft materials in a noninstrumented canine interspinous implantation model, *Tissue Eng.–Part A*. 23 (2017) 1310–1320. <https://doi.org/10.1089/ten.tea.2016.0347>.
- [81] N. Davison, H. Yuan, J.D. De Bruijn, F. Barrere-De Groot, In vivo performance of microstructured calcium phosphate formulated in novel water-free carriers, *Acta Biomater.* 8 (2012) 2759–2769. <https://doi.org/10.1016/J.ACTBIO.2012.04.007>.
- [82] R.V. Baier, I.B. Wijnhoven, V.I. Del Valle, C.M. Giovanetti, J.F. Vivanco, Microporosity clustering assessment in calcium phosphate bioceramic particles, *Front. Bioeng. Biotechnol.* 7 (2019) 281. <https://doi.org/10.3389/FBIOE.2019.00281/BIBTEX>.
- [83] H. Lapczynska, L. Galea, S. Wüst, M. Böhner, S. Jerban, A. Sweedy, N. Doebelin, N. van Garderen, S. Hofmann, G. Baroud, R. Müller, B. von Rechenberg, Effect of grain size and microporosity on the in vivo behaviour of  $\beta$ -tricalcium phosphate scaffolds, *Eur. Cells Mater.* 28 (2014) 299–319. <https://doi.org/10.22203/eCM.v028a21>.
- [84] L.E. Rustom, T. Boudou, S. Lou, I. Pignot-Paintrand, B.W. Nemke, Y. Lu, M.D. Markel, C. Picart, A.J. Wagoner Johnson, Micropore-induced capillarity enhances bone distribution in vivo in biphasic calcium phosphate scaffolds, *Acta Biomater.* 44 (2016) 144–154. <https://doi.org/10.1016/j.actbio.2016.08.025>.
- [85] K.A. Hing, B. Annaz, S. Saeed, P.A. Revell, T. Buckland, Microporosity enhances bioactivity of synthetic bone graft substitutes, in: *J. Mater. Sci. Mater. Med., J Mater Sci Mater Med*, 2005: pp. 467–475. <https://doi.org/10.1007/s10856-005-6988-1>.
- [86] J.D. DE BRUIJN, K. DE GROOT, C.A. VAN BLITTERSWIJK, H. YUAN, Osteoinductive ceramic materials, (n.d.). <https://lens.org/180-790-096-112-249>.
- [87] C. Klein, K. de Groot, W. Chen, Y. Li, X. Zhang, Osseous substance formation induced in porous calcium phosphate ceramics in soft tissues, *Biomaterials*. 15 (1994) 31–34. [https://doi.org/10.1016/0142-9612\(94\)90193-7](https://doi.org/10.1016/0142-9612(94)90193-7).

- [88] Z. Yang, H. Yuan, W. Tong, P. Zou, W. Chen, X. Zhang, Osteogenesis in extraskeletally implanted porous calcium phosphate ceramics: variability among different kinds of animals, *Biomaterials*. 17 (1996) 2131–2137. [https://doi.org/10.1016/0142-9612\(96\)00044-0](https://doi.org/10.1016/0142-9612(96)00044-0).
- [89] Z. Jian Yang, H. Yuan, P. Zou, W. Tong, S. Qu, X. Dong Zhang, Osteogenic responses to extraskeletally implanted synthetic porous calcium phosphate ceramics: an early stage histomorphological study in dogs, *J. Mater. Sci. Mater. Med.* 8 (1997) 697–701. <https://doi.org/10.1023/A:1018540024082>.
- [90] H. Yuan, Z. Yang, Y. Li, X. Zhang, J.D. De Bruijn, K. De Groot, Osteoinduction by calcium phosphate biomaterials, *J. Mater. Sci. Mater. Med.* 9 (1998) 723–726. <https://doi.org/10.1023/A:1008950902047>.
- [91] H.O. Mayr, M. Dietrich, F. Fraedrich, R. Hube, A. Nerlich, R. von Eisenhart-Rothe, W. Hein, A. Bernstein, Microporous Pure  $\beta$ -Tricalcium Phosphate Implants for Press-Fit Fixation of Anterior Cruciate Ligament Grafts: Strength and Healing in a Sheep Model, *Arthrosc.–J. Arthrosc. Relat. Surg.* 25 (2009) 996–1005. <https://doi.org/10.1016/j.arthro.2009.02.019>.
- [92] M. Nouri-Goushki, L. Angeloni, K. Modaresifar, M. Minneboo, P.E. Boukany, M.J. Mirzaali, M.K. Ghatkesar, L.E. Fratila-Apachitei, A.A. Zadpoor, 3D-Printed Submicron Patterns Reveal the Interrelation between Cell Adhesion, Cell Mechanics, and Osteogenesis, *ACS Appl. Mater. Interfaces*. 13 (2021) 33767. <https://doi.org/10.1021/ACSAMI.1C03687>.
- [93] M. Nouri-Goushki, A. Isaakidou, B.I.M. Eijkel, M. Minneboo, Q. Liu, P.E. Boukany, M.J. Mirzaali, L.E. Fratila-Apachitei, A.A. Zadpoor, 3D printed submicron patterns orchestrate the response of macrophages, *Nanoscale*. 13 (2021) 14304. <https://doi.org/10.1039/D1NR01557E>.
- [94] M.J. Vassey, G.P. Figueredo, D.J. Scurr, A.S. Vasilevich, S. Vermeulen, A. Carlier, J. Luckett, N.R.M. Beijer, P. Williams, D.A. Winkler, J. de Boer, A.M. Ghaemmaghami, M.R. Alexander, Immune Modulation by Design: Using Topography to Control Human Monocyte Attachment and Macrophage Differentiation, *Adv. Sci.* 7 (2020). <https://doi.org/10.1002/ADVS.201903392>.
- [95] D. Xiao, J. Zhang, C. Zhang, D. Barbieri, H. Yuan, L. Moroni, G. Feng, The role of calcium phosphate surface structure in osteogenesis and the mechanisms involved, *Acta Biomater.* 106 (2020) 22–33. <https://doi.org/10.1016/j.actbio.2019.12.034>.
- [96] P. Habibovic, H. Yuan, M. van den Doel, T.M. Sees, C.A. van Blitterswijk, K. de Groot, Relevance of osteoinductive biomaterials in critical-sized orthotopic defect, *J. Orthop. Res.* 24 (2006) 867–876. <https://doi.org/10.1002/jor.20115>.
- [97] J. Zhang, D. Barbieri, H. Ten Hoopen, J.D. De Bruijn, C.A. Van Blitterswijk, H. Yuan, Microporous calcium phosphate ceramics driving osteogenesis through surface architecture, *J. Biomed. Mater. Res. A*. 103 (2015) 1188–1199. <https://doi.org/10.1002/JBM.A.35272>.
- [98] D. Xiao, J. Zhang, C. Zhang, D. Barbieri, H. Yuan, L. Moroni, G. Feng, The role of calcium phosphate surface structure in osteogenesis and the mechanisms involved, *Acta Biomater.* 106 (2020) 22–33. <https://doi.org/10.1016/J.ACTBIO.2019.12.034>.
- [99] C. Zhao, X. Wang, L. Gao, L. Jing, Q. Zhou, J. Chang, The role of the micro-pattern and nano-topography of hydroxyapatite bioceramics on stimulating osteogenic differentiation

- of mesenchymal stem cells, *Acta Biomater.* 73 (2018) 509–521. <https://doi.org/10.1016/j.ACTBIO.2018.04.030>.
- [100] W. Habraken, P. Habibovic, M. Epple, M. Böhner, Calcium phosphates in biomedical applications: Materials for the future?, *Mater. Today.* 19 (2016) 69–87. <https://doi.org/10.1016/j.mattod.2015.10.008>.
- [101] M.R. Urist, Bone: formation by autoinduction, *Science.* 150 (1965) 893–899. <https://doi.org/10.1126/SCIENCE.150.3698.893>.
- [102] M.R. Urist, B.S. Strates, Bone morphogenetic protein, *J. Dent. Res.* 50 (1971) 1392–1406. <https://doi.org/10.1177/00220345710500060601>.
- [103] A.M.C. Barradas, H. Yuan, C.A. van Blitterswijk, P. Habibovic, Osteoinductive biomaterials: current knowledge of properties, experimental models and biological mechanisms., *Eur. Cell. Mater.* (2011). <https://doi.org/10.22203/eCM.v021a31>.
- [104] H. Yuan, Z. Yang, J.D. De Bruijn, K. De Groot, X. Zhang, Material-dependent bone induction by calcium phosphate ceramics: a 2.5-year study in dog, *Biomaterials.* 22 (2001) 2617–2623. [https://doi.org/10.1016/S0142-9612\(00\)00450-6](https://doi.org/10.1016/S0142-9612(00)00450-6).
- [105] H. Yuan, C.A. Van Blitterswijk, K. De Groot, J.D. De Bruijn, Cross-species comparison of ectopic bone formation in biphasic calcium phosphate (BCP) and hydroxyapatite (HA) scaffolds, *Tissue Eng.* 12 (2006) 1607–1615. <https://doi.org/10.1089/TEN.2006.12.1607>.
- [106] H. Yuan, C.A. Van Blitterswijk, K. De Groot, J.D. De Bruijn, A comparison of bone formation in biphasic calcium phosphate (BCP) and hydroxyapatite (HA) implanted in muscle and bone of dogs at different time periods, *J. Biomed. Mater. Res. A.* 78 (2006) 139–147. <https://doi.org/10.1002/JBM.A.30707>.
- [107] J.D. de Bruijn, H. Yuan, Osteoinductive microparticles, (2011).
- [108] U. Ripamonti, The Morphogenesis of Bone in Replicas of Porous Hydroxyapatite Obtained from Conversion of Calcium Carbonate Exoskeletons of CoraT, (1991).
- [109] C. Klein, K. de Groot, W. Chen, Y. Li, X. Zhang, Osseous substance formation induced in porous calcium phosphate ceramics in soft tissues, *Biomaterials.* 15 (1994) 31–34. [https://doi.org/10.1016/0142-9612\(94\)90193-7](https://doi.org/10.1016/0142-9612(94)90193-7).
- [110] S. Fujibayashi, M. Neo, H.M. Kim, T. Kokubo, T. Nakamura, Osteoinduction of porous bioactive titanium metal, *Biomaterials.* 25 (2004) 443–450. [https://doi.org/10.1016/S0142-9612\(03\)00551-9](https://doi.org/10.1016/S0142-9612(03)00551-9).
- [111] H. Yuan, Y. Li, J. De Bruijn, K. De Groot, X. Zhang, Tissue responses of calcium phosphate cement: a study in dogs, *Biomaterials.* 21 (2000) 1283–1290. [https://doi.org/10.1016/S0142-9612\(00\)00016-8](https://doi.org/10.1016/S0142-9612(00)00016-8).
- [112] R. Duan, D. Barbieri, F. De Groot, J.D. De Bruijn, H. Yuan, Modulating Bone Regeneration in Rabbit Condyle Defects with Three Surface-Structured Tricalcium Phosphate Ceramics, *ACS Biomater. Sci. Eng.* 4 (2018) 3347–3355. <https://doi.org/10.1021/acsbomaterials.8b00630>.
- [113] R. Duan, D. Barbieri, X. Luo, J. Weng, J.D. de Bruijn, H. Yuan, Submicron-surface structured tricalcium phosphate ceramic enhances the bone regeneration in canine spine environment, *J. Orthop. Res.* 34 (2016) 1865–1873. <https://doi.org/10.1002/jor.23201>.



- [114] H. Yuan, H. Fernandes, P. Habibovic, J. De Boer, A.M.C. Barradas, A. De Ruiter, W.R. Walsh, C.A. Van Blitterswijk, J.D. De Bruijn, Osteoinductive ceramics as a synthetic alternative to autologous bone grafting, *Proc. Natl. Acad. Sci. U. S. A.* 107 (2010) 13614–13619. <https://doi.org/10.1073/pnas.1003600107>.
- [115] X. Chen, M. Wang, F. Chen, J. Wang, X. Li, J. Liang, Y. Fan, Y. Xiao, X. Zhang, Correlations between macrophage polarization and osteoinduction of porous calcium phosphate ceramics, *Acta Biomater.* 103 (2020) 318–332. <https://doi.org/10.1016/j.actbio.2019.12.019>.
- [116] D. Zukic, J. Vicory, M. McCormick, L. Wisse, G. Gerig, P. Yushkevich, S. Aylward, N-D morphological contour interpolation, *Insight J.* 2016 Janua (2016) 1–8. <http://hdl.handle.net/10380/3563%0Ahttp://insight-journal.org/browse/publication/977>.
- [117] U. Ripamonti, L.C. Roden, C. Ferretti, R.M. Klar, Biomimetic matrices self-initiating the induction of bone formation, *J. Craniofac. Surg.* 22 (2011) 1859–1870. <https://doi.org/10.1097/SCS.0b013e31822e83fe>.
- [118] U. Ripamonti, L.N. Ramoshebi, T. Matsaba, J. Tasker, J. Crooks, J. Teare, Bone induction by BMPs/OPs and related family members in primates, *J. Bone Joint Surg. Am.* 83-A Suppl 1 (2001). <https://doi.org/10.2106/00004623-200100002-00006>.
- [119] U. Ripamonti, P.W. Richter, R.W.N. Nilen, L. Renton, The induction of bone formation by smart biphasic hydroxyapatite tricalcium phosphate biomimetic matrices in the non-human primate *Papio ursinus*, *J. Cell. Mol. Med.* 12 (2008) 2609–2621. <https://doi.org/10.1111/J.1582-4934.2008.00312.X>.
- [120] N.L. Davison, J. Su, H. Yuan, J.J.J.P. van den Beucken, J.D. de Bruijn, F.B. de Groot, Influence of surface microstructure and chemistry on osteoinduction and osteoclastogenesis by biphasic calcium phosphate discs, *Eur. Cells Mater.* 29 (2015) 314–329. <https://doi.org/10.22203/eCM.v029a24>.
- [121] G. Song, P. Habibovic, C. Bao, J. Hu, C.A. van Blitterswijk, H. Yuan, W. Chen, H.H.K. Xu, The homing of bone marrow MSCs to non-osseous sites for ectopic bone formation induced by osteoinductive calcium phosphate, *Biomaterials.* 34 (2013) 2167–2176. <https://doi.org/10.1016/j.biomaterials.2012.12.010>.
- [122] M.R. Urist, R.J. DeLange, G.A.M. Finerman, Bone cell differentiation and growth factors, *Science.* 220 (1983) 680–686. <https://doi.org/10.1126/SCIENCE.6403986>.
- [123] P. Habibovic, H. Yuan, C.M. Van Der Valk, G. Meijer, C.A. Van Blitterswijk, K. De Groot, 3D microenvironment as essential element for osteoinduction by biomaterials, *Biomaterials.* 26 (2005) 3565–3575. <https://doi.org/10.1016/j.biomaterials.2004.09.056>.
- [124] U. Ripamonti, Osteoinduction in porous hydroxyapatite implanted in heterotopic sites of different animal models, *Biomaterials.* 17 (1996) 31–35. [https://doi.org/10.1016/0142-9612\(96\)80752-6](https://doi.org/10.1016/0142-9612(96)80752-6).
- [125] M. Li, X. Guo, W. Qi, Z. Wu, J.D. De Bruijn, Y. Xiao, C. Bao, H. Yuan, Macrophage polarization plays roles in bone formation instructed by calcium phosphate ceramics, *J. Mater. Chem. B* 8 (2020) 1863–1877. <https://doi.org/10.1039/c9tb02932j>.

- [126] S.R. Radin, P. Ducheyne, The effect of calcium phosphate ceramic composition and structure on in vitro behavior. II. Precipitation, *J. Biomed. Mater. Res.* 27 (1993) 35–45. <https://doi.org/10.1002/JBM.820270106>.
- [127] Y.R. Duan, Z.R. Zhang, C.Y. Wang, J.Y. Chen, X.D. Zhang, Dynamic study of calcium phosphate formation on porous HA/TCP ceramics, *J. Mater. Sci. Mater. Med.* 16 (2005) 795–801. <https://doi.org/10.1007/s10856-005-3577-2>.
- [128] M. Heughebaert, R.Z. LeGeros, M. Gineste, A. Guilhem, G. Bonel, Physicochemical characterization of deposits associated with HA ceramics implanted in nonosseous sites, *J. Biomed. Mater. Res.* 22 (1988) 257–268. <https://doi.org/10.1002/jbm.820221406>.
- [129] M. Bohner, R.J. Miron, A proposed mechanism for material-induced heterotopic ossification, *Mater. Today.* 22 (2019) 132–141. <https://doi.org/10.1016/J.MATTOD.2018.10.036>.
- [130] T. Kokubo, H. Takadama, How useful is SBF in predicting in vivo bone bioactivity?, *Biomaterials.* 27 (2006) 2907–2915. <https://doi.org/10.1016/J.BIOMATERIALS.2006.01.017>.
- [131] A.A. Zadpoor, Relationship between in vitro apatite-forming ability measured using simulated body fluid and in vivo bioactivity of biomaterials, *Mater. Sci. Eng. C. Mater. Biol. Appl.* 35 (2014) 134–143. <https://doi.org/10.1016/J.MSEC.2013.10.026>.
- [132] Elliot J. C., *Structure and Chemistry of the Apatites and Other Calcium Orthophosphates*, 1st ed., Elsevier, Amsterdam, 1994. [https://books.google.com.mx/books?hl=es&lr=&id=dksXBQAAQBAJ&oi=fnd&pg=PP1&dq=Structure+and+chemistry+of+the+apatites+and+other+calcium+orthophosphates.+Studies+in+inorganic+chemistry&ots=xqNFMG\\_Pt2&sig=ISkXSk5wAus8VTnsyftTLZO\\_PMc#v=onepage&q=Structure and](https://books.google.com.mx/books?hl=es&lr=&id=dksXBQAAQBAJ&oi=fnd&pg=PP1&dq=Structure+and+chemistry+of+the+apatites+and+other+calcium+orthophosphates.+Studies+in+inorganic+chemistry&ots=xqNFMG_Pt2&sig=ISkXSk5wAus8VTnsyftTLZO_PMc#v=onepage&q=Structure and) (accessed May 29, 2022).
- [133] M. Kohri, K. Miki, D.E. Waite, H. Nakajima, T. Okabe, In vitro stability of biphasic calcium phosphate ceramics, *Biomaterials.* 14 (1993) 299–304. [https://doi.org/10.1016/0142-9612\(93\)90122-1](https://doi.org/10.1016/0142-9612(93)90122-1).
- [134] H.K. Koerten, J. Van Der Meulen, Degradation of calcium phosphate ceramics, (1999). [https://doi.org/10.1002/\(SICI\)1097-4636\(199901\)44:1](https://doi.org/10.1002/(SICI)1097-4636(199901)44:1).
- [135] R.G.T. Geesink, K. De Groot, C.P.A.T. Klein, Bonding of bone to apatite-coated implants, <https://doi.org/10.1302/0301-620X.70B1.2828374>. 70 (1988) 17–22. <https://doi.org/10.1302/0301-620X.70B1.2828374>.
- [136] T. Hanawa, Y. Kamiura, S. Yamamoto, T. Kohgo, A. Amemiya, H. Ukai, K. Murakami, K. Asaoka, Early bone formation around calcium-ion-implanted titanium inserted into rat tibia, (1997). [https://doi.org/10.1002/\(SICI\)1097-4636\(199707\)36:1](https://doi.org/10.1002/(SICI)1097-4636(199707)36:1).
- [137] R.G.T. Geesink, M.T. Manley, *Hydroxylapatite coatings in orthopaedic surgery*, Raven Press (ID), 1993.
- [138] J.C. Le Huec, D. Clément, B. Brouillaud, N. Barthe, B. Dupuy, B. Foliguet, B. Basse-Cathalinat, Evolution of the local calcium content around irradiated  $\beta$ -tricalcium phosphate ceramic implants: in vivo study in the rabbit, *Biomaterials.* 19 (1998) 733–738. [https://doi.org/10.1016/S0142-9612\(97\)00189-0](https://doi.org/10.1016/S0142-9612(97)00189-0).




- [139] G.D. Winter, B.J. Simpson, Heterotopic bone formed in a synthetic sponge in the skin of young pigs, *Nature*. 223 (1969) 88–90. <https://doi.org/10.1038/223088a0>.
- [140] S. Miyamoto, K. Takaoka, K. Ono, Bone induction in monkeys by bone morphogenetic protein: A trans-filter technique, *J. Bone Jt. Surg.–Ser. B*. 75 (1993) 107–110. <https://doi.org/10.1302/0301-620X.75B1.8421005>.
- [141] A. Marušić, V. Katavić, D. Grčević, I.K. Lukić, Genetic variability of new bone induction in mice, *Bone*. 25 (1999) 25–32. [https://doi.org/10.1016/S8756-3282\(99\)00095-2](https://doi.org/10.1016/S8756-3282(99)00095-2).
- [142] Y. Hou, W. Xie, L. Yu, L.C. Camacho, C. Nie, M. Zhang, R. Haag, Q. Wei, Surface Roughness Gradients Reveal Topography-Specific Mechanosensitive Responses in Human Mesenchymal Stem Cells, *Small*. 16 (2020). <https://doi.org/10.1002/SMLL.201905422>.
- [143] S. Mascharak, P.L. Benitez, A.C. Proctor, C.M. Madl, K.H. Hu, R.E. Dewi, M.J. Butte, S.C. Heilshorn, YAP-dependent mechanotransduction is required for proliferation and migration on native-like substrate topography, *Biomaterials*. 115 (2017) 155–166. <https://doi.org/10.1016/J.BIOMATERIALS.2016.11.019>.
- [144] D. Xiao, J. Zhang, C. Zhang, D. Barbieri, H. Yuan, L. Moroni, G. Feng, The role of calcium phosphate surface structure in osteogenesis and the mechanisms involved, *Acta Biomater.* 106 (2020) 22–33. <https://doi.org/10.1016/J.ACTBIO.2019.12.034>.
- [145] J. Zhang, L. Sun, X. Luo, D. Barbieri, J.D. de Bruijn, C.A. van Blitterswijk, L. Moroni, H. Yuan, Cells responding to surface structure of calcium phosphate ceramics for bone regeneration, *J. Tissue Eng. Regen. Med.* 11 (2017) 3273–3283. <https://doi.org/10.1002/TERM.2236>.
- [146] J. Zhang, M.T. Dalbay, X. Luo, E. Vrij, D. Barbieri, L. Moroni, J.D. de Bruijn, C.A. van Blitterswijk, J.P. Chapple, M.M. Knight, H. Yuan, Topography of calcium phosphate ceramics regulates primary cilia length and TGF receptor recruitment associated with osteogenesis, *Acta Biomater.* 57 (2017) 487–497. <https://doi.org/10.1016/j.actbio.2017.04.004>.
- [147] J. Zhang, X. Luo, D. Barbieri, A.M.C. Barradas, J.D. De Bruijn, C.A. Van Blitterswijk, H. Yuan, The size of surface microstructures as an osteogenic factor in calcium phosphate ceramics, *Acta Biomater.* 10 (2014) 3254–3263. <https://doi.org/10.1016/J.ACTBIO.2014.03.021>.
- [148] R.J. Miron, H. Zohdi, M. Fujioka-Kobayashi, D.D. Bosshardt, Giant cells around bone biomaterials: Osteoclasts or multi-nucleated giant cells?, *Acta Biomater.* 46 (2016) 15–28. <https://doi.org/10.1016/j.actbio.2016.09.029>.
- [149] T. Stessuk, J. Husch, I.A. Hermens, S. Hofmann, J.J. van den Beucken, Osteogenic differentiation driven by osteoclasts and macrophages, *J. Immunol. Regen. Med.* 12 (2021) 100044. <https://doi.org/10.1016/J.REGEN.2021.100044>.
- [150] N.L. Davison, A.L. Gamblin, P. Layrolle, H. Yuan, J.D. de Bruijn, F. Barrère-de Groot, Liposomal clodronate inhibition of osteoclastogenesis and osteoinduction by submicrostructured beta-tricalcium phosphate, *Biomaterials*. 35 (2014) 5088–5097. <https://doi.org/10.1016/j.biomaterials.2014.03.013>.
- [151] N.L. Davison, X. Luo, T. Schoenmaker, V. Everts, H. Yuan, F. Barrère-de Groot, J.D. de Bruijn, Submicron-scale surface architecture of tricalcium phosphate directs osteogenesis in vitro and in vivo, *Eur. Cells Mater.* 27 (2014) 281–297. <https://doi.org/10.22203/eCM.v027a20>.

- [152] N.L. Davison, B. ten Harkel, T. Schoenmaker, X. Luo, H. Yuan, V. Everts, F. Barrère-de Groot, J.D. de Bruijn, Osteoclast resorption of beta-tricalcium phosphate controlled by surface architecture, *Biomaterials*. 35 (2014) 7441–7451. <https://doi.org/10.1016/j.biomaterials.2014.05.048>.
- [153] C. Schlundt, H. Fischer, C.H. Bucher, C. Rendenbach, G.N. Duda, K. Schmidt-Bleek, The multifaceted roles of macrophages in bone regeneration: A story of polarization, activation and time, *Acta Biomater*. 133 (2021) 46–57. <https://doi.org/10.1016/J.ACTBIO.2021.04.052>.
- [154] H.Y. Dar, Z. Azam, R. Anupam, R.K. Mondal, R.K. Srivastava, Osteoimmunology: The Nexus between bone and immune system, *Front. Biosci. (Landmark Ed)*. 23 (2018) 464–492. <https://doi.org/10.2741/4600>.
- [155] T. Ono, H. Takayanagi, Osteoimmunology in Bone Fracture Healing, *Curr. Osteoporos. Rep.* 15 (2017) 367–375. <https://doi.org/10.1007/s11914-017-0381-0>.
- [156] J. Richardson, A.M. Hill, C.J.C. Johnston, A. McGregor, A.R. Norrish, D. Eastwood, C.B.D. Lavy, Fracture healing in HIV-positive populations, *J. Bone Jt. Surg.–Ser. B*. 90 (2008) 988–994. <https://doi.org/10.1302/0301-620X.90B8.20861>.
- [157] O. Bissinger, K. Kreutzer, C. Götz, A. Hapfelmeier, C. Pautke, S. Vogt, G. Wexel, K.D. Wolff, T. Tischer, P.M. Proding, A biomechanical, micro-computertomographic and histological analysis of the influence of diclofenac and prednisolone on fracture healing in vivo, *BMC Musculoskelet. Disord.* 17 (2016). <https://doi.org/10.1186/s12891-016-1241-2>.
- [158] K. Satoh, H. Mark, P. Zachrisson, B. Rydevik, G. Byröd, S.I. Kikuchi, S.I. Konno, M. Sekiguchi, Effect of methotrexate on fracture healing., *Fukushima J. Med. Sci.* 57 (2011) 11–18. <https://doi.org/10.5387/fms.57.11>.
- [159] J.M. Morais, F. Papadimitrakopoulos, D.J. Burgess, Biomaterials/tissue interactions: Possible solutions to overcome foreign body response, *AAPS J.* (2010). <https://doi.org/10.1208/s12248-010-9175-3>.
- [160] L. Chung, D.R. Maestas, F. Housseau, J.H. Elisseeff, Key players in the immune response to biomaterial scaffolds for regenerative medicine, *Adv. Drug Deliv. Rev.* (2017). <https://doi.org/10.1016/j.addr.2017.07.006>.
- [161] C. Zhang, M. Yang, A.C. Ericsson, Function of Macrophages in Disease: Current Understanding on Molecular Mechanisms, *Front. Immunol.* 12 (2021) 635. <https://doi.org/10.3389/FIMMU.2021.620510/BIBTEX>.
- [162] A. Viola, F. Munari, R. Sánchez-Rodríguez, T. Scolaro, A. Castegna, The metabolic signature of macrophage responses, *Front. Immunol.* 10 (2019) 1462. <https://doi.org/10.3389/FIMMU.2019.01462/BIBTEX>.
- [163] K. Kierdorf, M. Prinz, F. Geissmann, E. Gomez Perdiguero, Development and function of tissue resident macrophages in mice, *Semin. Immunol.* 27 (2015) 369. <https://doi.org/10.1016/J.SMIM.2016.03.017>.
- [164] C.D. Mills, K. Kincaid, J.M. Alt, M.J. Heilman, A.M. Hill, M-1/M-2 macrophages and the Th1/Th2 paradigm, *J. Immunol.* 164 (2000) 6166–6173. <https://doi.org/10.4049/JIMMUNOL.164.12.6166>.



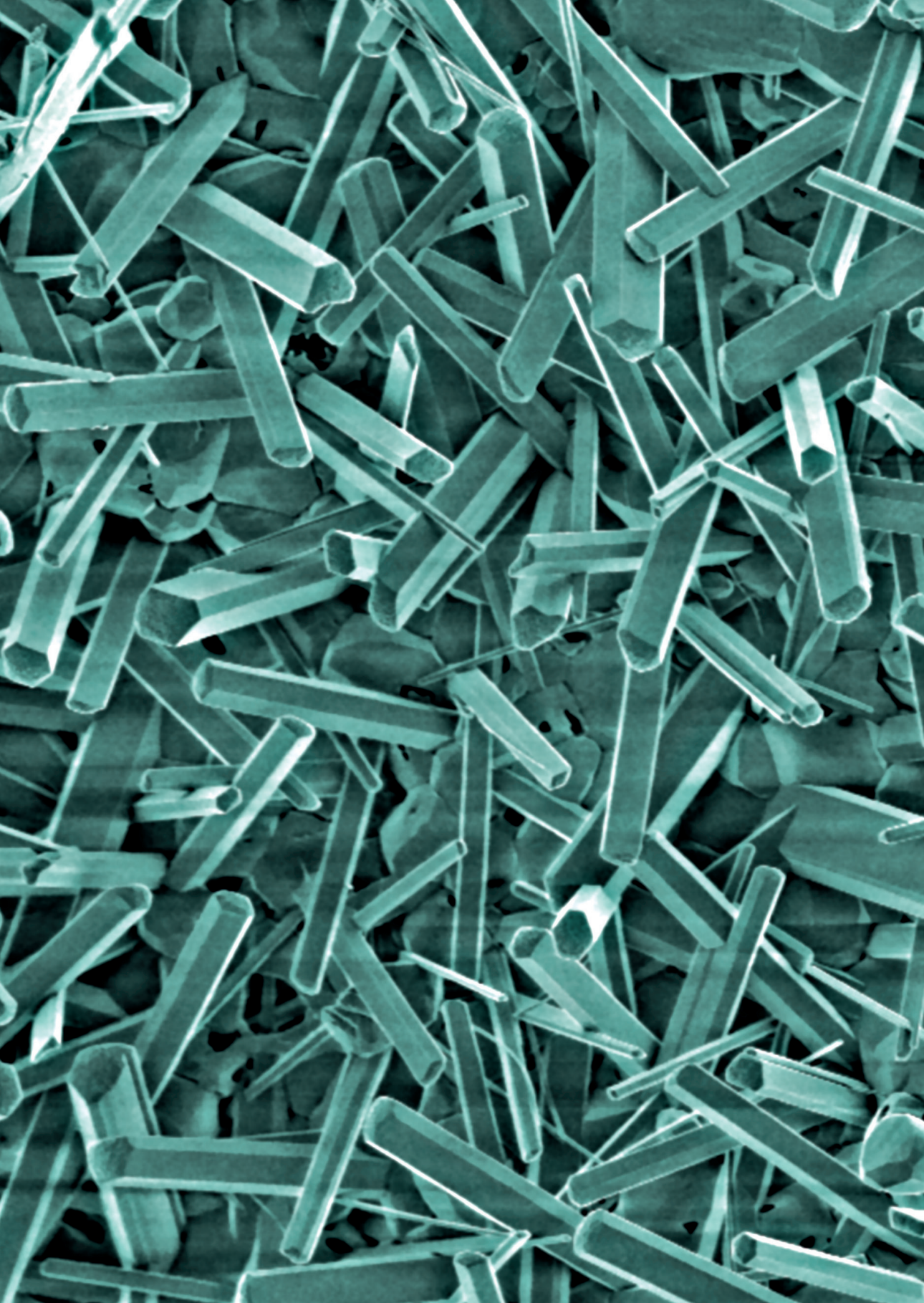
- [165] A. Mantovani, S.K. Biswas, M.R. Galdiero, A. Sica, M. Locati, Macrophage plasticity and polarization in tissue repair and remodelling, *J. Pathol.* (2013). <https://doi.org/10.1002/path.4133>.
- [166] F. Taraballi, M. Sushnitha, C. Tsao, G. Bauza, C. Liverani, A. Shi, E. Tasciotti, Biomimetic Tissue Engineering: Tuning the Immune and Inflammatory Response to Implantable Biomaterials, *Adv. Healthc. Mater.* (2018). <https://doi.org/10.1002/adhm.201800490>.
- [167] T.A. Wynn, K.M. Vannella, Macrophages in Tissue Repair, Regeneration, and Fibrosis, *Immunity.* 44 (2016) 450–462. <https://doi.org/10.1016/j.immuni.2016.02.015>.
- [168] K.A. Alexander, M.K. Chang, E.R. Maylin, T. Kohler, R. Müller, A.C. Wu, N. Van Rooijen, M.J. Sweet, D.A. Hume, L.J. Raggatt, A.R. Pettit, Osteal macrophages promote in vivo intramembranous bone healing in a mouse tibial injury model, *J. Bone Miner. Res.* (2011). <https://doi.org/10.1002/jbmr.354>.
- [169] L.J. Raggatt, M.E. Wulschleger, K.A. Alexander, A.C.K. Wu, S.M. Millard, S. Kaur, M.L. Maughan, L.S. Gregory, R. Steck, A.R. Pettit, Fracture healing via periosteal callus formation requires macrophages for both initiation and progression of early endochondral ossification, *Am. J. Pathol.* (2014). <https://doi.org/10.1016/j.ajpath.2014.08.017>.
- [170] J. Pajarinen, T. Lin, E. Gibon, Y. Kohno, M. Maruyama, K. Nathan, L. Lu, Z. Yao, S.B. Goodman, Mesenchymal stem cell-macrophage crosstalk and bone healing, *Biomaterials.* (2019). <https://doi.org/10.1016/j.biomaterials.2017.12.025>.
- [171] P. Humbert, M. Brennan, N. Davison, P. Rosset, V. Trichet, F. Blanchard, P. Layrolle, Immune modulation by transplanted calcium phosphate biomaterials and human mesenchymal stromal cells in bone regeneration, *Front. Immunol.* (2019). <https://doi.org/10.3389/fimmu.2019.00663>.
- [172] C. Schlundt, T. El Khassawna, A. Serra, A. Dienelt, S. Wendler, H. Schell, N. van Rooijen, A. Radbruch, R. Lucius, S. Hartmann, G.N. Duda, K. Schmidt-Bleek, Macrophages in bone fracture healing: Their essential role in endochondral ossification, *Bone.* 106 (2018) 78–89. <https://doi.org/10.1016/j.bone.2015.10.019>.
- [173] C. Dou, N. Ding, C. Zhao, T. Hou, F. Kang, Z. Cao, C. Liu, Y. Bai, Q. Dai, Q. Ma, F. Luo, J. Xu, S. Dong, Estrogen Deficiency–Mediated M2 Macrophage Osteoclastogenesis Contributes to M1/M2 Ratio Alteration in Ovariectomized Osteoporotic Mice, *J. Bone Miner. Res.* 33 (2018) 899–908. <https://doi.org/10.1002/jbmr.3364>.
- [174] D. He, X. Kou, R. Yang, D. Liu, X. Wang, Q. Luo, Y. Song, F. Liu, Y. Yan, Y. Gan, Y. Zhou, M1-like Macrophage Polarization Promotes Orthodontic Tooth Movement, *J. Dent. Res.* 94 (2015) 1286–1294. <https://doi.org/10.1177/0022034515589714>.
- [175] D. He, X. Kou, Q. Luo, R. Yang, D. Liu, X. Wang, Y. Song, H. Cao, M. Zeng, Y. Gan, Y. Zhou, Enhanced M1/M2 macrophage ratio promotes orthodontic root resorption, *J. Dent. Res.* 94 (2015) 129–139. <https://doi.org/10.1177/0022034514553817>.
- [176] A. Viniegra, H. Goldberg, Çil, N. Fine, Z. Sheikh, M. Galli, M. Freire, Y. Wang, T.E. Van Dyke, M. Glogauer, C. Sima, Resolving Macrophages Counter Osteolysis by Anabolic Actions on Bone Cells, *J. Dent. Res.* 97 (2018) 1160–1169. <https://doi.org/10.1177/0022034518777973>.



- 
- [177] F. Wehrhan, P. Moebius, K. Amann, J. Ries, R. Preidl, F.W. Neukam, M. Weber, Macrophage and osteoclast polarization in bisphosphonate associated necrosis and osteonecrosis, *J. Cranio-Maxillofacial Surg.* 45 (2017) 944–953. <https://doi.org/10.1016/j.jcms.2017.02.023>.
- [178] W. Zhu, R. Xu, J. Du, Y. Fu, S. Li, P. Zhang, L. Liu, H. Jiang, Zoledronic acid promotes TLR-4-mediated M1 macrophage polarization in bisphosphonate-related osteonecrosis of the jaw, *FASEB J.* 33 (2019) 5208–5219. <https://doi.org/10.1096/fj.201801791RR>.
- [179] S. Shi, Q. Zhang, I. Atsuta, S. Liu, C. Chen, S. Shi, A.D. Le, IL-17-mediated M1/M2 macrophage alteration contributes to pathogenesis of bisphosphonate-related osteonecrosis of the jaws, *Clin. Cancer Res.* 19 (2013) 3176–3188. <https://doi.org/10.1158/1078-0432.CCR-13-0042>.
- [180] J. Löffler, F.A. Sass, S. Filter, A. Rose, A. Ellinghaus, G.N. Duda, A. Dienelt, Compromised Bone Healing in Aged Rats Is Associated With Impaired M2 Macrophage Function, *Front. Immunol.* 10 (2019). <https://doi.org/10.3389/FIMMU.2019.02443>.
- [181] J. Zhang, H. Shi, N. Zhang, L. Hu, W. Jing, J. Pan, Interleukin-4-loaded hydrogel scaffold regulates macrophages polarization to promote bone mesenchymal stem cells osteogenic differentiation via TGF- $\beta$ 1/Smad pathway for repair of bone defect, *Cell Prolif.* (2020). <https://doi.org/10.1111/cpr.12907>.
- [182] Z. wei Zheng, Y. hong Chen, D. yu Wu, J. bing Wang, M. ming Lv, X. song Wang, J. Sun, Z.Y. Zhang, Development of an accurate and proactive immunomodulatory strategy to improve bone substitute material-mediated osteogenesis and angiogenesis, *Theranostics.* 8 (2018) 5482–5500. <https://doi.org/10.7150/thno.28315>.
- [183] D. Hachim, S.T. LoPresti, C.C. Yates, B.N. Brown, Shifts in macrophage phenotype at the biomaterial interface via IL-4 eluting coatings are associated with improved implant integration, *Biomaterials.* (2017). <https://doi.org/10.1016/j.biomaterials.2016.10.019>.
- [184] D.W. Zhao, K.Q. Zuo, K. Wang, Z.Y. Sun, Y.P. Lu, L. Cheng, G.Y. Xiao, C. Liu, Interleukin-4 assisted calcium-strontium-zinc-phosphate coating induces controllable macrophage polarization and promotes osseointegration on titanium implant, *Mater. Sci. Eng. C.* (2021). <https://doi.org/10.1016/j.msec.2020.111512>.
- [185] I.M. Castaño, R.M. Raftery, G. Chen, B. Cavanagh, B. Quinn, G.P. Duffy, F.J. O'Brien, C.M. Curtin, Rapid bone repair with the recruitment of CD206+M2-like macrophages using non-viral scaffold-mediated miR-133a inhibition of host cells, *Acta Biomater.* (2020). <https://doi.org/10.1016/j.actbio.2020.03.042>.
- [186] O.R. Mahon, D.C. Browe, T. Gonzalez-Fernandez, P. Pitacco, I.T. Whelan, S. Von Euw, C. Hobbs, V. Nicolosi, K.T. Cunningham, K.H.G. Mills, D.J. Kelly, A. Dunne, Nano-particle mediated M2 macrophage polarization enhances bone formation and MSC osteogenesis in an IL-10 dependent manner, *Biomaterials.* 239 (2020) 119833. <https://doi.org/10.1016/j.biomaterials.2020.119833>.
- [187] M.R. Convente, S.A. Chakkalakal, E.J. Yang, R.J. Caron, D. Zhang, T. Kambayashi, F.S. Kaplan, E.M. Shore, Reply to: Macrophages Driving Heterotopic Ossification: Convergence of Genetically-Driven and Trauma-Driven Mechanisms, *J. Bone Miner. Res.* 33 (2018) 367–368. <https://doi.org/10.1002/JBMR.3349>.

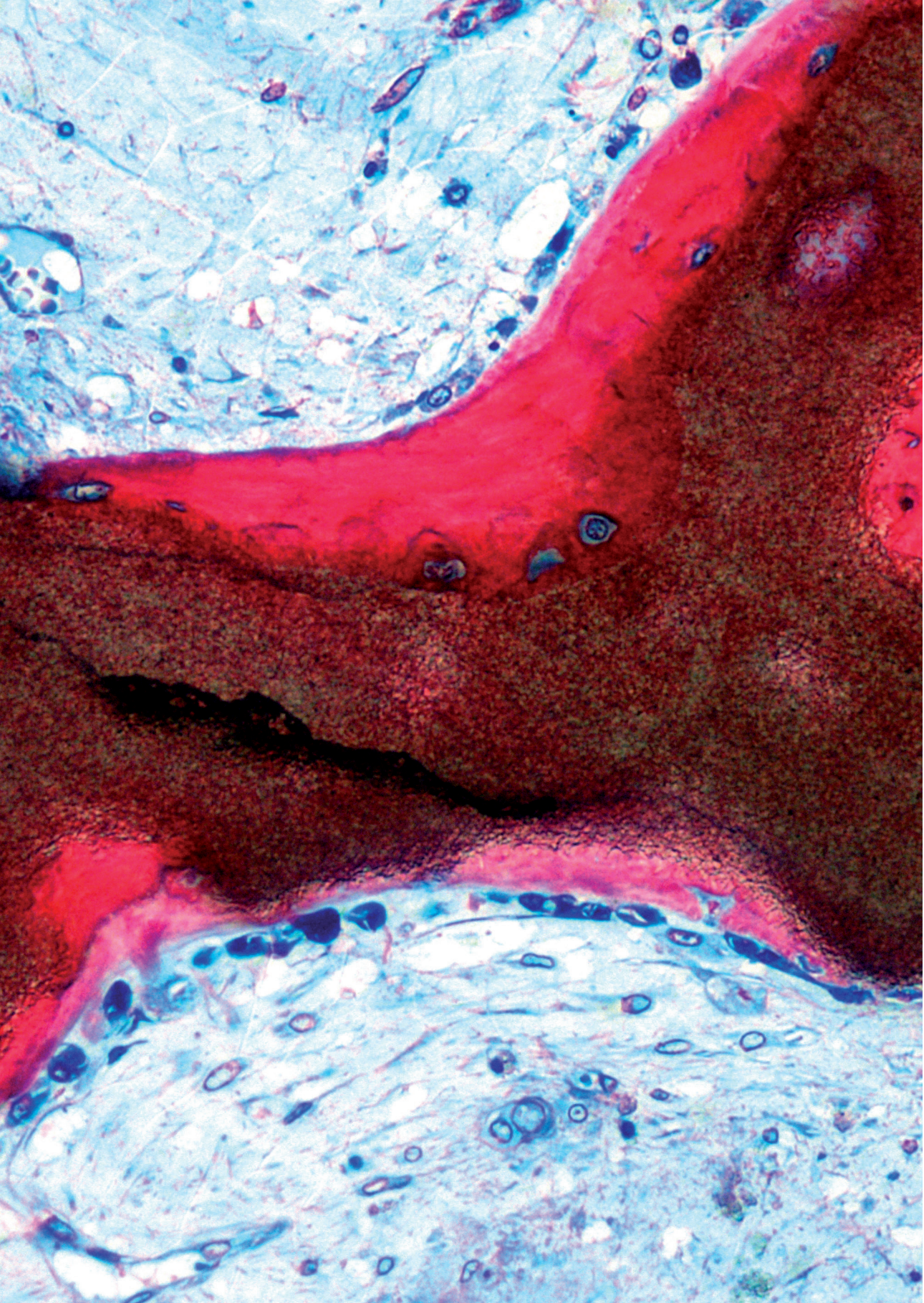
- [188] M.R. Convente, S.A. Chakkalakal, E.J. Yang, R.J. Caron, D. Zhang, T. Kambayashi, F.S. Kaplan, E.M. Shore, Depletion of Mast Cells and Macrophages Impairs Heterotopic Ossification in an Acvr1R206H Mouse Model of Fibrodysplasia Ossificans Progressiva, *J. Bone Miner. Res.* 33 (2018) 269–282. <https://doi.org/10.1002/jbmr.3304>.
- [189] J.P. Levesque, N.A. Sims, A.R. Pettit, K.A. Alexander, H.W. Tseng, F. Torossian, F. Genêt, J.J. Lataillade, M.C. Le Bousse-Kerdilès, Macrophages Driving Heterotopic Ossification: Convergence of Genetically-Driven and Trauma-Driven Mechanisms, *J. Bone Miner. Res.* 33 (2018) 365–366. <https://doi.org/10.1002/JBMR.3346>.
- [190] E. Olmsted-Davis, J. Mejia, E. Salisbury, Z. Gugala, A.R. Davis, A Population of M2 Macrophages Associated With Bone Formation, *Front. Immunol.* 12 (2021). <https://doi.org/10.3389/FIMMU.2021.686769>.
- [191] K.N. Bailey, B.D. Furman, J. Zeitlin, K.A. Kimmerling, C.L. Wu, F. Guilak, S.A. Olson, Intra-articular depletion of macrophages increases acute synovitis and alters macrophage polarity in the injured mouse knee, *Osteoarthr. Cartil.* 28 (2020) 626–638. <https://doi.org/10.1016/j.joca.2020.01.015>.
- [192] J.E. Bader, R.T. Enos, K.T. Velázquez, M.S. Carson, M. Nagarkatti, P.S. Nagarkatti, I. Chatzistamou, J.M. Davis, J.A. Carson, C.M. Robinson, E.A. Murphy, Macrophage depletion using clodronate liposomes decreases tumorigenesis and alters gut microbiota in the AOM/DSS mouse model of colon cancer, *Am. J. Physiol.-Gastrointest. Liver Physiol.* 314 (2018) G22–G31. <https://doi.org/10.1152/ajpgi.00229.2017>.
- [193] X. Li, G. Mu, C. Song, L. Zhou, L. He, Q. Jin, Z. Lu, Role of M2 macrophages in sepsis-induced acute kidney injury, *Shock.* 50 (2018) 233–239. <https://doi.org/10.1097/SHK.0000000000001006>.





# PART I

**IMPROVING THE SURFACE  
TOPOGRAPHY OF CALCIUM  
PHOSPHATES TO ENHANCE THEIR  
OSTEOINDUCTIVE POTENTIAL**



# CHAPTER 2

## ACCELERATED BONE FORMATION BY BIPHASIC CALCIUM PHOSPHATE WITH A NOVEL SUB- MICRON SURFACE TOPOGRAPHY

---

Rongquan Duan  
Lukas A. van Dijk  
Davide Barbieri  
Florence de Groot  
Huipin Yuan  
Joost D. de Bruijn

*European Cells & Materials, 2019, 37:60-73*

# ABSTRACT

Osteoinductive calcium phosphate (CaP) bone grafts have been shown to have equivalent performance to autograft in repairing critical-sized bone defects. The osteoinductive potential of CaP has been linked to the size of surface topographical features. We performed a study in which two novel biphasic calcium phosphate (BCP) bone grafts were synthesized with either submicron (BCP<sub><μm</sub>) or micron-scale (BCP<sub>μm</sub>) needle-shaped surface topography and compared to dimensionally similar tricalcium phosphate with grain-shaped surface structures (TCP<sub><μm</sub> and TCP<sub>μm</sub>). To clarify the possible function of surface morphology (needle-like vs. grain-like) in initiating bone formation, the four CaP test materials were physicochemically characterized and implanted in the dorsal muscle of beagles for 12 weeks. The submicron needle-shaped topography of BCP<sub><μm</sub> triggered earlier bone formation (3 - 6 weeks) compared to the grain-shaped surface topography of TCP<sub><μm</sub> which formed bone at 6 - 9 weeks. After 12 weeks, the amount of induced bone formation in both materials was equivalent based on histomorphometry. The micron-sized needle-shaped surface topography of BCP<sub>μm</sub> led to limited formation of new bone tissue, whereas its counterpart, TCP<sub>μm</sub> with grain-shaped surface topography, failed to trigger *de novo* bone formation. We found that the relative strength of effect on CaP-driven bone induction is as follows: surface feature size > surface feature morphology > substrate chemistry. BCP materials with needle-shaped submicron surface topography gave rise to accelerated bone formation and a slower rate of resorption than a comparable TCP in this intramuscular implantation model. These characteristics may translate to improved bone healing in orthotopic defects.



## 1. INTRODUCTION

---

Owing to their similarity to the inorganic component of bone, their bioactivity, biocompatibility and osteoconductivity, calcium phosphate (CaP) materials are used clinically as bone void fillers[1,2]. However, because they have historically lacked osteoinductivity, their efficacy has been perceived as being lower than that of the gold standard bone graft, autologous bone, in repairing critical-sized bone defects[3,4].

Unless osteogenic agents were added to the graft material pre-implantation, osteoinduction of CaP bone grafts on their own was not reported until the beginning of the 1990s. Since then, initiation of bone formation by various CaP bone grafts with specific physicochemical properties has been observed in studies of non-skeletal defect sites (e.g. subcutis and muscle) [5–8].

Studies comparing osteoinductive versus non-osteoinductive CaP in orthotopic skeletal sites have demonstrated the benefits of osteoinductivity in bone regeneration [9]. Osteoinductive CaP bone grafts not only trigger ectopic bone formation, but also enhance orthotopic bone formation via inducing osteogenic differentiation of mesenchymal stem cells (MSCs) [10]. One such osteoinductive CaP bone graft substitute has been shown to have equivalent performance to autograft, considered the gold standard bone graft, in repairing critical-sized bone defects [11]. Having now established a link between osteoinductivity and bone-forming potential in orthotopic sites, researchers are focused on developing osteoinductive CaP bone grafts that can trigger high quality bone formation as early as possible after implantation.

It has been proven that osteoinduction by CaP bone grafts is material-dependent, and the osteoinductive potential varies with their physicochemical properties [12,13], such as chemistry (i.e. the ratio HA/ TCP) [14], microporosity (i.e. the volume percentage of pores < 10  $\mu\text{m}$  in the material) [15,16], surface architecture and geometry [17–19]. Among them, the presence of a microporous structure has been shown as essential. For example, one study demonstrated that microporous hydroxyapatite (HA) induced ectopic bone formation, while a non-microporous HA did not [20]. Furthermore, it has been shown that reducing the size of features on a microporous surface is critical to endowing CaP materials with osteoinductive properties. For instance, submicron scale surface structured TCP could induce ectopic bone formation, while an equivalent but micron scale surface structured alternative failed [18,21]. The influence of surface feature size was also seen in biphasic calcium phosphates (BCP), where materials with smaller grain crystals initiated ectopic bone formation, while materials with larger structures did not[19,22]. This research

confirms that the size of surface features plays an important role in initiating bone formation by CaP materials in ectopic defect sites.

Nowadays, there is still limited knowledge regarding the molecular mechanism underlying surface topography induced differentiation of MSCs. It has been reported that geometrical features can enhance the actomyosin contractility and facilitate osteogenesis via enhancement of c-Jun N-terminal kinase and with the activation of the extracellular related kinase in conjunction with elevated wingless-type (Wnt) signaling [23]. Furthermore, Zhang et al. reported that the surface topography of CaPs can tune MSCs with respect to morphology, primary cilia length and TGF $\beta$ R recruitment to the cilium, all of which have been associated with osteogenic differentiation *in vitro* and bone formation *in vivo* [24].

Next to the size of features on the surface structure, the morphology is another characterization of surface topography which has been reported to evoke specific cellular responses *in vitro* [25–29]. For example, Kolhar et al. found that rod-shaped nanoparticles had higher affinity with endothelial cells in *in vitro* and *in vivo* experiments compared with their spherical counterparts [25]. Similarly, Agarwal et al. reported that elongated nanoparticles exhibited higher efficiency for the adhesion of cells and facilitated the multivalent interaction between cells and surface, compared to spherical nanoparticles [26]. Dasgupta and co-workers observed that the elongated particles with higher aspect ratio had extensive cellular uptake compared to spherical particles with the average diameter [27]. Furthermore, *In vitro* studies have indicated that surface morphology changes modulate adhesion, cytokine release, and gene expression of osteogenic cells [28,29]. Based on the data above, we hypothesize that, besides the surface feature size, the morphology of the surface structure may play a crucial role in triggering bone formation in CaP materials.

We investigated the relative influence of surface feature size, surface morphology and substrate chemistry on osteoinductivity of CaP bone grafts by employing a hydrothermal treatment to obtain two needle-shaped surface structures on BCP at submicron and micron scale, and by comparing their *in vivo* bone-forming potential to submicron and micron grain-shaped TCP counterparts.

## 2. MATERIALS AND METHODS

### 2.1. Engineering the surface morphology

Submicron grain-like-surface-structured osteoinductive CaP (TCP<sub><sub>μm</sub></sub>, positive control) and micron grain-like-surface-structured non-osteoinductive CaP (TCP<sub>μm</sub>, negative control) were prepared in granular format (1 - 2 mm) as previously described.

The two novel CaP materials were manufactured by Kuros Biosciences B.V. (the Netherlands). Briefly, BCP powder was synthesized using a wet precipitation of apatite powder, followed by foaming with H<sub>2</sub>O<sub>2</sub> (1 % in distilled water, Merck, Darmstadt, Germany), and sintering at either 1125 °C or 1200 °C for 6 h respectively to obtain BCP plaques. After crushing the plaques and sieving, BCP granules (1 - 2 mm) were then prepared and autoclaved at 135 °C for 99 min to form novel CaP materials with either submicron (BCP<sub><sub>μm</sub></sub>) or micron scale (BCP<sub>μm</sub>) surface topography. All materials were sterilized with gamma irradiation (dose 25 - 40 kGy, Isotron Nederland B.V., Ede, the Netherlands) prior to use.

### 2.2. Physicochemical characterization of CaP materials

The chemical composition of the CaP materials (n=1 per material) was identified by X-ray diffraction (XRD; Miniflex II, Rigaku, Tokyo, Japan) using a scanning range of 25 - 45 deg., step size of 0.01 deg., and a scanning rate of 1 deg. per min. The amount of HA phase was determined by using an internal calibration system.

The surface structure of the CaP materials was analyzed with scanning electron microscope (SEM; JEOL JSM-5600, JEOL Ltd, Tokyo, Japan). The surface grain size (i.e. the vertical length crossing the center of each grain) and the shortest axis of the needles were measured with AxioVision LE (Carl Zeiss MicroImaging, Inc., Breda, the Netherlands) for at least 100 random grains or needles visualized from 10 SEM images (magnification: 5000×).

The microporosity and the specific surface area were determined with mercury intrusion porosimetry (n=1 per material; Micromeritics Autopore 9600 Mercury Porosimeter, Norcross, USA) with a mercury temperature of 18.36 °C, and Hg contact angle of (I) 130.00°, (E) 130.00°.

### 2.3. In vitro assay: dissolution rate

Calcium ion release was evaluated by soaking 0.5 mL of CaP granules (n=5 per material) in 100 mL of simulated physiological saline (SPS; 0.8 % NaCl, 50 mM HEPES, 0.4 mM NaN<sub>3</sub>; 37 °C; pH = 7.3) solution for 200 min. While carefully stirring at 150 rpm to avoid the contact between the stirring bar and granules, the calcium ion concentration in SPS was recorded every minute using a calcium electrode (Metrohm, Herisau, Switzerland).

## 2.4. In vitro assay: protein adsorption

Protein adsorption was measured for two types of protein solutions. Sterile CaP granules (0.2 mL, n = 5 per material) were added to 2 mL of 1 % vol. fetal bovine serum (FBS) solution or 2 mL of 400 µg/mL bovine serum albumin (BSA) solution at 37 °C and 5 % CO<sub>2</sub> for 1 week. Protein adsorption was measured after 12 h, 1, 4 and 7 d using a micro BCA assay kit (Micro BCA Protein Assay Kit, Thermo Scientific, Rockford, IL) and a spectrophotometer with an absorbance filter of 595 nm. The amount of proteins adsorbed by the samples (expressed in mg/mL for FBS, and in µg/mL for BSA) was estimated via internal calibration protein curves and was then reported per 1 mL which corresponds to the volume of material implanted *in vivo*.

## 2.5. In vivo assay: intramuscular implantation

All surgeries were performed following ethical approval by the local animal care committee (i.e. the management committee of experimental animals of Sichuan province, China) and in accordance with the local laws and institutional guidelines. To evaluate their osteoinductive potential, the four CaP materials (n = 8 for each group) were implanted in the dorsal muscles of healthy beagles (n = 8, 2 - 4 years, 10 - 15 kg), for 12 weeks as described previously [9,18]. Briefly, under general anesthesia by intravenous injection of sodium pentobarbital (30 mg/kg body weight) and in sterile conditions, 1 mL of each test group was implanted into paraspinal muscle pockets created by blunt dissection. The pockets were kept isolated from each other to prevent contact between the samples. Subsequently, the muscle wound was closed with non-resorbable sutures and the skin incisions were closed layer by layer. Following the surgeries, buprenorphine (0.1 mg per animal) was injected intramuscularly for 2 d to relieve pain, while penicillin (40 mg/kg) was injected intramuscularly for 3 consecutive days to prevent infection. Animals were allowed to undertake full activity and received a normal diet immediately after surgery. To determine the time of onset for bone formation, we utilized three fluorescent histological labels to indicate osteogenesis at: 1 - 3 weeks (calcein; green staining); 3 - 6 weeks (xylenol orange; red staining), and 6 - 9 weeks (tetracycline; yellow staining). Fluorochromes were intravenously injected at 3 weeks (calcein, Sigma, Louis, USA, 5 mg/mL 2% NaHCO<sub>3</sub> solution, pH=7.41, injection volume: 2 mL/kg body mass), 6 weeks (xylenol orange, Sigma, 50 mg/mL 1% NaHCO<sub>3</sub> solution, pH=7.38, injection volume: 2 mL/kg body mass) and 9 weeks (tetracycline, Sigma, 10 mg/mL 0.9% NaCl solution, pH=7.41, injection volume: 2 mL/kg body mass) after implantation.

## 2.7. In vivo assay: implants harvest and histological processing

Twelve weeks after implantation, animals were sacrificed by intravenous injection of an excessive dose of sodium pentobarbital and the implants were harvested with their surrounding soft tissue, trimmed and then fixed in 4 % buffered formaldehyde solution (pH = 7.4) at 4 °C for at least 1 week. Following fixation, the samples were dehydrated using a

series of gradient ethanol solutions and embedded in methyl methacrylate (MMA, K-plast, LTI, Bilthoven, the Netherlands). Consecutive histological sections (10 - 20  $\mu\text{m}$ ) of non-decalcified samples were obtained by sectioning the whole samples using a diamond saw blade microtome (SP-1600, Leica, Wetzlar, Germany). The sections were alternately not stained and stained with 1 % methylene blue (Sigma-Aldrich, Louis, USA) and 0.3 % basic fuchsin (Sigma-Aldrich) after etching with acidic ethanol (Merck, Darmstadt, Germany). The stained sections were analyzed with light microscopy (Nikon Eclipse E200, Tokyo, Japan) and histomorphometry. Non-stained sections were used for fluorescence microscopy using a FITC Texas Red filter (Nikon, Tokyo, Japan) at bandpass mirror wavelengths of 510 - 555 nm and 585 - 665 nm.

## 2.8. In vivo assay: histology and histomorphometry

Stained histological sections were scanned with a slide scanner (Dimage Scan Elite 5400II, Konica Minolta Photo Imaging Inc, Tokyo, Japan) to obtain overview images for histomorphometric analysis (i.e. the area percentage of *de novo* bone formation and residual material). The amount of multinucleated osteoclast-like cells was counted from 40 randomly selected histological images (magnification 20 $\times$ ) and expressed as number of cells per  $\text{mm}^2$ . Histomorphometric analysis was performed using Adobe Photoshop Elements 4.0 software (CS5, v12, Adobe Systems Benelux BV, Amsterdam-Zuidoost, the Netherlands) as follows. First, the area encompassing the whole sample was selected as a region of interest and the corresponding number of pixels was read as ROI. Then the bone tissue and residual material areas were pseudo-colored, and their respective pixels were counted as B and Me respectively. The percentage of bone in the available space was determined as  $B \% = B * 100 / (\text{ROI} - \text{Me})$ , while the percentage of residual material was calculated as  $\text{Me} \% = \text{Me} * 100 / \text{ROI}$ . The percent area of material resorbed (M %) was calculated as  $M \% = (\text{M}_0 - \text{Me}) * 100 / \text{M}_0$ , where  $\text{M}_0$  was the mean pixel area of similarly embedded, sectioned, and pseudo-colored materials (1 mL, n = 8) that had not been implanted.

Unstained histological sections were observed using fluorescence microscopy (Nikon Eclipse E600, Japan; camera Nikon FDX-35) to determine the time of onset of bone formation and material biomineralization. The incidence (for total animals operated) of three fluorescent labels in the explants was recorded, while the number of xylenol orange staining spots (6 weeks, red color) in the samples was counted. A quantitative index ( $X_{\text{fluor}}$ ), which indicates early bone formation (< 6 weeks), was calculated as the ratio between the total spots counted in all animals and the incidence of fluorescent labels.

## 2.9. Statistical analysis

Normality of the data was assessed using the Shapiro-Wilk test ( $p > 0.05$  for normally distributed data), and statistical comparisons were carried out by one-way ANOVA and

Tukey's post hoc tests, where a p-value smaller than 0.05 was considered statistically significant.

### 3. RESULTS

#### 3.1. Physicochemical characterization of materials

X-ray diffraction analysis confirmed that the two novel CaP materials were BCP (i.e. BCP<sub><math>\lt; \mu\text{m}</math>: 25 % HA/ 75 % TCP, BCP<sub>: 22 % HA/ 78 % TCP), while both the positive and the negative controls were pure  $\beta$ -TCP (Fig. 1a and Table 1).</sub></sub>

SEM imaging revealed that the two novel CaP materials had either submicron (median, 0.60  $\mu\text{m}$ ) or micron-scale needles (median, 1.52  $\mu\text{m}$ ) on their surface, comprising an epitaxial polygon surface structure. Both TCP<sub><math>\lt; \mu\text{m}</math></sub> and TCP <sub>possessed grain-shaped surface features, at the submicron scale for TCP<sub><math>\lt; \mu\text{m}</math></sub> (median, 0.70  $\mu\text{m}$ ) and micron-scale for TCP <sub>(median, 1.96  $\mu\text{m}$ ) (Fig. 1b, 1c and Table 1).</sub></sub>

Mercury intrusion porosimetry indicated that BCP<sub><math>\lt; \mu\text{m}</math></sub> and BCP <sub>had lower microporosity (9.0 % and 5.1 % respectively), compared to TCP<sub><math>\lt; \mu\text{m}</math></sub> and TCP <sub>(22.0% and 23.0 % respectively). By volume, TCP<sub><math>\lt; \mu\text{m}</math></sub> had a slightly larger surface area (2.02 m<sup>2</sup>/mL) than BCP<sub><math>\lt; \mu\text{m}</math></sub> (1.78 m<sup>2</sup>/mL), followed by TCP <sub>(0.72 m<sup>2</sup>/mL) and BCP <sub>(0.65 m<sup>2</sup>/mL) (Table 1).</sub></sub></sub></sub>

**Table 1. Physicochemical properties of the calcium phosphate ceramic implants.** <sup>a</sup> as determined by X-ray diffractometry; <sup>b</sup> as determined by quantitative measurements on scanning microscopic images (5000 $\times$ ); <sup>c</sup> as determined by mercury intrusion.

Materials	BCP <sub>&lt;math&gt;\lt; \mu\text{m}&lt;/math&gt;</sub>	TCP <sub>&lt;math&gt;\lt; \mu\text{m}&lt;/math&gt;</sub>	BCP <sub><math&gt;\mu\text{m}&lt; math&gt;<="" sub=""></math&gt;\mu\text{m}&lt;></sub>	TCP <sub><math&gt;\mu\text{m}&lt; math&gt;<="" sub=""></math&gt;\mu\text{m}&lt;></sub>	
Chemistry <sup>a</sup>	25 % HA/ 75 % TCP	0 % HA/ 100 % TCP	22 % HA/ 78 % TCP	0 % HA/ 100 % TCP	
Grain/needle size ( $\mu\text{m}$ ) <sup>b</sup>	0.33-0.90 Median 0.60	0.10-1.20 Median 0.70	1.01-2.28 Median 1.52	1.30-2.45 Median 1.96	
Microporosity (< 10 $\mu\text{m}$ ) <sup>c</sup>	9.0 %	22.0 %	5.1 %	23.0 %	
Specific surface area	by weight (m <sup>2</sup> /g) <sup>c</sup>	2.77	1.71	1.21	0.79
	by volume (m <sup>2</sup> /mL) <sup>c</sup>	1.78	2.02	0.65	0.72
Ca <sup>2+</sup> ion released (ppm, after 200 min)	9.5 $\pm$ 0.8	18.0 $\pm$ 1.8	5.2 $\pm$ 0.9	11.1 $\pm$ 1.7	
Proteins adsorbed after 7 d	BSA ( $\mu\text{g}/\text{mL}$ )	1722.9 $\pm$ 104.5	1796.5 $\pm$ 172.7	786.3 $\pm$ 48.1	920.5 $\pm$ 62.5
	FBS (mg/mL)	114.9 $\pm$ 3.7	127.6 $\pm$ 7.2	49.8 $\pm$ 4.1	60.6 $\pm$ 3.9



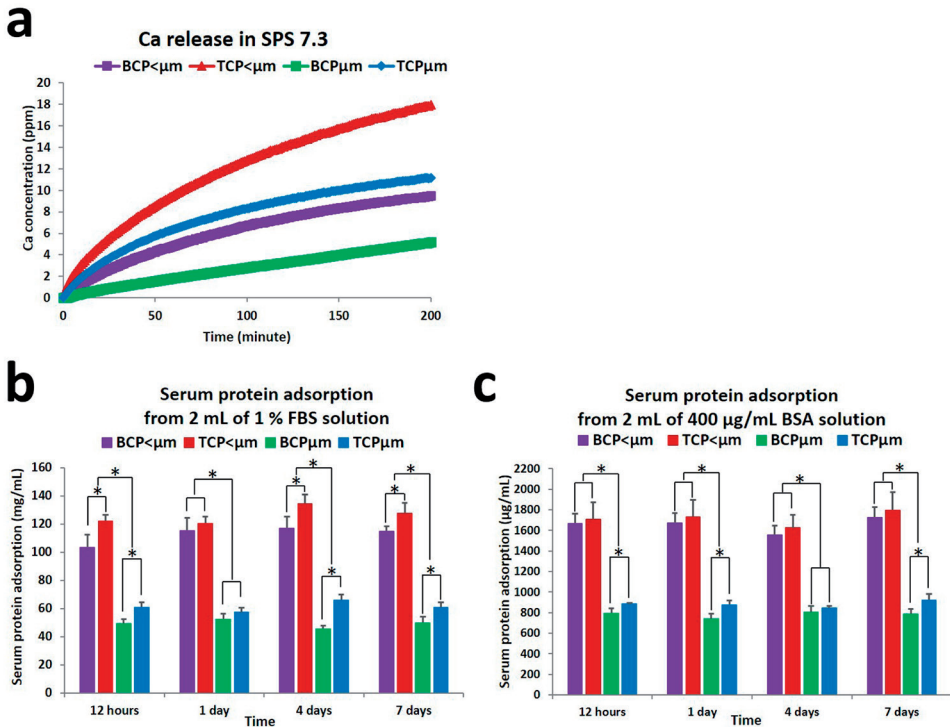


**Fig. 2.** a: calcium ion release from the materials into SPS over 200 min; b, c: percentage of proteins adsorbed from 2 ml 1 % FBS and 2 ml of 200 μg BSA ml<sup>-1</sup> solution onto 0.2 cc CaP granules for up to 7 d (\*  $p < 0.05$ ).

### 3.3. In vitro assays: protein adsorption

As shown in Fig. 2b and 2c, BCP<sub><math>\mu\text{m}</math></sub> and TCP<sub><math>\mu\text{m}</math></sub> adsorbed similar amount of proteins from BSA but TCP<sub><math>\mu\text{m}</math></sub> absorbed more protein from FBS. Both TCP<sub><math>\mu\text{m}</math></sub> and BCP<sub><math>\mu\text{m}</math></sub> absorbed significantly less protein from BSA and FBS than their submicron counterpart test materials (Table 1).

### 3.4. Histology and histomorphometry

After 12 weeks intramuscular implantation, all explants were encapsulated by a thin layer of connective tissue which was also infiltrated into the CaP materials. *De novo* bone formation was observed in 8 out of 8 BCP<sub><math>\mu\text{m}</math></sub> and TCP<sub><math>\mu\text{m}</math></sub> (positive control) explants, 7 out of 8 BCP<sub><math>\mu\text{m}</math></sub> explants and 0 out of 8 TCP<sub><math>\mu\text{m}</math></sub> (negative control) explants (Fig. 3a, Table 2). As shown in the detailed histological images (Fig. 3b, 3c), osteoid with a seam of cuboidal osteoblasts lying on its outer surface as well as osteocytes entrapped in lacunae of lamellar and woven bone were clearly observed in BCP<sub><math>\mu\text{m}</math></sub>, TCP<sub><math>\mu\text{m}</math></sub> and BCP<sub><math>\mu\text{m}</math></sub> explants. In addition, multinucleated osteoclast-like cells phagocytizing small fragments of CaP were localized on the surface of the test CaP material for BCP<sub><math>\mu\text{m}</math></sub> ( $22 \pm 7$  cells/mm<sup>2</sup>) and TCP<sub><math>\mu\text{m}</math></sub> ( $14 \pm 6$





**Table 2. A summary of the explants from muscle of beagles after 12 weeks.**

Explants		BCP <sub>&lt;μm</sub>	TCP <sub>&lt;μm</sub>	BCP <sub>μm</sub>	TCP <sub>μm</sub>
<b>3 weeks (green color)</b>	Calcein incidence	8/8	8/8	8/8	0/8
	Xylenol orange incidence	5/8	2/8	0/8	0/8
<b>6 weeks (red color)</b>	Σ(spots)	21	2	0	0
	Xfluor	4.2	1.0	0	0
<b>9 weeks (yellow color)</b>	Tetracycline incidence	8/8	8/8	0/8	0/8
	Bone incidence	8/8	8/8	7/8	0/8
<b>12 weeks</b>	Bone area in available space (B %)	24.5 ± 4.3	23.9 ± 6.3	2.1 ± 1.7	0
	Material resorption (%)	28.1 ± 4.1	53.8 ± 5.7	9.3 ± 2.4	4.7 ± 2.1

Looser connective tissue, with very limited presence of blood vessels, was detected in TCP<sub>μm</sub>.

Under the fluorescent microscopy (Fig. 5, Table 2), xylenol orange was detected in 5 out of 8 BCP<sub><μm</sub> and in 2 out of 8 of TCP<sub><μm</sub> explants. Calcein and tetracycline were observed in all the BCP<sub><μm</sub> and TCP<sub><μm</sub> explants. Only calcein was found in BCP<sub>μm</sub> explants, and no fluorescent signal was seen in any of the TCP<sub>μm</sub> explants. Xylenol orange was detected in the bone inside the BCP<sub><μm</sub> implants, indicating that the marked bone formed between 3- and 6-weeks post-implantation. Whereas, tetracycline was the predominant fluorophore observed in the bone formed in TCP<sub><μm</sub>, revealing that it formed between 6 and 9 weeks. No xylenol orange or tetracycline fluorophores were detected in BCP<sub>μm</sub>, indicating that any bone found in these defects was formed after 9 weeks post-implantation. These qualitative observations were corroborated by the quantitative data. In fact, the  $X_{\text{fluor}}$  index and the xylenol orange incidence (Table 2) indicate that much more bone was formed between week 3 and week 6 in BCP<sub><μm</sub> as compared to the positive control (TCP<sub><μm</sub>). In sharp contrast, BCP<sub>μm</sub> and TCP<sub>μm</sub> showed no xylenol orange incidence (Table 2).

BCP<sub><μm</sub> led to faster bone formation, but by the time of sacrifice at 12 weeks BCP<sub><μm</sub> and the positive control, TCP<sub><μm</sub>, led to similar amounts of bone tissue, as measured by histomorphometry: 24.5 ± 4.3 % and 23.9 ± 6.3 % respectively, followed by BCP<sub>μm</sub> (2.1 ± 1.7 %). No bone formed in TCP<sub>μm</sub> (Fig. 6a). In addition, the percent area of resorbed material (by histomorphometry) profoundly varied among the four materials: TCP<sub><μm</sub> underwent the most material resorption (53.8 ± 5.7 %), followed by BCP<sub><μm</sub> (28.1 ± 4.1 %), BCP<sub>μm</sub> (9.3 ± 2.4 %) and TCP<sub>μm</sub> (4.7 ± 2.1 %) (Fig. 6b).

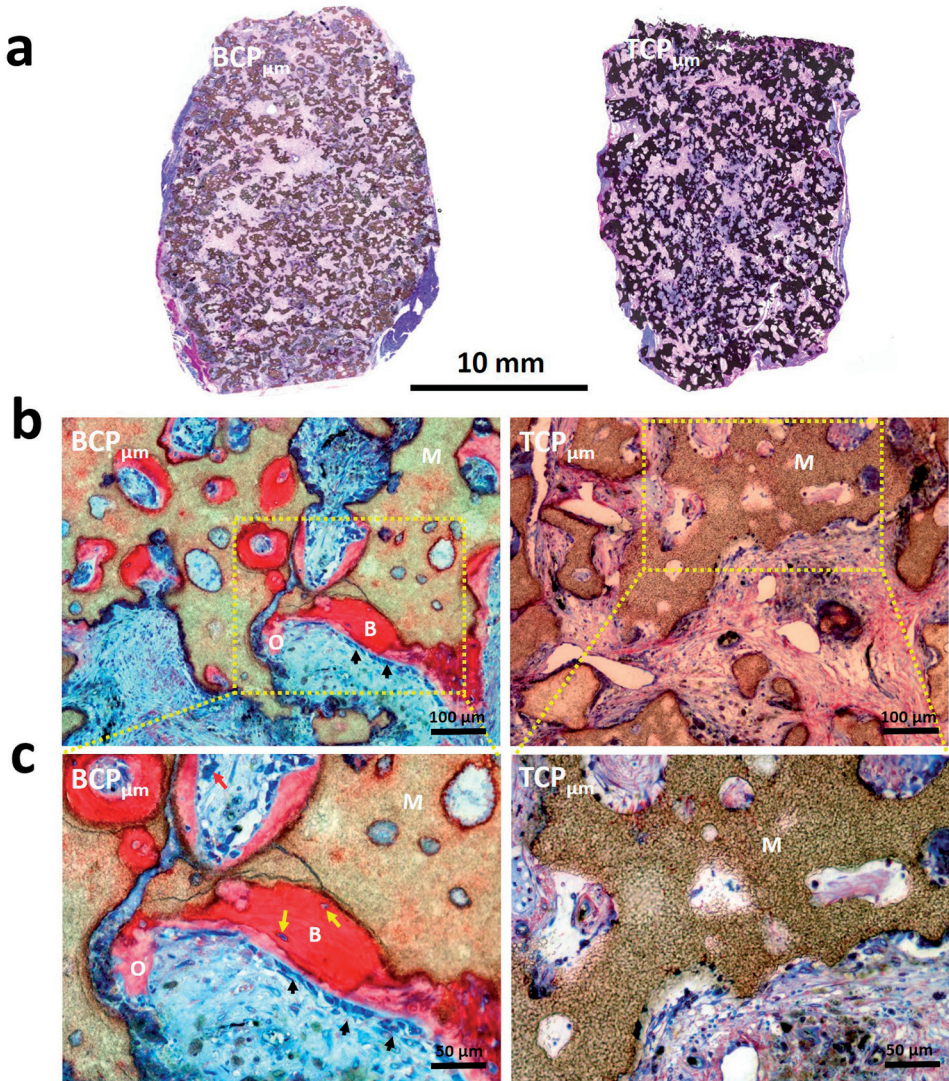


**Fig. 4.** Histological images of BCP<sub>μm</sub> and TCP<sub>μm</sub> after 12 weeks implantation. **a:** histological overviews showing the bone regeneration and material resorption of CaP materials; **b, c:** detailed histological images showing bone formation and remodeling as well as degradation of CaP substrates (non-decalcified sections stained with methylene blue and basic fuchsin, B: bone; M: material; black arrow: osteoblast; yellow arrow: osteocytes; red arrow: phagocytic cells).



## 4. DISCUSSION

In the present study, a hydrothermal treatment was employed to promote the growth of a layer of epitaxial crystals on the surface of BCP materials, leading to a novel needle-shaped surface topography. By adjusting the sintering temperature (i.e. 1125 °C or 1200 °C) of the BCP materials, needle-like crystals at either the submicron or micron scale were achieved (Fig. 1). *In vivo*, the novel CaP with submicron needle-shaped topography (BCP<sub><μm</sub>) triggered earlier bone formation (3 - 6 weeks) compared to TCP with a submicron grain-shaped surface topography (TCP<sub><μm</sub>) which mainly formed bone at 6-9 weeks (Fig. 5). By 12 weeks post-implantation, the amount of bone formed by the positive control, TCP<sub><μm</sub>, was equivalent to the amount formed by the novel needle-like surface topography of BCP<sub><μm</sub> (Fig. 6a). Similarly, BCP<sub>μm</sub> with a micron scale needle-shaped surface topography underwent *in vivo* biomineralization and gave rise to ectopic bone formation, while its counterpart TCP<sub>μm</sub> with micron-scaled grain-like crystals did not (Fig. 5, 6a).

In agreement with previous reports, the feature size of the surface structure greatly affected the osteoinductive potential of CaP materials[9,11,18,19,21,30]. As expected, inductive bone formation occurred in greater amounts for the submicron surface structured BCP<sub><μm</sub> and TCP<sub><μm</sub> grafts but very limited bone formed in BCP<sub>μm</sub> and no bone formed in TCP<sub>μm</sub> with a micron-scale surface topography (Fig. 3, 4, 5 and 6). The strength of the observed effect suggests that the scale of topography influences osteoinductivity independently from chemistry and surface morphology. Based on the available data for grain size, surface area and protein adsorption for BCP<sub><μm</sub> and TCP<sub><μm</sub> versus BCP<sub>μm</sub> and TCP<sub>μm</sub>, this could either be due to a direct or an indirect effect of the smaller surface feature size on bone formation.

Let us first consider whether the specific surface topography could exert a direct effect on bone formation by affecting attached cells. In the absence of chemical factors, surface topographies ranging from nano- to micron scale have been reported to evoke specific cell attachment, orientation, proliferation and guide their differentiation towards various lineages[31–36]. At the micron scale, surface structure has been shown to enhance adipogenic differentiation of MSCs, while submicron scaled surface structures favored osteogenic differentiation [9,35,37]. More recently, research has demonstrated that submicron surface topographies can preferentially direct early wound healing toward the bone-forming pathway by influencing macrophage polarization [30,38–40]. The role of macrophages as either mediators of a pro-inflammatory response or mediating a wound-healing and angiogenic response is well-understood [38]. The key to successful bone healing, that is to promote osteogenesis and avoid the formation of scar tissue, is to tip the balance of wound healing toward the M2, or deactivated, macrophage response following an initial phase of inflammation [39,40]. CaP materials with a submicron surface

topography have been shown to direct the transition of macrophages to the M2 phenotype, as shown by the higher production of TGF- $\beta$  and CCL18 from cells cultured on CaP with sub-micron surface structures[30]. At the same time, CaP materials with micron surface topography displayed more M1 macrophages formation as indicated by an enhanced TNF- and IL-1 $\beta$  secretion[30]. The conditioned media harvested from THP-1 cells cultured on CaP with submicron surface topography enhanced tube formation by human umbilical vein endothelial cells (HUVECs) *in vitro*. Furthermore, submicron surface topography enhanced angiogenesis and triggered bone formation in ectopic defect sites[30].

Let us next consider whether the specific surface topography could exert an indirect effect on bone formation. Protein adsorption is often suggested as crucial in inductive bone formation [41–43], where osteoinduction of CaP materials is thought to be a secondary response following the adsorption of growth factors/ cytokines from body fluids *in vivo* [44–46]. Since the function of growth factors/cytokines is dose-dependent[47,48], theoretically the more proteins concentrated in the implants should lead to higher osteoinductive potential. In this study, TCP<sub><math>\lt; \mu\text{m}</math></sub> adsorbed significantly more proteins from FBS per implant than BCP<sub><math>\lt; \mu\text{m}</math></sub> (Fig. 2b, 2c and Table 1), while the latter triggered earlier bone formation than the former. Similarly, BCP<sub><math>\mu\text{m}</math></sub> adsorbed similar or little more proteins than TCP<sub><math>\mu\text{m}</math></sub>, but the former triggered bone formation, the latter did not (Fig. 2b, 2c and Table 1). Therefore, we conclude that the initiation and enhancement of inductive bone formation in BCP<sub><math>\lt; \mu\text{m}</math></sub> and TCP<sub><math>\lt; \mu\text{m}</math></sub> is less likely to have been due to a higher surface area (and associated increased protein adsorption) but, more likely, instructed by the possible physical cues created by the smaller features in the surface topography.

It is important to consider which of the other effects of chemistry and surface feature morphology is most dominant in driving earlier bone formation in ectopic defects, as observed for BCP<sub><math>\lt; \mu\text{m}</math></sub> (3 - 6 weeks), compared to TCP<sub><math>\lt; \mu\text{m}</math></sub> (6 - 9 weeks). Firstly, BCP<sub><math>\lt; \mu\text{m}</math></sub> consists of 25 % HA/ 75 %  $\beta$ -TCP, while TCP<sub><math>\lt; \mu\text{m}</math></sub> is phase-pure  $\beta$ -TCP. Although the role of chemical composition appears, according to some literature, not to be an essential material factor to trigger inductive bone formation in CaP materials [21], it is generally thought that a higher content of TCP can affect the dissolution of CaP and thus the ion release (e.g. calcium and phosphate) from its surface. This increased ion release may, in turn, enhance inductive bone formation [14,49–52]. However, in this study, BCP<sub><math>\lt; \mu\text{m}</math></sub> released less calcium ions *in vitro* than TCP<sub><math>\lt; \mu\text{m}</math></sub> (Fig. 2a) and resorbed at a slower rate than TCP<sub><math>\lt; \mu\text{m}</math></sub> *in vivo* (Fig. 6b). Therefore, the earlier trigger or enhancement of bone formation observed in our study for BCP<sub><math>\lt; \mu\text{m}</math></sub> seems not to be attributed to the rate of calcium ion release.

Both BCP test materials had resorption rates between those observed for TCP<sub><math>\lt; \mu\text{m}</math></sub> and TCP<sub><math>\mu\text{m}</math></sub> *in vivo* (Fig. 6b), contrary to the general view that a higher TCP content would lead to faster resorption. Since BCP<sub><math>\mu\text{m}</math></sub> had the lowest dissolution *in vitro* (Fig. 2a) but a faster rate of

resorption compared to TCP<sub>μm</sub> *in vivo*, it indicates that cell-mediated resorption played the major role in the *in vivo* resorption for the BCP test articles. This is further corroborated by the histological analysis (Fig. 3b, 3c), in which multinucleated osteoclast-like cells were observed on the surface of the materials. Could chemistry dictate the mechanism of resorption and indirectly drive earlier bone formation for BCP<sub><μm</sub>? We suggest this is not a dominant factor, since abundant resorption by multi-nucleated giant cells was also observed using histological analysis for TCP<sub><μm</sub> (Fig. 3c). The slower resorption we observed for BCP<sub>μm</sub> compared to BCP<sub><μm</sub> corroborates the findings of Davison et al. that CaP ceramic with submicron scaled surface structures favored the formation of osteoclasts from mononuclear cells and facilitated material resorption as compared to its micron scale structured counterpart [53]. Therefore, if the presence of multinucleated osteoclast-like cells is a driver for osteoinductive potential, according to our research, the size of feature in the surface topography is more likely to be the dominant factor than the chemistry.

It is worth noting that the BCP and TCP families contained a different level of microporosity (Table 1). Microporosity is often suggested to determine the osteoinductive potential of CaP materials because it creates an ideal microenvironment for protein adsorption and/or cell attachment, differentiation and proliferation [9,11,15,16,18,21], where higher microporosity has been reported to lead to higher osteoinductive potential [15]. Since lower microporosity was detected in the BCP family than in the TCP family, the trigger of earlier inductive bone formation observed in BCP<sub><μm</sub> is not likely to be linked to microporosity.

Based on our data and the supporting literature, we conclude that the most dominant secondary factor (after surface feature size) for CaP driven osteoinductivity is the surface feature morphology of the substrate. In the case of this study, we found that needle-shaped surface features gave rise to earlier bone formation than grain-shaped surfaces. As chemistry is still likely to have a certain level of influence in osteoinductivity, we propose the strength of effect to be as follows: surface feature size > surface feature morphology > substrate chemistry. The improved bone formation outcomes for BCP<sub><μm</sub> and BCP<sub>μm</sub> in this intramuscular model indicates that they have higher osteoinductive potential than TCP<sub><μm</sub> and TCP<sub>μm</sub> respectively. Previous studies have shown that osteoinductive materials facilitated bone regeneration in orthotopic skeletal sites compared to non-osteoinductive materials [9,11], and that a higher osteoinductive potential correlates with faster bone repair in orthotopic defects [49]. Therefore, of all the articles tested in this study, BCP<sub><μm</sub> may be expected to have good bone regeneration potential in clinical applications.

Using the current settings, the superiority of BCP<sub><μm</sub> to other 3 materials in the study was seen. However, besides the histological and histomorphometrical data, more analyses such as quantitative μCT, biochemical assays of bone forming signals and immunohistostaining of bone markers would make the conclusion stronger. Fluorescent labeling was used to

monitor the onset of bone formation at different timepoints, without the need to include more animals in the study. Another approach could have been to use animal cohorts at each time point, which would allow for a more precise analysis and include bone quantity assessment at each time point. Finally, a clinically relevant animal study (i.e. orthotopic implantation) would be required to more accurately predict the potential clinical efficacy of these materials.

## **5. CONCLUSIONS**

Evaluation of ectopic bone formation by two novel CaP materials with a needle-like surface topography showed that they can give rise to earlier and accelerated bone formation as compared to their counterparts with grain-like surface structures. Our data suggests that the relative strength of effect on osteoinductive potential is as follows: surface feature size > surface feature morphology > substrate chemistry. Of all materials tested in this study, BCP<sub><sub>µm</sub></sub> with a needle-shaped surface topography is expected to have the best bone regeneration potential in clinical applications, although the performance of this material still needs to be evaluated in an orthotopic implantation site.

### **Acknowledgements**

The authors would like to thank the Netherlands Institute for Regenerative Medicine (NIRM), the Rapid Prototyping of Custom-Made Bone-Forming Tissue Engineering Constructs (RAPIDOS Project, Ref. NMP-2013-EU-China, no. 604517), the Seventh Framework Programme of the European Union (no. 241879) and the Horizon 2020 Framework Programme (no. 674282) for their financial support in this study. The authors also acknowledge financial support of Kuros Biosciences BV (the Netherlands) and Sichuan University (China) for the animal study and histological analysis.



## REFERENCES

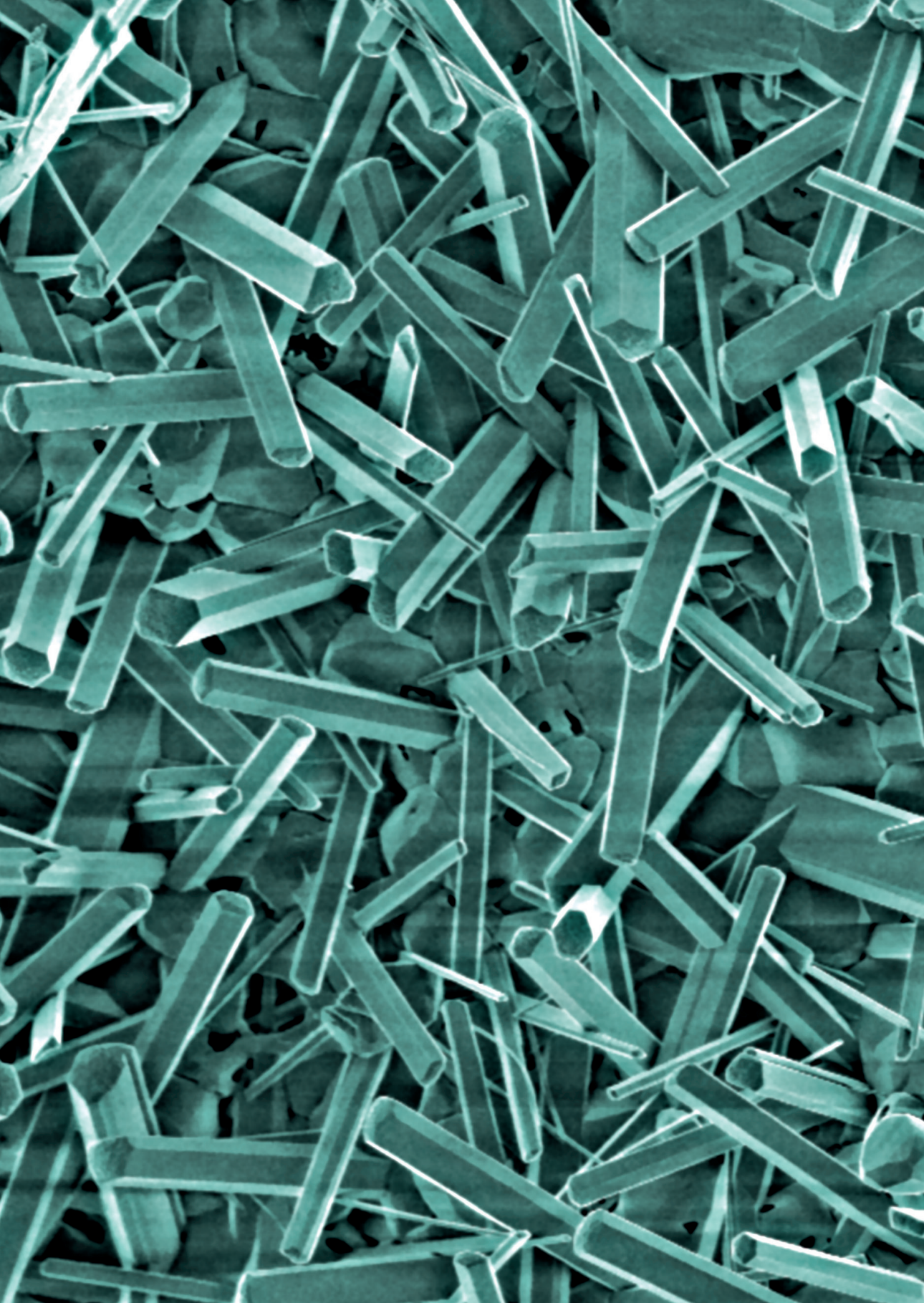
- [1] W. Habraken, P. Habibovic, M. Epple, M. Bohner, Calcium phosphates in biomedical applications: Materials for the future?, *Mater. Today*. 19 (2016) 69–87. <https://doi.org/10.1016/j.mattod.2015.10.008>.
- [2] S. Samavedi, A.R. Whittington, A.S. Goldstein, Calcium phosphate ceramics in bone tissue engineering: a review of properties and their influence on cell behavior, *Acta Biomater*. 9 (2013) 8037–8045.
- [3] M. Miyazaki, H. Tsumura, J.C. Wang, A. Alanay, An update on bone substitutes for spinal fusion, *Eur Spine J*. 18 (2009) 783–799.
- [4] N.K. Acharya, R.J. Kumar, H.K. Varma, V.K. Menon, Hydroxyapatite- bioactive glass ceramic composite as stand alone graft substitute for posterolateral fusion of lumbar spine: a prospective, matched, and controlled study, *J Spine Disord Tech*. 12 (2008) 106–111.
- [5] H. Yamasaki, H. Sakai, Osteogenic response to porous hydroxyapatite ceramics under the skin of dogs, *Biomaterials*. 13 (1992) 308–312. [https://doi.org/10.1016/0142-9612\(92\)90054-R](https://doi.org/10.1016/0142-9612(92)90054-R).
- [6] X. Zhang, P. Zhou, J. Zhang, W. Chen, C. Wu, A study of porous block of HA ceramics and its osteogenesis, in: *Bioceramics and the human body*, Elsevier Science, Amsterdam, 1991.
- [7] U. Ripamonti, Bone induction in nonhuman primates: An experimental study on the baboon, *Clin Orthop Relat Res*. 269 (1991) 284–294.
- [8] S. Pollick, E.C. Shors, R.E. Holmes, R.A. Kraut, Bone formation and implant degradation of coralline porous ceramics placed in bone and ectopic sites, *J Oral Maxillofac Surg*. 53 (1995) 915–922.
- [9] R. Duan, D. Barbieri, X. Luo, J. Weng, J.D. de Bruijn, H. Yuan, Submicron-surface structured tricalcium phosphate ceramic enhances the bone regeneration in canine spine environment, *J. Orthop. Res*. 34 (2016) 1865–1873. <https://doi.org/10.1002/jor.23201>.
- [10] N.L. Davison, X. Luo, T. Schoenmaker, V. Everts, H. Yuan, F. Barrre-de Groot, J.D. de Bruijn, Submicronscales surface architecture of tricalcium phosphate directs osteogenesis in vitro and in vivo, *Eur Cell Mater*. 27 (n.d.) 281–297.
- [11] H. Yuan, H. Fernandes, P. Habibovic, J. De Boer, A.M.C. Barradas, A. De Ruitter, W.R. Walsh, C.A. Van Blitterswijk, J.D. De Bruijn, Osteoinductive ceramics as a synthetic alternative to autologous bone grafting, *Proc. Natl. Acad. Sci. U. S. A*. 107 (2010) 13614–13619. <https://doi.org/10.1073/pnas.1003600107>.
- [12] R.Z. LeGeros, Calcium phosphate-based osteoinductive materials, *Chem Rev*. 108 (2008) 4742–4753.
- [13] A.M.C. Barradas, H. Yuan, C.A. van Blitterswijk, P. Habibovic, Osteoinductive biomaterials: current knowledge of properties, experimental models and biological mechanisms., *Eur. Cell. Mater*. (2011). <https://doi.org/10.22203/eCM.v021a31>.

- [14] P. Habibovic, T.M. Sees, M.A. van den Doel, van Blitterswijk C.A., K. de Groot, Osteoinduction by biomaterials - Physicochemical and structural influences, *J Biomed Mater Res A*. 77 (2006) 747–762.
- [15] O. Chan, M.J. Coathup, A. Nesbitt, C.Y. Ho, K.A. Hing, T. Buckland, C. Champion, G.W. Blunn, The effects of microporosity on osteoinduction of calcium phosphate bone graft substitute biomaterials, *Acta Biomater*. 8 (2012) 2788–2794. <https://doi.org/10.1016/j.actbio.2012.03.038>.
- [16] A. Barba, A. Diez-Escudero, Y. Maazouz, K. Rappe, M. Espanol, E.B. Montufar, M. Bonany, J.M. Sadowska, J. Guillem-Marti, C. Öhman-Mägi, C. Persson, M.C. Manzanares, J. Franch, M.P. Ginebra, Osteoinduction by foamed and 3D-printed calcium phosphate scaffolds: effect of nanostructure and pore architecture, *ACS Appl Mater Interfaces*. 9 (2017) 41722–41736.
- [17] M.J. Dalby, N. Gadegaard, R. Tare, A. Andar, M.O. Riehle, P. Herzyk, C.D. Wilkinson, R.O. Oreffo, The control of human mesenchymal cell differentiation using nanoscale symmetry and disorder, *Nat Mater*. 6 (2007) 997–1003.
- [18] N.L. Davison, X. Luo, T. Schoenmaker, V. Everts, H. Yuan, F. Barrère-de Groot, J.D. de Bruijn, Submicron-scale surface architecture of tricalcium phosphate directs osteogenesis in vitro and in vivo, *Eur. Cells Mater*. 27 (2014) 281–297. <https://doi.org/10.22203/eCM.v027a20>.
- [19] P. Habibovic, H. Yuan, C.M. Van Der Valk, G. Meijer, C.A. Van Blitterswijk, K. De Groot, 3D microenvironment as essential element for osteoinduction by biomaterials, *Biomaterials*. 26 (2005) 3565–3575. <https://doi.org/10.1016/j.biomaterials.2004.09.056>.
- [20] H. Yuan, K. Kurashina, J.D. De Bruijn, Y. Li, K. De Groot, X. Zhang, A preliminary study on osteoinduction of two kinds of calcium phosphate ceramics, *Biomaterials*. 20 (1999) 1799–1806. [https://doi.org/10.1016/S0142-9612\(99\)00075-7](https://doi.org/10.1016/S0142-9612(99)00075-7).
- [21] R. Duan, D. Barbieri, X. Luo, J. Weng, C. Bao, J.D. de Bruijn, H. Yuan, Variation of bone forming ability with the physicochemical properties of calcium phosphate bone substitutes, *Biomater Sci*. 6 (2017) 136–145.
- [22] N.L. Davison, J. Su, H. Yuan, J.J.J.P. van den Beucken, J.D. de Bruijn, F.B. de Groot, Influence of surface microstructure and chemistry on osteoinduction and osteoclastogenesis by biphasic calcium phosphate discs, *Eur. Cells Mater*. 29 (2015) 314–329. <https://doi.org/10.22203/eCM.v029a24>.
- [23] K.A. Kilian, B. Bugarija, B.T. Lahn, M. Mrksich, Geometric cues for directing the differentiation of mesenchymal stem cells, *Proc. Natl. Acad. Sci. U. S. A.* 107 (2010) 4872–4877. <https://doi.org/10.1073/pnas.0903269107>.
- [24] J. Zhang, M.T. Dalbay, X. Luo, E. Vrij, D. Barbieri, L. Moroni, J.D. de Bruijn, C.A. van Blitterswijk, J.P. Chapple, M.M. Knight, H. Yuan, Topography of calcium phosphate ceramics regulates primary cilia length and TGF receptor recruitment associated with osteogenesis, *Acta Biomater*. 57 (2017) 487–497. <https://doi.org/10.1016/j.actbio.2017.04.004>.
- [25] P. Kolhar, A.C. Anselmo, V. Gupta, K. Pant, P. Prabhakarpanthian, E. Ruoslahti, S. Mitragotri, Using shape effects to target antibody-coated nanoparticles to lung and brain endothelium, *Proc Natl Acad Sci USA*. 110 (2013) 10753–10758.

- [26] R. Agarwal, V. Singh, P. Journey, L. Shi, S. Sreenivasan, K. Roy, Mammalian cells preferentially internalize hydrogel nanodiscs over nanorods and use shape-specific uptake mechanisms, *Proc Natl Acad Sci.* 110 (2013) 17247–17252.
- [27] S. Dasgupta, T. Auth, G. Gompper, Shape and orientation matter for the cellular uptake of nonspherical particles, *Nano Lett.* 14 (2014) 687–693.
- [28] K. Metavarayuth, P. Sitasuwan, X. Zhao, Y. Lin, Q. Wang, Influence of surface topographical cues on the differentiation of mesenchymal stem cells in vitro, *ACS Biomater Sci Eng.* 2 (2016) 142–151.
- [29] A.M. Ross, Z. Jiang, M. Bastmeyer, J. Lahann, Physical Aspects of Cell Culture Substrates: Topography, Roughness, and Elasticity, *Small.* 8 (2012) 336–355.
- [30] R. Duan, Y. Zhang, L.A. van Dijk, D. Barbieri, F. de Groot, J.D. de Bruijn, J.J.P. van den Beucken, Y. Huipin, Relation Between Macrophage Differentiation, Angiogenesis and Topology-Directed Osteoinduction of Calcium Phosphate Ceramics., in: *Pap. Present. 64th Annu. Meet. Orthop. Res. Soc.* March 10–13, 2018; New Orleans, LA., 2018.
- [31] S. Mitragotr, J. Lahann, Physical approaches to biomaterial design, *Nat Mater.* 8 (2009) 15–23.
- [32] S. Dupont, L. Morsut, M. Aragona, E. Enzo, S. Giullitti, M. Cordenonsi, F. Zanconato, J. Le Digabel, M. Forcato, S. Bicciato, N. Elvassore, S. Piccolo, Role of YAP/TAZ in mechanotransduction, *Nature.* 474 (2011) 179–183.
- [33] S. Oh, K.S. Brammer, Y.S. Li, D. Teng, A.J. Engler, S. Chien, S. Jin, Stem cell fate dictated solely by altered nanotube dimension, *Proc Natl Acad Sci.* 106 (2009) 2130–2135.
- [34] K. Kolind, D. Kraft, T. Bøggild, M. Duch, J. Lovmand, F.S. Pedersen, D.A. Bindslev, C.E. Bünger, M. Foss, F. Besenbacher, Control of proliferation and osteogenic differentiation of human dental-pulp-derived stem cells by distinct surface structures, *Acta Biomater.* 10 (2014) 641–650.
- [35] G. Abagnale, M. Steger, V.H. Nguyen, N. Hersch, A. Sechi, S. Joussem, B. Denecke, R. Merkel, B. Hoffmann, A. Dreser, U. Schnakenberg, A. Gillner, W. Wagner, Surface topography enhances differentiation of mesenchymal stem cells towards osteogenic and adipogenic lineages, *Biomaterials.* 61 (2015) 316–326.
- [36] A. Phadke, Y. Hwang, S.H. Kim, S.H. Kim, T. Yamaguchi, K. Masuda, S. Varghese, Effect of scaffold microarchitecture on osteogenic differentiation of human mesenchymal stem cells, *Eur Cell Mater.* 25 (2013) 114–129.
- [37] N.L. Davison, B. ten Harkel, T. Schoenmaker, X. Luo, H. Yuan, V. Everts, F. Barrère-de Groot, J.D. de Bruijn, Osteoclast resorption of beta-tricalcium phosphate controlled by surface architecture, *Biomaterials.* 35 (2014) 7441–7451. <https://doi.org/10.1016/j.biomaterials.2014.05.048>.
- [38] P. Italiani, D. Boraschi, From monocytes to M1/M2 macrophages: Phenotypical vs. functional differentiation, *Front. Immunol.* 5 (2014). <https://doi.org/10.3389/fimmu.2014.00514>.
- [39] F. Loi, L.A. Córdova, R. Zhang, J. Pajarinen, T.H. Lin, S.B. Goodman, Z. Yao, The effects of immunomodulation by macrophage subsets on osteogenesis in vitro, *Stem Cell Res. Ther.* 7 (2016) 15. <https://doi.org/10.1186/s13287-016-0276-5>.
- [40] K.L. Spiller, D.O. Freytes, G. Vunjak-Novakovic, Macrophages modulate engineered human tissues for enhanced vascularization and healing, *Ann Biomed Eng.* 43 (2015) 616–627.

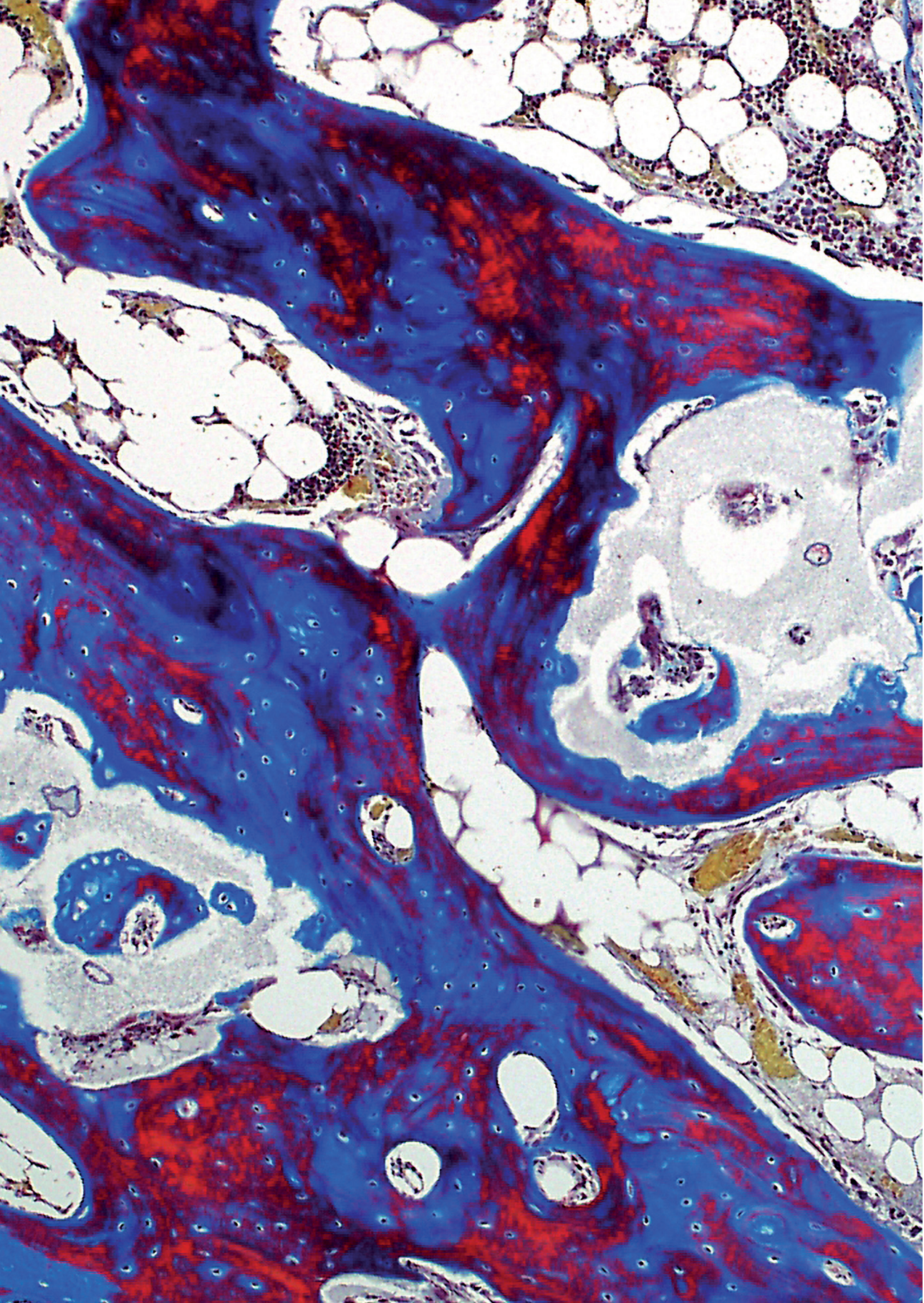
- [41] J. Bolander, W. Ji, L. Geris, V. Bloemen, Y.C. Chai, J. Schrooten, F.P. Luyten, The combined mechanism of bone morphogenetic protein- and calcium phosphate-induced skeletal tissue formation by human periosteum derived cells, *Eur Cell Mater.* 31 (2016) 11–25.
- [42] T. Ariizumi, A. Ogose, N. Kondo, H. Kawashima, T. Hotta, N. Kudo, M. Hoshino, H. Inoue, H. Irie, N. Endo, The role of microstructure of highly purified beta-tricalcium phosphate for osteoinduction in canine dorsal muscles, *J Biomater Nanobiotechnol.* 4 (2013) 189–193.
- [43] T.J. Webster, L.S. Schadler, R.W. Siegel, R. Bizios, Mechanism of enhanced osteoblast adhesion on nanophase alumina involve vitronectin, *Tissue Eng.* 7 (2001) 291–301.
- [44] Q.M. Jin, H. Takita, T. Kohgo, K. Atsumi, H. Itoh, Y. Kuboki, Effects of geometry of hydroxyapatite as a cell substratum in BMP-induced ectopic bone formation, *J Biomed Mater Res.* 52 (2000) 491–499.
- [45] A.H. Reddi, Morphogenesis and tissue engineering of bone and cartilage: inductive signals, stem cells, and biomimetic biomaterials, *Tissue Eng.* 6 (2000) 351–359.
- [46] J. De Groot, Carriers that concentrate native bone morphogenetic protein in vivo, *Tissue Eng.* 4 (1998) 337–341.
- [47] M. Bonilla-Claudio, J. Wang, Y. Bai, E. Klysiak, J. Selever, J.F. Martin, BMP signaling regulates a dose-dependent transcriptional program to control facial skeletal development, *Development.* 139 (2012) 709–719.
- [48] E.B. Hunziker, J. Jovanovic, A. Horner, M.J. Keel, K. Lippuner, N. Shintani, Optimisation of BMP-2 dosage for the osseointegration of porous titanium implants in an ovine model, *Eur Cell Mater.* 32 (2016) 241–256.
- [49] H. Yuan, C.A. Van Blitterswijk, K. De Groot, J.D. De Bruijn, A comparison of bone formation in biphasic calcium phosphate (BCP) and hydroxyapatite (HA) implanted in muscle and bone of dogs at different time periods, *J. Biomed. Mater. Res. - Part A.* 78 (2006) 139–147. <https://doi.org/10.1002/jbm.a.30707>.
- [50] Y.C. Chai, S.J. Roberts, E. Desmet, G. Kerckhofs, N. van Gastel, L. Geris, G. Carmeliet, J. Schrooten, F.P. Luyten, Mechanisms of ectopic bone formation by human osteoprogenitor cells on CaP biomaterial carriers, *Biomaterials.* 33 (2012) 3127–3142.
- [51] S. Nakamura, T. Matsumoto, J. Sasaki, H. Egusa, K.Y. Lee, T. Nakano, T. Sohmura, A. Nakahira, Effect of calcium ion concentrations on osteogenic differentiation and hematopoietic stem cell niche-related protein expression in osteoblasts, *Tissue Eng Part A.* 16 (2010) 2467–2473.
- [52] Y.R. Shih, Y. Hwang, A. Phadke, H. Kang, N.S. Hwang, E.J. Caro, S. Nguyen, M. Siu, E.A. Theodorakis, N.C. Gianneschi, K.S. Vecchio, S. Chien, O.K. Lee, S. Varghese, Calcium phosphate-bearing matrices induce osteogenic differentiation of stem cells through adenosine signaling, *Proc Natl Acad Sci USA.* 111 (2014) 990–995.
- [53] N.L. Davison, A.L. Gamblin, P. Layrolle, H. Yuan, J.D. de Bruijn, F. Barrère-de Groot, Liposomal clodronate inhibition of osteoclastogenesis and osteoinduction by submicrostructured beta-tricalcium phosphate, *Biomaterials.* 35 (2014) 5088–5097. <https://doi.org/10.1016/j.biomaterials.2014.03.013>.





# PART II

**EFFICACY OF OSTEOINDUCTIVE  
CALCIUM PHOSPHATE AS BONE  
GRAFT MATERIAL IN SPINAL  
FUSION**





# CHAPTER 3

## **EFFICACY OF A SYNTHETIC CALCIUM PHOSPHATE WITH SUBMICRON SURFACE TOPOGRAPHY AS AUTOGRAFT EXTENDER IN LAPINE POSTEROLATERAL SPINAL FUSION**

---

Lukas A. van Dijk  
Davide Barbieri  
Florence Barrère-de Groot  
Huipin Yuan  
Rema Oliver  
Chris Christou  
William R. Walsh  
Joost D. de Bruijn

*Journal of Biomedical Materials Research Part B: Applied Biomaterials,*  
2019, 107(6):2080-2090

# ABSTRACT

Posterolateral spinal fusion (PLF) is a common procedure in orthopaedic surgery that is performed to fuse adjacent vertebrae to reduce symptoms related to spinal conditions. In the current study, a novel synthetic calcium phosphate with submicron scale surface topography was evaluated as an autograft extender in a validated rabbit model of PLF.

Fifty-nine skeletally mature New Zealand white rabbits were divided into three groups and underwent single-level intertransverse process PLF at L4-5 using (1) autologous bone graft (ABG) alone or in a 1:1 combination with the (2) calcium phosphate granules (ABG/BCP<sub>granules</sub>) or (3) granules embedded in fast-resorbing polymeric carrier (ABG/BCP<sub>putty</sub>). After 6, 9 and 12 weeks, animals were sacrificed and spinal fusion was assessed by manual palpation, X-rays, micro-CT, mechanical testing (12 weeks only), histology and histomorphometry.

Based on all endpoints, all groups showed a gradual progression in bone formation and maturation during time, leading to solid fusion masses between the transverse processes after 12 weeks. Fusion assessments by manual palpation, radiography and histology were consistent and demonstrated equivalent fusion rates between groups, with high bilateral fusion rates after 12 weeks. Mechanical tests after 12 weeks indicated substantially lower range of motion for all groups, compared to non-operated controls. By histology and histomorphometry, the gradual formation and maturation of bone in the fusion mass was confirmed for each graft type.

With these results, we describe the equivalent performance between autograft and a novel calcium phosphate material as an autograft extender in a rabbit model of PLF using an extensive range of evaluation techniques.

## INTRODUCTION

---

Spinal fusion is a frequent procedure in orthopaedic surgery which is performed to fuse adjacent vertebrae of the spine to improve symptoms resulting from spinal trauma, degenerative conditions, scoliosis or tumor resections. The posterolateral fusion (PLF) technique is commonly performed in the lumbar spine and involves bilateral implantation of bone graft between the transverse processes of adjacent vertebrae. Although autologous bone is the gold standard graft for spinal fusion procedures, pseudoarthrosis and non-unions are still frequently reported complications of this treatment [1-6]. Moreover, the required harvesting of large autograft volumes, usually obtained from the iliac crest, leads to morbidity [7, 8] and persistent post-surgical pain in up to 60% of patients [2].

In order to improve the fusion rate of PLF procedures and to reduce the amount of bone autograft to be harvested, there has been an increasing interest in calcium phosphate materials that can support spinal bone formation as autograft extenders [9, 10]. Synthetic calcium phosphates are generally osteoconductive and highly biocompatible, making them suitable biomaterials for use in bone surgery. As mere osteoconductive materials, their regenerative potential is limited and the presence of an osteogenic or osteoinductive adjunct is favored for bone growth to occur. However, a subset of calcium phosphates with optimized physicochemical properties was demonstrated to have exceptional bone-inducing properties on its own [11, 12, 13], showing enhanced regenerative performance in pre-clinical studies [11-14]. Specifically, the presence of a submicron surface topography was related to the enhanced bone-inducing potential of these calcium phosphates [11, 13-15]. Interestingly, studies have demonstrated that surface properties of biomaterials can influence the phenotype of macrophages [16-18], immune cells that govern the foreign body response and wound healing response [19]. An increase in anti-inflammatory M2 macrophages following an initial inflammatory phase has been shown to be beneficial for bone formation [20] and vascularization [21] and recently, macrophages cultured on calcium phosphates with submicron surface topography were demonstrated to adopt the M2 phenotype [22]. This suggests a connection between surface topography, macrophage phenotype and the enhanced vascularization [22] and bone formation observed with submicron surface structured calcium phosphates *in vivo*.

The current study describes the evaluation of a novel synthetic calcium phosphate with surface topography consisting of submicron polygon crystals in a validated rabbit model of PLF, which is well-described for studies of autograft extender efficacy [23-26]. Either in granular form or as granules embedded within a fast-resorbing polymeric carrier material designed to improve handling properties, the calcium phosphate was combined with iliac crest-derived bone graft in a 1:1 ratio, after which the graft composites were implanted.

Study outcomes included fusion rate by manual palpation, radiography, micro-computed tomography and histology at 6, 9 and 12 weeks post-surgery. Furthermore, biomechanical analysis of the spines and histomorphometry of bone and material in the fusion mass were performed.

## MATERIALS AND METHODS

---

### Graft materials

Calcium phosphate granules. Commercially-available biphasic calcium phosphate (BCP) bone graft (MagnetOs; Kuros Biosciences) was provided in granule and putty formulations. Both formulations contained 1-2 mm granules of bioactive bone graft comprising 65-75% Tri-Calcium Phosphate (TCP-Ca<sub>3</sub>(PO<sub>4</sub>)<sub>2</sub>) and 25-35% Hydroxyapatite (HA-Ca<sub>10</sub>(PO<sub>4</sub>)<sub>6</sub>(OH)<sub>2</sub>). The granules were manufactured from porous BCP blocks produced by use of calcium orthophosphate powder, foaming agent and porogen. Blocks were dried, sintered and crushed to obtain granules (1-2 mm) which were subsequently exposed to a hydrothermal treatment to create submicron-scale surface topography (**Fig. 1 A**). Submicron size of surface crystals was confirmed by scanning electron microscopy (SEM, JEOL JSM-5600, JEOL Ltd, Tokyo, Japan), revealing an average crystal diameter of 0.58 ± 0.21 µm.

Polymeric carrier. For the putty formulation, a tri-block copolymer was synthesized from polyethylene glycol (PEG, 80-90 mol%) and L-lactide monomer (10-20 mol%), with a molecular weight of 2-3 kDa. The resulting polymer is water-soluble and dissolves near body temperature, leading to rapid dispersion after implantation (<48h). The BCP granules and binder were combined to obtain a mouldable putty. The materials were sterilized by gamma irradiation (25 kGy).

Autologous bone graft and graft composites. The iliac crests were exposed from the caudal aspect of the midline incision used to approach the spine. Corticocancellous bone was harvested from both iliac crests using a Miltex Rongeur. Volume and weight of the autologous bone graft (ABG) particles (< 5 mm in size) was measured in a 3 ml syringe (tip removed) and a laboratory balance (**Fig. 1 B**). A volume of 1 cc (~ 0.8 g) of autograft particles was blended with 1 cc of the BCP granules (ABG/BCP<sub>granules</sub>) (**Fig. 1 C,D**). Likewise, 1 cc of autograft particles was blended with 1 cc of putty (ABG/BCP<sub>putty</sub>) (**Fig. 1 E,F**). Volumes of 2 cc of ABG, ABG/BCP<sub>granules</sub> and ABG/BCP<sub>putty</sub> were determined for implantation on each side of the spine (4 cc total per level). The volume of 2 cc autograft per side is the standard amount of autograft that facilitates fusion in the rabbit spine, as is reported in literature

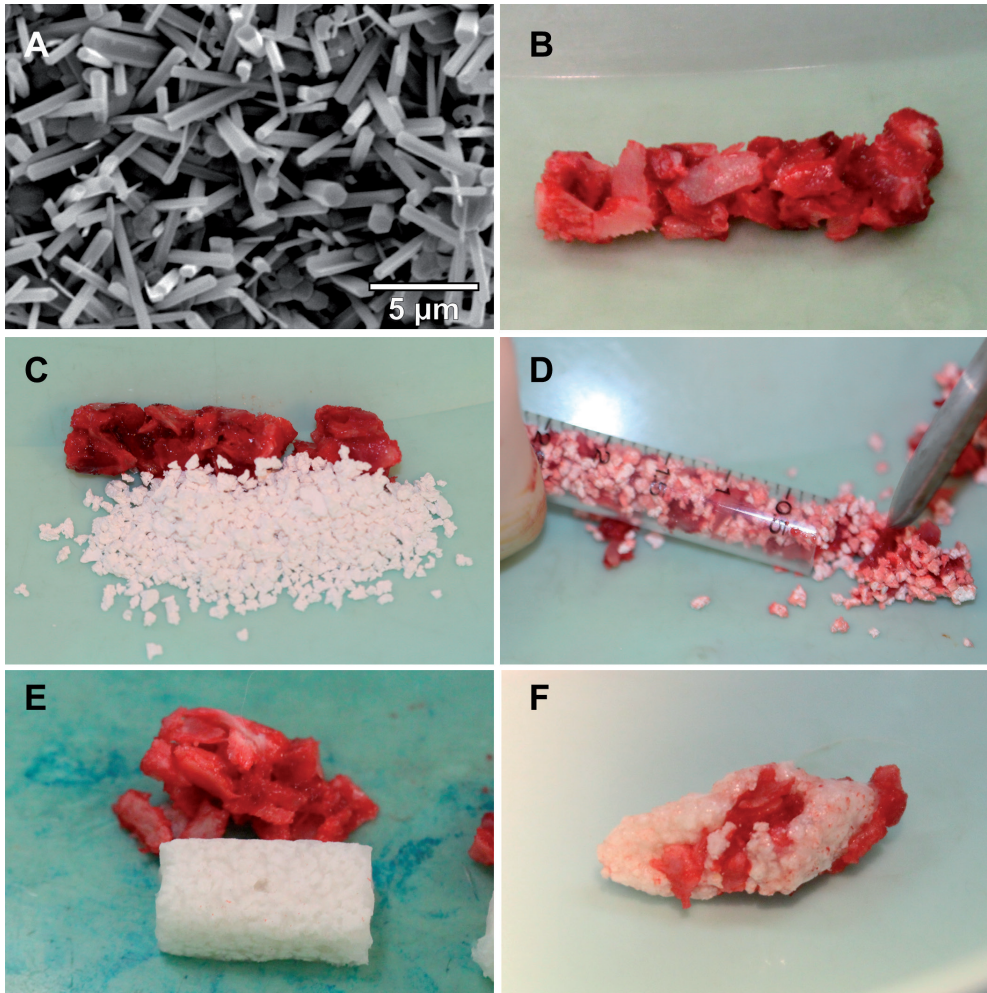


**Fig. 1.** Graft materials used in PLF model, including **(A)** surface of submicron epitaxial polygon crystals observed on BCP granules by SEM, **(B)** iliac crest-derived autologous bone graft particles (ABG), **(C,D)** ceramic granules and autograft particles combined in a 1:1 ratio (ABG/BCP<sub>granules</sub>) and **(E,F)** granules embedded in polymeric carrier combined with autograft particles in a 1:1 ratio (ABG/BCP<sub>putty</sub>).

[27]. Furthermore, a volume of 1 cc of autograft was reported to be unable to achieve fusion in this model [28].

### Animal model and surgical procedure

After approval of the Institutional Animal Care and Ethics Committee (ACEC approval 14/110A, UNSW, Australia), fifty-four adult New Zealand white rabbits underwent single-level bilateral posterolateral intertransverse process spine arthrodesis at L4-5. Skeletal

maturity was confirmed prior to being enrolled in the study by radiographic confirmation of the closure of the growth plates of the proximal tibia. The animals were sedated with a mixture of midazolam (5 mg/ml at 0.3-0.5 mg/kg) and buprenorphine (0.326 mg/ml at 0.03-0.05 mg/kg) intramuscularly. Anesthesia was applied and maintained via isoflurane inhalation (2-3%) with oxygen. Once the rabbits were anesthetized, the skin was incised from the L3-L5 levels. The intermuscular plane between the multifidus and longissimus muscles was separated in a blunt fashion to expose the transverse processes as well as the intertransverse membrane. A pneumatic burr (Midax Rex) was used with an M8 matchstick burr to prepare the host bone between the levels by decortication. The transverse processes were carefully decorticated for a distance of 10 mm from the vertebral body and pars to a level where bleeding bone beds were visually present to the surgeon.

The animals were divided into 3 groups: (1) ABG, (2) ABG/BCP<sub>granules</sub>, and (3) ABG/BCP<sub>putty</sub>. For each group, a total volume of 2 cc graft material per side (4 cc per level) was implanted between the L4-5 transverse processes in the paraspinal bed. After implant placement, the muscle layers were allowed to return to their native position and the fascial incisions were closed with 3-0 absorbable sutures and the skin approximated using 3-0 sutures. Post-operative pain was managed using a non-steroid anti-inflammatory drug (Carprofen, 50 mg/ml, dose 2-4 mg/kg) for the first 2-3 days. The animals were housed in individual cages, fed *ad libitum* and monitored daily for the first 7 days following surgery and weekly thereafter. Animals were euthanized at 6 (n=5), 9 (n=5) and 12 (n=8) weeks after surgery, and spinal fusion was determined by manual palpation, radiography (Faxitron and micro-CT), mechanical testing (range of motion testing at 12 weeks only) and histology (decalcified and undecalcified). For the mechanical testing, 5 non-operated animals were included as baseline controls. For determining BCP material percentage in the implantation bed after surgery at time-point zero, 12 animals were used.

## **Radiographic analysis**

Faxitron Radiography. After harvest, the spines were immediately radiographed in the posteroanterior plane using a Faxitron (Faxitron Bioptics LLC, Arizona, USA) and digital plates (Agfa CR MD 4.0 cassette, Agfa, Germany). An Agfa Digital Developer and workstation was used to process the digital images (Agfa CR 75.0 Digitizer Musica, Agfa, Germany). The DICOM data was converted to bitmap images using DICOM Works (ezDICOM medical viewer, 2002). Radiographic status of the posterolateral spinal fusion was evaluated on the post-sacrifice anteroposterior faxitron radiographs utilizing the Lenke four-point grading scale [29]. A grade A was given to a fusion where it was deemed definitely solid with bilateral robust bridging bone. A grade B was given to a fusion where it was deemed probably solid with unilateral robust bridging bone and contralateral thin fusion mass. A grade C was given to a fusion where it was deemed probably not solid with a thin unilateral fusion mass and a probable pseudarthrosis on the contralateral side. A grade D was given to a fusion

where it was deemed definitely not solid with thin fusion masses bilaterally with obvious pseudarthrosis or bone graft dissolution bilaterally. The occurrence of each grade (A-D) was determined based on faxitron image review by two independent observers blinded to treatment group and time-points.

**Micro-computed tomography (CT).** Micro computed tomography ( $\mu$ CT) scanning was performed on all animals following radiography using an Inveon in-vivo micro computed tomography scanner (Siemens Medical, PA, USA) to obtain high-resolution radiographic images of the spinal fusions in three planes. Spines were scanned and the raw images reconstructed to DICOM data using Siemens software at a resolution of 53 microns. Images were examined in the axial, sagittal and coronal planes to assess the overall quality of the fusion mass from transverse process to transverse process in a similar manner to the other radiographic data. Anterior and posterior 3D models were also created for each animal. The  $\mu$ CT reconstructions were assessed for fusion between the treated levels by two trained and experienced observers who reviewed the coronal and sagittal planes in a blinded manner to treatment groups and time-points. The  $\mu$ CTs were graded using the four-point Lenke radiographic grading score [29] as described above.

### Manual palpation

Immediately after harvest, the stability of the lumbar spine of all animals was assessed by manual palpation according to Boden *et al.* [23]. Two trained and experienced observers assessed the treated motion segment in a blinded manner in lateral bending and flexion/extension and compared it to the proximal and distal motion segments. The motion segments at L4-5 were graded as either fused (rigid, no detectable movement at the disc space) or not fused (not rigid, movement detected at the disc space).

### Biomechanical testing

Non-destructive range of motion testing was performed at 12 weeks to provide a kinematic, multidirectional flexibility analysis of the rabbit lumbar spine. Spines were tested with pure moments using a Denso robot (simVITRO; Cleveland Clinic BioRobotics Lab, Cleveland, OH) to avoid off axis moments and spurious loading. After fixing the spines in custom molds with resin, moments as per Grauer *et al.* [30] (270 N·mm) were applied in axial rotation (AR), flexion-extension (FE) and lateral bending (LB). Moments of 270 N·mm were applied at a rate of 33.3 N·mm per second to a maximum of 300 N·mm, and was held for 15 seconds. A total of 4.5 load – unload cycles were run in each profile. The last 3 cycles were analysed and a mean value at 270 N·mm was taken for each cycle and averaged. Range of motion testing was performed using robotic testing and intact, non-operated skeletally mature female rabbit spines (n=5) that had no previous surgery were evaluated to provide a comparison.

## **Histology and histomorphometric analysis**

All spines were immediately fixed for a minimum of 96 hours in 10% formalin in 0.145 M phosphate buffered saline under gentle rotation, following mechanical testing. The spines were cut in the sagittal plane through the middle of vertebral body using a hacksaw and one side was randomly processed for decalcified paraffin histology and the other side processed for undecalcified polymethyl methacrylate (PMMA) histology. Decalcified histology was used to determine general tissue response and the presence of histological fusion. Undecalcified histology was used for the quantitative determination of bone formation and graft resorption.

Decalcified histology. The portion of the spines allocated for paraffin histology was decalcified in 10% formic acid in phosphate buffered formalin at room temperature for 3 to 4 days prior to further processing. The decalcified spines were then sectioned to provide detailed histology from the entire fusion mass from medial to lateral, which resulted in to at least 4 blocks from the treated spinal unit from transverse processes in the posterolateral fusion space. The blocks (~3 mm in thickness) were then embedded in paraffin and sectioned (5 microns) using a Leica Microtome (Leica Microsystems Pty Ltd, North Ryde, Australia). A minimum of three sections were cut from each paraffin block and stained with hematoxylin and eosin (H&E). Stained sections were examined in a blinded fashion (to treatment groups and time-points) using an Olympus light microscope (Olympus, Japan) with a DP72 high-resolution video camera (Olympus, Japan). Examination included qualitative assessment of general tissue response, the presence of inflammatory cells or tissue necrosis, evidence of graft resorption, new bone formation, marrow space development and bony fusion between both transverse processes. In addition, Rallis' Tetrachrome [31] staining was performed on decalcified sections in order to visualize bone maturation.

Undecalcified histology. The portion of the spines allocated for histomorphometric analysis was dehydrated through a series of ethanol and embedded in PMMA. A Leica SP1600 saw-microtome (Leica Microsystems Pty Ltd, North Ryde, Australia) was used to cut ~15 micron thick sections in the sagittal plane that were stained with methylene blue (Sigma, 1% in 0.1 M borax buffer, pH 8.5) and basic fuchsin (Sigma, 0.3% in water) [13]. Three sections were cut from each PMMA block, with a ~2 mm interval to evaluate the entire fusion mass from medial to lateral. Low magnification images were used for histomorphometric analysis.

Histomorphometry. Three low magnification images (1.25 $\times$ , 1 mm scale bar) taken from the transverse process, the middle of the fusion and the other transverse process were used for quantitative analysis. The region-of-interest (ROI) was determined by an observer blinded to treatment groups or time-points, using a polygon technique and graft material or bone tissue (mineralized bone and bone marrow elements) was identified by pixel color



and morphology assessment. Their respective area was determined as a percentage of the ROI, and a mean value was obtained for each animal based on the three PMMA sections.

### Statistical analysis

SPSS for Windows (SPSS, Chicago, IL) was used for statistical analysis. Fusion grading data were analyzed using a Kruskal Wallis analysis of variance. Biomechanical testing data was analyzed using a 1-way analysis of variance followed by a Games Howell post-hoc test when appropriate. Analysis of variance followed by a Games Howell post hoc test was performed on the histomorphometry data. Statistical significance was set at  $p < 0.05$ .

3

## RESULTS

### Surgery

Surgery was uneventful and no post-operative complications were observed. All animals ambulated normally throughout the study and were euthanized at their allocated time-points.

### Radiographic analysis

Post-operative radiographs demonstrated proper implantation position for all animals, which was maintained for all graft types for the entire study duration. No migration of BCP granules from the implantation site was observed for ABG/BCP<sub>granules</sub> and ABG/BCP<sub>putty</sub> on radiographs and by micro-CT. For all groups, a progression in healing was observed during time. Radiographs showed the progression of a fusion mass with autograft and BCP particles with well-defined borders at 6 weeks towards a more homogeneous mass by 12 weeks for all groups (**Fig. 2, A-C**). By micro-CT, evidence of bone formation on the decorticated host bone transverse processes was observed at 6 weeks with all groups. During time, the autograft and BCP particles coalesced by new bone formation and bone remodeling, leading to solid fusion mass by 12 weeks for all groups (**Fig. 2, D-F**). Fusion grading was performed according to the Lenke scale on radiographs (**Fig. 3, B**) and micro-CT (**Fig. 3, C**). Grading distributions were similar between all groups at each time-point, with no statistically significant differences. A high occurrence of solid bilateral fusion (grade A) was determined after 12 weeks, corresponding to fusion rates of 75%, 87.5% and 75% by radiography and 87.5%, 100% and 87.5% by micro-CT for ABG, ABG/BCP<sub>granules</sub> and ABG/BCP<sub>putty</sub>, respectively.

### Manual palpation

Fusion assessment by manual palpation revealed a similar fusion distribution across groups at each time-point (**Fig. 3, A**). At 6 weeks, bilateral fusion was determined in only

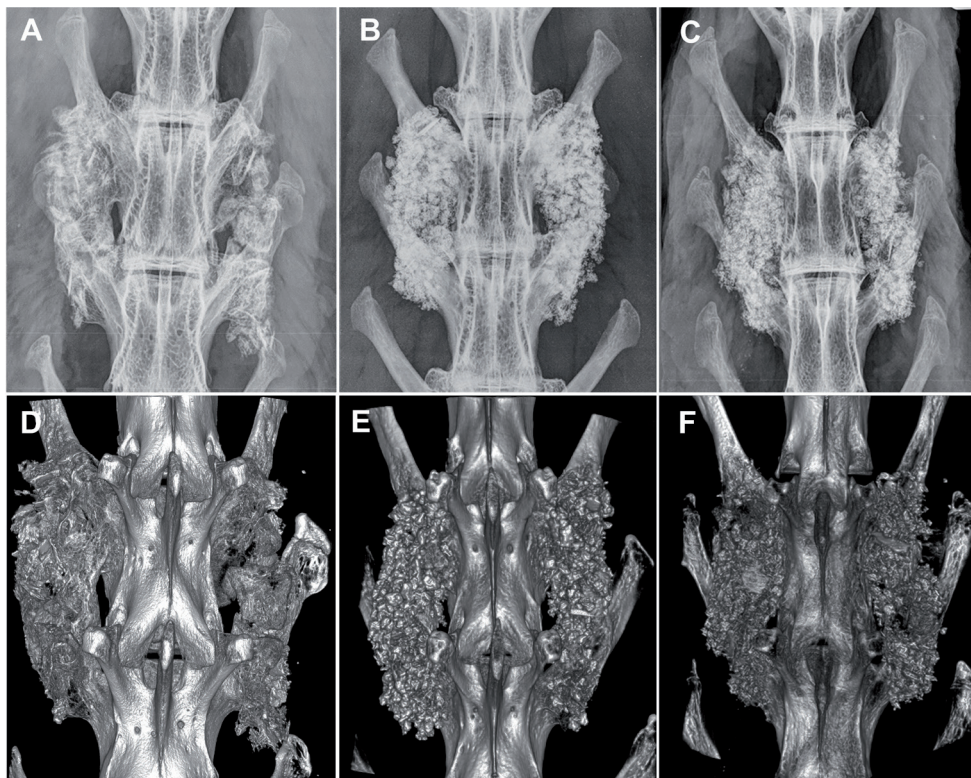


**Fig. 2.** Radiography. (A-C) Examples of Faxitron radiographs taken after 12 weeks for (A) ABG, (B) ABG/BCP<sub>granules</sub> and (C) ABG/BCP<sub>putty</sub>. (D-F) Examples of 3D micro-CT reconstructions taken after 12 weeks for (D) ABG, (E) ABG/BCP<sub>granules</sub> and (F) ABG/BCP<sub>putty</sub>. Faxitron radiographs and micro-CT reconstructions show the presence of graft material bridging the intertransverse process space of the treated levels in all groups.

1 of 5 spines for both ABG/BCP<sub>granules</sub> and ABG/BCP<sub>putty</sub>, while no fusion was observed for ABG. During time, fusion had increased to 3 of 5 at 9 weeks and 6 of 8 at 12 weeks for all groups, corresponding to a fusion rate of 75% for the latest time-point. No statistically significant differences were determined between treatments.

### Biomechanical testing

Results of range-of-motion (ROM) analysis measured after 12 weeks are presented in **Table 1**. Non-operated control spines had a ROM of  $18.8 \pm 1.9$  in LB and  $20.7 \pm 2.9$  FE, indicating baseline ROM. With a difference of  $\pm 50\%$  or more as compared to the controls, the ROM of treated spines in LB and FE after 12 weeks was significantly lower for all groups ( $p < 0.001$ ). Between treatments, ROM of ABG and ABG/BCP<sub>granules</sub> were equivalent in both measuring movements, with no significant differences. Also, ROM between ABG/BCP<sub>granules</sub> and ABG/BCP<sub>putty</sub> was similar in LB. For ABG/BCP<sub>putty</sub>, ROM was slightly higher than other treatments

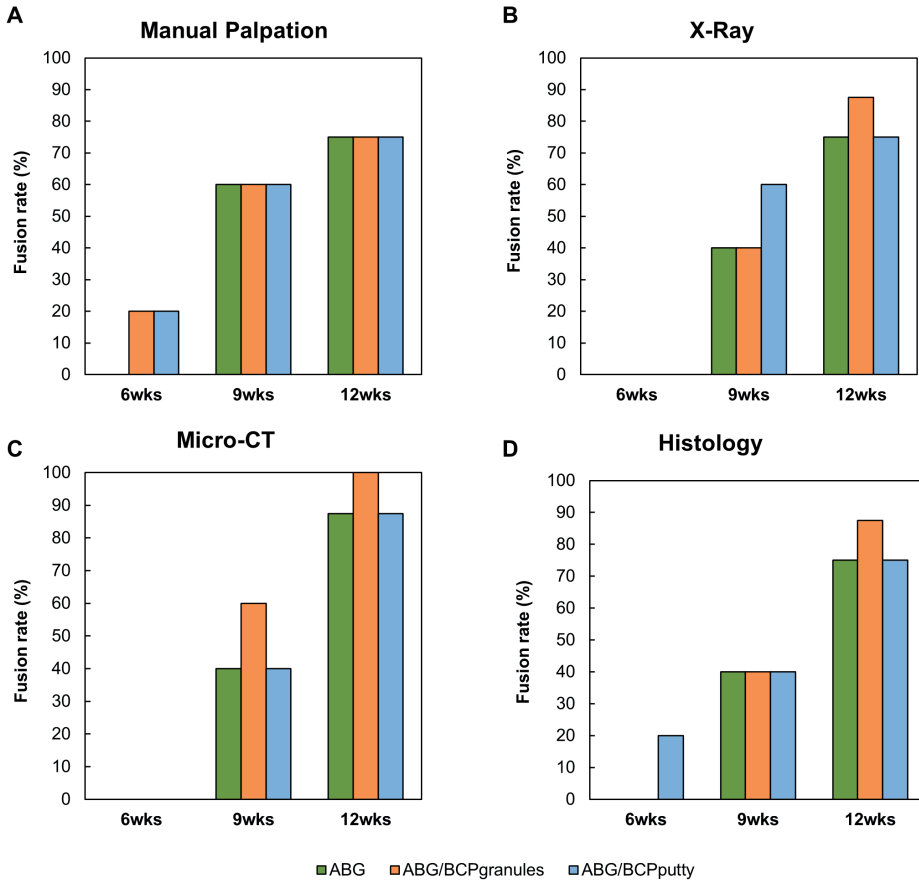


**Fig. 3.** Diagrams presenting the fusion rate as determined by **(A)** manual palpation, **(B)** X-Ray, **(C)** Micro-CT and **(D)** histology. For **A** and **B**, only the percentage of treated levels that achieved solid bilateral fusion (Lenke grade A) are shown. For all assessment methods, no significant differences in fusion rate between treatments were determined at all time-points.

**Table 1.** Mean range of motion (°) of treated spine levels in response to pure moment loading after 12 weeks

Parameter	Control	ABG	ABG/BCP <sub>granules</sub>	ABG/BCP <sub>putty</sub>
Lateral bending	18.8 ± 1.9° (*)	5.3 ± 2.2°	7.7 ± 3.9°	10.7 ± 2.1° (#)
Flexion extension	20.7 ± 2.9° (†)	8.0 ± 2.2°	7.9 ± 2.8°	11.6 ± 2.0° (‡)

Data presented in mean ± sd.

\* significantly different from all other groups, p<0.001

# significantly different from ABG, p<0.001

† significantly different from all other groups, p<0.001

‡ significantly different from ABG, p<0.05

in LB (ABG  $p < 0.001$ ) and FE (ABG  $p < 0.05$ , ABG/BCP<sub>granules</sub>  $p < 0.05$ ). There was no significant difference ( $p > 0.05$ ) in axial rotation between the negative control (un-operated spine) and the positive control (autograft). Furthermore, there were no differences between the BCP treatments and either control.

### Histology and histological grading

Histological observations are presented in examples of low-magnification overviews (Fig. 4) and high magnification micrographs (Fig. 5, 6). On the histological overviews, fusion was

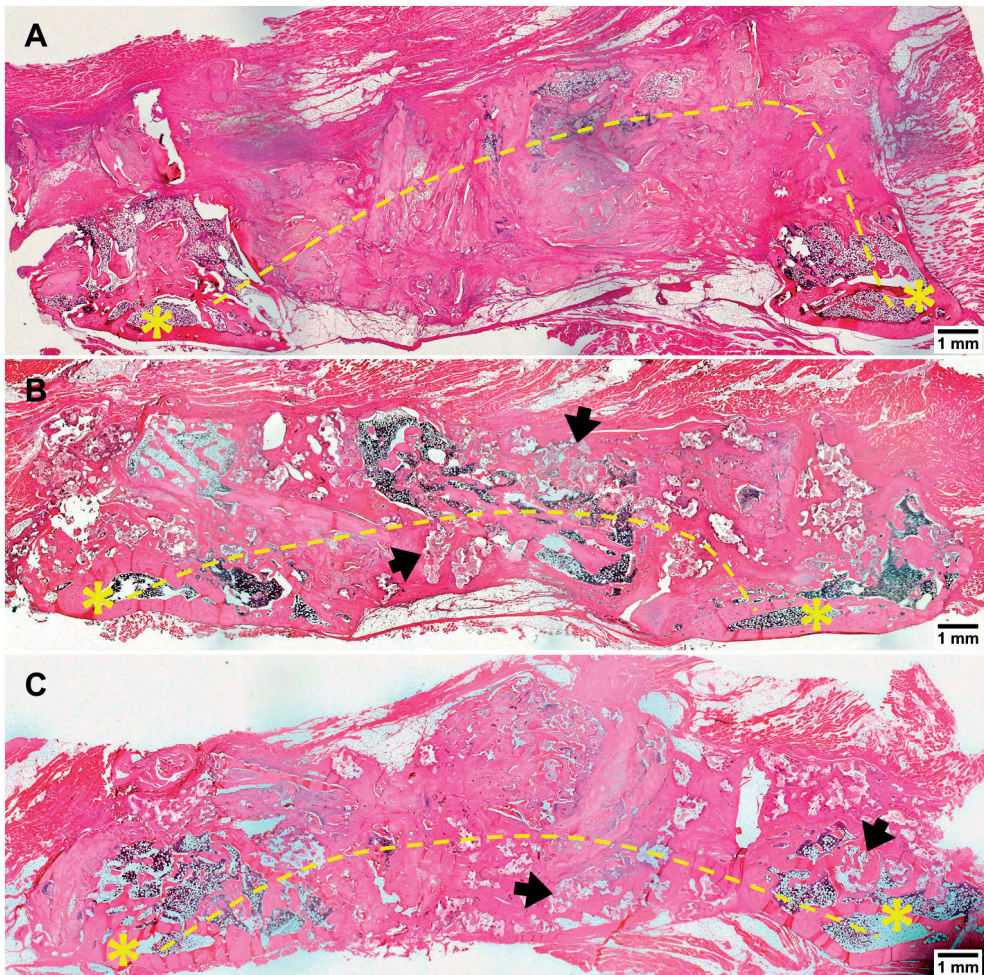


**Fig 4.** Histological panel overviews (H&E) of fusion masses of spines treated with **(A)** ABG, **(B)** ABG/BCP<sub>granules</sub> and **(C)** ABG/BCP<sub>putty</sub> at 12 weeks post-surgery. All these fusion masses were determined to be fused, as indicated by the continuous bone mass (dashed line) between the adjacent transverse processes (yellow asterisks). The presence of ceramic granules in the fusion mass was observed in the autograft extender groups (black arrows).

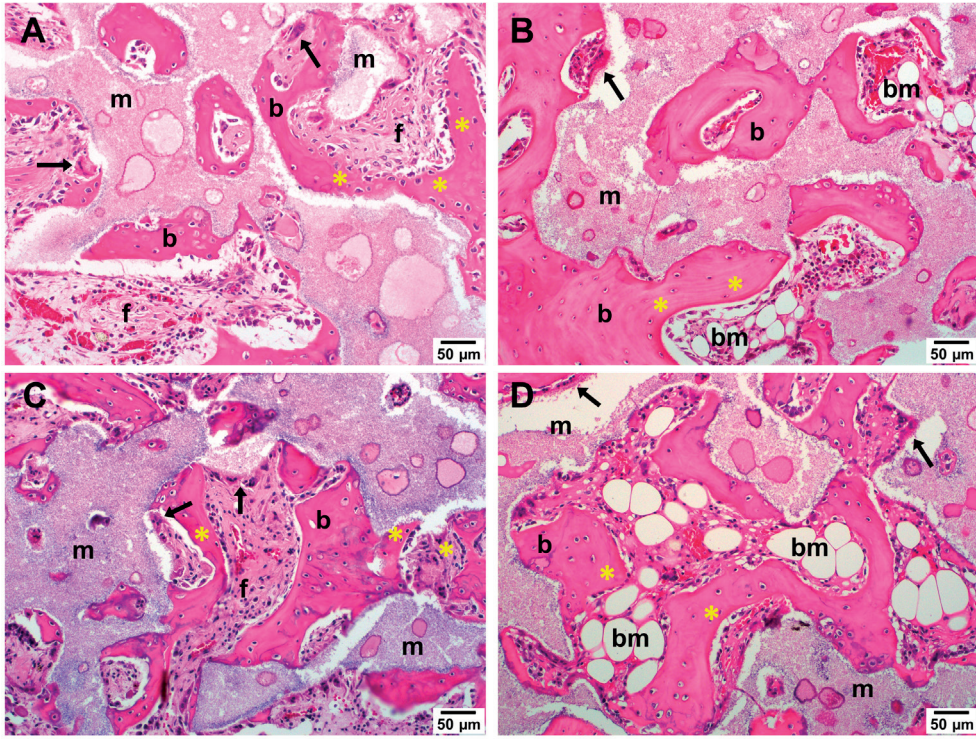


**Fig 5.** Histological micrographs (H&E) of the fusion masses of **(A,B)** ABG/BCP<sub>granules</sub> and **(C,D)** ABG/BCP<sub>putty</sub> at **(A,C)** 6 weeks and **(B,D)** 12 weeks. At 6 weeks, bone tissue was characterized by woven bone and fibrous tissue and was observed at the material surface and inside of the pores. After 12 weeks, bone tissue had developed towards mature bone phenotype as determined by the presence of hematopoietic bone marrow spaces. Osteoblasts were observed depositing new bone matrix (yellow asterisks) and large, multi-nucleated cells were seen at the material surface resorbing material (black arrows). Legend: *m* ceramic material; *b* bone; *f* fibrous tissue; *bm* bone marrow.

determined in case of a bridge of bone tissue in the fusion mass connecting the adjacent transverse processes. By this method, fusion rates of 0-20% at 6 weeks, 40% at 9 weeks and 75-87.5% at 12 weeks were determined, with no significant differences between graft types (**Fig. 3, D**).

Histological micrographs showed the presence of residual particles, BCP granules and new bone formation with typical bone cells (**Fig 5, 6**). After 6 weeks, the formation of new bone on and between the BCP granules and the residual autograft particles was observed (**Fig 5 A,C; Fig. 6 A, B, D, E**). New bone tissue at 6 weeks had infiltrated the BCP pores and was characterized by early, woven bone phenotype and fibrous tissue. Histology at 9 and 12 weeks showed healing progression by new bone formation and remodeling of bone into

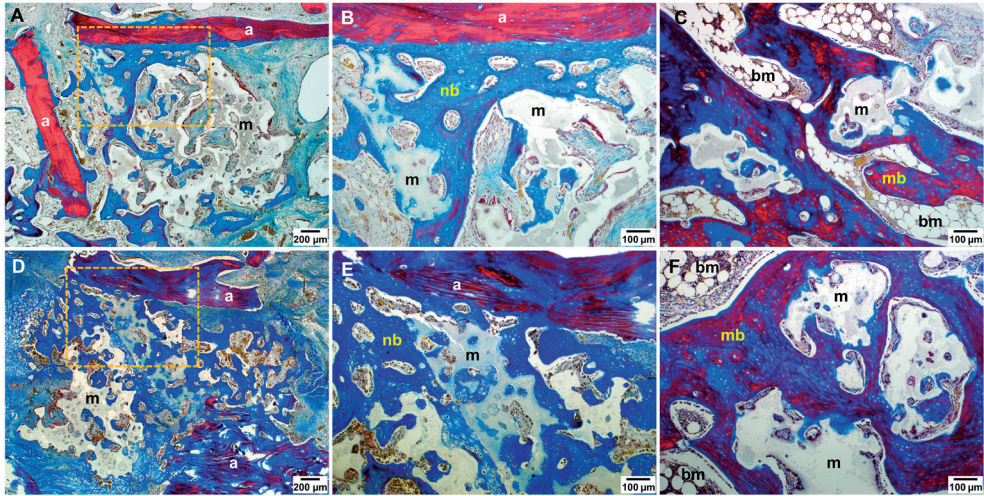


**Fig 6.** Histological micrographs (Tetrachrome) of the fusion masses of **(A-C)** ABG/BCP<sub>granules</sub> and **(D-F)** ABG/BCP<sub>putty</sub> at **(A,D; frames B,E)** 6 weeks and **(C,F)** 12 weeks. After 6 weeks, newly formed woven bone (blue) was observed growing from autograft particles, forming a direct connection between ceramic granules and autograft particles. After 12 weeks, bone maturation was evident from the development of mature bone matrix (red) between granules as well as the presence of large bone marrow spaces. Legend: *a* autograft particle; *m* ceramic material; *nb* new bone; *bm* bone marrow; *mb* matured bone.

lamellar bone in and around the BCP material, as well as the development of bone marrow spaces with hematopoietic cells (**Fig 5 B,D; Fig. 6 C, F**).

Osteoblasts were observed typically lining the surface of new bone in the process of bone formation (**Fig 5**) as well as osteocytes residing in lacunae. Multi-nucleated cells were present on the surface of the BCP material (**Fig. 5**), indicating foreign body giant cell- and osteoclast-mediated resorption of the material.

### Histomorphometric analysis

Quantitative histomorphometry results of bone tissue and material in the fusion mass are presented in **Figure 7**. At all time-points, bone percentage was between 30% and 40% with no significant differences between groups and no trends being apparent over the different time-points. Regarding the percentage of BCP material, a gradual reduction in material percentage during time was apparent for both BCP<sub>granules</sub> and BCP<sub>putty</sub>. However, the percentage of material for ABG/BCP<sub>putty</sub> was significantly higher than for ABG/BCP<sub>granules</sub> at all time-points except time-point zero.

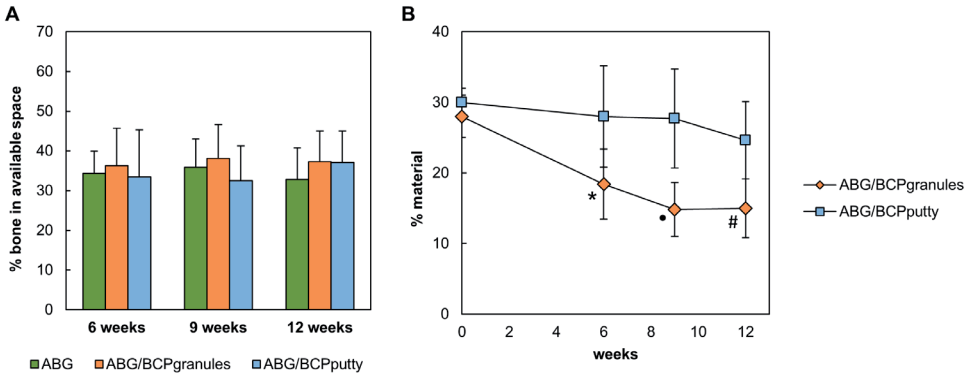


**Fig. 7.** Diagrams presenting the results of histomorphometrical analysis, showing percentage of bone in available space **(A)** and material **(B)** in the fusion mass over time (means ± sd). Symbols: \* significantly different from material, ABG/BCP<sub>putty</sub>, 6 weeks p<0.01; • significantly different from material, ABG/BCP<sub>putty</sub>, 9 weeks p<0.001; # significantly different from material, ABG/BCP<sub>putty</sub>, 12 weeks p<0.001

## DISCUSSION

The objective of this study was to evaluate the performance of a novel BCP bone graft with submicron scale surface topography as an autograft extender against autograft alone in a validated model of PLF in rabbit. The BCP was applied either as granules or as granules embedded in a fast-dissolving polymeric carrier, both in combination with an equal volume of autologous iliac crest bone. Outcomes were determined by an extensive range of assessment methods, including manual palpation, X-ray, micro-CT, mechanical testing, histology and histomorphometry at endpoints of 6, 9 and 12 weeks post-surgery.

Based on all endpoints, all the three groups (ABG, ABG/BCP<sub>granules</sub>, ABG/BCP<sub>putty</sub>) showed a gradual progression in bone formation and maturation during time, leading to solid fusion masses between the transverse processes after 12 weeks. Results of fusion assessment by manual palpation, radiography (X-ray, microCT) and histology revealed equivalent fusion rates between all groups at all time-points, with satisfactory fusion rates after 12 weeks corresponding to literature [23,32]. Previous research has demonstrated that certain methods of fusion assessment (e.g. micro-CT) are more sensitive than other techniques (e.g. manual palpation, X-ray) [23,33], although each technique has advantages and disadvantages. Manual palpation and X-ray assessments are of a more subjective nature and allow global assessment of the fusion mass as compared to the high level of detail offered by micro-CT and histology. However, while histology is an excellent method to show bone formation, it is suboptimal for the assessment of fusion status as it may give false non-union results. A histological slide provides a 2-dimensional representation



of a more complex 3-dimensional fusion mass and apparent non-contiguity between bone islands in a 2-dimensional histological slide could still be contiguous in another plane. A disadvantage of fusion assessment by micro-CT (and X-ray) is that bone mineral and calcium phosphate-based graft materials have similar radiopacity, which can limit the ability to differentiate these components in a fusion mass. Despite all this, an advantage of preclinical investigation compared to the clinic is that multiple descriptive methods for fusion characterization can be used concurrently to develop a robust overall comparison between treatment outcomes. As expected, we noted variation in fusion rate depending on the analytical technique used, but our hypothesis that there would be no difference between autograft and BCP treatments was corroborated by each of the four analyses conducted.

In accordance with the fusion assessment results, mechanical testing of the spines after 12 weeks showed a substantially lower ROM (~50%) in LB and FE in all groups as compared to non-operated controls, indicating successful spinal fusion. There was no significant difference ( $p>0.05$ ) in ROM in LB or FE between the BCP treatments. There was more laxity for ABG/BCP<sub>putty</sub> compared to ABG, but this did not correspond with a lower fusion rate using radiographical or histological methods. Moreover, there was no difference between groups when characterizing the volume of new bone formation by histomorphometry. Furthermore, a recent study in a sheep PLF model in which BCP<sub>granules</sub> and BCP<sub>putty</sub> were implanted as stand-alone grafts and compared to an autograft positive control reported no difference in any mode of flexibility analysis [34]. We found no difference between the positive control, autograft, and the negative control, an un-operated spine, when tested in axial rotation in this study. This could be attributed either to the low sensitivity of the test method in this mode of flexibility or the possibility that more time was required to reach a complete fusion.

In line with the above results, histology and histomorphometry of the fusion mass showed the formation and maturation of bone tissue in the fusion mass during time in all groups, with typical bone morphology and bone-related cell types. Osteoclast-like, multinucleated cell-mediated were observed resorbing the BCP material, which are thought to play a role in the unique bone forming ability of calcium phosphates with submicron scale surface topography [15].

Although the fusion rate evidently increased between 6 and 12 weeks post-surgery, the percentage of bone tissue in available space in the fusion mass as determined by histomorphometry remained stable (30-40%) in all groups during this period. This suggests that bone formation had reached an equilibrium at 6 weeks and thereafter, as new bone formation was in balance with ongoing bone resorption and remodeling. Between 6 and 12 weeks, this process resulted in consolidation and maturation of the grafts into a stable fusion mass at 12 weeks. In retrospect, addition of an earlier time-point at 3 weeks



post-surgery would have provided insight in the progress of bone formation before the equilibrium was reached. With regard to the calcium phosphate material in the fusion mass, the higher percentage of material in the ABG/BCP<sub>putty</sub> group is likely the result of a higher density of granules in the implant bed related to implantation within the polymeric carrier, whereas granules implanted without carrier might become slightly more dispersed. However, this does not seem to have influenced fusion efficacy, as shown by the other assessment methods.

For the proper evaluation of autograft extender performance in this rabbit PLF model, the amount of autograft used in combination with the extender material is a critical factor. Indeed, several studies have noted the positive correlation between the amount of implanted autograft and the fusion rate [27,28,35]. By using a low quantity of autograft that is unable to achieve fusion by itself ( $\pm 1$  cc), the effect of an autograft extender on fusion success can be reliably evaluated (bone paucity model [27]). We have determined previously that 1cc of autograft alone was not able to achieve spinal fusion [unpublished data], a finding that has also been reported by others [27, 28]. However, almost all studies on calcium phosphate autograft extenders that have claimed equivalence to autograft in this model have used quantities of autograft considerably larger than 1 cc combined with the extender [36-39]. This may lead to a significant overestimation of the effect of these materials because the volume of autograft might be sufficient to achieve fusion by itself, as was clearly demonstrated in a study by Miller et al. [28]. In contrast, by use of 1cc of autograft combined with 1cc of BCP in the current study, we have unequivocally shown that this material with submicron scale surface topography is an effective autograft extender, since it enhanced the fusion success of 1 cc of autograft up to the level of the positive control (2 cc of autograft). These results suggest that calcium phosphates with submicron topography are highly effective bone graft materials for use in spinal fusion procedures.

It has been demonstrated that biomaterial surface properties can alter the phenotype of macrophages[16-18], which are key modulators in the tissue response to medical implants. These plastic cells are known to differentiate into various subtypes in response to environmental cues. Typically, they are classified into two main subpopulations that have different functionality: the M1 macrophage, which is microbicidal and promotes an inflammatory response that can contribute to tissue injury, and the pro-healing, anti-inflammatory, M2 macrophage, which is involved in tissue repair and healing [40]. Although having opposing functions, the presence of both subpopulations is important for normal wound repair and also for the integration and healing of bone grafts [40]. Studies have suggested that an upregulation in anti-inflammatory M2 macrophages after a transient phase of inflammation dominated by M1 macrophages is crucial for enhanced vascularization and osteogenesis[20, 21]. Recently, it has been shown that calcium phosphates with submicron surface topography promote naïve macrophages to adopt the

M2 phenotype *in vitro* [22]. The promotion of M2 macrophages on submicron topographies might be the underlying mechanism behind the enhanced angiogenesis and bone healing observed with calcium phosphates with submicron topography *in vivo* [11, 14, 22].

It should be mentioned that all pre-clinical studies are limited in the attempt to represent a model of a human scenario. The rabbit PLF model provides a biological bed to evaluate the *in vivo* performance of bone grafting options that may facilitate fusion. This model is limited in the anatomical and physiological differences between rabbit and human as well as the lack of fixation by instrumentation compared to human PLF. Although this study investigated calcium phosphates with submicron topography, no calcium phosphates without submicron topography were included as control. This would have allowed a more critical evaluation of the effect of submicron topography on bone graft performance in this model. Also, inclusion of additional time-points would have provided valuable information on the healing process, like the progression of bone formation early in the healing process (i.e. 3 weeks) and also the amount of remaining BCP material after a longer term of implantation (i.e. 26 weeks). A recommendation for future studies in this model is to include calcium phosphates with submicron topography as stand-alone grafts instead of autograft extenders, in order to evaluate the performance of these materials in the absence of autograft. However, recently, these materials have already shown potential as stand-alone grafts in an *Ovine* model of instrumented PLF [34].

## **CONCLUSIONS**

This study shows equivalent fusion rates between autologous bone graft and a novel synthetic BCP with submicron surface topography when used as a 1:1 graft extender in a single-level rabbit PLF model. Using an extensive range of evaluation techniques, a gradual progression of bone formation was determined, leading to high fusion rates after 12 weeks, with consistency between groups. Implantation of the BCP material within a fast-resorbing polymeric carrier did not affect treatment outcomes, indicating that the carrier did not inhibit the bone forming-ability of the material. By these findings, we can conclude that this novel BCP is a promising bone graft material for clinical spinal fusion procedures.

## **ACKNOWLEDGEMENTS**

This study was supported by the European Union's Horizon 2020 research and innovation program (grant agreement no. 674282). The authors are grateful to Dr. T. Wang (Surgical

and Orthopedic Research Laboratories, University of New South Wales, Sydney, Australia) for his help with the ROM measurements.



## REFERENCES

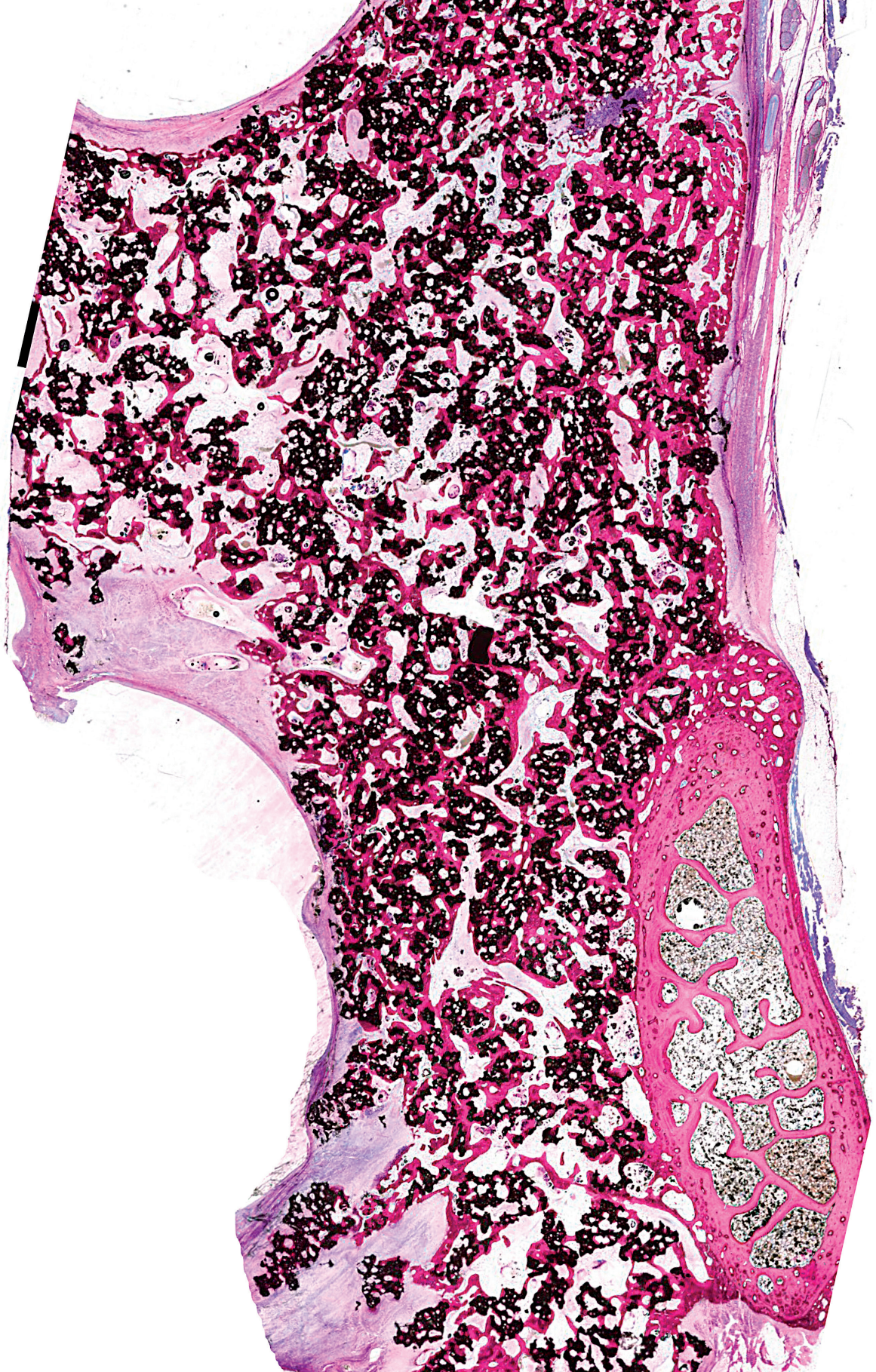
---

- [1] Dimar JR, Glassman SD, Burkus JK, Carreon LY. Clinical outcomes and fusion success at 2 years of single-level instrumented posterolateral fusions with recombinant human bone morphogenetic protein-2/compression resistant matrix versus iliac crest bone graft. *Spine* 2006;31:2534-2539.
- [2] Dimar JR, Glassman SD, Burkus JK, Pryor PW, Hardacker JW, Carreon LY. Two-year fusion and clinical outcomes in 224 patients treated with a single-level instrumented posterolateral fusion with iliac crest bone graft. *Spine J.* 2009;9:880-885.
- [3] Fischgrund JS, Mackay M, Herkowitz HN, Brower R, Montgomery DM, Kurz LT. Degenerative lumbar spondylolisthesis with spinal stenosis: a prospective, randomized study comparing decompressive laminectomy and arthrodesis with and without spinal instrumentation. *Spine.* 1997;22:2807-2812.
- [4] Glassman SD, Dimar JR, Burkus K, Hardacker JW, Pryor PW, Boden SD, Carreon LY. The efficacy of rhBMP-2 for posterolateral lumbar fusion in smokers. *Spine* 2007;32:1693-1698.
- [5] Vaccaro AR, Lawrence JP, Patel T, Katz LD, Anderson DG, Fischgrund JS, Krop J, Fehlings MG, Wong D. The safety and efficacy of OP-1 (rhBMP-7) as a replacement for iliac crest autograft in posterolateral lumbar arthrodesis – a long-term (>4 Years) pivotal study. *Spine.* 2008;33:2850-2862.
- [6] Zdeblick TA. A prospective, randomized study of lumbar fusion. Preliminary results. *Spine.* 1993;18:983-991.
- [7] Banwart JC, Asher MA, Hassanein RS. Iliac crest bone graft harvest donor site morbidity. A statistical evaluation. *Spine.* 1995;20:1055-1060.
- [8] Rihn JA, Kirkpatrick K, Albert TJ. Graft options in posterolateral and posterior interbody lumbar fusion. *Spine.* 2010;35:1629-1639.
- [9] Burger EL, Patel V. Calcium phosphates as bone graft extenders. *Orthopedics* 2007;30:939-942.
- [10] Nickoli MS, Hsu WK. Ceramic-based bone grafts as a bone graft extender for lumbar spine arthrodesis: a systematic review. *Global Spine J.* 2014;4:211-216.
- [11] Habibovic P, Yuan H, van den Doel M, Sees TM, van Blitterswijk CA, de Groot K. Relevance of osteoinductive biomaterials in critical-sized orthotopic defect. *J. Orthop. Res.* 2006;24:867-876.
- [12] Yuan H, van Blitterswijk CA, de Groot K, de Bruijn JD. A comparison of bone formation in biphasic calcium phosphate (BCP) and hydroxyapatite (HA) implanted in muscle and bone of dogs at different time periods. *J. Biomed. Mater. Res. A.* 2006;78:139-147.
- [13] Yuan H, Fernandes H, Habibovic P, de Boer J, Barradas AMC, de Ruiter A, Walsh WR, van Blitterswijk CA, de Bruijn JD. Osteoinductive ceramics as a synthetic alternative to autologous bone grafting. *Proc. Natl. Acad. Sci.* 2010;107:13614-13619.
- [14] Duan R, Barbieri D, Luo X, Weng J, de Bruijn JD, Yuan H. Submicron-surface structured tricalcium phosphate ceramic enhances the bone regeneration in canine spine environment. *J. Orthop. Res.* 2016;34:1865-1873.

- [15] Davison NL, Luo X, Schoenmaker T, Everts V, Yuan H, Barrère-de Groot F, de Bruijn JD. Submicron-scale surface architecture of tricalcium phosphate directs osteogenesis in vitro and in vivo. *Eur. Cell Mater.* 2014;27:281-297.
- [16] Bota, P. C. S. et al. Biomaterial topography alters healing in vivo and monocyte/macrophage activation in vitro. *J. Biomed. Mater. Res. Part A* 95A, 649–657 (2010).
- [17] Hotchkiss, K. M. et al. Titanium surface characteristics, including topography and wettability, alter macrophage activation. *Acta Biomater.* 31, 425–434 (2016).
- [18] Luu, T. U., Gott, S. C., Woo, B. W. K., Rao, M. P. & Liu, W. F. Micro- and Nanopatterned Topographical Cues for Regulating Macrophage Cell Shape and Phenotype. *ACS Appl. Mater. Interfaces* 7, 28665–72 (2015).
- [19] Italiani, P. & Boraschi, D. From Monocytes to M1/M2 Macrophages: Phenotypical vs. Functional Differentiation. *Front. Immunol.* 5, (2014).
- [20] Loi, F. et al. The effects of immunomodulation by macrophage subsets on osteogenesis in vitro. *Stem Cell Res. Ther.* 7, 15 (2016).
- [21] Spiller, K. L. et al. Sequential delivery of immunomodulatory cytokines to facilitate the M1-to-M2 transition of macrophages and enhance vascularization of bone scaffolds. *Biomaterials* 37, 194–207 (2015).
- [22] Duan, R. et al. Relation Between Macrophage Differentiation, Angiogenesis and Topology-Directed Osteoinduction of Calcium Phosphate Ceramics. in paper presented at: 64th Annual Meeting of the Orthopaedic Research Society, March 10-13, 2018; New Orleans, LA.
- [23] Boden SD, Schimandle JH, Hutton WC. An experimental lumbar intertransverse process spinal fusion model: radiographic, histologic, and biomechanical healing characteristics. *Spine* 1995;20:412-420.
- [24] Fredericks D, Petersen EB, Watson N, Grosland N, Gibson-Corley K, Smucker J. Comparison of two synthetic bone graft products in a rabbit posterolateral fusion model. *Iowa Orthop. J.* 2016;36:167-173.
- [25] Walsh WR, Oliver RA, Gage G, Yu Y, Bellemore J, Adkisson HD. Application of resorbable poly(lactide-co-glycolide) with entangled hyaluronic acid as an autograft extender for posterolateral intertransverse lumbar fusion in rabbits. *Tissue Eng. A.* 2011;17:213-220.
- [26] Walsh WR, Vizesi F, Cornwall GB, Bell D, Oliver RA, Yu Y. Posterolateral spinal fusion in a rabbit model using a collagen-mineral composite bone graft substitute. *Eur. Spine J.* 2009;18:1610-1620.
- [27] Curylo LJ, Johnstone B, Petersilge CA, Janicki JA, Yoo JU. Augmentation of spinal arthrodesis with autologous bone marrow in a rabbit posterolateral spine fusion model. *Spine* 1999;24:434-438.
- [28] Miller CP, Jegede K, Essig D, Garg H, Bible JE, Biswas D, Whang PG, Grauer JN. The efficacies of 2 ceramic bone graft extenders for promoting spinal fusion in a rabbit bone paucity model. *Spine* 2012;37:642-647.
- [29] Lenke LG, Bridwell KH, Bullis D, Betz RR, Baldus C, Schoenecker PL. Results of in situ fusion for isthmic spondylolisthesis. *J. Spinal Disord.* 1992;5:433-442.

- [30] Grauer JN, Erulkar JS, Patel TC, Panjabi MM. Biomechanical evaluation of the New Zealand white rabbit lumbar spine: a physiologic characterization. *Eur. Spine J.* 2000;9:250-255.
- [31] Rallis Z, Watkins G. Modified tetrachrome staining method for osteoid and defectively mineralized bone in paraffin sections. *Biotech Histochem* 1992;67(6):339-345. 27
- [32] Pelletier MH, Oliver RA, Christou C, Yu Y, Bertollo N, Irie H, Walsh WR. Lumbar spinal fusion with b-TCP granules and variable *Escherichia coli*-derived rhBMP-2 dose. *Spine J.* 2014;14:1758-1768.
- [33] Goldstein C, Drew B. When is a spine fused? *Injury.* 2011 Mar;42(3):306-13.
- [34] van Dijk LA, Duan R, Luo X, Barbieri D, Pelletier M, Christou C, Rosenberg AJWP, Yuan H, Barrère-de Groot F, Walsh WR, de Bruijn JD. Biphasic Calcium Phosphate with Submicron Surface Topography in an *Ovine* Model of Instrumented Posterolateral Spinal Fusion. *JOR Spine* (in press).
- [35] Ghodasra JH, Daley EL, Hsu EL, Hsu WK. Factors influencing arthrodesis in a rabbit posterolateral spine model with iliac crest autograft. *Eur. Spine J.* 2014;23:426-434.
- [36] Fredericks DC, Petersen EB, Sahai N, Corley KG, DeVries N, Grosland NM, Smucker JD. Evaluation of a novel silicate substituted hydroxyapatite bone graft substitute in a rabbit posterolateral fusion model. *Iowa Orthop J.* 2013;33:25-32.
- [37] Pugely AJ, Petersen EB, DeVries-Watson N, Fredericks DC. Influence of 45S5 Bioactive Glass in A Standard Calcium Phosphate Collagen Bone Graft Substitute on the Posterolateral Fusion of Rabbit Spine. *Iowa Orthop J.* 2017;37:193-198.
- [38] Smucker JD, Petersen EB, Fredericks DC. Assessment of MASTERGRAFT PUTTY as a graft extender in a rabbit posterolateral fusion model. *Spine.* 2012 May 20;37(12):1017-21.
- [39] Smucker JD, Petersen EB, Nepola JV, Fredericks DC. Assessment of Mastergraft® strip with bone marrow aspirate as a graft extender in a rabbit posterolateral fusion model. *Iowa Orthop J.* 2012;32:61-8.
- [40] Klopffleisch, R. Macrophage reaction against biomaterials in the mouse model—Phenotypes, functions and markers. *Acta Biomater.* 43, 3–13 (2016).







# CHAPTER 4

## **BIPHASIC CALCIUM PHOSPHATE WITH SUBMICRON SURFACE TOPOGRAPHY IN AN OVINE MODEL OF INSTRUMENTED POSTEROLATERAL SPINAL FUSION**

---

Lukas A. van Dijk  
Rongquan Duan  
Xiaoman Luo  
Davide Barbieri  
Matthew Pelletier  
Chris Christou  
Antoine J.W.P. Rosenberg  
Huipin Yuan  
Florence Barrère-de Groot  
William R. Walsh  
Joost D. de Bruijn

*JOR Spine, 2018, 1(4), e1039*

# ABSTRACT

As spinal fusions require large volumes of bone graft, different bone graft substitutes are being investigated as alternatives. A sub-class of calcium phosphate materials with submicron surface topography has been shown to be a highly effective bone graft substitute. In this work, a commercially available biphasic calcium phosphate (BCP) with submicron surface topography (MagnetOs™; Kuros Biosciences) was evaluated in an Ovine model of instrumented posterolateral fusion. The material was implanted standalone, either as granules (BCP<sub>granules</sub>) or as granules embedded within a fast-resorbing polymeric carrier (BCP<sub>putty</sub>) and compared to autograft bone (AG). Twenty-five adult, female Merino sheep underwent posterolateral fusion at L2-3 and L4-5 levels with instrumentation. After 6, 12 and 26 weeks, outcomes were evaluated by manual palpation, range of motion (ROM), micro-computed tomography, histology and histomorphometry. Fusion assessment by manual palpation 12 weeks after implantation revealed 100% fusion rates in all treatment groups. The three treatment groups showed a significant decrease in lateral bending at the fusion levels at 12 weeks ( $p < 0.05$ ) and 26 weeks ( $p < 0.001$ ) compared to the 6 week time point. Flexion-extension and axial rotation were also reduced over time, but statistical significance was only reached in flexion-extension for AG and BCP<sub>putty</sub> between the 6 and 26 week time points ( $p < 0.05$ ). No significant differences in ROM were observed between the treatment groups at any of the time points investigated. Histological assessment at 12 weeks showed fusion rates of 75%, 92% and 83% for AG, BCP<sub>granules</sub> and BCP<sub>putty</sub>, respectively. The fusion rates were further increased 26 weeks post-implantation. Similar trends of bone growth were observed by histomorphometry. The fusion mass consisted of at least 55% bone for all treatment groups 26 weeks after implantation. These results suggest that this BCP with submicron surface topography, in granules or putty form, is a promising alternative to autograft for spinal fusion.

## INTRODUCTION

---

The annual number of spinal fusion procedures in the US for the treatment of degenerative spine conditions has risen rapidly over the past two decades to >770,000[1]. The most commonly used spinal fusion technique is posterolateral fusion (PLF), which is either performed as an individual procedure (19%) or in combination with interbody cage fusion (45%)[2]. Because these procedures require large volumes of bone graft (12– 36 cc)[3], bone graft substitutes are frequently employed to reduce or avoid morbidity related to the harvesting of autologous bone[4]. Calcium phosphate-based bone grafts have been widely investigated because of their excellent biocompatibility, osteoconductivity and controllable resorption rates[5]. A commonly addressed disadvantage compared to autologous bone is their lack of osteogenic and osteoinductive capacity. However, efforts to modify the physicochemical properties of calcium phosphates (i.e. composition, porosity and, most recently, surface properties) have resulted in materials with bone-inducing properties. In particular, submicron surface topographies have been reported to enhance angiogenesis and bone healing properties following *in vivo* implantation[5–8].

Surface properties of biomaterials have been shown to influence the phenotype of macrophages[9–11], that are key modulators in the foreign body and wound healing responses[12,13]. For promotion of bone repair, an increase in anti-inflammatory macrophages following an initial phase with pre-dominantly pro-inflammatory macrophages has been suggested to be important[14,15]. Recently, calcium phosphates with submicron surface topography have been shown to promote the transition of macrophages to the pro-healing, anti-inflammatory M2 phenotype *in vitro*[8], which has been linked to enhanced angiogenesis and superior bone healing properties observed with these materials[6,7].

In the current study, a clinically relevant[16–18] *Ovine* model of instrumented PLF was used to compare treatment outcomes of a biphasic calcium phosphate (BCP) with submicron surface topography to bone autograft as a stand-alone treatment. The bone graft was implanted as granules alone and as a putty, with granules embedded in a fast-resorbing polymeric binder designed to improve handling properties. Study endpoints included fusion rate (FR) by manual palpation (MP), range of motion (ROM), histology and histomorphometrical analysis of bone in the fusion mass (FM) after 6, 12 and 26 weeks.



## MATERIAL AND METHODS

---

### Calcium phosphate:

Commercially-available BCP bone graft (MagnetOs™; Kuros Biosciences B.V., the Netherlands) was provided as granules (BCP<sub>granules</sub>) and putty (BCP<sub>putty</sub>). Both formulations contain 1-2 mm granules of bioactive bone graft comprising 65-75% Tri-Calcium Phosphate (TCP-Ca<sub>3</sub>(PO<sub>4</sub>)<sub>2</sub>) and 25-35% Hydroxyapatite (HA-Ca<sub>10</sub>(PO<sub>4</sub>)<sub>6</sub>(OH)<sub>2</sub>). The carrier in the putty formulation is a tri-block copolymer synthesized from polyethylene glycol (PEG) and L-lactide monomer. The resulting polymer is water-soluble and dissolves at near body temperature, leading to rapid dispersion after implantation (<48h)[19]. Scanning electron microscopy (SEM; JSM-5600, JEOL) was used to characterize the submicron surface topography. Bioactivity of the BCP surface was evaluated *in vitro* using the validated assay described by Kokubo et al.[20] Briefly, the materials were submerged in simulated body fluid (SBF) for 2, 4, 7 and 10 days and subsequently analysed for presence of an apatite-like-layer using SEM. The materials for the animal study were provided sterile having been sterilized by gamma irradiation (25 kGy).

### Animal Study:

The study design was based on a previously reported sheep model of PLF[18,21,22] and approved by the local Animal Care and Ethics Committee (ACEC). The surgery was performed on 25 adult, female Merino sheep (4-5 years, 80-90 Kg, at the University of New South Wales (UNSW), Australia). Animals were randomly distributed into 3 groups for the 6, 12 and 26-week time-points, with an *n* of 8, 9 and 8, respectively. Pre-operative, animals were administered fentanyl (2 µg/kg/hr, t.d.), buprenorphine (0.006 mg/kg, s.c.) and Carprofen (4 ml, s.c.) for pain relief and Zoletil (8-12 mg/kg, i.m.) for induction. Anesthesia was achieved and maintained by isoflurane (2-4% in 100% O<sub>2</sub>). Surgery consisted of multi-level instrumented spinal PLF procedure at levels L2-L3 and L4-L5. In short, facet joints and transverse processes (TPs) were exposed followed by destabilization of the motion segments and excision of the facet joints, spinous processes and ligaments. TPs were decorticated after which the operative levels were bilaterally instrumented with polyaxial pedicle screws (Ø 5.0mm x 35mm) and titanium rods (Ø 5.5mm, Wiltrom, Co Ltd Taiwan). Subsequently, 20cc of graft material was equally distributed to the bilateral arthrodesis sites in direct apposition with each of the TPs (10cc per side). The three graft materials were iliac crest- and proximal tibia-derived (1:1) autologous bone graft (AG), BCP<sub>granules</sub> and BCP<sub>putty</sub>, randomly allocated to the fusion levels (n=5 for 6 and 26 weeks, n=6 for 12 weeks). Post-surgery, the animals were housed at the laboratory animal facility where they were monitored and received proper post-operative care. After 6, 12 and 26 weeks, animals were euthanized by IV injection of Lethotarb (1 mL/2kg i.v., 325 mg/ml) for analyses of endpoints.

### **Manual palpation:**

After euthanasia, harvesting of the spines and removal of pedicle rods, the L2-L3 and L4-L5 segments were manually subjected to flexion – extension (FE) and lateral bending (LB) to assess spine mobility. All levels were graded as either fused (low mobility), partially fused (one-sided mobility) and not fused (high mobility) under FE and LB. The Fisher-Freeman-Halton Exact Test was performed for statistical analysis ( $p < 0.05$ ).

### **Micro-computed tomography**

Micro-computed tomography (micro-CT) was performed using an Inveon Scanner (Siemens, USA) at a slice thickness of 50 micron.

### **Biomechanical analysis**

The treated levels were separately mounted on a robotic six degree of freedom musculoskeletal simulator, simVITRO (Simulation Solutions and Cleveland Clinic, Ohio). A 7.5 Nm pure moment was applied to the segments in FE, LB and axial rotation (AR). Each loading profile was repeated three times for every specimen and the mean angular deformation was recorded. Data were analysed with a two-factor analysis of variance (ANOVA) with a significance level of  $p < 0.05$  using dedicated software (Graphpad version 5). Normal distribution of data was confirmed by Kolmogorov-Smirnov normality test.

### **Histology & Histomorphometry**

The treated spine levels were fixed in 4% phosphate-buffered formalin for 1 week at 4 degrees Celsius. After fixation, samples were dehydrated through a series of increasing ethanol concentrations and were subsequently embedded in methylmethacrylate. A Leica SP1600 saw-microtome was used to cut sagittal cross-sections (10-20 micron) from the region between TPs of each contralateral fusion mass. From each sample, three sections were obtained across the fusion mass for evaluation. Sections were stained with 1% methylene blue and 0.3% basic fuchsin to visualize bone tissue (bone matrix: pink, fibrous tissues: blue). Sections were visualized under a Leica microscope (Eclipse 50i, Nikon) for histological observation and were imaged using a slide scanner (DiMage scan 5400 Elite II, Konica Minolta) to obtain overviews for fusion assessment followed by histomorphometrical analysis. Each section was evaluated for histological fusion. Histological fusion was scored when a continuous presence of bone was observed between the TPs, connecting the adjacent spine segments. From each fusion mass, the most representative section was used for histomorphometry. Histomorphometry of the fusion mass was performed by pseudo-coloring pixels representing bone and remaining implant material in a region of interest (Adobe Photoshop Elements 2.0). Values were expressed in mean and standard deviation. For statistical evaluation, a two-factor ANOVA was performed ( $p < 0.05$ ). Normal distribution of data was confirmed by D'Agostina-Pearson normality test.



## RESULTS

### Material characterization

Surface structure analysis of the porous BCP granules (fig. 1a) by SEM demonstrated a surface topography of submicron-scale polygon crystals (fig. 1b). Average surface crystal diameter was determined to be  $0.58 \pm 0.21 \mu\text{m}$ . Surface mineralization, evident from the development of an apatite-like-layer of globules, was observed in an increasing manner with time following submersion in SBF (fig. 1b-1f). These results confirm the bioactivity of the BCP surface.

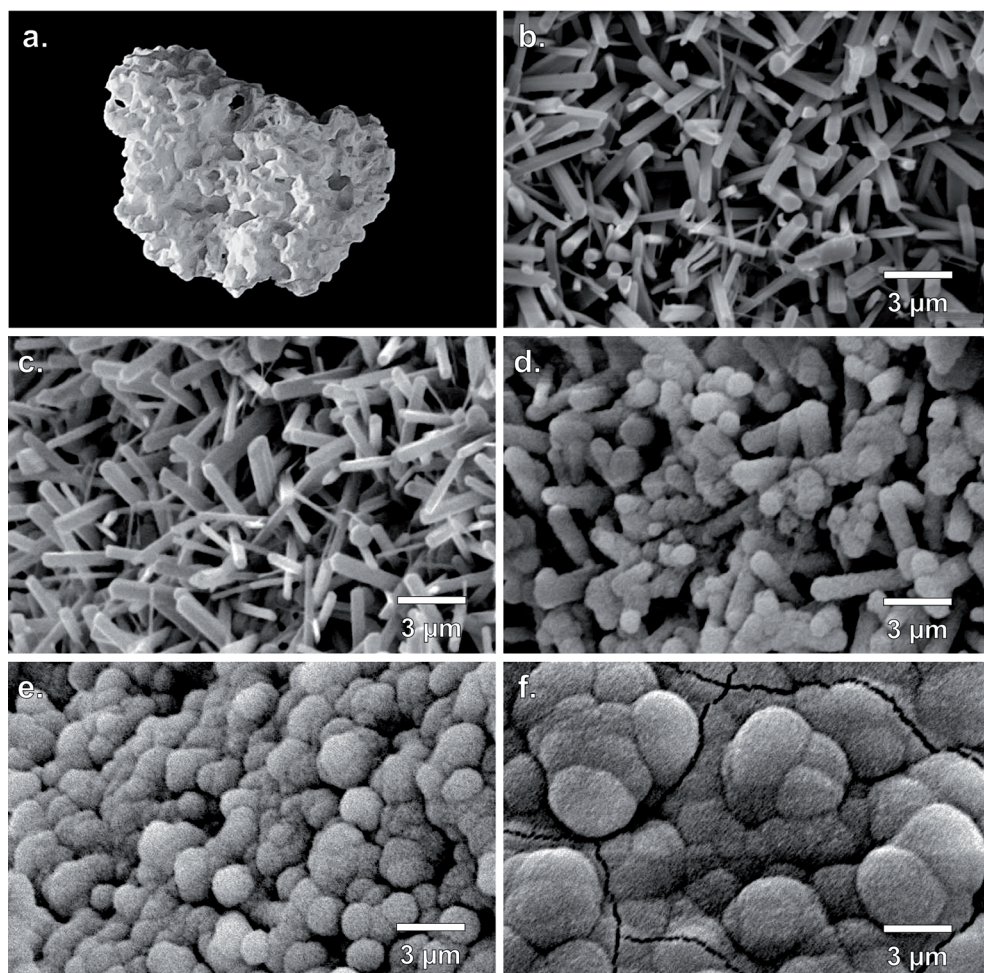


**Figure 1.** (a.) Porous BCP granule of 1-2 mm in size with (b.) submicron surface topography of epitaxial polygon crystals. Submersion in SBF resulted in the progressive formation of an apatite-like mineral layer on the material surface as shown by SEM after (c.) 2 days, (d.) 4 days, (e.) 7 days and (f.) 10 days.

## Micro-CT

Surgery and recovery proceeded without adverse events or adverse reactions to the implant materials. After 6, 12 and 26 weeks, animals were euthanized and the spine and surrounding tissues were harvested. Imaging by micro-CT showed that all graft materials were well-contained at the implantation sites and there was progression to a solid fusion mass between the spine segments over time (Figure 2). At 26 weeks, mature fusion masses were evident and were indicated by incorporation of the graft materials with host bone, and the inability to discriminate individual BCP particles. Evaluation of fusion masses suggested higher fusion mass volumes in the BCP groups at 12 and 26 weeks than with AG, indicating higher graft volume stability with the BCP treatments.

## Manual palpation

Results of fusion assessment by palpation in a blinded manner are presented in Table 1. The data indicate a 100% fusion rate in each group from 12 weeks onwards. No partially fused spines were found by manual palpation. No statistically significant differences in

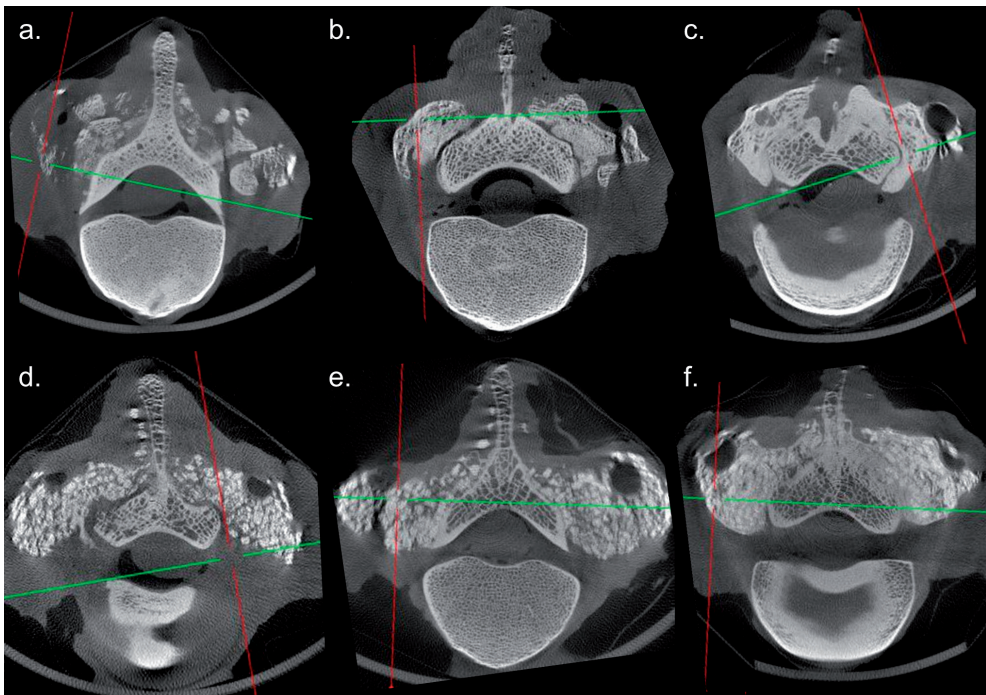


**Figure 2.** Examples of transversal micro-CT slices of the treated spine levels for AG (a-c) and BCP (d-f) at 6 (a,d), 12 (b,e) and 26 (c,f) weeks. During time, consolidation of the fusion mass was evident for all treatments and gradual integration of graft materials with the underlying host bone was observed. Graft volume at 12 and 26 weeks appear higher for BCP treatments than for AG, suggesting a higher graft volume stability for BCP.

**Table 1: Fusion rate by manual palpation**

Time-point	AG	BCP <sub>granules</sub>	BCP <sub>putty</sub>	p value*
6 weeks	3/5	1/5	1/5	0.50
12 weeks	6/6	6/6	6/6	0.99
26 weeks	5/5	5/5	5/5	0.99

\*Fisher-Freeman-Halton Exact Test

fusion between treatments at each time-point were determined (Fisher-Freeman-Halton Exact Test,  $P \geq 0.5$ ).

### Biomechanical evaluations

ROM testing was performed to determine whether treatment resulted in a reduction in mobility between the segments and thus a higher stability, which is the primary goal of spinal fusion. Results of ROM tests are presented in Figure 3. These results show decreasing trends in ROM in lateral bending (LB), flexion-extension (FE) and axial rotation (AR) with no differences between treatment groups. The decrease was strongest in LB for all materials, with an average decrease of  $5.50^\circ \pm 1.59$  between 6 and 26 weeks and statistical significance between 6 weeks and the later time-points (Two-Factor ANOVA,  $P < 0.05$ ). In FE, the average decrease was  $3.60^\circ \pm 1.65$  between 6 and 26 weeks, with significance for AG and BCP<sub>putty</sub>, but not for BCP<sub>granules</sub>. Although the data for AR show a slight decrease in ROM of an average  $1.67^\circ \pm 1.03$  between 6 and 26 weeks, statistical significance was not reached. No statistical differences between graft materials were seen

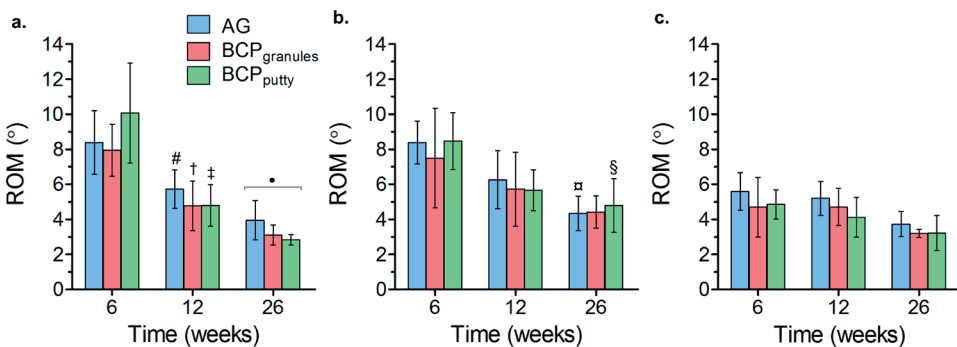


**Figure 3.** Diagrams presenting ROM data of treated segments in LB (a), FE (b) and AR (c). Decrease in ROM over time was evident for each loading direction, with no significant differences between groups. Symbols: # significantly different from AG, 6 weeks ( $p < 0.05$ ); † significantly different from BCP<sub>granules</sub>, 6 weeks ( $p < 0.01$ ); ‡ significantly different from BCP<sub>putty</sub>, 6 weeks ( $p < 0.05$ ); ¶ significantly different from 6 weeks ( $p < 0.001$ ); § significantly different from BCP<sub>putty</sub>, 6 weeks ( $p < 0.05$ ).



in any loading direction at any timepoint, indicating equivalent spinal stability between the positive control, autograft, and the treatment groups, BCP<sub>putty</sub> and BCP<sub>granules</sub>\*

## Histology and histomorphometry

All further evaluations were performed by histology. Presence of a bony fusion between the segments was assessed on sagittal cross-sections of the fusion mass, as presented in Figure 4. The fusion scores are given in Table 2. As the data show, fusion was rarely observed at 6 weeks. However, a steep increase was observed for all treatments at 12 weeks, with fusion rates of 75%, 92% and 83% for AG, BCP<sub>granules</sub> and BCP<sub>putty</sub>, respectively. Specimens of the 26-week endpoint showed a further increase in percentage of segments fused with 90%, 100% and 90% for AG, BCP<sub>granules</sub> and BCP<sub>putty</sub>, respectively. Differences in fusion rate between treatments were not of statistical significance, indicating equivalent performance between the three graft materials (Fisher-Freeman-Halton Exact Test,  $P > 0.05$ ).

**Table 2: Fusion rate by histology**

Time-point	AG			BCP <sub>granules</sub>			BCP <sub>putty</sub>			p value*
	U	B	FR	U	B	FR	U	B	FR	
6 weeks	1/5	0/5	10%	0/5	0/5	0%	0/5	0/5	0%	0.99
12 weeks	1/6	4/6	75%	1/6	5/6	92%	2/6	4/6	83%	0.85
26 weeks	1/5	4/5	90%	0/5	5/5	100%	1/5	4/5	90%	0.99

U: unilateral fusion; B: bilateral fusion; FR: fusion rate; \*Fisher-Freeman-Halton Exact Test

High and low magnification histological sections were examined to evaluate tissues within the fusion mass (Figure 4 and 5). Fibrous tissue and blood vessel infiltration was complete in the central region of the fusion at week 6 in all implants. In addition, bone formation was observed near the host bone bed after 6 weeks in all groups. During the healing period, progression of bone tissue throughout the fusion mass was observed, with an increased proportion of bone at 12 weeks and bone tissue occupying the full range of the fusion mass after 26 weeks. Bone tissue was observed growing directly on BCP material surface, with cuboidal osteoblasts colonizing the material surface and secreting osteoid. Maturation of bone tissue in the fusion mass was indicated by the transition from an early bone phenotype with abundant osteoid, woven bone and fibrous tissue towards a mature bone phenotype at 26 weeks, characterized by a large proportion of lamellar bone and bone marrow. Osteoclast-like multinucleated phagocytes were observed phagocytosing the BCP material indicating the cell-mediated resorption of the implanted material. Gradual degradation of BCP granules was evident by the presence of small particles of BCP separated from larger granules up to the 26-week time point.

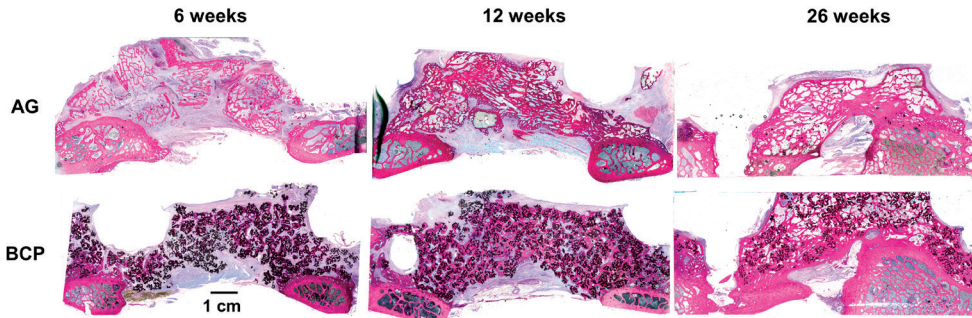


**Figure 4.** Sagittal histological sections (basic fuchsin-methylene blue) of spine levels grafted with AG or BCP, taken from the region between the TP's. These sections were used to score spinal fusion, i.e. the presence of a continuous bone bridge between the adjacent transverse processes. The 6 weeks sections shown on the left were scored as "not fused" whereas 12 and 26 weeks shown in the center and right side were scored as "fused". Fusion by histology was frequently observed from 12 weeks onwards.

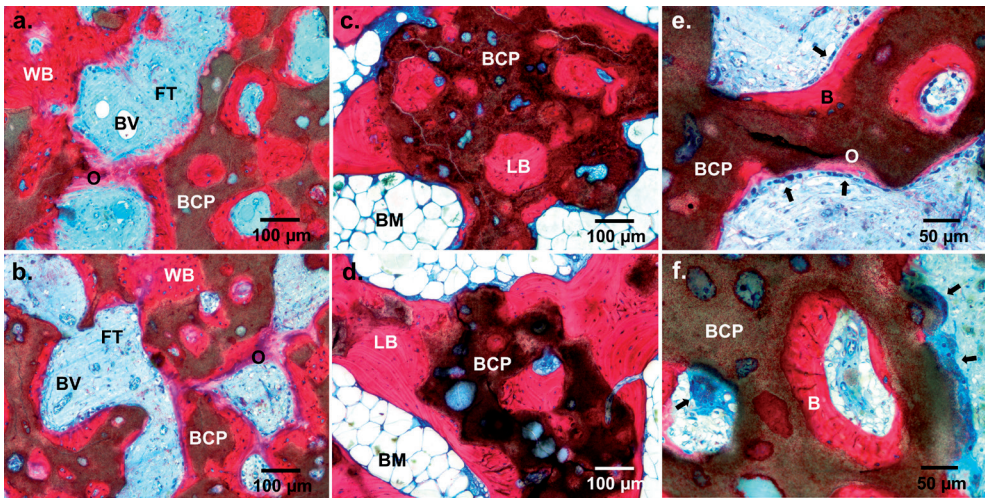


**Figure 5.** High magnification histology (basic fuchsin-methylene blue) of the grafts of levels treated with BCP<sub>granules</sub> (a,c,e) and BCP<sub>putty</sub> (b,d,f). Images show the progression and maturation of bone tissue from 6 weeks (a,b) to 26 weeks (c,d). Less mature bone tissue at 6 weeks is recognized by the presence of abundant fibrous tissue (FT), osteoid (O) and woven bone (WB). New bone tissue was observed forming around the BCP particles (BCP). At 26 weeks, more mature bone was recognized by the presence of lamellar bone (LB) and bone marrow (BM). Cuboidal osteoblasts were observed depositing osteoid directly on the BCP granule surface (e, arrows, 6 weeks). In addition, large multinucleated cells were observed resorbing the BCP material, with internalized fragments of material being apparent (f, arrows, 6 weeks).

Histomorphometry data, represented in Figure 6, are consistent with the general histological observation of the fusion mass. In all groups, the proportion of bone in the fusion mass steadily increased over time in a significant trend ( $P < 0.001$ ), leading up to over 55% of bone after 26 weeks. Between groups, at the 6-week time-point, a higher proportion of bone was determined in the AG group ( $25.2\% \pm 5.0$ ) compared to BCP<sub>granules</sub> ( $14.8\% \pm 7.1$ ,  $P < 0.01$ ) and BCP<sub>putty</sub> ( $14.8\% \pm 7.1$ ,  $P < 0.01$ ), which can be explained by the presence of autologous bone chips that were implanted at the fusion site. After healing periods of 12 and 26 weeks, no differences in bone volume were observed between all treatments ( $P > 0.05$ ).

The proportion of BCP graft in the fusion mass was determined for BCP<sub>granules</sub> and BCP<sub>putty</sub> (Figure 6). As is evident from the graph, a decrease in material volume was determined over time. In both BCP groups, the amount of material in the fusion mass decreased by 25% in the healing period from 6 weeks to 26 weeks, which was confirmed by statistical analysis ( $P < 0.001$ ). No significant difference in material decrease between 6 and 12 weeks was determined for BCP<sub>granules</sub> and BCP<sub>putty</sub>. A slightly higher proportion of BCP graft in the fusion mass was seen for BCP<sub>putty</sub> compared to BCP<sub>granules</sub> at 6 weeks ( $39.7 \pm 4.1\%$  vs  $33.2 \pm 5.7\%$ ,  $P < 0.01$ ) and 26 weeks ( $29.9\% \pm 3.2$  vs  $24.9 \pm 5.0\%$ ,  $P < 0.05$ ).

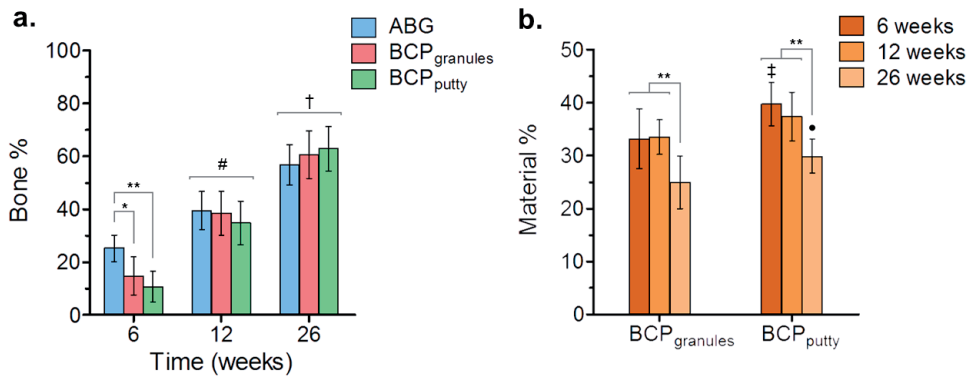


**Figure 6.** Diagrams presenting histomorphometry results of bone tissue **(a)** and BCP material **(b)** in the FM of the treated spine segments. Data are presented as percentage of the available space in a region of interest. A linear increase of bone tissue in the fusion mass during time is evident for all treatments **(a)**. At 6 weeks, a slightly higher percentage of bone is shown for AG, but no differences were observed at later time-points. A decrease in material percentage during time was observed for both BCP treatments **(b)**. A slight difference between BCP<sub>granules</sub> and BCP<sub>putty</sub> is apparent at 6 weeks and 26 weeks. Symbols: \*  $p < 0.01$ ; \*\*  $p < 0.001$ ; # all significantly different from 6 weeks,  $p < 0.001$ ; † all significantly different from 12 weeks and 6 weeks,  $p < 0.001$ ; ‡ significantly different from BCP<sub>granules</sub> 6 weeks,  $p < 0.01$ ; · significantly different from BCP<sub>granules</sub> 26 weeks,  $p < 0.05$ .

## DISCUSSION

---

The posterolateral spine environment is known to be challenging for bone graft substitute materials because it provides very limited contact with host bone from which bone growth can progress. In fact, a successful lumbar arthrodesis is achieved by controlled bone formation through the paraspinous soft tissues in between adjacent TPs[23]. Because of this, materials with physicochemical properties designed to beneficially control the foreign body and wound healing responses may be more effective bone graft substitutes for PLF, as these can promote bone formation in sites distant from native bone through mechanisms other than osteoconduction alone.

Although most commercially available bone grafts have undergone testing in lapine posterolateral fusion studies, only a handful have been tested in higher-order animals such as sheep using posterior pedicle screws and rods. Wheeler et al.[24] compared BCP (Mastergraft; 15% HA / 85%  $\beta$ -TCP) and autograft, and reported 57.1% and 100% fusion respectively at 16 weeks. Bone proportion in the fusion mass at 16 weeks was also significantly lower for the BCP ( $36.2 \pm 3.95$ ) than for autograft ( $55.1 \pm 7.59$ ). In another work, that studied macroporous BCP (MBCP; 65% HA / 35% TCP), Guigui et al.[25] reported that this material achieved fusion after 12 months while fusion by autograft was already observed after 6 months, as was confirmed by biomechanical testing. A third study by Baramki et al.[26] reported high fusion rates for autograft and interconnected porous HA after 20 weeks, but mechanical tests revealed poorer outcomes for the HA group. In the absence of posterior fixation,  $\beta$ -TCP alone has also shown inferior performance to autograft[27]. Other studies have reported more favorable outcomes for ceramics compared to autograft in this model[28–30], although certain limitations to those studies are evident when compared to the current work. First of all, fusion assessment by radiography (i.e. X-ray and  $\mu$ CT) for evaluation of calcium phosphate grafts is inconclusive and leads to overestimations, because the high radiopacity of calcium phosphate limits the ability to distinguish bone from material[31–33]. Since the formation of bone tissue is crucial for a successful spinal fusion, fusion assessment by histology is a more accurate and reliable indicator than radiographic assessment. Moreover, studies described in the prior art lacked internal references for mechanical testing (e.g. multiple time-points) and reported equivalent spinal fusion with autograft or ceramics at 16 weeks or later. Lastly, the age of the animal is often reported as 'skeletally mature' rather than the specific age or range. This is important, as fusion rates drop considerably for 5 year old ewes[34] as compared to 2-3 year old ewes[35], both of which are skeletally mature. The 4-5 year old sheep used in the present study present an additional relevant challenge for the graft to overcome.

In the current work, by a combination of histological fusion data and mechanical data (i.e. manual palpation and ROM testing) at multiple time-points, we demonstrated high spinal fusion success and equivalence to autograft as early as 12 weeks post-surgery by this BCP with submicron surface topography in both granule and putty form. Both BCP formulations showed equivalent and sustained efficacy for each endpoint, which indicates that the polymeric binder did not inhibit bone-healing performance of the granules. This is in line with expectations, since the binder was designed to rapidly dissolve after implantation and consists of a biologically inert composition. Although By histomorphometry at 6 weeks, levels treated with autograft showed a slightly but significantly larger proportion of bone tissue in the fusion mass, which may be explained by grafted autologous bone chips being included in the measurement of newly formed bone. Although manual palpation results suggest a higher fusion rate with autograft at 6 weeks (non-significant), the ROM and histological fusion data indicate similar healing progress between BCP treatments and autograft at the earliest time-point.

In comparison to previous studies, which show either an inferiority of calcium phosphates compared to autograft or equivalence evidenced through weaker endpoints, we demonstrate equivalent performance of AG, BCP<sub>granules</sub> and BCP<sub>putty</sub> by an array of strong assessment methods. In clinical literature, we can find conflicting evidence about the efficacy of calcium phosphate materials as bone graft materials for spine fusion[36,37]. Physicochemical properties of biomaterials are rarely discussed in clinical literature and it is often overlooked that these properties strongly influence the performance of calcium phosphate bone graft materials. Indeed, during preclinical *in vivo* studies, grafts with optimized physicochemical properties have presented better outcomes than those with suboptimal properties. For instance, calcium phosphate phase composition[38–43], macro-porosity[44–50] (i.e. macro-pore size and interconnectivity) and bioactivity[51] have been directly related to the *in vivo* tissue response, neovascularization and bone-forming potential in ectopic and orthotopic sites[40–43]. Moreover, presence of a submicron surface topography and micro-porosity has been linked to substantially enhanced bone-inducing properties of calcium phosphates[6,7].

One of the current hypotheses on the effectiveness of calcium phosphates with submicron topography involves the polarization of macrophages. Macrophages play a key role in the foreign body response and their reaction to medical implants is pivotal for the success or failure of an implant after implantation[52]. Being of a plastic nature, uncommitted macrophages can polarize towards a pro-inflammatory phenotype (M1) or anti-inflammatory phenotype (M2) in response to external triggers, including tissue damage or the implantation of a biomaterial [13,53]. Studies have suggested that an increase in anti-inflammatory M2 macrophages following an initial phase of M1-dominated inflammation results in enhanced vascularization and osteogenesis[14,15]. Moreover,



the surface properties of biomaterials have been demonstrated to influence macrophage phenotype after implantation[9–11] and recently, calcium phosphates with a submicron surface topography were shown to promote the transition of macrophages to the M2 phenotype *in vitro*[8]. The upregulation of M2 macrophages by submicron structured calcium phosphates may explain the enhanced angiogenesis and superior bone healing properties observed with these materials *in vivo*[6–8], including as well as the results obtained in the current work. However, the techniques used in the current study to assess bone formation and spinal fusion were not designed for macrophage characterization. The proposed mechanism remains to be further experimentally verified in future studies.

A limitation of the current study is that no materials with different surface topographies were compared. Therefore, a recommendation for future studies in this model is to include materials with no surface topography or with surface topographies of different geometries and dimensions (i.e. supermicron scale), in order to isolate the role of material surface topography on efficacy. In addition, with regard to mechanical testing, inclusion of a sham or “empty” control (i.e. no graft material) and baseline measurements immediately after surgery would provide more insight on the effect of spinal fusion by these graft materials on spine ROM.

We may conclude that this study provides solid evidence of the adequate performance of a BCP with tailored physicochemistry as stand-alone alternative to autograft in the clinically relevant *Ovine* model of PLF. By application of reliable fusion assessment by histology and supporting analyses at relevant time-points, we demonstrated a high fusion rate after 12 weeks for this material, with overall equivalence to autograft in fusion rate, mechanical integrity and bone formation over the entire healing period of 26 weeks. These findings support the premise that calcium phosphates with a submicron surface topography are highly effective bone graft substitutes for PLF and this justifies further clinical investigation of these materials.

## **ACKNOWLEDGEMENTS**

This study was supported by the European Union's Horizon 2020 research and innovation program (grant agreement no. 674282) and Kuros Biosciences BV. LvD, RD, XL, DB, FBdG, HY and JdB are employees or former employees of Kuros Biosciences BV. HY and JdB are stockholders of Kuros Biosciences BV.

## REFERENCES

- [1] Millennium Research Group, Orthopedic Biomaterials | Medtech 360 | Market Analysis | US | 2017, Toronto, 2016.
- [2] W.C. Pannell, D.D. Savin, T.P. Scott, J.C. Wang, M.D. Daubs, Trends in the surgical treatment of lumbar spine disease in the United States, *Spine J.* 15 (2015) 1719–1727. <https://doi.org/10.1016/j.spinee.2013.10.014>.
- [3] E.J. Carragee, G.C. Comer, M.W. Smith, Local bone graft harvesting and volumes in posterolateral lumbar fusion: A technical report, *Spine J.* 11 (2011) 540–544. <https://doi.org/10.1016/j.spinee.2011.02.014>.
- [4] K.M. Scheufler, D. Diesing, Einsatz von Knochenersatzmaterialien bei Fusionen der Wirbelsäule, *Orthopade.* 44 (2015) 146–153. <https://doi.org/10.1007/s00132-014-3069-5>.
- [5] S. V. Dorozhkin, Calcium orthophosphate-based bioceramics, *Materials (Basel).* 6 (2013) 3840–3942. <https://doi.org/10.3390/ma6093840>.
- [6] P. Habibovic, H. Yuan, M. van den Doel, T.M. Sees, C.A. van Blitterswijk, K. de Groot, Relevance of osteoinductive biomaterials in critical-sized orthotopic defect, *J. Orthop. Res.* 24 (2006) 867–876. <https://doi.org/10.1002/jor.20115>.
- [7] H. Yuan, H. Fernandes, P. Habibovic, J. De Boer, A.M.C. Barradas, A. De Ruiter, W.R. Walsh, C.A. Van Blitterswijk, J.D. De Bruijn, Osteoinductive ceramics as a synthetic alternative to autologous bone grafting, *Proc. Natl. Acad. Sci. U. S. A.* 107 (2010) 13614–13619. <https://doi.org/10.1073/pnas.1003600107>.
- [8] R. Duan, Y. Zhang, L.A. van Dijk, D. Barbieri, F. de Groot, J.D. de Bruijn, J.J.P. van den Beucken, Y. Huipin, Relation Between Macrophage Differentiation, Angiogenesis and Topology-Directed Osteoinduction of Calcium Phosphate Ceramics., in: *Pap. Present. 64th Annu. Meet. Orthop. Res. Soc. March 10-13, 2018; New Orleans, LA., 2018.*
- [9] K.M. Hotchkiss, G.B. Reddy, S.L. Hyzy, Z. Schwartz, B.D. Boyan, R. Olivares-Navarrete, Titanium surface characteristics, including topography and wettability, alter macrophage activation, *Acta Biomater.* 31 (2016) 425–434. <https://doi.org/10.1016/j.actbio.2015.12.003>.
- [10] T.U. Luu, S.C. Gott, B.W.K. Woo, M.P. Rao, W.F. Liu, Micro- and Nanopatterned Topographical Cues for Regulating Macrophage Cell Shape and Phenotype, *ACS Appl. Mater. Interfaces.* 7 (2015) 28665–28672. <https://doi.org/10.1021/acsami.5b10589>.
- [11] P.C.S. Bota, A.M.B. Collie, P. Puolakkainen, R.B. Vernon, E.H. Sage, B.D. Ratner, P.S. Stayton, Biomaterial topography alters healing in vivo and monocyte/macrophage activation in vitro, *J. Biomed. Mater. Res.–Part A.* 95 A (2010) 649–657. <https://doi.org/10.1002/jbm.a.32893>.
- [12] P. Italiani, D. Boraschi, From monocytes to M1/M2 macrophages: Phenotypical vs. functional differentiation, *Front. Immunol.* 5 (2014). <https://doi.org/10.3389/fimmu.2014.00514>.
- [13] R. Klopfleisch, Macrophage reaction against biomaterials in the mouse model – Phenotypes, functions and markers, *Acta Biomater.* 43 (2016) 3–13. <https://doi.org/10.1016/j.actbio.2016.07.003>.



- [14] F. Loi, L.A. Córdova, R. Zhang, J. Pajarinen, T.H. Lin, S.B. Goodman, Z. Yao, The effects of immunomodulation by macrophage subsets on osteogenesis in vitro, *Stem Cell Res. Ther.* 7 (2016) 15. <https://doi.org/10.1186/s13287-016-0276-5>.
- [15] K.L. Spiller, S. Nassiri, C.E. Witherell, R.R. Anfang, J. Ng, K.R. Nakazawa, T. Yu, G. Vunjak-Novakovic, Sequential delivery of immunomodulatory cytokines to facilitate the M1-to-M2 transition of macrophages and enhance vascularization of bone scaffolds, *Biomaterials.* 37 (2015) 194–207. <https://doi.org/10.1016/j.biomaterials.2014.10.017>.
- [16] A.I. Pearce, R.G. Richards, S. Milz, E. Schneider, S.G. Pearce, Animal models for implant biomaterial research in bone: A review, *Eur. Cells Mater.* 13 (2007) 1–10. <https://doi.org/10.22203/eCM.v013a01>.
- [17] M. Mageed, D. Berner, H. Jülke, C. Hohaus, W. Brehm, K. Gerlach, Is sheep lumbar spine a suitable alternative model for human spinal researches? Morphometrical comparison study, *Lab. Anim. Res.* 29 (2013) 183. <https://doi.org/10.5625/lar.2013.29.4.183>.
- [18] M. Kanayama, B.W. Cunningham, T.J.C. Setter, J.A. Goldstein, G. Stewart, K. Kaneda, P.C. McAfee, Does spinal instrumentation influence the healing process of posterolateral spinal fusion? An in vivo animal model, *Spine (Phila. Pa. 1976).* 24 (1999) 1058–1065. <https://doi.org/10.1097/00007632-199906010-00003>.
- [19] F. Barrère-de Groot, D. Barbieri, D.W. Grijpma, J.D. de Bruijn, United States Patent No. US2018/0028720A1, Anhydrous Biocompatible Composite Materials, US2018/0028720A1, 2018.
- [20] T. Kokubo, S. Ito, Z.T. Huang, T. Hayashi, S. Sakka, T. Kitsugi, T. Yamamuro, Ca, P-rich layer formed on high-strength bioactive glass-ceramic A-W, *J. Biomed. Mater. Res.* 24 (1990) 331–343. <https://doi.org/10.1002/jbm.820240306>.
- [21] M. Kanayama, B.W. Cunningham, J.C. Weis, L.M. Parker, K. Kaneda, P.C. McAfee, Maturation of the posterolateral spinal fusion and its effect on load-sharing of spinal instrumentation, *J. Bone Jt. Surg.-Ser. A.* 79 (1997) 1710–1720. <https://doi.org/10.2106/00004623-199711000-00013>.
- [22] W.R. Walsh, J. Harrison, A. Loeffler, T. Martin, D. Van Sickle, M.K.C. Brown, D.H. Sonnabend, Mechanical and histologic evaluation of Collagraft® in an ovine lumbar fusion model, *Clin. Orthop. Relat. Res.* (2000) 258–266. <https://doi.org/10.1097/00003086-200006000-00031>.
- [23] M.R. Foster, M.J. Allen, J.E. Schoonmaker, H.A. Yuan, A. Kanazawa, S.A. Park, B. Liu, Characterization of a developing lumbar arthrodesis in a sheep model with quantitative instability, *Spine J.* 2 (2002) 244–250. [https://doi.org/10.1016/S1529-9430\(02\)00189-4](https://doi.org/10.1016/S1529-9430(02)00189-4).
- [24] D.L. Wheeler, J.M. Lane, H.B. Seim, C.M. Puttlitz, S. Itescu, A.S. Turner, Allogeneic mesenchymal progenitor cells for posterolateral lumbar spine fusion in sheep, *Spine J.* 14 (2014) 435–444. <https://doi.org/10.1016/j.spinee.2013.09.048>.
- [25] P. Guigui, P. Hardouin, Évaluation Histologique Et Biomécanique D'Une Arthrodèse Postérolatérale Utilisant Comme Substitut Osseux Une Céramique Biphase De Phosphate De Calcium. Étude Expérimentale Chez Le Mouton, *Bull. Acad. Natl. Med.* 184 (2000) 403–414. <http://www.embase.com/search/results?subaction=viewrecord&from=export&id=L31367943%5Cnhttp://findit.library.jhu.edu/resolve?sid=>



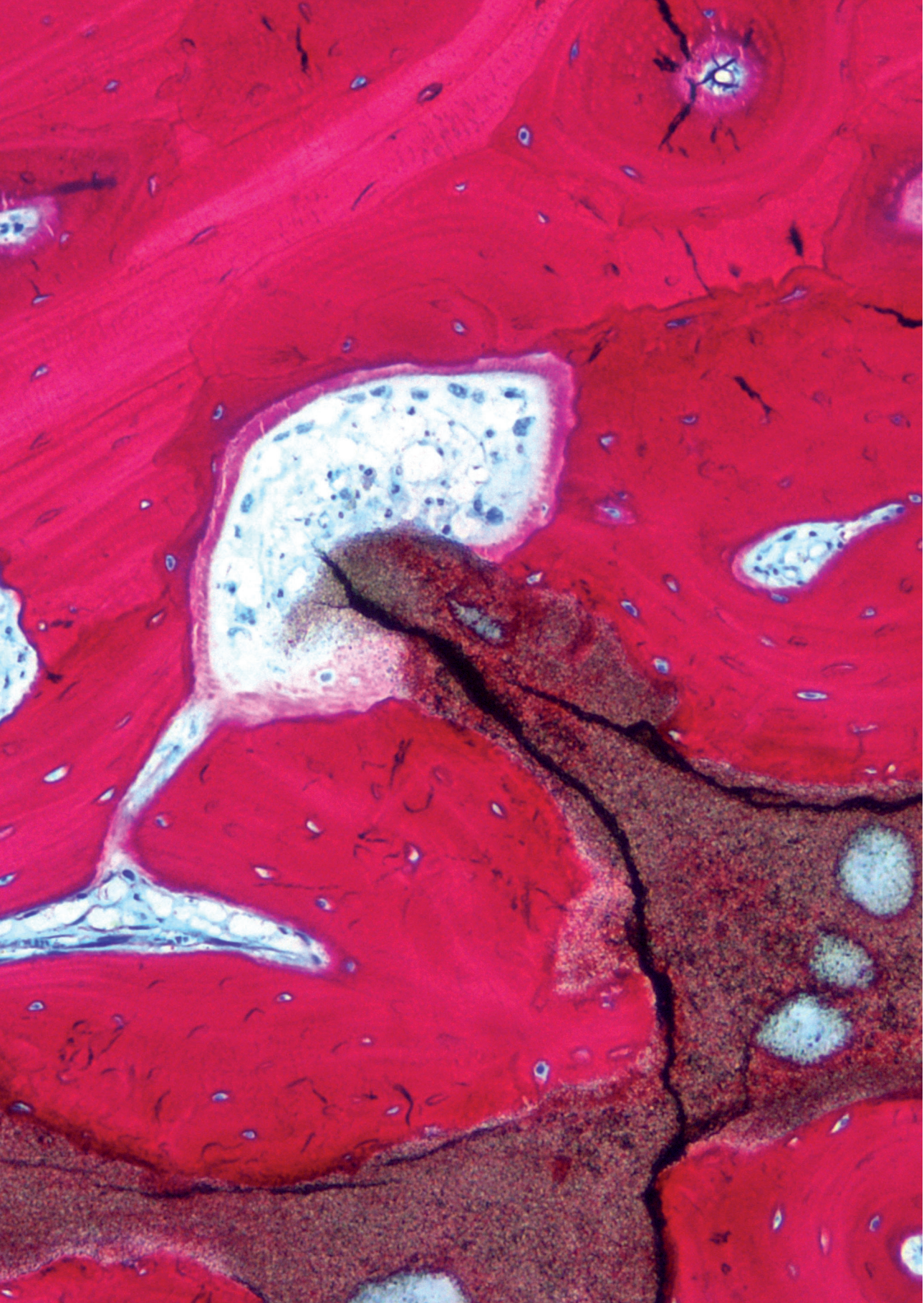
- EMBASE&issn=00014079&id=doi:&atitle=Histologic+and+biomechanic+evaluation +of+posterolateral+arthrodesis+using+a+biphasic+cerami.
- [26] H.G. Baramki, T. Steffen, P. Lander, M. Chang, D. Marchesi, The efficacy of interconnected porous hydroxyapatite in achieving posterolateral lumbar fusion in sheep, *Spine (Phila. Pa. 1976)*. 25 (2000) 1053–1060. <https://doi.org/10.1097/00007632-200005010-00003>.
- [27] M.H. Pelletier, R.A. Oliver, C. Christou, Y. Yu, N. Bertollo, H. Irie, W.R. Walsh, Lumbar spinal fusion with  $\beta$ -TCP granules and variable *Escherichia coli*-derived rhBMP-2 dose, *Spine J.* 14 (2014) 1758–1768. <https://doi.org/10.1016/j.spinee.2014.01.043>.
- [28] P. Guigui, P.Y. Plais, B. Flautre, E. Viguier, M.C. Blary, D. Chopin, F. Lavaste, P. Hardouin, Experimental model of posterolateral spinal arthrodesis in sheep: Part 2. application of the model: Evaluation of vertebral fusion obtained with coral (porites) or with a biphasic ceramic (triosite), *Spine (Phila. Pa. 1976)*. 19 (1994) 2798–2803. <https://doi.org/10.1097/00007632-199412150-00012>.
- [29] D.L. Wheeler, L.G. Jenis, M.E. Kovach, J. Marini, A.S. Turner, Efficacy of silicated calcium phosphate graft in posterolateral lumbar fusion in sheep, *Spine J.* 7 (2007) 308–317. <https://doi.org/10.1016/j.spinee.2006.01.005>.
- [30] D. Delawi, M.C. Kruyt, Y. Huipin, K.L. Vincken, J.D. De Bruijn, F.C. Oner, W.J.A. Dhert, Comparing autograft, allograft, and tricalcium phosphate ceramic in a goat instrumented posterolateral fusion model, *Tissue Eng.–Part C Methods*. 19 (2013) 821–828. <https://doi.org/10.1089/ten.tec.2012.0576>.
- [31] A.E. Brodsky, E.S. Kovalsky, M.A. Khalil, Correlation of radiologic assessment of lumbar spine fusions with surgical exploration, *Spine (Phila. Pa. 1976)*. 16 (1991) S261–S265. <https://doi.org/10.1097/00007632-199106001-00017>.
- [32] C. Goldstein, B. Drew, When is a spine fused?, *Injury*. 42 (2011) 306–313. <https://doi.org/10.1016/j.injury.2010.11.041>.
- [33] L.Y. Carreon, M. Djurasovic, S.D. Glassman, P. Sailer, Diagnostic accuracy and reliability of fine-cut CT scans with reconstructions to determine the status of an instrumented posterolateral fusion with surgical exploration as reference standard, *Spine (Phila. Pa. 1976)*. 32 (2007) 892–895. <https://doi.org/10.1097/01.brs.0000259808.47104.dd>.
- [34] Y. Kotani, B.W. Cunningham, A. Cappuccino, K. Kaneda, P.C. McAfee, The role of spinal instrumentation in augmenting lumbar posterolateral fusion, *Spine (Phila. Pa. 1976)*. 21 (1996) 278–287. <https://doi.org/10.1097/00007632-199602010-00005>.
- [35] W.R. Walsh, A. Loeffler, S. Nicklin, D. Arm, R.E. Stanford, Y. Yu, R. Harris, R.M. Gillies, Spinal fusion using an autologous growth factor gel and a porous resorbable ceramic, *Eur. Spine J.* 13 (2004) 359–366. <https://doi.org/10.1007/s00586-003-0597-9>.
- [36] K.A.M. Alsaleh, C.A. Tougas, D.M. Roffey, E.K. Wai, Osteoconductive bone graft extenders in posterolateral thoracolumbar spinal fusion: A systematic review, *Spine (Phila. Pa. 1976)*. 37 (2012). <https://doi.org/10.1097/BRS.0b013e3182518859>.



- [37] A. Kadam, P.W. Millhouse, C.K. Kepler, K.E. Radcliff, M.G. Fehlings, M.E. Janssen, R.C. Sasso, J.J. Benedict, A.R. Vaccaro, Bone substitutes and expanders in spine surgery: A review of their fusion efficacies, *Int. J. Spine Surg.* 10 (2016). <https://doi.org/10.14444/3033>.
- [38] S. Ghanaati, M. Barbeck, R. Detsch, U. Deisinger, U. Hilbig, V. Rausch, R. Sader, R.E. Unger, G. Ziegler, C.J. Kirkpatrick, The chemical composition of synthetic bone substitutes influences tissue reactions in vivo: Histological and histomorphometrical analysis of the cellular inflammatory response to hydroxyapatite, beta-tricalcium phosphate and biphasic calcium phosphate cer, *Biomed. Mater.* 7 (2012) 15005. <https://doi.org/10.1088/1748-6041/7/1/015005>.
- [39] Y. Chen, J. Wang, X.D. Zhu, Z.R. Tang, X. Yang, Y.F. Tan, Y.J. Fan, X.D. Zhang, Enhanced effect of  $\beta$ -tricalcium phosphate phase on neovascularization of porous calcium phosphate ceramics: In vitro and in vivo evidence, *Acta Biomater.* 11 (2015) 435–448. <https://doi.org/10.1016/j.actbio.2014.09.028>.
- [40] H. Yuan, C.A. Van Blitterswijk, K. De Groot, J.D. De Bruijn, A comparison of bone formation in biphasic calcium phosphate (BCP) and hydroxyapatite (HA) implanted in muscle and bone of dogs at different time periods, *J. Biomed. Mater. Res.–Part A.* 78 (2006) 139–147. <https://doi.org/10.1002/jbm.a.30707>.
- [41] L. Chen, Y. Xu, J. Zhao, Z. Zhang, R. Yang, J. Xie, X. Liu, S. Qi, Conditioned medium from hypoxic bone marrow-derived mesenchymal stem cells enhances wound healing in mice, *PLoS One.* 9 (2014) e96161. <https://doi.org/10.1371/journal.pone.0096161>.
- [42] N.M. Fariña, F.M. Guzón, M.L. Peña, A.G. Cantalapiedra, In vivo behaviour of two different biphasic ceramic implanted in mandibular bone of dogs, in: *J. Mater. Sci. Mater. Med.*, 2008: pp. 1565–1573. <https://doi.org/10.1007/s10856-008-3400-y>.
- [43] S.S. Jensen, M.M. Bornstein, M. Dard, D.D. Bosshardt, D. Buser, Comparative study of biphasic calcium phosphates with different HA/TCP ratios in mandibular bone defects. A long-term histomorphometric study in minipigs, *J. Biomed. Mater. Res.–Part B Appl. Biomater.* 90 B (2009) 171–181. <https://doi.org/10.1002/jbm.b.31271>.
- [44] O. Gauthier, J.M. Bouler, E. Aguado, P. Pilet, G. Daculsi, Macroporous biphasic calcium phosphate ceramics: Influence of macropore diameter and macroporosity percentage on bone ingrowth, *Biomaterials.* 19 (1998) 133–139. [https://doi.org/10.1016/S0142-9612\(97\)00180-4](https://doi.org/10.1016/S0142-9612(97)00180-4).
- [45] F.M. Klenke, Y. Liu, H. Yuan, E.B. Hunziker, K.A. Siebenrock, W. Hofstetter, Impact of pore size on the vascularization and osseointegration of ceramic bone substitutes in vivo, *J. Biomed. Mater. Res.–Part A.* 85 (2008) 777–786. <https://doi.org/10.1002/jbm.a.31559>.
- [46] L. Galois, D. Mainard, Bone ingrowth into two porous ceramics with different pore sizes: An experimental study, *Acta Orthop. Belg.* 70 (2004) 598–603.
- [47] J. Li, W. Zhi, T. Xu, F. Shi, K. Duan, J. Wang, Y. Mu, J. Weng, Ectopic osteogenesis and angiogenesis regulated by porous architecture of hydroxyapatite scaffolds with similar interconnecting structure in vivo, *Regen. Biomater.* 3 (2016) 285–297. <https://doi.org/10.1093/rb/rbw031>.
- [48] M. Mastrogiacomo, S. Scaglione, R. Martinetti, L. Dolcini, F. Beltrame, R. Cancedda, R. Quarto, Role of scaffold internal structure on in vivo bone formation in macroporous calcium

- phosphate bioceramics, *Biomaterials*. 27 (2006) 3230–3237. <https://doi.org/10.1016/j.biomaterials.2006.01.031>.
- [49] P.S. Eggli, W. Muller, R.K. Schenk, Porous hydroxyapatite and tricalcium phosphate cylinders with two different pore size ranges implanted in the cancellous bone of rabbits. A comparative histomorphometric and histologic study of bone ingrowth and implant substitution, *Clin. Orthop. Relat. Res.* (1988) 127–138. <https://doi.org/10.1097/00003086-198807000-00017>.
- [50] F. Bai, Z. Wang, J. Lu, J. Liu, G. Chen, R. Lv, J. Wang, K. Lin, J. Zhang, X. Huang, The correlation between the internal structure and vascularization of controllable porous bioceramic materials in vivo: A quantitative study, *Tissue Eng.-Part A*. 16 (2010) 3791–3803. <https://doi.org/10.1089/ten.tea.2010.0148>.
- [51] M. Kobayashi, T. Nakamura, Y. Okada, A. Fukumoto, T. Furukawa, H. Kato, T. Kokubo, T. Kikutani, Bioactive bone cement: Comparison of apatite and wollastonite containing glass-ceramic, hydroxyapatite, and  $\beta$ -tricalcium phosphate fillers on bone- bonding strength, *J. Biomed. Mater. Res.* 42 (1998) 223–237. [https://doi.org/10.1002/\(SICI\)1097-4636\(199811\)42:2<223::AID-JBM7>3.0.CO;2-R](https://doi.org/10.1002/(SICI)1097-4636(199811)42:2<223::AID-JBM7>3.0.CO;2-R).
- [52] M.E. Ogle, C.E. Segar, S. Sridhar, E.A. Botchwey, Monocytes and macrophages in tissue repair: Implications for immunoregenerative biomaterial design, *Exp. Biol. Med.* 241 (2016) 1084–1097. <https://doi.org/10.1177/1535370216650293>.
- [53] P.J. Murray, J.E. Allen, S.K. Biswas, E.A. Fisher, D.W. Gilroy, S. Goerdt, S. Gordon, J.A. Hamilton, L.B. Ivashkiv, T. Lawrence, M. Locati, A. Mantovani, F.O. Martinez, J.L. Mege, D.M. Mosser, G. Natoli, J.P. Saeij, J.L. Schultze, K.A. Shirey, A. Sica, J. Suttles, I. Udalova, J.A. vanGinderachter, S.N. Vogel, T.A. Wynn, Macrophage Activation and Polarization: Nomenclature and Experimental Guidelines, *Immunity*. 41 (2014) 14–20. <https://doi.org/10.1016/j.immuni.2014.06.008>.





# CHAPTER 5

## **MAGNETOS, VITOSS, AND NOVABONE IN A MULTI-ENDPOINT STUDY OF POSTEROLATERAL FUSION: A TRUE FUSION OR NOT?**

---

Lukas A. van Dijk  
Florence Barrère-de Groot  
Antoine J.W.P. Rosenberg  
Matthew Pelletier  
Chris Christou  
Joost D. de Bruijn  
William R. Walsh

*Clinical Spine Surgery, 2020, 33(6):E276-E287*



## INTRODUCTION

---

Spinal fusion procedures involve the use of bone grafts to mechanically and biologically conjoin two or more consecutive spinal segments. Posterolateral spinal fusion (PLF) is one of the more challenging bone grafting indications performed clinically, because it requires the formation of a large, consolidated bone mass through the paraspinous soft tissues with limited host bone contact. To avoid adverse effects related to harvesting of iliac crest-derived bone graft[1], synthetic bone graft materials are used as extenders or substitutes of autograft bone. Numerous synthetic bone grafts are available on the market, of which many are based on calcium phosphate and bioactive glass[2,3]. Calcium phosphate materials are suitable bone graft materials due to their similar composition and structure to mineralized inorganic bone matrix, which facilitates excellent osteoconductive and bone-bonding properties[4]. Besides this, specific surface characteristics of calcium phosphates have been shown to strongly affect bone regeneration *in vivo*. Submicron size and morphology of calcium phosphate surface features have been linked to an ability to induce bone formation in tissues distant from host bone without the addition of stem cells or growth factors, resulting in enhanced performance in orthotopic sites[5–9]. Bioactive glasses have been shown to release ionic dissolution products that can stimulate the activity of osteogenic cells *in vitro*[10–12], termed osteostimulation. Bioactive glasses have also been shown to elicit deposition of a crystalline calcium phosphate surface layer in simulated body fluid[13,14], which has been related to osteoconduction and strong bone-bonding *in vivo*[15,16]. Although different types of bioactive glass have been studied in recent years, 45S5 bioactive glass (i.e. Bioglass) developed by Hench et al. has been most well-known as a bone graft substitute material[3].

The selection of the most appropriate bone graft for PLF may be challenging for surgeons, because preclinical studies on these materials have mostly been performed in non-clinically relevant models. Only few studies have compared materials from different classes of synthetic bone grafts (e.g. calcium phosphate, Bioglass) in spinal fusion models *in vivo*. However, side-by-side comparison of such materials in well-designed, clinically relevant animal models could provide valuable insights that could aid surgeons in the selection of treatment options for spinal surgery.

Recently, this research team demonstrated equivalent performance between a calcium phosphate with submicron topography and the gold standard, autograft, in clinically relevant animal models of posterolateral spinal fusion[17,18]. One of these studies involved a challenging *Ovine* model of instrumented PLF with implantation as a standalone bone graft. In the current work, this *Ovine* PLF model was again utilized to compare three commercially available bone grafts based on calcium phosphate and 45S5 Bioglass. The

groups included were (1) a putty formulation of BCP (biphasic calcium phosphate) with submicron surface topography, previously shown to have equivalent performance to autograft in this model[17,18], (2) a putty formulation of 45S5 bioactive glass, (3) a collagen- $\beta$ -tricalcium phosphate ( $\beta$ TCP) composite with a 45S5 bioactive glass adjunct. Autograft bone (AB) was included as the “gold standard” reference treatment. Twelve weeks following implantation, the treated segments were evaluated by a range of assessment methods, including fusion assessment (manual palpation, X-ray, micro-CT and histology), biomechanical range of motion (ROM) testing, fusion mass volume quantification (micro-CT), histological evaluation of tissue responses and histomorphometry of bone tissue and residual graft material.

## METHODS

### Materials

Three commercially available bone grafts were examined in this study. The submicron structured biphasic calcium phosphate bone graft was provided in putty formulation (BCP<sub><sub>µm</sub></sub>; MagnetOs Putty, Kuros Biosciences BV, NL). This formulation contained 1–2 mm calcium phosphate granules with a submicron surface topography[6] and a phase composition of 65–75%  $\beta$ TCP and 25–35% hydroxyapatite (HA), embedded in a fast-resorbing polymer carrier. The polymer carrier consisted of polyethylene glycol (PEG) and L-lactide monomer and occupied the granule pores and intergranular space. MagnetOs Putty is currently not labeled for use as standalone bone graft in spinal fusion surgery in the United States.

The bioactive glass-based bone graft was a putty formulation (BG; Novabone Putty, Novabone Products LLC, USA) and consisted of  $\pm 70$  v/v% bioactive glass (45S5) particles of 32–710  $\mu$ m in a water-soluble carrier of PEG and glycerine. 45S5 bioactive glass is composed of  $\pm 45\%$  silica ( $\text{SiO}_2$ ), 24.5% calcium oxide (CaO), 24.5% sodium oxide ( $\text{Na}_2\text{O}$ ) and 6% phosphorous pentoxide ( $\text{P}_2\text{O}_5$ ) (wt%)[15].

The collagen- $\beta$ TCP composite with 45S5 Bioglass (TCP/BG; Vitoss BA2X Foam pack, Orthovita, Inc) was comprised of a bovine type I collagen carrier containing  $\beta$ TCP particles ( $\geq 95$ –100%  $\beta$ TCP) of 1–4 mm, with a separate vial of 1.5 g 45S5 bioactive glass particles of 90 – 150  $\mu$ m. The implant was prepared according to the instructions for use. In short, the bioactive glass particles were loaded onto the collagen- $\beta$ TCP composite, after which physiological saline was added and the composite was thoroughly mixed. The final composition of the graft was  $\pm 55\%$   $\beta$ TCP, 27% 45S5 and 18% collagen (wt%).



## Animal study

A previously described *Ovine* model of two-level instrumented posterolateral spinal fusion (PLF) was used in this study[18]. Nine (9) female, skeletally mature sheep (*Ovis Aries*, Border Leicester Merino Cross, 4-5 years, 80-90 kg) were used at the University of New South Wales, Australia following approval from the local Animal Care and Ethics Committee (ACEC). The animals were randomly allocated treatments at levels L2-L3 and L4-L5 according to a randomization scheme, with n=6 for AB, n=6 for BCP<sub>sum</sub>, n=3 for BG and n=3 for TCP/BG. After administration of appropriate antibiotics, analgesics and anaesthetics, surgery was performed as previously described[18]. In brief, the animal was positioned in sternal recumbency and draped using sterile technique. The correct levels were identified and marked pre-operatively using fluoroscopy. A skin incision was made in the dorsal midline, after which facet joints and transverse processes (TPs) for the relevant levels were exposed and decorticated. The two operative levels (L2-L3 and L4-L5) were instrumented bilaterally with polyaxial pedicle screws (Ø 5.5mm x 25 mm) and solid titanium rods (Ø 5.5mm). Thereafter, two single-level posterolateral arthrodeses were performed at the exposed levels. For each graft material, 10 cc of material was placed into both posterolateral gutters (20 cc total per level) at the appropriate level in direct apposition with the decorticated TPs, spanning the intertransverse process space. Corticancellous autograft was obtained from the bilateral *Osi Iliums* using rongeurs. after removal of the cortex. Autograft was reduced to 2-5 mm bone chips which were mixed to obtain a 1:1 ratio of both donor sites. The surgical sites were closed in layers. Post-operatively, the animals were monitored and received proper post-operative care, antibiotics and analgesics. At 12 weeks follow-up, animals were anaesthetized and euthanized by lethal injection of Lethobarb (325 mg/2 kg i.v.). The lumbar spines were excised and harvested for endpoint analyses.

## Manual Palpation

Directly after harvesting of the spines and removal of the pedicle rods two trained observers assessed fusion rigidity of the treated spinal levels in a blinded manner by manual palpation, as previously described[19]. All levels were graded as fused (rigid, low mobility) or not fused (not rigid, high mobility) in lateral bending (LB) and flexion-extension (FE), with an untreated level used as a relative comparison.

## Radiography

### Faxitron

Harvested spines were radiographed in the posteroanterior plane using a Faxitron (Faxitron Bioptics LLC, Arizona, USA) and digital plates (Agfa CR MD 4.0 cassette, Agfa, Germany). An Agfa Digital Developer and workstation was used to process the digital images (Agfa CR 75.0 Digitizer Musica, Agfa, Germany). Radiographic status of the spinal arthrodesis

was evaluated by two experienced observers in a blinded manner on anteroposterior radiographs using the Lenke four-point grading scale[20] (**Table 1**).

**Table 1. Fusion grading scale for X-ray and micro-CT assessment based on the Lenke classification<sup>20</sup>**

Grade	Definition
A	Bilateral robust bridging fusion masses (definitely solid)
B	Unilateral robust bridging fusion mass and contralateral thin fusion mass (probably solid)
C	Unilateral thin bridging fusion mass and probable pseudarthrosis on the contralateral aspect (probably not solid)
D	Bilateral thin fusion masses with obvious pseudarthrosis or bone graft resorption (definitely not solid)

### ***Micro Computed Tomography***

Micro Computed tomography (micro-CT) was performed on the spines using an Inveon Scanner (Siemens Medical Solutions USA, Inc., Knoxville, TN, USA). Scans were made with a slice thickness of 53  $\mu\text{m}$  and were stored in DICOM format. Three-dimensional reconstructions were generated from the scans. Status of the spinal arthrodesis was evaluated by two experienced observers in a blinded manner in three orthogonal planes (i.e. axial, sagittal, coronal) and anterior and posterior 3D reconstructions. As per for the radiographs, the Lenke four-point grading scale was used to grade fusion status.

### ***Quantification of fusion mass volume***

Fusion mass volume quantification was performed on TIFF stacks generated from the DICOM scans of the treated spinal levels using dedicated image computing software (3D Slicer 4.10 [21]). This was achieved by performing manual, intensity-based selection of the separate left and right fusion masses on interspersed axial slices (53  $\mu\text{m}$ ) throughout the micro-CT files, taking care to exclude the host vertebrae and transverse processes. Subsequently, interpolation of boundaries between adjacent scan layers was performed using a contour interpolation algorithm[22], resulting in segmentations of the fusion mass. The total volume of each fusion mass in  $\text{cm}^3$  was derived from the number of voxels in each segmentation, including both (new) mineralized bone and residual graft material.

### ***Biomechanical analysis***

Non-destructive biomechanical ROM testing was performed to obtain a multidirectional flexibility profile of the treated spinal levels. After removal of pedicle rods, each of the spinal levels was mounted onto a six axis simVITRO robotic musculoskeletal simulator (Simulation Solutions Ltd., Stockport, UK and Cleveland Clinic Biorobotics Lab, Cleveland, OH, USA). A  $\pm 7.5$  Nm pure moment was applied to the spinal levels in lateral bending (LB), flexion-extension (FE) and axial rotation (AR). Each loading profile was repeated 3 times and a mean value for LB, FE and AR was recorded in range of motion degrees ( $^\circ$ ).

## **Histology and histomorphometry**

Following mechanical testing, spines were fixed at room temperature in 10% formalin in 0.145 M phosphate buffered saline under gentle rotation for at least 96 hours. Subsequently, specimens were processed for poly-methylmethacrylate embedding. A Leica SP1600 saw microtome was used to cut sections in the sagittal plane from the region between TPs lateral of the spine at both sides. From each side, a minimum of three sections separated by 300  $\mu\text{m}$  was obtained. A histological staining of methylene blue (Sigma, 1% in 0.1 M borax buffer, pH 8.5) and basic fuchsin (Sigma, 0.3% in demi water) was performed to visualize bone tissue (bone matrix: pink, fibrous tissues: blue). Sections were examined under a Leica microscope (Eclipse 50i, Nikon) and were scanned with a slide scanner (DiMage scan 5400 Elite II, Konica Minolta, Tokyo, Japan) to obtain low magnification overviews.

### ***Histological evaluation and fusion assessment***

Histological evaluation included qualitative assessment of the tissue response, including evidence of inflammation, evidence of graft resorption, new bone formation and bone marrow space development. Low magnification overviews of each section were used for fusion assessment and histomorphometry. Fusion assessment by histology was performed by two trained observers in a blinded manner on three sections from each lateral side of the treated spinal level, resulting in two scores per level. Each section was scored as histologically fused if a continuous bridge of bone tissue was observed between the TPs of L2-L3 or L4-L5, thus connecting the adjacent spinal levels. When at least one out of the three sections was scored as fused, the sample was considered 'fused' on that side of the spine. If no fusion was determined in any of the three slides, the sections were digitally stacked and re-evaluated for fusion.

### ***Histomorphometry***

Histomorphometry of the fusion mass was performed on three sections from each side of the treated spinal level. Pixels representing bone (B) and remaining implant material (M) in a region of interest (ROI) were pseudo-colored using image editing software (Adobe Photoshop 5.0). Next, the number of pixels for B, M and ROI was recorded and the area percentage of bone in the available space was calculated by the formula:  $B/(ROI-M) \times 100\%$ . In addition, the area percentage of remaining implant material was calculated by the formula:  $M/ROI \times 100\%$ .

## **Statistical analysis**

Statistical analysis of data was performed using dedicated software tools (GraphPad Prism, San Diego, USA; SPSS, Chicago, USA). Fusion grading data from manual palpation, X-ray, Micro-CT and histology were analyzed by the Fisher-Freeman-Halton Exact Test. Data from micro-CT volume quantification, biomechanical ROM testing and histomorphometry were analyzed by Analysis of Variance (ANOVA) followed by Tukey's Honest Significant Difference

test for post-hoc analysis. Normal distribution of data was assessed by the Shapiro-Wilk normality test. For all statistical tests, a significance level of  $P < 0.05$  was utilized.

## RESULTS

### Surgery

All surgeries and study procedures proceeded as planned. All graft materials handled well, as they were moldable and easy to implant into the posterolateral gutters. No adverse events occurred in any animal during surgery and the 12-week follow-up period.

### Manual palpation

Results of fusion assessment by manual palpation are presented in **Table 2**. Successful arthrodesis was confirmed in all levels treated with AB, with 100% of specimens graded as rigid in both LB and FE. Results varied between treatment groups. While  $\text{BCP}_{<\mu\text{m}}$  showed a similar fusion rate to AB with all specimens scored as rigid, both bone grafts (BG and TCP/BG) containing bioactive glass were graded as rigid in only 1 out of 3 treated levels. All fusion grades by manual palpation were coherent between reviewers and between the different modes LB and FE. The difference between groups was confirmed by statistical analysis.

**Table 2. Outcomes of fusion assessment per evaluation method.**

	AB	$\text{BCP}_{<\mu\text{m}}$	BG	TCP/BG	Sig. <sup>a</sup>
Manual palpation	6/6	6/6	1/3	1/3	$p < 0.013$
X-Ray	A: 4/6 B: 2/6	A: 5/6 B: 1/6	B: 2/3 D: 1/3	C: 1/3 D: 2/3	$P < 0.008$
Micro-CT	A: 3/6 B: 3/6	A: 5/6 B: 1/6	B: 2/3 D: 1/3	C: 1/3 D: 2/3	$P < 0.010$
Histology	9/12	10/12	0/6	0/6	$P < 0.001$

<sup>a</sup> Fisher-Freeman-Halton Exact Test

### Radiographic evaluation and fusion assessment

Faxitron radiographs (**Figure 1**) were evaluated for evidence of bone formation and residual graft material in the posterolateral regions in between TPs of L2-L3 and L4-L5. In the AB group (**Fig. 1, A**), a consolidated mass of mineralized bone was observed in the bilateral intertransverse process regions. Individual autogenous bone particles could not be discriminated. In the  $\text{BCP}_{<\mu\text{m}}$  group (**Fig. 1, B**), a large, radiopaque fusion mass was evident in the region between the bilateral TPs. Although individual  $\text{BCP}_{<\mu\text{m}}$  particles could still be discriminated, the grafts had consolidated into a dense, continuous fusion

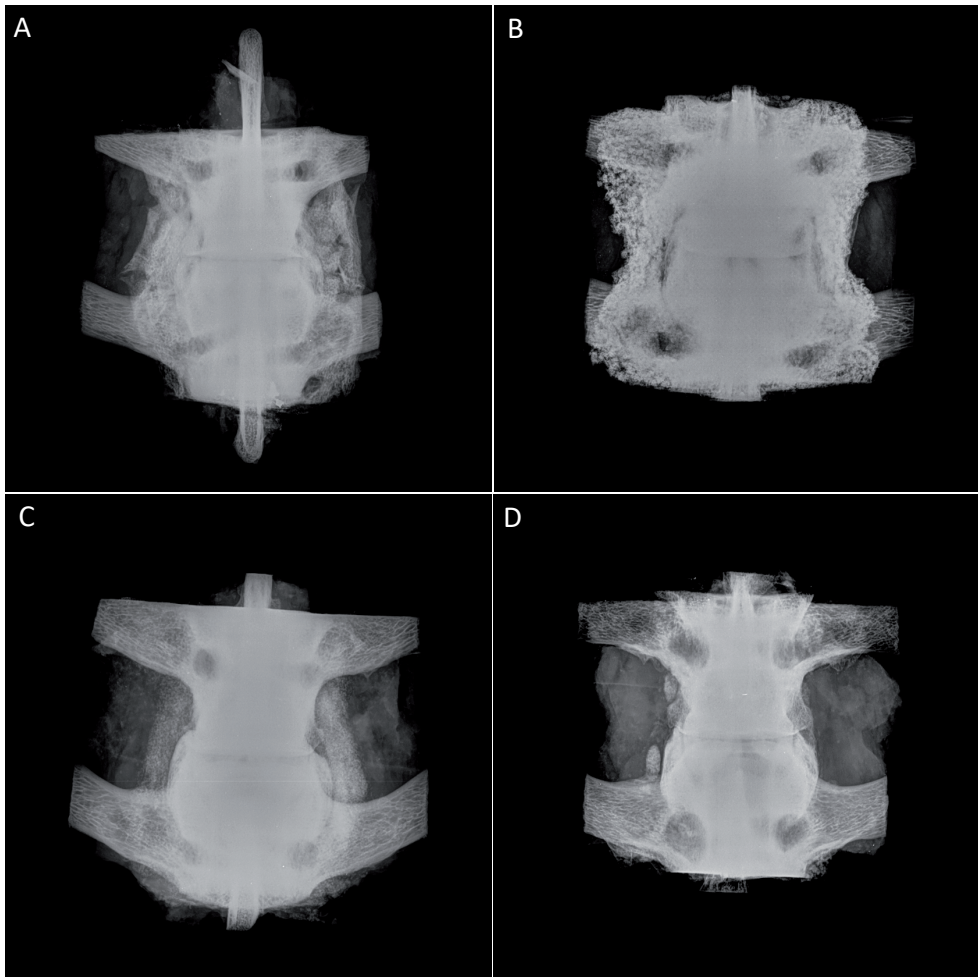


**Figure 1.** Representative examples of faxitron radiographs of the spinal levels treated with AB **(A)**, BCP<sub>5μm</sub> **(B)**, BG **(C)** and TCP/BG **(D)**, after removal of instrumentation.

mass between the TPs. At levels treated with BG **(Fig. 1, C)**, thin masses of radiopaque material, which were of variable intensity and continuity, were observed between TPs. In the TCP/BG group **(Fig. 1, D)**, there was a significant lack of radiopaque substance in the intertransverse regions of all treated levels. The TCP/BG grafts had a low radiopacity with a granular appearance and did not form a consolidated mass at the treated levels.

On Micro-CT reconstructions **(Figure 2)**, a bony fusion mass forming a bridge between L2-3 or L4-5, was commonly observed in the AB group **(Fig. 2, A)**. In many cases, the fusion masses were well-developed, showing a smooth, continuous bone mass with a *de novo* cortex. Occasionally, fusion masses were not yet completely consolidated and matured,

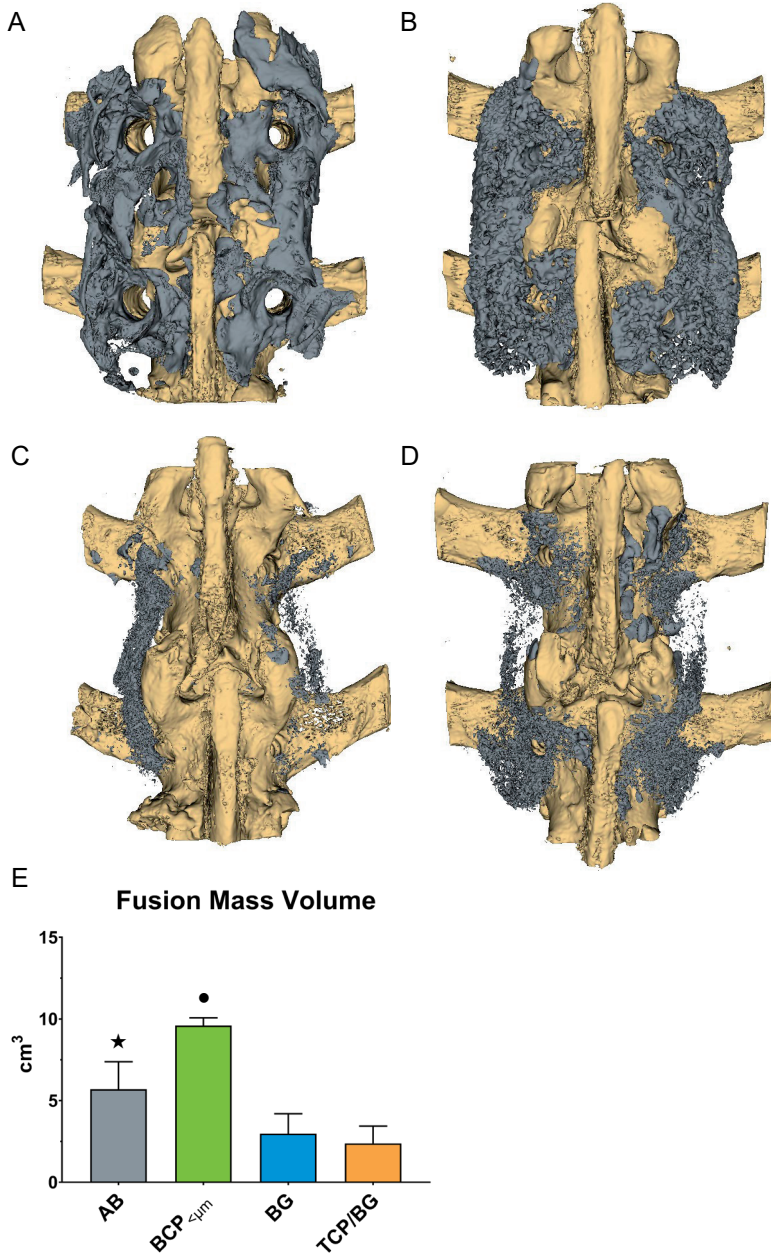


**Figure 2.** Representative examples of 3-dimensional micro-CT reconstructions (**A-D**) of spinal levels treated AB (**A**), BCP<sub>≤4μm</sub> (**B**), BG (**C**) and TCP/BG (**D**). The host spinal bone (off-white) and fusion mass (grey) including (new) bone and residual implant material are shown as individual segmentations. For each treatment group, unilateral fusion mass volume (bone + graft material) was determined by performing voxel-based quantification (**E**). Data shown as mean and SD.

★ significantly different from AB, BG and TCP/BG ( $P < 0.001$ )

• significantly different from BCP<sub>≤4μm</sub>, BG and TCP/BG ( $P < 0.001$ )

as an outer cortex had not yet developed, and autograft chips could be distinguished in the developing bone mass.

The BCP<sub><math>\lt; \mu\text{m}</math></sub> grafts (**Fig. 2, B**) formed uniform, solid and continuous fusion bridges between the TPs. The center of the BCP<sub><math>\lt; \mu\text{m}</math></sub> grafts were compact and individual BCP particles could be hardly distinguished on axial, sagittal and transversal slices, indicating bone formation between the granules. New bone growth into the calcium phosphate grafts could be observed in the regions near host bone.

The spinal levels treated with BG (**Fig. 2, C**) presented thin, underdeveloped fusion masses versus AB and BCP<sub><math>\lt; \mu\text{m}</math></sub> as observed by Micro-CT. The radiopaque mass in the region between TPs (if present), had a fine, granular appearance with localized, dense regions in the center or in apposition with TPs. A continuous mass between TPs was lacking and Bioglass granules were few and dispersed.

None of the treated levels presented a consolidated fusion mass in between TPs with TCP/BG (**Fig. 2, D**). A small amount of dispersed, granular material was occasionally observed in the intertransverse regions. In some cases, regions of minor osteoconductive bone growth were observed near the host bone.

Results of fusion grading on radiographs and micro-CT according to the Lenke scale are presented in **Table 2**. Both AB and BCP<sub><math>\lt; \mu\text{m}</math></sub> obtained high fusion scores, with either unilateral or bilateral robust bone bridging in all treated levels. Radiographic fusion scores were lower in the other groups, while the BG group obtained more favourable grades than TCP/BG. The differences in radiographical fusion grades reached statistical significance, although no between-group comparisons were analyzed.

### Fusion mass volume

Micro-CT quantification (**Fig. 2, E**) revealed the levels treated with AB had an average unilateral, mineralized fusion mass volume of  $5.70 \pm 1.59 \text{ cm}^3$ . The volume in the BCP<sub><math>\lt; \mu\text{m}</math></sub> group was significantly higher at  $9.60 \pm 0.45 \text{ cm}^3$ . Volumes were significantly lower in BG and TCP/BG, at approximately  $3 \text{ cm}^3$ . Statistical significance was reached for all group comparisons, except for BG versus TCP/BG.

### Biomechanical testing

Functional treatment efficacy was quantified by use of biomechanical ROM testing (**Figure 3**). The BCP<sub><math>\lt; \mu\text{m}</math></sub> group revealed an equivalent ROM to AB in all modes, while ROM for levels treated with BG and TCP/BG was evidently higher in LB and FE. Statistical analysis revealed equivalence between AB and BCP<sub><math>\lt; \mu\text{m}</math></sub> in all modes, while ROM in these groups was

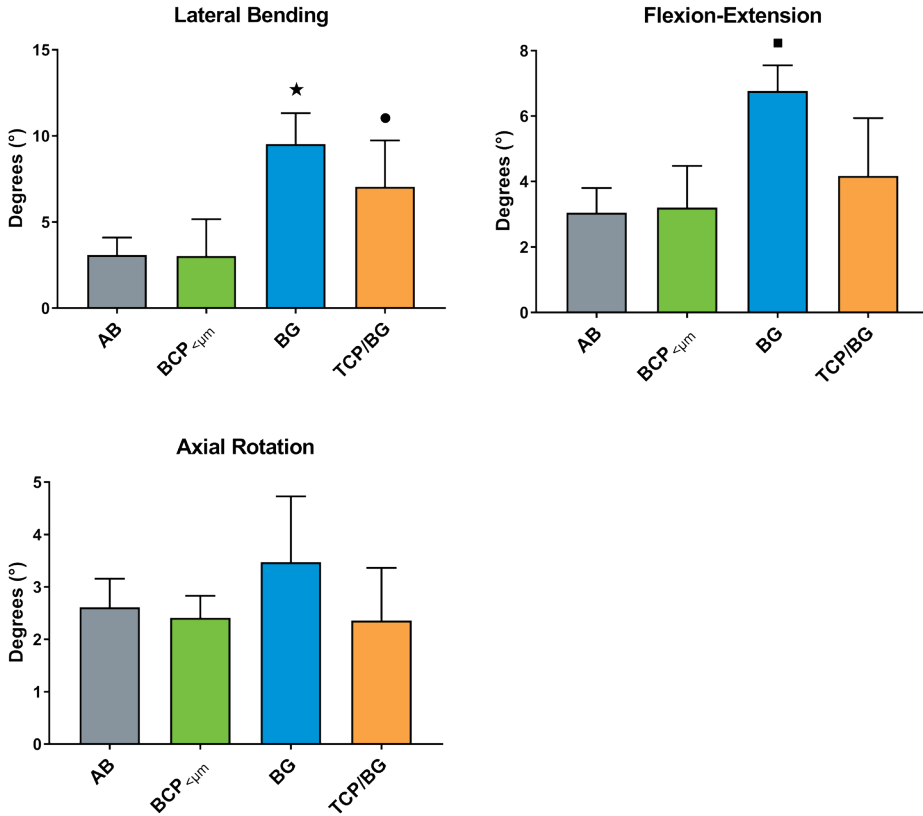


**Figure 3.** Diagrams of non-destructive biomechanical ROM testing results, as performed in LB (A), FE (B) and AR (C). Data are presented as ROM degrees in mean and SD.

- ★ significantly different from AB and BCP<sub>4μm</sub> ( $P < 0.005$ )
- significantly different from AB and BCP<sub>4μm</sub> ( $P < 0.05$ )
- significantly different from AB and BCP<sub>4μm</sub> ( $P < 0.005$ )

significantly lower in LB and FE compared to BG and significantly lower in FE compared to TCP/BG. No significant difference in AR ROM was determined between all treatments.

### **Histological evaluation and fusion assessment**

Histology of the spinal levels treated with AB (Fig. 4, A) revealed the presence of abundant new and remodeling bone tissue in the intertransverse process space. The implanted AB particles had been remodeled into uniform bone mass in the intertransverse process space.

In BCP<sub>4μm</sub> specimens (Fig. 4, B; Fig. 5, A-D), a large area consisting of calcium phosphate granules integrated in trabecular bone was observed throughout the implant sites (Fig. 4, B). Bone was of mature, lamellar morphology including new bone marrow spaces (Fig. 5,





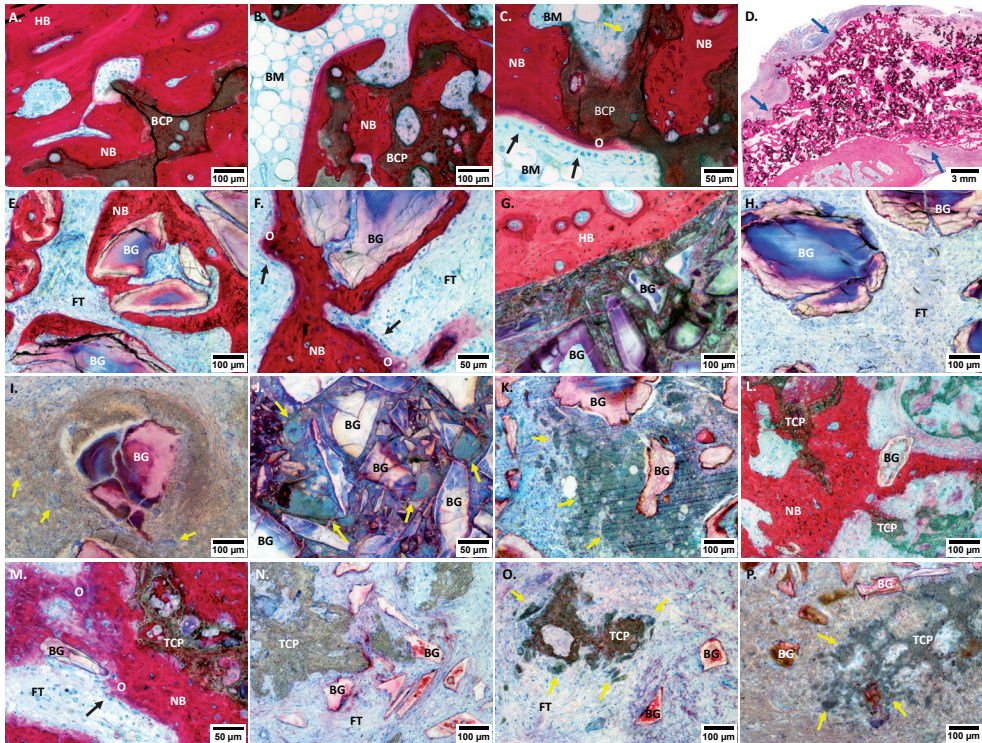


**Figure 5.** Representative micrographs from histological sections of the spinal levels treated with BCP<sub><math>\leq 5 \mu\text{m}</math> (A-D), BG (E-K) and TCP/BG (L-P). Micrographs were obtained from regions near the host TP (A, E-G, L-M) and the intertransverse central region (B-C, H-K, N-P). A pseudo-cortex on the outside of the fusion mass was observed in specimens treated with BCP<sub><math>\leq 5 \mu\text{m}</math> (D – blue arrows). High magnification images show cellular processes observed near the graft materials, including osteoblasts (C, F, M–black arrows) depositing osteoid and cell-mediated resorption of materials by multinucleated cells (C, O, P – yellow arrows). Inflammatory foreign body reaction was observed in BG and TCP/BG specimens, as evidenced by encapsulation of material (I), high numbers of lymphocytes (I,P) and foreign body giant cells (I-K, P – yellow arrows). HB: host bone; NB: new bone; BM: bone marrow; O: osteoid; FT: fibrous tissue.</sub></sub>

calcium phosphate particles, which were commonly in the process of disintegration due to cell-mediated resorption (Fig. 5, N-O). The Bioglass particles were very small and could only be observed by high magnification, with a similar appearance to those observed in the BG group (Fig. 5, L-P). An inflammatory reaction around the bioglass particles was generally not observed. Newly formed bone tissue was absent in the central region of the implants, although some specimens exhibited new bone formation in the vicinity of TPs. Calcium phosphate and Bioglass particles were occasionally observed being integrated in the bone matrix (Fig. 5, L-M). One specimen presented a region with graft material enclosed by granulation tissue that contained high numbers of lymphocytes and resorbing multinucleated giant cells, indicating a foreign body granuloma (Fig. 5, P).

Results of fusion assessment by histology are presented in **Table 2**. Histological fusion scores in the AB and BCP<sub><math>\leq 50\mu\text{m}</math> groups were significantly higher than in the BG and TCP/BG groups. For levels treated with AB, the positive control, fusion was reported in 9 out of 12 samples, corresponding to a fusion rate of 75%. In the BCP<sub><math>\leq 50\mu\text{m}</math> group, 10 out of 12 samples were scored as fused, which translates to a fusion rate of 83%. For the BG and TCP/BG groups, a bony fusion between TPs was not reported in any of the specimens, thus corresponding to a fusion rate of 0%. Statistical analysis revealed that the differences in histological fusion rate were statistically significant ( $P < 0.05$ ).</sub></sub>

### Histomorphometry

As determined by histomorphometry (**Figure 6**), the fusion masses of levels treated with AB and BCP<sub><math>\leq 50\mu\text{m}</math> contained a substantially higher percentage of bone as compared to the BG and TCP/BG groups (**Fig. 6, A**). Bone proportions were similar for AB and BCP<sub><math>\leq 50\mu\text{m}</math>, with over >40% of bone in available space in both groups. This percentage was significantly lower for the other groups, the lowest being BG, followed by TCP/BG. Statistical analysis confirmed equivalence for AB vs BCP<sub><math>\leq 50\mu\text{m}</math> and BG vs TCP/BG, while all other comparisons were significantly different. Area percentage of remaining graft material (**Fig. 6, B**) was highest for BCP<sub><math>\leq 50\mu\text{m}</math> implants, followed by BG, with the TCP/BG graft the lowest. Statistical significance was reached for all group comparisons in material percentage.</sub></sub></sub></sub>

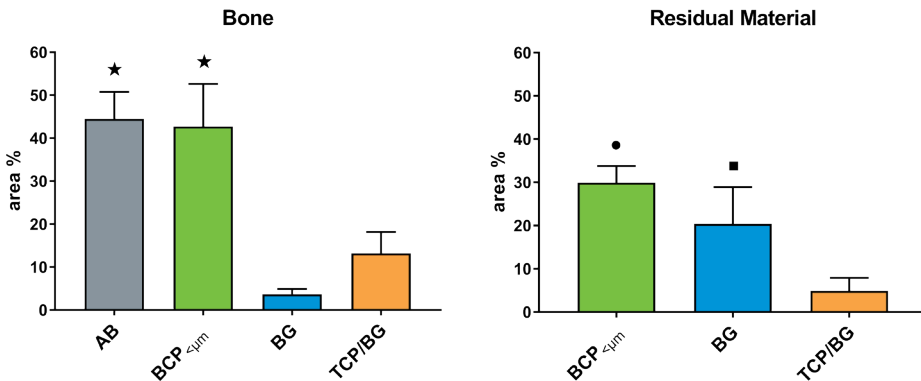


**Figure 6.** Histomorphometry diagrams of **(A)** bone and **(B)** residual material, performed on low magnification micrographs of histological sections. Data is presented as area%, in mean and SD.

- ★ significantly different from BG and TCP/BG ( $P < 0.001$ )
- significantly different from BG ( $P < 0.005$ ) and TCP/BG ( $P < 0.001$ )
- significantly different from BCP<sub><math>\leq 50\mu\text{m}</math> ( $P < 0.005$ ) and TCP/BG ( $P < 0.001$ )</sub>

## DISCUSSION

---

The posterolateral spine environment is a challenging biological and biomechanical environment, as it provides limited host bone contact and significant exposure to soft tissues. Even with use of the “gold standard” of autograft, surgeons commonly deal with revision surgery rates of  $\pm$  10-20%[23–26]. Considering this, it is important that the selection of graft materials is based on preclinical evidence obtained in studies of high methodological quality, using clinically relevant animal models and multiple evaluation techniques. A large number of bone grafts are commercially available for clinical use, which makes selection of the most appropriate challenging for the surgeon community. Most reports on commercial graft materials in literature are of preclinical studies performed in rabbits, and involve the repair of small, cancellous bone defects with a high ratio of bone surface to defect volume[27–33]. Although critically-sized, i.e. they won't completely spontaneously heal without the use of a graft, such defects are less challenging than, and do not properly model, the posterolateral spine environment. This limits extrapolation of results from these models to PLF indications. Moreover, many studies have been of poor methodological design, e.g. no use of critical-sized defects, lack of proper positive and/or negative controls, use of limited endpoints and assessment methods with low sensitivity[27–29,34]. Clinical reports for the use of synthetic bone grafts are limited in number and often of low methodological strength (i.e. observational studies). Furthermore, outcomes can only be determined using techniques with low sensitivity and/or specificity, such as radiographical evaluation and patient-reported outcomes.

Of the available animal models of PLF, the instrumented *Ovine* PLF[35] model is among the most translational, since bone remodeling properties and spine biomechanics of sheep are similar to those of humans and the model allows the use of relevant graft volumes and pedicle instrumentation[36–39]. For comparison, the Boden rabbit PLF model[19], which is used to obtain market approval for bone graft materials in the US, is noninstrumented and differs in anatomy, biomechanics and bone turnover rate from the clinical reality in human[40]. Note, the current study used aged sheep (4-5 years old) which challenges the model due to age[41].

With regard to assessment techniques used for fusion evaluation, it is important that a range of different methods is applied, since they may individually give limited information and vary in sensitivity. Classically, fusion assessment in pre-clinical models was performed by the less sensitive techniques of manual palpation and plain film radiography[19]. Recently, more sensitive techniques have been added, including micro-CT, histology and biomechanical testing. For synthetic bone grafts, fusion evaluation by radiography (e.g. X-ray, CT) may lead to an overestimation of fusion, since bone mineral and radiopaque

implant materials cannot easily be distinguished by these methods. Histology provides a unique insight and accurate representation of a fusion mass at the tissue and cell level, allowing investigators to differentiate bone, graft material and to evaluate tissue and cellular responses. Lastly, biomechanical testing is an important quantitative method performed in conjunction with the other techniques to determine whether fusion outcomes also have a functional significance, i.e. reduction of mobility between spinal segments. Here, a robotic musculoskeletal simulator was used to apply controlled loading regimens to the spinal segments.

Using this validated, multi-endpoint, clinically relevant, *Ovine* model of instrumented PLF, three commercially available bone grafts implanted as a standalone graft were compared against autograft bone, the current gold standard for bone grafting. Of the evaluated synthetic bone grafts, BCP<sub><math>\text{<math>\mu\text{m}</math></math></sub> was the only material that presented substantial, solid fusion masses between TPs that contained mature bone, resulting in similar fusion scores to AB by all assessment methods and equivalent biomechanical ROM. These outcomes were corroborated by all assessment techniques and were in line with previous results[17,18]. In contrast to BCP<sub><math>\text{<math>\mu\text{m}</math></math></sub>, spinal levels treated with BG and TCP/BG significantly underperformed to the positive control by all evaluation methods. Although by biomechanical testing no significant differences between treatments were determined in AR, it is recognized that flexibility testing in AR has a lower sensitivity than the other modes[42,43].

These results confirm the limitations of fusion evaluation by radiographical techniques when synthetic bone graft materials are used in PLF. While spinal levels treated with BG obtained a moderate fusion grade B of the Lenke scale in two out of three specimens by both X-ray and Micro-CT, histology revealed that all apparent fusion bridges did not contain any bone tissue. These results show that the option to use histology is a significant advantage of pre-clinical models over clinical investigation. Histology also allows the evaluation of local tissue reactions as the materials resorb and participate in the bone repair and remodeling process, which is not possible by other techniques.

Fusion mass volume quantification is a more novel method for evaluation of PLF outcomes that assists in further differentiation of radiographic endpoints. It should be noted that the use of micro-CT, which is not available clinically, provides a level of detail beyond traditional radiographs or clinical CT. The technique can provide meaningful information on graft volume stability, as too fast or too severe resorption of a graft may potentially result in atrophic pseudarthrosis[44]. Here, clear differences in fusion mass volumes were determined between groups. While the same starting volume of 10 cc was implanted in each posterolateral gutter for all groups, the mineralized volume after 12 weeks was around 3 cc for BG and TCP/BG grafts, while for BCP<sub><math>\text{<math>\mu\text{m}</math></math></sub> it was just under 10 cc. Although the initial radiopaque volume of the grafts was not determined and the data represent

the volume of both new bone and residual graft material, we may still assume that BG and TCP/BG have undergone substantial resorption after implantation. This notion was supported by histological observations and histomorphometry results. The finding that spinal levels treated with AB had lower fusion mass volumes compared to BCP<sub><μm</sub> may be potentially related to a lower initial radiopaque volume, but could also suggest resorption. Indeed, autograft bone has been reported to undergo resorption and remodeling after implantation in the posterolateral spine, leading to a volume loss of up to ±35% during the first year[45–47].

The above findings demonstrate a clear difference in performance of commercially available synthetic bone grafts in instrumented PLF in sheep. Correlation of performance outcomes to specific bone graft factors is challenging due to the many physicochemical differences between the grafts that could affect bone regeneration potential, e.g. composition, surface properties, carrier materials, particle size and graft-to-carrier ratio. However, the submicron surface topography of BCP<sub><μm</sub> seems to play a leading role in bone graft performance[48] and may explain its enhanced efficacy in this PLF model.

In recent years, research has consistently demonstrated that calcium phosphates with a submicron topography show enhanced performance to conventional calcium phosphates, following from their ability to induce bone formation in regions far from host bone or with minimal bone contact[7–9,48]. This property is particularly desirable for use in PLF, in which bone formation should occur in the paraspinous soft tissues with limited host bone surface contact. A suggested mechanism underlying the enhanced efficacy of calcium phosphates with submicron topography is the upregulation of anti-inflammatory M2 macrophages at the material surface, which have been associated with bone regeneration[49–52].

Bone induction by the TCP component of the TCP/BG group has been evaluated in two previous studies[48,53]. Both studies demonstrated the absence of submicron topography correlated with the lack of ectopic bone induction, even in the presence of Bioglass[53]. Furthermore, the TCP component in TCP/BG reportedly consists of 100% phase pure βTCP and has a porosity of 78%[53]. A calcium phosphate with these properties is expected to have a high resorption rate, with potentially detrimental effects on bone healing[54]. This notion is in agreement with the findings of the current study as well as other works[32,33,53,54].

The presence of 45S5 Bioglass in BG and TCP/BG grafts, resulting in enhanced osteoblast activity and osteogenic differentiation of stem cells *in vitro*[10–12,55–57], did not promote spinal fusion in this PLF model. To our knowledge, there is no literature on use of Bioglass as standalone graft in PLF models and beneficial effects of osteostimulation have not been demonstrated in other *in vivo* models. We may therefore conclude that osteostimulative

Bioglass, whether used alone or as an adjunct to calcium phosphate, has little biological relevance to use of bone graft materials in spinal fusion. Moreover, the inflammatory foreign body reaction observed around Bioglass particles, which has also been reported in other studies[58–60], is presumably not beneficial for bone formation. However, foreign body reaction against Bioglass particles was not observed in TCP/BG, which contained a lower content of Bioglass than BG (25% vs 100%), suggesting that only larger proportions of Bioglass may induce such reactions.

## **CONCLUSION**

---

Using a challenging, clinically relevant, *Ovine* model of instrumented PLF, this study reveals clear differences in performance between commercially available bone graft materials implanted as a standalone graft, after evaluation by a full range of assessment techniques. The results demonstrated favorable outcomes with a putty formulation of BCP<sub><μm</sub>, that has a submicron topography, versus two other bone graft materials, being a putty formulation of 45S5 Bioglass and a collagen-βTCP with a 45S5 Bioglass adjunct. Through all outcomes, the BCP<sub><μm</sub> reached equivalence to the positive control, autograft, in achieving functional spinal fusion, while the other two materials significantly underperformed, showing an inability to form a solid, bony fusion between the spinal segments during the 12-week follow-up period. These results corroborate previous findings on the efficacy of BCP<sub><μm</sub> with submicron topography in spinal PLF models, following from its ability to promote bone formation in soft tissues distant from host bone. These findings emphasize the importance of side-by-side comparison of commercial bone graft materials in clinically relevant, multi-endpoint animal models in determining spinal fusion efficacy.

## **ACKNOWLEDGEMENTS**

---

We thank Dr Huipin Yuan and Dr Davide Barbieri for assistance with histology and data collection and Dr Charlie Champion for his helpful suggestions with the writing of this manuscript.



## REFERENCES

---

- [1] R. Dimitriou, G.I. Mataliotakis, A.G. Angoules, N.K. Kanakaris, P. V. Giannoudis, Complications following autologous bone graft harvesting from the iliac crest and using the RIA: A systematic review, *Injury*. 42 (2011). <https://doi.org/10.1016/j.injury.2011.06.015>.
- [2] T. Kurien, R.G. Pearson, B.E. Scammell, Bone graft substitutes currently available in orthopaedic practice: The evidence for their use, *Bone Jt. J.* 95 B (2013) 583–597. <https://doi.org/10.1302/0301-620X.95B5.30286>.
- [3] J.R. Jones, D.S. Brauer, L. Hupa, D.C. Greenspan, Bioglass and Bioactive Glasses and Their Impact on Healthcare, *Int. J. Appl. Glas. Sci.* 7 (2016) 423–434. <https://doi.org/10.1111/ijag.12252>.
- [4] R.Z. LeGeros, Properties of osteoconductive biomaterials: Calcium phosphates, in: *Clin. Orthop. Relat. Res.*, 2002: pp. 81–98. <https://doi.org/10.1097/00003086-200202000-00009>.
- [5] P. Habibovic, H. Yuan, C.M. Van Der Valk, G. Meijer, C.A. Van Blitterswijk, K. De Groot, 3D microenvironment as essential element for osteoinduction by biomaterials, *Biomaterials*. 26 (2005) 3565–3575. <https://doi.org/10.1016/j.biomaterials.2004.09.056>.
- [6] R. Duan, L.A. van Dijk, D. Barbieri, F. de Groot, H. Yuan, J.D. de Bruijn, Accelerated bone formation by biphasic calcium phosphate with a novel sub-micron surface topography, *Eur. Cell. Mater.* 37 (2019) 60–73. <https://doi.org/10.22203/eCM.v037a05>.
- [7] P. Habibovic, H. Yuan, M. van den Doel, T.M. Sees, C.A. van Blitterswijk, K. de Groot, Relevance of osteoinductive biomaterials in critical-sized orthotopic defect, *J. Orthop. Res.* 24 (2006) 867–876. <https://doi.org/10.1002/jor.20115>.
- [8] H. Yuan, H. Fernandes, P. Habibovic, J. De Boer, A.M.C. Barradas, A. De Ruiter, W.R. Walsh, C.A. Van Blitterswijk, J.D. De Bruijn, Osteoinductive ceramics as a synthetic alternative to autologous bone grafting, *Proc. Natl. Acad. Sci. U. S. A.* 107 (2010) 13614–13619. <https://doi.org/10.1073/pnas.1003600107>.
- [9] R. Duan, D. Barbieri, X. Luo, J. Weng, J.D. de Bruijn, H. Yuan, Submicron-surface structured tricalcium phosphate ceramic enhances the bone regeneration in canine spine environment, *J. Orthop. Res.* 34 (2016) 1865–1873. <https://doi.org/10.1002/jor.23201>.
- [10] I.D. Xynos, M.V.J. Hukkanen, J.J. Batten, L.D. Buttery, L.L. Hench, J.M. Polak, Bioglass®45S5 stimulates osteoblast turnover and enhances bone formation in vitro: Implications and applications for bone tissue engineering, *Calcif. Tissue Int.* 67 (2000) 321–329. <https://doi.org/10.1007/s002230001134>.
- [11] I.D. Xynos, A.J. Edgar, L.D.K. Buttery, L.L. Hench, J.M. Polak, Gene-expression profiling of human osteoblasts following treatment with the ionic products of Bioglass® 45S5 dissolution, *J. Biomed. Mater. Res.* 55 (2001) 151–157. [https://doi.org/10.1002/1097-4636\(200105\)55:2<151::AID-JBM1001>3.0.CO;2-D](https://doi.org/10.1002/1097-4636(200105)55:2<151::AID-JBM1001>3.0.CO;2-D).



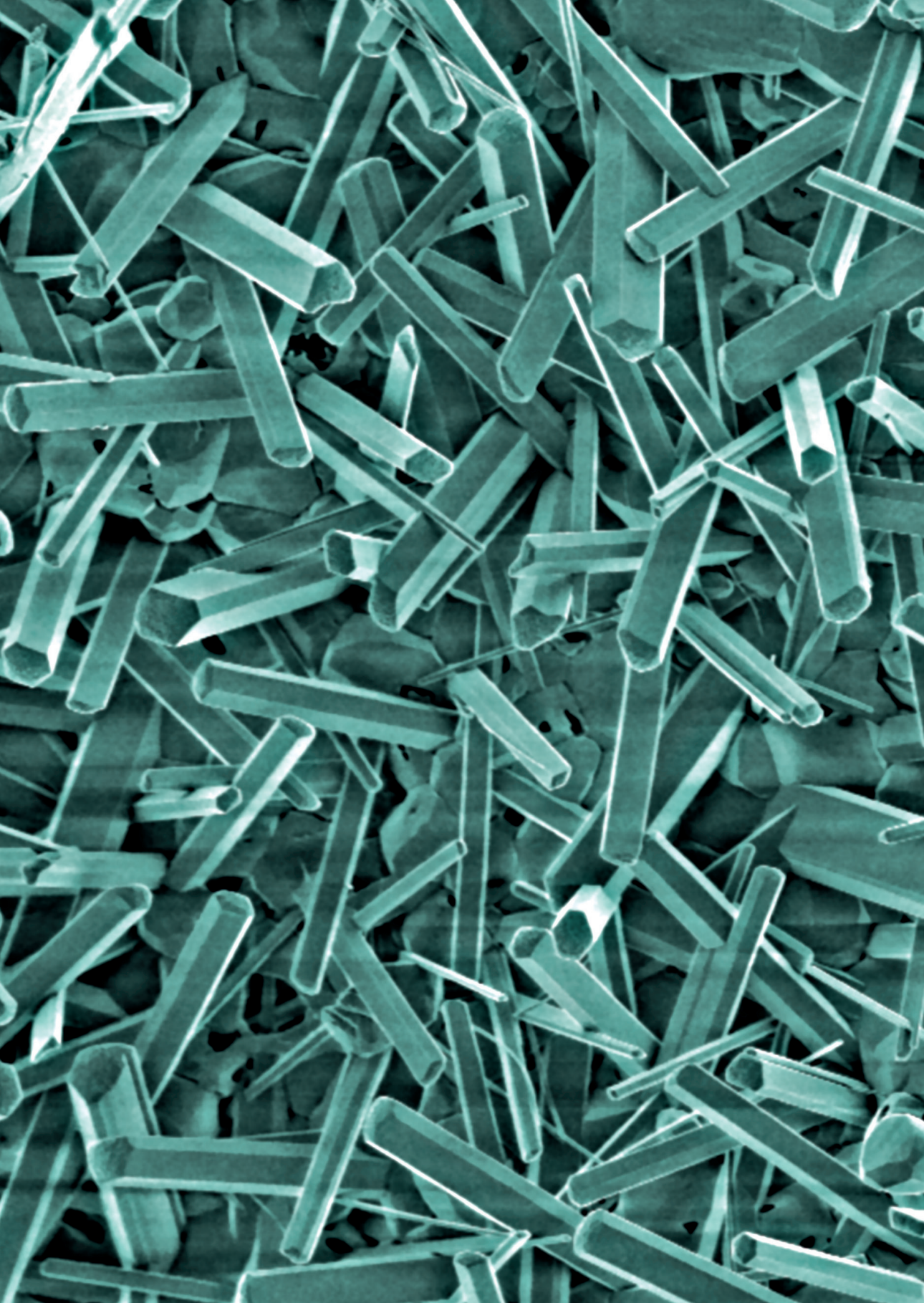
- [12] Z. Qiu, H. Yang, J. Wu, L. Wei, J. Li, Ionic dissolution products of NovaBone® promote osteoblastic proliferation via influences on the cell cycle, *J. Int. Med. Res.* 37 (2009) 737–745. <https://doi.org/10.1177/147323000903700317>.
- [13] H. Andersson, I. Kangasniemi, Calcium phosphate formation at the surface of bioactive glass in vitro, *J. Biomed. Mater. Res.* 25 (1991) 1019–1030. <https://doi.org/10.1002/jbm.820250808>.
- [14] M.R. Filgueiras, G. La Torre, L.L. Hench, Solution effects on the surface reactions of a bioactive glass, *J. Biomed. Mater. Res.* 27 (1993) 445–453. <https://doi.org/10.1002/jbm.820270405>.
- [15] L.L. Hench, R.J. Splinter, W.C. Allen, T.K. Greenlee, Bonding mechanisms at the interface of ceramic prosthetic materials, *J. Biomed. Mater. Res.* 5 (1971) 117–141. <https://doi.org/10.1002/jbm.820050611>.
- [16] L.L. Hench, Bioceramics: From Concept to Clinic, *J. Am. Ceram. Soc.* 74 (1991) 1487–1510. <https://doi.org/10.1111/j.1151-2916.1991.tb07132.x>.
- [17] L.A. van Dijk, D. Barbieri, F. Barrère-de Groot, H. Yuan, R. Oliver, C. Christou, W.R. Walsh, J.D. de Bruijn, Efficacy of a synthetic calcium phosphate with submicron surface topography as autograft extender in lapine posterolateral spinal fusion, *J. Biomed. Mater. Res.–Part B Appl. Biomater.* 107 (2019) 2080–2090. <https://doi.org/10.1002/jbm.b.34301>.
- [18] L.A. van Dijk, R. Duan, X. Luo, D. Barbieri, M. Pelletier, C. Christou, A.J.W.P. Rosenberg, H. Yuan, F. Barrère-de Groot, W.R. Walsh, J.D. de Bruijn, Biphasic calcium phosphate with submicron surface topography in an Ovine model of instrumented posterolateral spinal fusion, *JOR Spine.* 1 (2018) e1039. <https://doi.org/10.1002/jsp2.1039>.
- [19] S.D. Boden, J.H. Schimandle, W.C. Hutton, An experimental lumbar intertransverse process spinal fusion model: Radiographic, histologic, and biomechanical healing characteristics, *Spine (Phila. Pa. 1976)*. 20 (1995) 412–420. <https://doi.org/10.1097/00007632-199502001-00003>.
- [20] L.G. Lenke, K.H. Bridwell, D. Bullis, R.R. Betz, C. Baldus, P.L. Schoenecker, Results of In Situ Fusion for Isthmic Spondylolisthesis, *J. Spinal Disord.* 5 (1992) 433–442. <https://doi.org/10.1097/00002517-199212000-00008>.
- [21] A. Fedorov, R. Beichel, J. Kalpathy-Cramer, J. Finet, J.C. Fillion-Robin, S. Pujol, C. Bauer, D. Jennings, F. Fennessy, M. Sonka, J. Buatti, S. Aylward, J. V. Miller, S. Pieper, R. Kikinis, 3D Slicer as an image computing platform for the Quantitative Imaging Network, *Magn. Reson. Imaging.* 30 (2012) 1323–1341. <https://doi.org/10.1016/j.mri.2012.05.001>.
- [22] D. Zukic, J. Vicory, M. McCormick, L. Wisse, G. Gerig, P. Yushkevich, S. Aylward, N-D morphological contour interpolation, *Insight J.* 2016 Janua (2016) 1–8. <http://hdl.handle.net/10380/3563%0Ahttp://insight-journal.org/browse/publication/977>.
- [23] T. Mabud, J. Norden, A. Veeravagu, C. Swinney, T. Cole, B.A. McCutcheon, J. Ratliff, Complications, Readmissions, and Revisions for Spine Procedures Performed by Orthopedic Surgeons Versus Neurosurgeons, *Clin. Spine Surg.* 30 (2017) E1376–E1381. <https://doi.org/10.1097/BSD.0000000000000426>.
- [24] R.A. Deyo, B.I. Martin, W. Kreuter, J.G. Jarvik, H. Angier, S.K. Mirza, Revision surgery following operations for lumbar stenosis, *J. Bone Jt. Surg.–Ser. A.* 93 (2011) 1979–1986. <https://doi.org/10.2106/JBJS.J.01292>.

- [25] B.I. Martin, S.K. Mirza, B.A. Comstock, D.T. Gray, W. Kreuter, R.A. Deyo, Reoperation rates following lumbar spine surgery and the influence of spinal fusion procedures, *Spine (Phila. Pa. 1976)*. 32 (2007) 382–387. <https://doi.org/10.1097/01.brs.0000254104.55716.46>.
- [26] A.D. Malter, B. McNeney, J.D. Loeser, R.A. Deyo, 5-Year Reoperation Rates After Different Types of Lumbar Spine Surgery, *Spine (Phila. Pa. 1976)*. 23 (1998) 814–820. <https://doi.org/10.1097/00007632-199804010-00015>.
- [27] H. Oonishi, S. Kushitani, E. Yasukawa, H. Iwaki, L.L. Hench, J. Wilson, E. Tsuji, T. Sugihara, Particulate bioglass compared with hydroxyapatite as a bone graft substitute, *Clin. Orthop. Relat. Res.* (1997) 316–325. <https://doi.org/10.1097/00003086-199701000-00041>.
- [28] Y. Fujishiro, L.L. Hench, H. Oonishi, Quantitative rates of in vivo bone generation for Bioglass® and hydroxyapatite particles as bone graft substitute, *J. Mater. Sci. Mater. Med.* 8 (1997) 649–652. <https://doi.org/10.1023/A:1018527621356>.
- [29] H. Oonishi, L.L. Hench, J. Wilson, F. Sugihara, E. Tsuji, M. Matsuura, S. Kin, T. Yamamoto, S. Mizokawa, Quantitative comparison of bone growth behavior in granules of Bioglass®, A-W glass-ceramic, and hydroxyapatite, *J. Biomed. Mater. Res.* 51 (2000) 37–46. [https://doi.org/10.1002/\(SICI\)1097-4636\(200007\)51:1<37::AID-JBM6>3.0.CO;2-T](https://doi.org/10.1002/(SICI)1097-4636(200007)51:1<37::AID-JBM6>3.0.CO;2-T).
- [30] Z. Wang, B. Lu, L. Chen, J. Chang, Evaluation of an osteostimulative putty in the sheep spine, *J. Mater. Sci. Mater. Med.* 22 (2011) 185–191. <https://doi.org/10.1007/s10856-010-4175-5>.
- [31] D.L. Wheeler, K.E. Stokes, R.G. Hoellrich, D.L. Chamberland, S.W. McLoughlin, Effect of bioactive glass particle size on osseous regeneration of cancellous defects, in: *J. Biomed. Mater. Res.*, 1998: pp. 527–533. [https://doi.org/10.1002/\(SICI\)1097-4636\(19980915\)41:4<527::AID-JBM3>3.0.CO;2-E](https://doi.org/10.1002/(SICI)1097-4636(19980915)41:4<527::AID-JBM3>3.0.CO;2-E).
- [32] W.R. Walsh, R.A. Oliver, C. Christou, V. Lovric, E.R. Walsh, G.R. Prado, T. Haider, Critical size bone defect healing using collagen-calcium phosphate bone graft materials, *PLoS One*. 12 (2017). <https://doi.org/10.1371/journal.pone.0168883>.
- [33] W.R. Walsh, F. Vizesi, D. Michael, J. Auld, A. Langdown, R. Oliver, Y. Yu, H. Irie, W. Bruce,  $\beta$ -TCP bone graft substitutes in a bilateral rabbit tibial defect model, *Biomaterials*. 29 (2008) 266–271. <https://doi.org/10.1016/j.biomaterials.2007.09.035>.
- [34] A. Elshahat, M.A. Shermak, N. Inoue, E.Y.S. Chao, P. Manson, The Use of Novabone and Norian in Cranioplasty: A Comparative Study, *J. Craniofac. Surg.* 15 (2004) 483–489. <https://doi.org/10.1097/00001665-200405000-00029>.
- [35] M. Kanayama, B.W. Cunningham, T.J.C. Setter, J.A. Goldstein, G. Stewart, K. Kaneda, P.C. McAfee, Does spinal instrumentation influence the healing process of posterolateral spinal fusion? An in vivo animal model, *Spine (Phila. Pa. 1976)*. 24 (1999) 1058–1065. <https://doi.org/10.1097/00007632-199906010-00003>.
- [36] A.I. Pearce, R.G. Richards, S. Milz, E. Schneider, S.G. Pearce, Animal models for implant biomaterial research in bone: A review, *Eur. Cells Mater.* 13 (2007) 1–10. <https://doi.org/10.22203/eCM.v013a01>.

- [37] H.J. Wilke, A. Kettler, K.H. Wenger, L.E. Claes, Anatomy of the sheep spine and its comparison to the human spine, *Anat. Rec.* 247 (1997) 542–555. [https://doi.org/10.1002/\(SICI\)1097-0185\(199704\)247:4<542::AID-AR13>3.0.CO;2-P](https://doi.org/10.1002/(SICI)1097-0185(199704)247:4<542::AID-AR13>3.0.CO;2-P).
- [38] H.J. Wilke, A. Kettler, L.E. Claes, Are sheep spines a valid biomechanical model for human spines?, *Spine (Phila. Pa. 1976)*. 22 (1997) 2365–2374. <https://doi.org/10.1097/00007632-199710150-00009>.
- [39] I.H. Drespe, G.K. Polzhofer, A.S. Turner, J.N. Grauer, Animal models for spinal fusion, *Spine J.* 5 (2005) S209–S216. <https://doi.org/10.1016/j.spinee.2005.02.013>.
- [40] L.M. Wancket, Animal Models for Evaluation of Bone Implants and Devices: Comparative Bone Structure and Common Model Uses, *Vet. Pathol.* 52 (2015) 842–850. <https://doi.org/10.1177/0300985815593124>.
- [41] W.R. Walsh, A. Loeffler, S. Nicklin, D. Arm, R.E. Stanford, Y. Yu, R. Harris, R.M. Gillies, Spinal fusion using an autologous growth factor gel and a porous resorbable ceramic, *Eur. Spine J.* 13 (2004) 359–366. <https://doi.org/10.1007/s00586-003-0597-9>.
- [42] R.J. Kroeze, A.J. Van Der Veen, B.J. Van Royen, R.A. Bank, M.N. Helder, T.H. Smit, Relation between radiological assessment and biomechanical stability of lumbar interbody fusion in a large animal model, *Eur. Spine J.* 22 (2013) 2731–2739. <https://doi.org/10.1007/s00586-013-3003-2>.
- [43] T. Wang, J.R. Ball, M.H. Pelletier, W.R. Walsh, Biomechanical evaluation of a biomimetic spinal construct, *J. Exp. Orthop.* 1 (2014) 1–8. <https://doi.org/10.1186/s40634-014-0003-z>.
- [44] M.H. Heggeness, S.I. Esses, Classification of pseudarthroses of the lumbar spine, *Spine (Phila. Pa. 1976)*. 16 (1991) 449–454. <https://doi.org/10.1097/00007632-199108001-00028>.
- [45] M.K. Aghi, B.P. Walcott, B. V. Nahed, G.L. Cvetanovich, K.T. Kahle, N. Redjal, J.V. Coumans, Determinants of initial bone graft volume loss in posterolateral lumbar fusion, *J. Clin. Neurosci.* 18 (2011) 1193–1196. <https://doi.org/10.1016/j.jocn.2011.02.017>.
- [46] K.Y. Ha, J.S. Lee, K.W. Kim, Bone graft volumetric changes and clinical outcomes after instrumented lumbar or lumbosacral fusion: A prospective cohort study with a five-year follow-up, *Spine (Phila. Pa. 1976)*. 34 (2009) 1663–1668. <https://doi.org/10.1097/BRS.0b013e3181aacab5>.
- [47] K.W. Kim, K.Y. Ha, M.S. Moon, Y.S. Kim, S.Y. Kwon, Y.K. Woo, Volumetric change of the graft bone after intertransverse fusion, *Spine (Phila. Pa. 1976)*. 24 (1999) 428–433. <https://doi.org/10.1097/00007632-199903010-00003>.
- [48] R. Duan, D. Barbieri, X. Luo, J. Weng, C. Bao, J.D. De Bruijn, H. Yuan, Variation of the bone forming ability with the physicochemical properties of calcium phosphate bone substitutes, *Biomater. Sci.* 6 (2018) 136–145. <https://doi.org/10.1039/c7bm00717e>.
- [49] R. Duan, Y. Zhang, L. van Dijk, D. Barbieri, J. van den Beucken, H. Yuan, J. de Bruijn, Coupling between Macrophage Phenotype, Angiogenesis and Bone Formation by Calcium Phosphates, *Mater. Sci. Eng. C.* 122 (2021) Manuscript submitted for publication. <https://doi.org/10.2139/ssrn.3507484>.

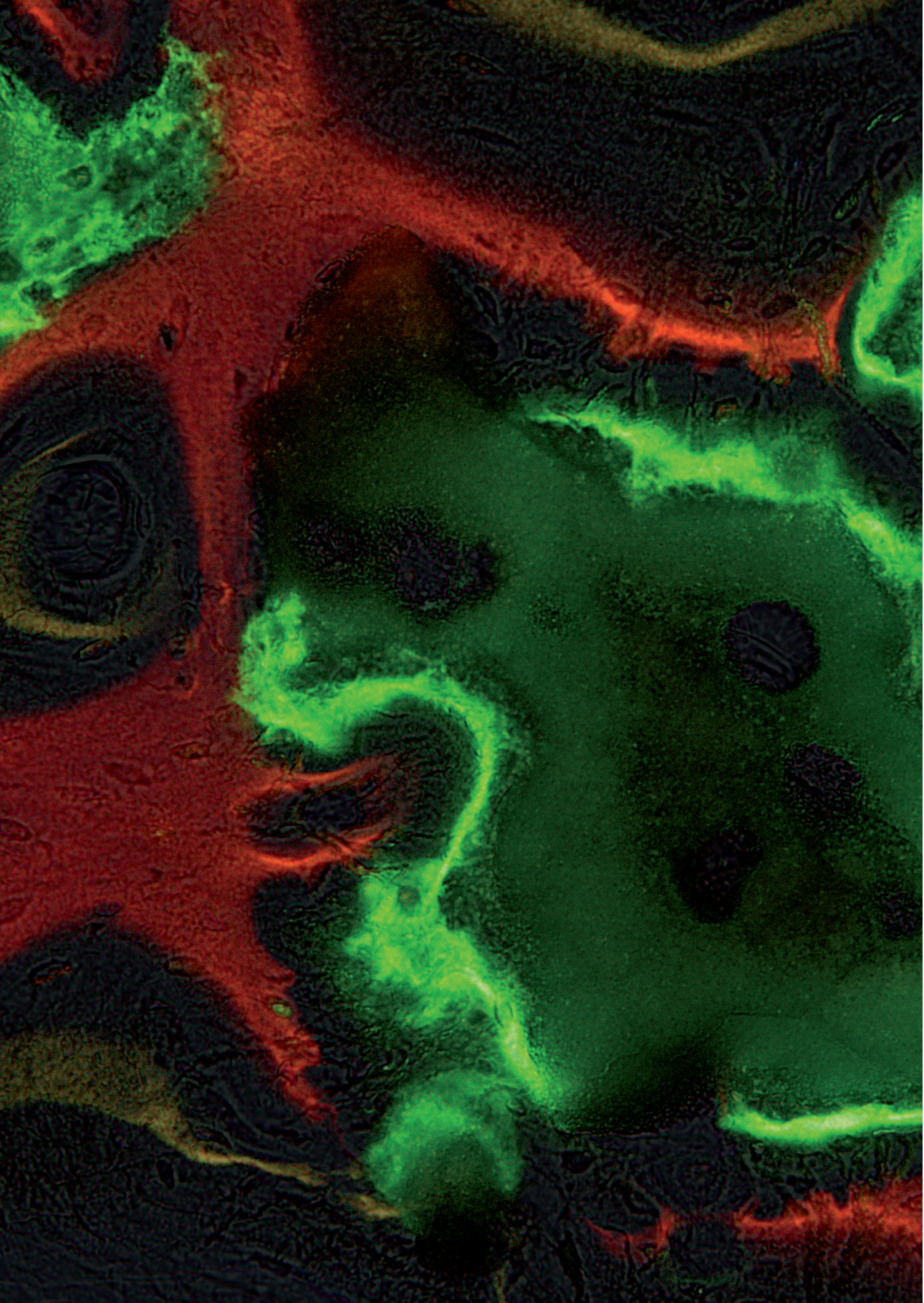
- [50] R. Zhang, Y. Liang, S. Wei, M2 macrophages are closely associated with accelerated clavicle fracture healing in patients with traumatic brain injury: A retrospective cohort study, *J. Orthop. Surg. Res.* 13 (2018) 213. <https://doi.org/10.1186/s13018-018-0926-7>.
- [51] Z. wei Zheng, Y. hong Chen, D. yu Wu, J. bing Wang, M. ming Lv, X. song Wang, J. Sun, Z.Y. Zhang, Development of an accurate and proactive immunomodulatory strategy to improve bone substitute material-mediated osteogenesis and angiogenesis, *Theranostics.* 8 (2018) 5482–5500. <https://doi.org/10.7150/thno.28315>.
- [52] Z. Jamalpoor, A. Asgari, M.H. Lashkari, A. Mirshafiey, M. Mohsenzadegan, Modulation of macrophage polarization for bone tissue engineering applications, *Iran. J. Allergy, Asthma Immunol.* 17 (2018) 398–408. <https://doi.org/10.18502/ijaa.v17i5.298>.
- [53] D. Barbieri, H. Yuan, A.S. Ismailo lu, J.D. De Bruijn, Comparison of two moldable calcium phosphate-based bone graft materials in a noninstrumented canine interspinous implantation model, *Tissue Eng.–Part A.* 23 (2017) 1310–1320. <https://doi.org/10.1089/ten.tea.2016.0347>.
- [54] K.A. Hing, L.F. Wilson, T. Buckland, Comparative performance of three ceramic bone graft substitutes, *Spine J.* 7 (2007) 475–490. <https://doi.org/10.1016/j.spinee.2006.07.017>.
- [55] J.E. Gough, I. Notingher, L.L. Hench, Osteoblast attachment and mineralized nodule formation on rough and smooth 45S5 bioactive glass monoliths, *J. Biomed. Mater. Res.–Part A.* 68 (2004) 640–650. <https://doi.org/10.1002/jbm.a.20075>.
- [56] J.E. Gough, J.R. Jones, L.L. Hench, Nodule formation and mineralisation of human primary osteoblasts cultured on a porous bioactive glass scaffold, *Biomaterials.* 25 (2004) 2039–2046. <https://doi.org/10.1016/j.biomaterials.2003.07.001>.
- [57] F. Westhauser, M. Karadjian, C. Essers, A.S. Senger, S. Hagmann, G. Schmidmaier, A. Moghaddam, Osteogenic differentiation of mesenchymal stem cells is enhanced in a 45S5-supplemented  $\beta$ -TCP composite scaffold: An in-vitro comparison of Vitoss and Vitoss BA, *PLoS One.* 14 (2019) e0212799. <https://doi.org/10.1371/journal.pone.0212799>.
- [58] J.M. Schmitt, D.C. Buck, S.-P. Joh, S.E. Lynch, J.O. Hollinger, Comparison of Porous Bone Mineral and Biologically Active Glass in Critical-Sized Defects, *J. Periodontol.* 68 (1997) 1043–1053. <https://doi.org/10.1902/jop.1997.68.11.1043>.
- [59] A. Moreira-Gonzalez, C. Loboeki, K. Barakat, L. Andrus, M. Bradford, M. Gilsdorf, I.T. Jackson, Evaluation of 45S5 bioactive glass combined as a bone substitute in the reconstruction of critical size calvarial defects in rabbits, *J. Craniofac. Surg.* 16 (2005) 63–70. <https://doi.org/10.1097/00001665-200501000-00013>.
- [60] H. Kobayashi, A.S. Turner, H.B. Seim, T. Kawamoto, T.W. Bauer, Evaluation of a silica-containing bone graft substitute in a vertebral defect model, *J. Biomed. Mater. Res.–Part A.* 92 (2010) 596–603. <https://doi.org/10.1002/jbm.a.32397>.





# PART III

**EFFICACY OF OSTEOINDUCTIVE  
CALCIUM PHOSPHATE IN  
MAXILLARY SINUS FLOOR  
AUGMENTATION**





# CHAPTER 6

## **OSTEOINDUCTIVE CALCIUM PHOSPHATE WITH SUBMICRON TOPOGRAPHY AS BONE GRAFT SUBSTITUTE FOR MAXILLARY SINUS FLOOR AUGMENTATION: A TRANSLATIONAL STUDY**

---

Lukas A. van Dijk  
Nard G. Janssen  
Silke J. Nurmohamed  
Marvick S.M. Muradin  
Alessia Longoni  
Rob C. Bakker  
Florence G. de Groot  
Joost D. de Bruijn  
Debby Gawlitta  
Antoine J.W.P. Rosenberg

*Submitted*

# A B S T R A C T

## **Objectives:**

The aim of this study was the preclinical and clinical evaluation of osteoinductive calcium phosphate with submicron surface topography as bone graft substitute for maxillary sinus floor augmentation (MSFA).

## **Material and methods:**

A preclinical sheep model of MSFA was used to compare a calcium phosphate with submicron needle-shaped topography (BCP<sub>N</sub>) to a calcium phosphate with submicron grain-shaped topography (BCP<sub>G</sub>) and autologous bone graft (ABG) as control. Secondly, a 10-patient, prospective, randomized, controlled trial was performed to compare BCP<sub>N</sub> to ABG in MSFA with two-stage implant placement (Netherlands Trial Register, NL6436).

## **Results:**

The pre-clinical study demonstrated that both BCP<sub>N</sub> and BCP<sub>G</sub> were highly biocompatible, supported bony ingrowth with direct bone apposition against the material and exhibited osteoinductive bone formation as early as 3 weeks, post-implantation. However, BCP<sub>N</sub> demonstrated significantly more bone formation than BCP<sub>G</sub> at the study endpoint of 12 weeks. Only BCP<sub>N</sub> reached an equivalent amount of bone formation in available space and a greater proportion of calcified material (bone + graft material) in the maxillary sinus compared to the 'gold standard' ABG after 12 weeks. These results were validated in the clinical study, in which BCP<sub>N</sub> was found equivalent to ABG in implant stability, bone height, new bone formation in trephine core biopsies and in overall clinical outcome.

## **Conclusion:**

This translational work demonstrates that osteoinductive calcium phosphates are promising bone graft substitutes for maxillofacial surgery involving dental implants, whereas their bone forming potential depends on the design of their surface features.

## INTRODUCTION

Endosseous dental implants are frequently employed to achieve esthetic and functional restoration of missing teeth and molars. Rehabilitation of the posterior maxilla using dental implants is often challenging, due to prevalence of inadequate quality and quantity of alveolar bone as a result of post-extraction bone resorption and sinus pneumatization [1,2]. Maxillary sinus floor augmentation (MSFA) is performed for almost 40% of posterior maxillary implants to restore bone mass required for implant insertion and integration [3,4]. In general, the procedure has been associated with favorable short- and long-term outcomes in terms of implant survival [5]. Autologous bone grafts (ABGs), which may be harvested from the iliac crest, calvarium or from local sites, *i.e.* chin or intra-oral bone, is considered the 'gold standard' graft material for MSFA due to its osteogenic, osteoinductive and osteoconductive properties [6]. However, ABG harvesting from the iliac crest or calvarium donor sites is associated with donor site morbidity, extended operating time and costs [7,8]. Also, some donor sites provide for limited availability of bone [9]. Furthermore, significant early graft resorption has been reported with the use of ABG for maxillary bone augmentation [10,11].

A variety of bone graft substitutes has been developed to overcome these limitations for MSFA, including allografts, xenografts and alloplastic or synthetic bone substitutes, which all consist of calcified matrices that comprise or mimic the mineral phase of bone [6,12]. An important benefit of such bone substitutes is that they can be used off-the-shelf, surpassing invasive harvesting procedures of ABG. However, while the use of bone graft substitutes in MSFA is generally recommended, variable outcomes have been reported when compared to ABG in clinical settings [12,13]. As developments in the field of bone graft substitutes continue to advance, screening of novel bone graft substitute materials as treatment option for MSFA remains an important research aim.

A disadvantage of most bone substitutes is that they are predominantly osteoconductive, and thus rely on bone ingrowth from the bone surrounding the defect [6]. However, recent efforts to improve the efficacy of calcium phosphate bone graft substitutes have resulted in materials with substantial osteoinductive capacity, as demonstrated by their ability to induce bone formation in non-osseous soft tissues, *i.e.* intramuscularly [14–19]. Harboring both osteoconductive and osteoinductive properties, these calcium phosphates meet 2 out of 3 of the essential properties that autologous bone grafts possess [6]. These materials have been reliably demonstrated to enhance bone healing when compared to materials with mere osteoconductive capacity, as well as equivalence to ABG in orthotopic defects [14–16,20–22]. Moreover, excellent results have been achieved with clinical use of osteoinductive calcium phosphates, such as their use for alveolar cleft reconstruction

in patients with cleft lip and palate and related craniofacial anomalies [23,24], and in extraction sockets in anterior maxilla regions [25]. Osteoinductive materials also have potential for use in MSFA, as they may promote faster and more extensive bone formation than conventional materials, which could ultimately benefit implant osseointegration.

The biocompatibility and performance of bone substitute biomaterials, including calcium phosphates, is dependent on their physicochemical properties, which include phase composition, micro- and macroporosity and surface topography. Osteoinductive capacity has been shown to vary strongly between different calcium phosphate-based materials. It has been repeatedly demonstrated that a critical factor for osteoinductive capacity is the presence of a submicron surface topography, *i.e.* a topography of elongated surface crystals smaller than 1  $\mu\text{m}$  in diameter [14–18]. Moreover, we have recently demonstrated that besides dimension, also the needle-like shape of submicron surface crystals can influence osteoinductive capacity [18].

The aim of the present work was to evaluate osteoinductive calcium phosphate with submicron surface topography as bone graft substitute for MSFA, performing a study in a pre-clinical sheep model as well as a prospective, randomized, controlled, clinical trial.

In the pre-clinical study, two different biphasic calcium phosphate materials with submicron topography were compared to the 'gold standard' iliac crest-derived ABG. The synthetic bone substitutes exhibited either needle-shaped ( $\text{BCP}_N$ ) or grain-shaped ( $\text{BCP}_G$ ) submicron surface crystal morphology. MSFA treatment outcomes were assessed using micro-computed tomography (micro-CT) and histology after 3, 6 and 12 weeks of healing. The clinical study was a prospective, open-label, randomized, controlled trial in which the  $\text{BCP}_N$  bone substitute was compared to ABG in a cohort of 10 patients receiving lateral window MSFA with two-stage implant placement. Outcome measures during 17 months of follow-up included implant stability, bone height by radiography, histology and histomorphometry of trephine bone core biopsies, and clinical outcomes.

## **MATERIALS AND METHODS**

---

### **In vivo evaluation in a sheep MSFA model**

#### ***Bone graft substitutes***

Two commercially available, calcium phosphate bone substitute materials were evaluated in this study. Both materials were used as porous granules, featuring a submicron topography (Fig. 1), *i.e.* a surface crystal diameter  $<1 \mu\text{m}$  and were of biphasic composition,

*i.e.* consisting of  $\beta$ -tricalcium phosphate ( $\beta$ TCP or  $\text{Ca}_3(\text{PO}_4)_2$ ) and hydroxyapatite ( $\text{HA-Ca}_{10}(\text{PO}_4)_6(\text{OH})_2$ ).

In brief, the first formulation,  $\text{BCP}_\text{N}$  (MagnetOs™, Kuros Biosciences BV, the Netherlands), had a surface topography of submicron needle-shaped crystals and a phase composition of 70%  $\beta$ TCP and 30% HA. The granule size range was 0.25 – 1 mm. The second formulation,  $\text{BCP}_\text{G}$ , (MBCP™, Biomatlante, France), had a topography of submicron grain-shaped crystals, a composition of 60%  $\beta$ TCP / 40% HA and a granule size of 0.5 – 1 mm. Both materials were sterile and used according to the manufacturer's instructions for use. Figure 1 shows the surface features of  $\text{BCP}_\text{N}$  and  $\text{BCP}_\text{G}$  as observed by scanning electron microscope. The material properties of  $\text{BCP}_\text{N}$  and  $\text{BCP}_\text{G}$  are detailed in supplementary Table 1.

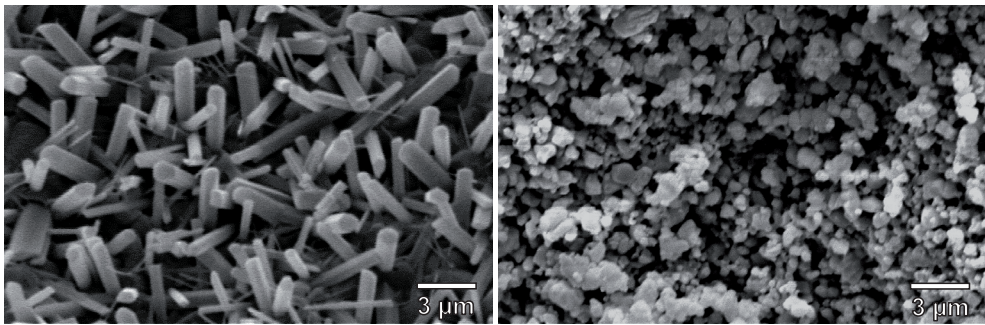


**Figure 1.** SEM micrographs of the submicron topography on  $\text{BCP}_\text{N}$  and  $\text{BCP}_\text{G}$ . The different morphologies of submicron surface crystals are evident, with needle-shaped crystals on  $\text{BCP}_\text{N}$  and grain-shaped crystals on  $\text{BCP}_\text{G}$ .

### **Animals**

Following approval of the study protocol by the Central Authority for Scientific Procedures on Animals (Dutch national CCD, under AVD115002015344), twenty-four sheep (*Ovis Aries*) were admitted in the study. All animals were female, had reached maturity (age 3-6 years), and weighed between 60–100 kg. The animals were randomized into 3 groups for 3-, 6- and 12-week follow-up periods, with 6, 9 and 9 animals per group, respectively. No animals were excluded. Animals were housed at the 'Gemeenschappelijk Dierenlaboratorium' in Utrecht. Animal housing and care was compliant with the national guidelines and regulations. A weight loss of >20% (checked weekly), severe wound abscess (checked daily) or strongly reduced mobility (checked daily) were used as humane endpoints. An experimental timeline of the study is shown in Figure 2A. This study was compliant with the ARRIVE guidelines.

### **Surgical procedure**

Bilateral MSFA in this sheep model was performed following the lateral window approach, as previously described [26]. Prior to surgery, animals were pre-medicated with analgesics

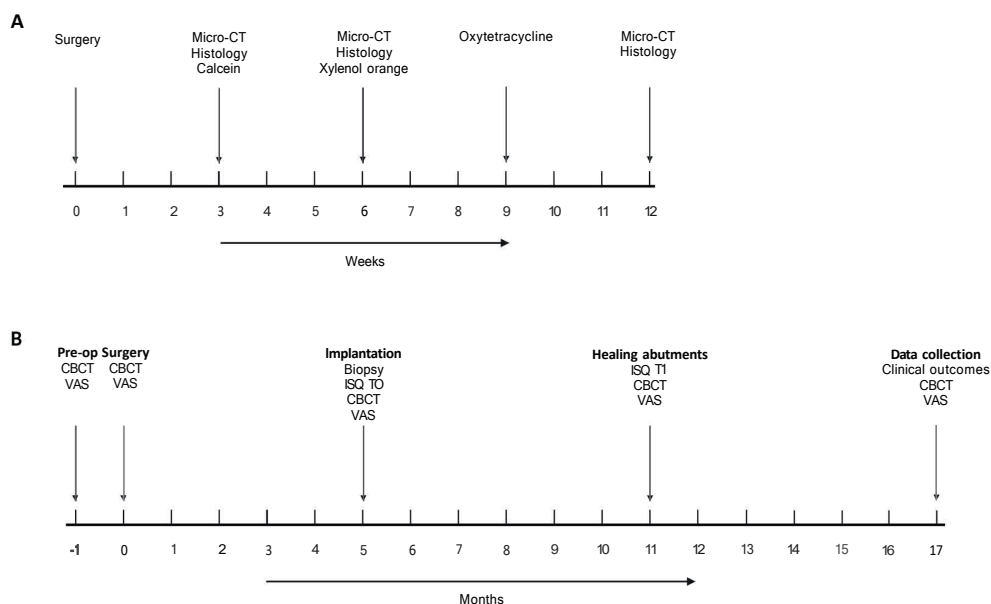


**Figure 2.** Study timelines. **(A)** Experimental timeline for the sheep MSFA study. **(B)** Study timeline of the clinical MSFA trial.

buprenorphine (*t.d.* 5  $\mu\text{g/hr}$ ) and meloxicam (*i.v.* 0.5 mg/kg) and antibiotic amoxicillin/clavulanic acid (*i.v.* 10 mg/kg). Anesthesia was initiated with detomidine (*i.m.* 0.05 mg/kg) and propofol (*i.v.* 5-7 mg/kg) and was maintained using propofol (*i.v.* 10 mg/kg/h) and sufentanil (*i.v.* 0.003 mg/kg/h). Animals were connected to an inhalation ventilator and positioned in sternal recumbency. Operation sites were washed, shaved, disinfected and sterile drapes were applied. Corticocancellous ABG was harvested from the iliac crest and was reduced to 2-5 mm particles. The maxillary sinuses were approached via the facial lateral wall, which was exposed by sharp and blunt dissection. Using a high-speed dental burr, a bony window of  $\pm 1 \times 1 \text{ cm}^2$  was created under continuous irrigation, taking care not to perforate the underlying Schneiderian membrane. After removal of the bony window, the Schneiderian membrane was carefully elevated with blunt dissectors, to expose the bony surface of the maxillary sinus floor and walls. Next, 2 cc of either ABG, BCP<sub>N</sub> or BCP<sub>G</sub> was implanted on the exposed maxillary sinus floor. Both BCP<sub>N</sub> and BCP<sub>G</sub> were mixed with 1-2 cc of local blood prior to implantation, to improve handling. Each animal received a bilateral implantation and the three graft/substitute materials were assigned in a randomized manner for each timepoint (3 weeks ( $n=4$ ), 6 weeks ( $n=6$ ) and 12 weeks ( $n=6$ )). The soft tissues at the surgical site were closed in layers using resorbable sutures (Vicryl 3-0, Ethicon, Brussels, Belgium). After surgery, animals received meloxicam (*s.c.* 0.5 mg/kg, 1x/day for 3 days) for pain management and penicillin-neomycin (0.05 mg/kg, 1x/day for 3 days) as antibiotic, in addition to standard care and monitoring.

**Calcium-binding fluorochrome labeling**

Polychrome sequential labeling with calcium-binding fluorochromes was performed on the 12-week group, in order to visualize active sites of mineralization during bone formation. Treatment with three different fluorescent calcium-binding labels was performed, one at each time point. The sequentially injected fluorochrome labels used were calcein at 3 weeks (CN, 10mg/kg, *i.v.* – green), xylenol Orange at 6 weeks (XO, 90 mg/kg, *i.v.* – red) and oxytetracycline at 9 weeks (OTC, 20 mg/kg, *i.m.*–yellow), respectively.

**Sample harvesting and processing**

After reaching the experimental endpoint, animals were euthanized by pentobarbital. The maxillary sinuses were excised, trimmed and fixed in 4% formaldehyde solution for 1 week at 4° C. The samples were then dehydrated through a series of increasing ethanol concentrations (70-100%) and subsequently embedded in polymethyl-methacrylate (PMMA).

**Micro-computed tomography**

PMMA-embedded samples were scanned in Micro-CT scanner (QuantumFX, Perkin Elmer) with a voxel size of 59 x 59 x 59  $\mu\text{m}^3$ , voltage at 90 kV and a tube current of 180  $\mu\text{A}$ . On TIFF stacks derived from the scans, vertical bone height was measured in the bucco-palatal plane at the center of each graft, in a straight line from lowest level of the sinus floor to the highest level of the graft, using dedicated software (3D Slicer 4.10).

**Histology**

A Leica SP1600 saw microtome was used to cut ~ 15-micron thick sections from the center of each graft in bucco-palatal direction. On these sections, a histological staining of methylene blue (Sigma; 1% in 0.1 M borax buffer, pH 8.5) and basic fuchsin (Sigma; 0.3% in demi water) was performed to visualize bone tissue (bone matrix: pink, fibrous tissues: blue). Sections were examined under a Leica microscope (Eclipse 50i; Nikon) and were scanned with a slide scanner (DiMage scan 5400 Elite II; Konica Minolta, Tokyo, Japan).

A fluorescence microscope (BX51, Olympus) was used to visualize fluorochrome label deposition in otherwise unstained sections. Fluorescent signals in each section were captured using appropriate excitation and emission wavelength filters for CN (ex:436-495, em:517-540), XO (ex:377-570, em:610-615) and OTC (ex:365-490, em:520-570). The polychrome fluorescent signals were then digitally merged with a transmission light microscopy image (15% opacity) using software (Adobe Photoshop CS5) to visualize the deposition of each label in the sections.

### ***Histomorphometry***

Histomorphometry of methylene blue/basic fuchsin-stained PMMA sections was performed on digitalized scans by pseudo-coloring of pixels representing bone (B; mineralized + osteoid) and bone graft material (M, only for bone graft substitutes) in the entire area of new bone formation as region of interest (ROI). The examiners were blinded for the treatments. The number of pixels for B, M, and ROI were used to calculate the area percentage of bone in the available space using the following formula:  $B/(ROI-M) \times 100$ . In addition, the area percentage of remaining implant material was calculated by the following formula:  $M/ROI \times 100$ . Lastly, the combined proportion of bone + material was calculated by:  $(B+M)/ROI \times 100$ .

## **Evaluation in a clinical MSFA study**

### ***Study Design***

This was a single-center, prospective, open-label, randomized controlled trial conducted at a university hospital in the Netherlands, at the department of Oral and Maxillofacial Surgery. Ethical approval was provided by the Medical Research Ethics Committee Utrecht (NL61242.041.17), in accordance with the principles of the Declaration of Helsinki (version October 2008) and the Medical Research Involving Human Subjects Act. Each participant provided written informed consent after receiving adequate verbal and written explanation prior to inclusion in the study. Based on computerized block randomization (1:1), patients were allocated to the parallel treatment arms of the test group, BCP<sub>N</sub>, or the control group ABG. Study investigators were blinded for the treatment allocation, apart from the treating clinicians and study coordinator. A timeline of the study presented in Figure 2B.

### ***Study inclusion criteria***

The most important inclusion criteria were age between 18 and 75 years and participants qualifying for MSFA with two-stage implant placement. Indications for surgery were presence of a unilateral or bilateral (partial) atrophic posterior maxilla in the premolar/molar areas, with a residual vertical bone height between 2 and 6 millimetres. The full inclusion and exclusion criteria of the study are presented in the appendix, Table 2.

### ***Intervention***

MSFA was performed using the lateral-window technique with trapdoor approach to access the sinus and elevate the Schneiderian membrane. Depending on the treatment arm, the thus created sub-Schneiderian void was implanted with BCP<sub>N</sub> granules of 0.25-1 mm or morselized autograft harvested locally (*i.e.* mandibular ramus) or from the iliac crest. The amount of graft or material used depended on the individual's sinus volume, the desired vertical height, and the number of planned implants per side. The surgery was ended by replacement of the mucoperiosteal flap and primary wound closure.



Primary implant placement was performed after 5 months of healing. During osteotomy of the implant bed a trephine core bone biopsy was harvested using a trephine burr (2 mm internal / 3 mm external diameter, Meisinger, Neuss, Germany). The trephine core biopsies were preserved in 10% formalin and stored until histological processing. After implant insertion (OsseoSpeed® EV, Astra Tech Implant System, Dentsply Sirona Implants, Mölndal, Sweden), cover screws were installed on the fixtures and primary wound closure was attained. After another 6 months of healing, at 11 months follow-up, patients were invited to the outpatient clinic for installation of healing abutments. The prosthetic restorations were installed after the soft tissues had healed. Following another 6 months, at 17 months follow-up, the patients were invited to the outpatient clinic for a final visit during which clinical assessment of peri-implant health was performed. At all study visits throughout the follow-up period, a cone beam computed tomography (CBCT) scan was made.

### ***Outcome Measures***

#### ***Implant stability***

Implant stability quotient (ISQ) of dental implants in the posterior maxilla was measured by resonance frequency analysis (RFA) using the Penguin<sup>RFA</sup> system (Integration Diagnostics AB, Gothenburg, Sweden). Primary stability was recorded immediately after implantation (T0, 5 months) and secondary stability was measured prior to installation of the healing abutments (T1, 11 months). The intra-implant difference in primary and secondary stability was calculated using the formula  $\Delta ISQ = ISQ_{T1} - ISQ_{T0}$ .

#### ***Bone height***

Bone height of the maxillary sinus floor was measured by CBCT pre-operatively (baseline), post-operatively and at 5 months, 11 months and 17 months of follow-up.

#### ***New bone formation***

Formalin-fixed trephine core biopsies were decalcified in EDTA, dehydrated using an ethanol series and embedded in paraffin for histology. Specimens were sectioned using a microtome and subsequently stained with hematoxylin and eosin. Sections were examined under a Leica microscope (Eclipse 50i; Nikon) and were scanned with a slide scanner (DiMage scan 5400 Elite II; Konica Minolta, Tokyo, Japan).

Histomorphometry of biopsy sections was performed on the digitalized scans by pseudo-coloring of pixels representing bone (B) and remaining material (M, only for BCP<sub>N</sub>) in the region of interest (ROI) using Photoshop (Photoshop CS5). The area percentage of bone and remaining implant material was calculated as described for the sheep study.



### ***Clinical outcomes***

Clinical outcomes included implant survival rate, adverse events and pain by visual analog scale (0-100) recorded on all visits throughout the follow-up period. Moreover, peri-implant health was assessed after 17 months of follow-up using the gingival index [27], supra-gingival plaque index[28] and dichotomous bleeding index. Lastly, probing depth of the implants in the posterior maxilla was also measured after 17 months of follow-up (buccal, palatal, mesial, distal).

### ***Statistical analysis***

For the animal study, sample size was determined based on a statistical power of 80%, a p-value of 0.05 and detectable effect size of  $\pm 30\%$ , considering one-way ANOVA. For the clinical study, sample size was determined for a non-inferiority parallel group trial, using  $\alpha$ -error probability of 2.5% and power at 80%. All data are presented as mean  $\pm$  standard deviation. Quantitative data were analyzed using statistical analysis software, Graphpad Prism (version 7, Graphpad, San Diego, CA). Normal distribution of the data was confirmed by the Shapiro-Wilk normality test. In the preclinical and clinical study, vertical bone height, histomorphometry and implant stability data were analyzed using Analysis of Variance, followed by the Holm-Sidak test for *post hoc* analysis. All other data in the clinical study were analyzed using Mann-Whitney U test (for non-normal data) or Fisher's exact test (for categorical data). A significance level of  $P < 0.05$  was used. The following notation was used to indicate statistical significance: \*  $p < 0.05$ , \*\*  $p < 0.01$ , \*\*\*  $p < 0.001$ .

## **RESULTS**

### **Sheep MSFA model**

All MSFA surgeries and graft implantations were completed uneventful. The animals recovered without complications and all reached the final endpoint in healthy condition. In all groups, no adverse reactions to the graft materials were observed.

### ***Micro-CT***

On micro-CT scans (Fig. 3 A,B), the implanted bone substitutes were localized beneath the Schneiderian membrane in direct contact with the bony floor of the maxillary sinus and walls.. In all groups, the implants were contained at their implantation sites and there was no evidence of graft migration. Over time, the ABG particles remodeled and fused to one another and onto the host bone surfaces, resulting in a solid trabeculated bone mass at 12 weeks. For the synthetic bone substitutes, progressive mineralized growth into the implants could be observed over time. For both bone substitutes, mineralized matrix gradually invaded the intergranular space, resulting in compact, consolidated grafts at the

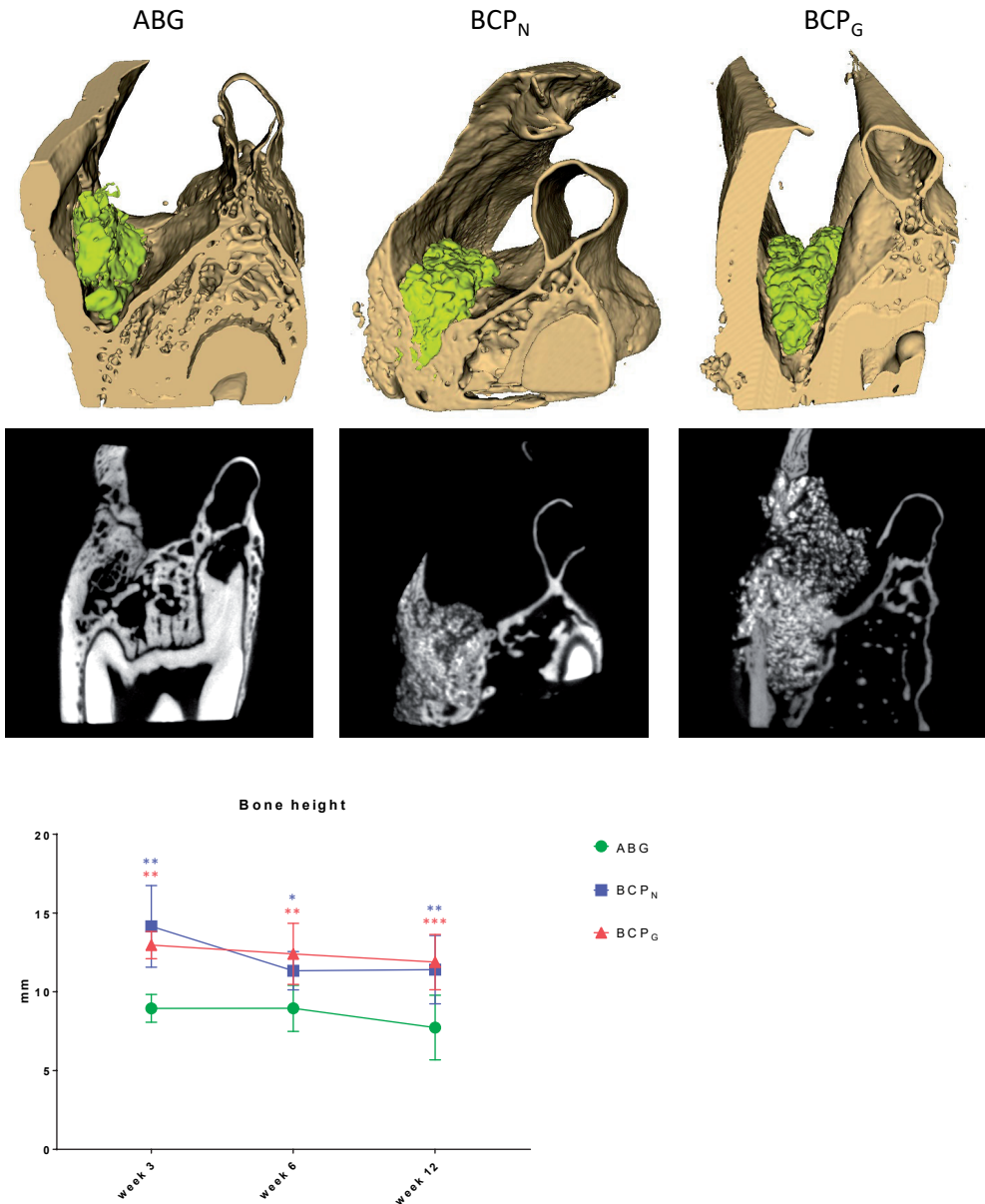


**Figure 3.** Evaluation of MSFA by micro-CT. **(A)** Representative 3D reconstructions of bone grafts (yellow) implanted beneath the Schneiderian membrane on the bony floor the maxillary sinus after 12 weeks of healing. The bone grafts can be observed in contact with the host bony sinus floor and walls (off-white). **(B)** Representative micro-CT slices from the center of the implanted grafts at 12 weeks. Radiodense calcium phosphate granules and mineralized bone matrix can be observed. The more homogeneous regions in BCP<sub>N</sub> and BCP<sub>G</sub> specimens represent integration of calcium phosphate in new mineralized bone matrix. **(C)** Vertical bone height, as measured by micro-CT in the center of the grafts at week 3, 6 and 12. Blue asterisks indicate significance for BCP<sub>N</sub> vs ABG, red asterisks for BCP<sub>G</sub> vs ABG.

12 week timepoint. Some specimens of BCP<sub>N</sub> and BCP<sub>G</sub> showed regions without mineralized ingrowth after 12 weeks, often located near the lateral window or in the superior aspect of the graft, *i.e.* regions most distant from the host bone surfaces. Overall, the augmentations with the synthetic grafts appeared to have more volume compared to ABG implants.

Vertical augmentation height (Fig. 3 C) of the different graft types was measured on micro-CT scans to determine MSFA success and graft stability during the follow-up period. The augmentation height range was 5.31–11.52 mm for ABG, 8.67–16.98 mm for BCP<sub>N</sub> and 8.97–14.46 mm for BCP<sub>G</sub>. At each timepoint, augmentation height of BCP<sub>N</sub> and BCP<sub>G</sub> was significantly higher than that of ABG, while the two synthetic bone substitutes did not result in significantly different height from each other. After 12 weeks follow-up, the difference in mean augmentation height between the synthetic bone substitutes (BCP<sub>N</sub>: 11.88 ± 2.17 mm ; BCP<sub>G</sub> 11.40 ± 1.75 mm) and ABG (7.73 ± 2.05 mm) was ± 4.0 mm, corresponding to roughly 1.5-fold greater augmentation height for the synthetic implants versus ABG. All graft types demonstrated a decreasing trend in augmentation height between 3 and 12 weeks, being the largest for BCP<sub>N</sub> (2.75 mm), followed by ABG (1.22 mm) and BCP<sub>G</sub> (1.08 mm).

### ***Histology***

Histological analyses were performed to complement the micro-CT data and further investigate new bone formation in the implants. On low magnification histological overviews (Fig. 4 A) of ABG specimens, individual ABG segments could still be clearly distinguished at the 3-week timepoint, while embedded in a matrix of fibrous tissue. The initiation of new bone formation on the surface of the ABG particles as well as on the sinus floor and walls could be observed. After 6 weeks, the individual bone pieces were more interconnected as a result of new bone formation. By 12 weeks, the ABG implants had consolidated into a single, interconnected bone mass and were fused to the bony floor of the sinus. The proportion of newly formed and remodeled bone had increased, although original ABG fragments could still be recognized. Regions of fibrous tissue could still be discerned in the graft area after 12 weeks.

For the synthetic bone graft substitutes, calcium phosphate granules could be recognized on the histological sections (Fig. 4 A). On low magnification histological overviews of 3-week specimens, the graft materials were entirely embedded in soft tissue and early osteoconductive bone ingrowth originating from the host bone could be observed with both materials. Interestingly, 2/3 implants of BCP<sub>N</sub> and 1/4 of BCP<sub>G</sub> exhibited regions with new bone that were suspected to originate from osteoinductive bone formation, in areas at the center of the implants or near the Schneiderian membrane (Fig. 4 B). Further progression of both osteoconductive and osteoinductive bone formation was observed at 6 weeks while at 12 weeks, mineralized bone was bridging between granules throughout the grafts, resulting in a trabeculated, interconnected mass of bone and calcium phosphate

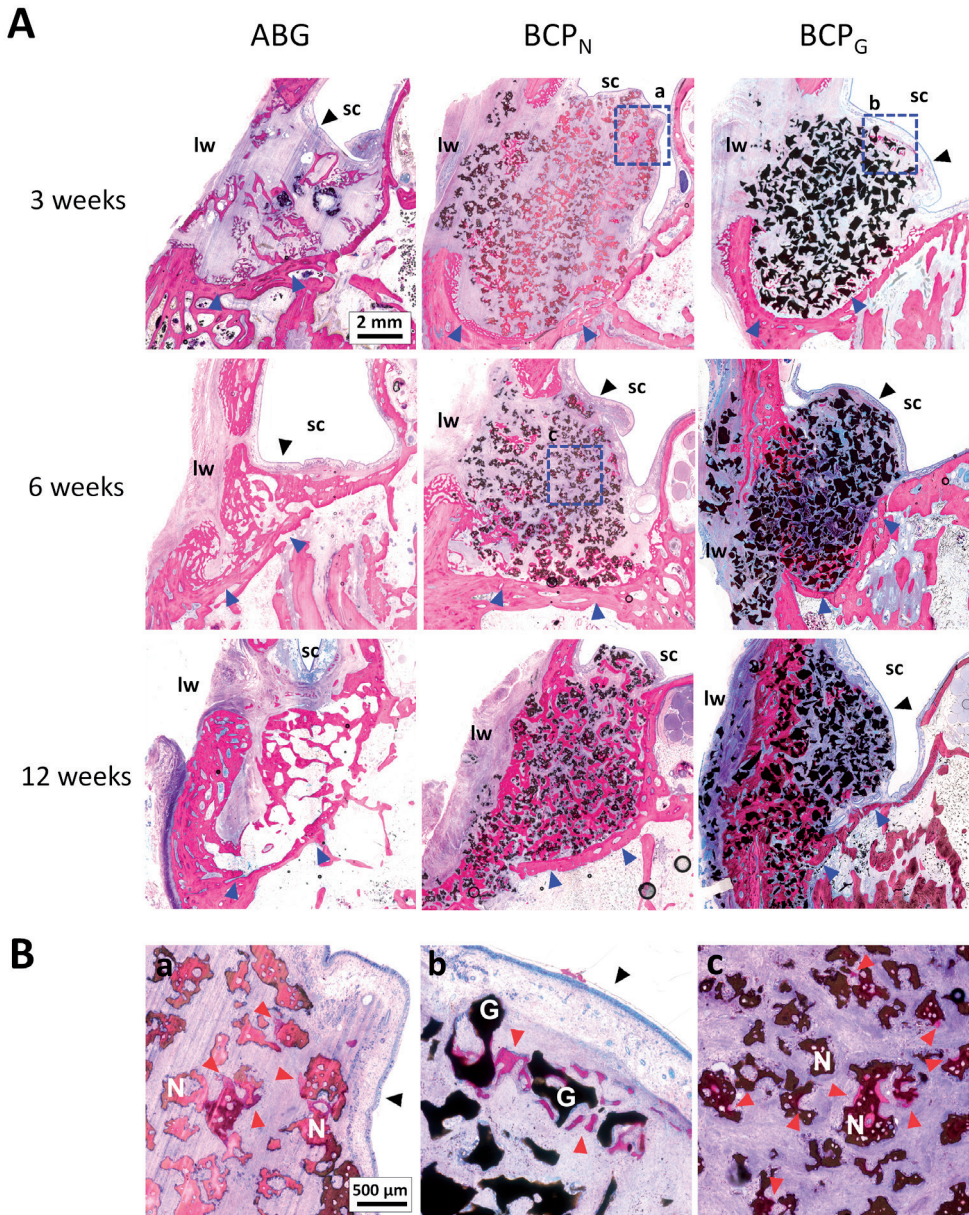


**Figure 4.** Histology of bone grafts implanted beneath the maxillary sinus floor (basic fuchsin-methylene blue). **(A)** Representative sections of ABG, BCP<sub>N</sub> and BCP<sub>G</sub> at time-points 3, 6 and 12 weeks are presented. ABG particles and calcium phosphate granules can be observed in direct contact with the bony sinus floor under the elevated Schneiderian membrane. Progressive bone formation and graft consolidation with time is evident. **(B)** Regions of osteoinductive bone formation observed in BCP<sub>N</sub> and BCP<sub>G</sub>, often near the Schneiderian membrane, are shown in higher magnification (**blue dashed frames a-c, panel A**). *pink*: bone matrix, *black/brown*: calcium phosphate granules, *sc*: sinus cavity, *lw*: lateral window, *black arrowheads*: Schneiderian membrane, *blue arrowheads*: sinus floor, *red arrowheads*: osteoinductive bone formation, *N*: BCP<sub>N</sub>, *G*: BCP<sub>G</sub>.

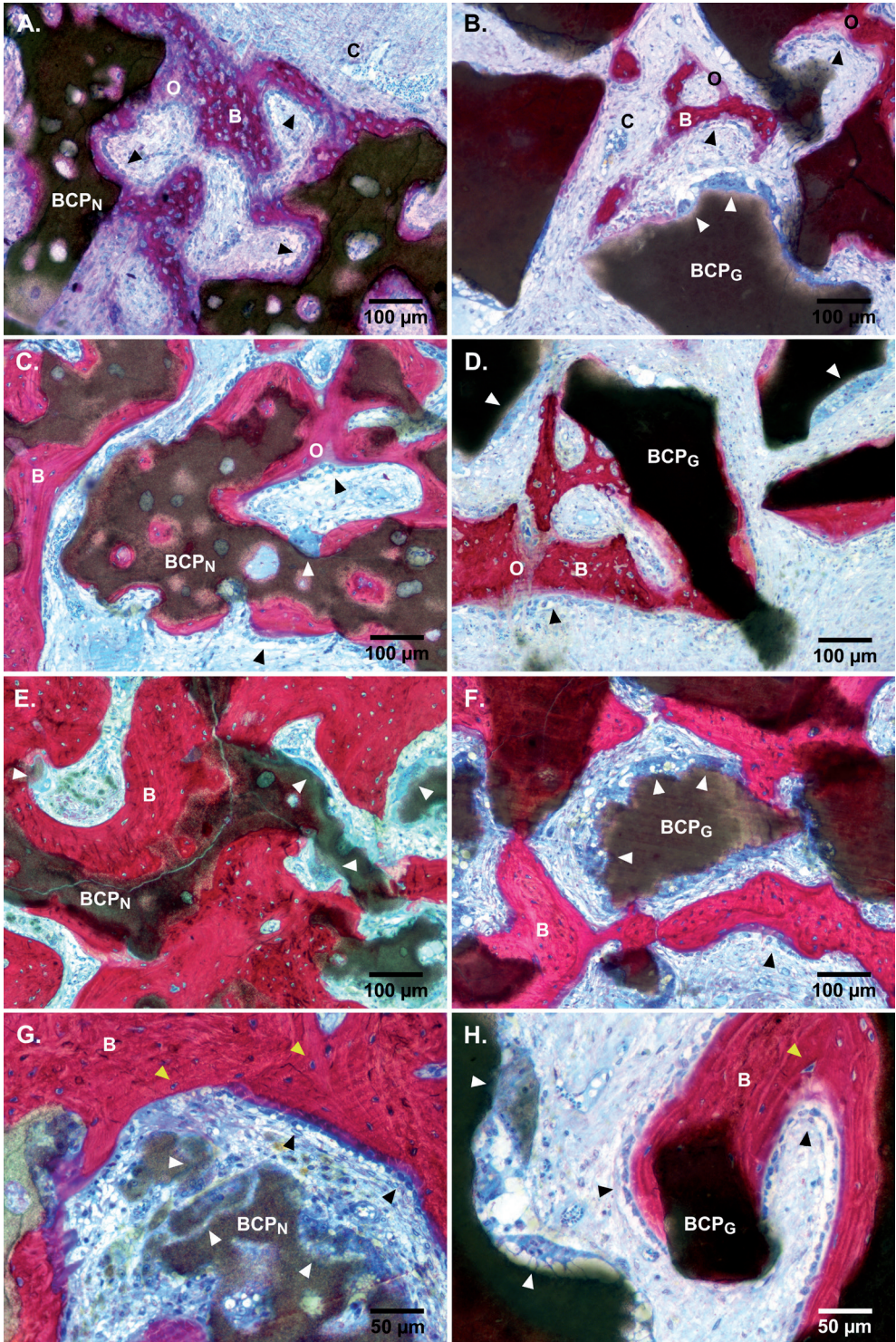
particles. As with ABG, specimens of either synthetic material presented local regions with fibrous tissue after 12 weeks.

High magnification microscopy of BCP<sub>N</sub> and BCP<sub>G</sub> specimens (Fig. 5) revealed new bone formation around and directly against BCP particles at 3 weeks. Presence of ample osteoblasts actively depositing osteoid as well as a woven bone morphology were indicative of ongoing primary osteogenesis. No adverse tissue reactions to the synthetic implants were observed. A lamellar bone phenotype was observed at 6 weeks, demonstrating that the woven bone matrix was remodeled into mature, secondary bone tissue. BCP granules were progressively engulfed by the ongoing bone formation process that incorporated them in the mineralized bone matrix. After 12 weeks, sites of new bone deposition were less frequently observed. By this time, the regions between BCP granules were predominantly occupied by dense lamellar bone matrix that bridged the adjacent granules. Overall, the bone tissue that had formed around both synthetic materials had all characteristics of normal, healthy bone tissue, including bone marrow spaces, concentric lamellae, osteocytes and capillaries. Large, phagocytosing multinucleated cells were frequently observed on the exposed surfaces of either BCP material at all timepoints. Degraded BCP material was commonly observed in the cytoplasm of these cells, indicating their ability to actively resorb the BCP material (Fig. 5 G,H).

### ***Histomorphometry***

Histomorphometry performed on histological sections allowed the quantitative analysis of bone formation in the implants over time (Fig. 6). Morphometry of bone matrix (Fig. 6 A) revealed a higher area percentage of bone in available space for ABG compared to the synthetic grafts at 6 weeks. It must be noted that the percentage of bone in the ABG specimens includes the implanted autograft particles as well as newly formed bone, while for the synthetic materials it only includes newly formed bone. At the study endpoint at 12 weeks, bone formation in BCP<sub>N</sub> ( $38.3 \pm 9.8\%$ ) was comparable to the ABG control ( $44.0 \pm 8.5\%$ ). However, with BCP<sub>G</sub> the percentage of bone formation at 12 weeks ( $26.8 \pm 11.4\%$ ) was 11.4% lower than BCP<sub>N</sub> and 17.2% lower than ABG. This corresponded to approximately one third less bone formation in the available space for BCP<sub>G</sub> than with ABG and BCP<sub>N</sub>. Area

**Figure 5 (right).** High magnification histology (basic fuchsin-methylene blue). Representative sections of BCP<sub>N</sub> (A,C,E,G) and BCP<sub>G</sub> (B,D,F,H) are presented at 3 weeks (A,B), 6 weeks (C,D) and 12 weeks (E,F) post-surgery. Bone matrix is observed between and in direct contact with calcium phosphate granules. Maturation of bone tissue over time can be appreciated, with early bone characterized by woven bone morphology and sites of osteoid deposition, while mature bone is characterized by lamellar phenotype. Aligned, cuboidal osteoblasts and osteocytes can be observed at all time-points. Active phagocytosis of calcium phosphate material by large multinucleated cells was observed at all timepoints (G,H). *B*: bone, *O*: osteoid, *C*: capillary, *black arrowheads*: osteoblasts, *white arrowheads*: phagocytosing multinucleated cells, *yellow arrowheads*: osteocytes.



6

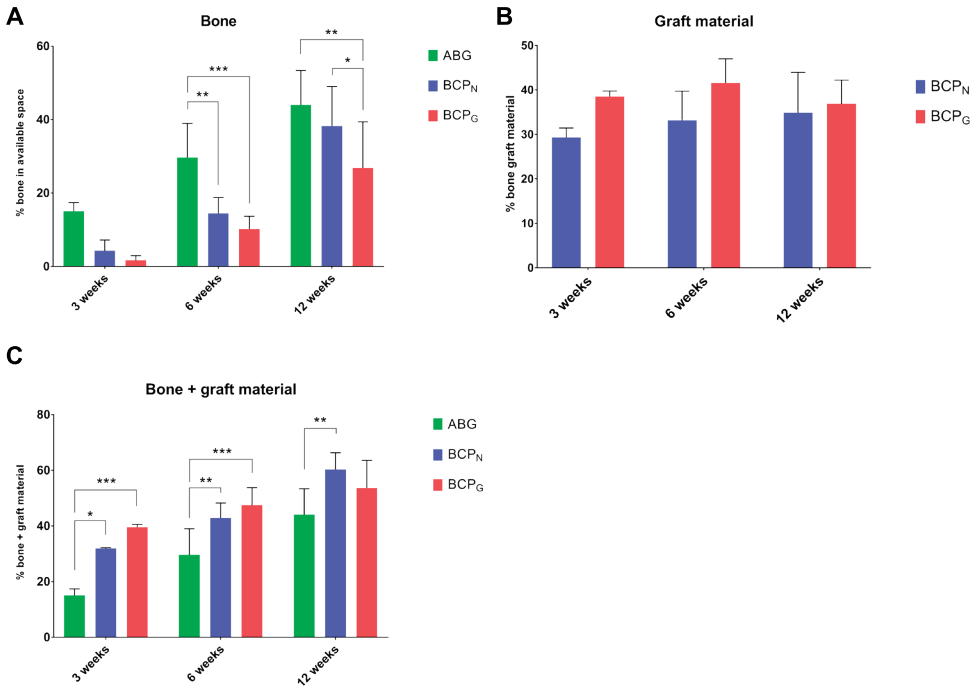


**Figure 6.** Histomorphometry of graft tissue. **(A)** Percentage of bone matrix in available space for ABG, BCP<sub>N</sub> and BCP<sub>G</sub>. **(B)** Percentage of bone and graft material in graft tissue for ABG, BCP<sub>N</sub> and BCP<sub>G</sub>. **(C)** Percentage of residual graft material for calcium phosphate bone graft substitutes BCP<sub>N</sub> and BCP<sub>G</sub>.

percentages occupied by BCP<sub>N</sub> and BCP<sub>G</sub> bone graft substitute materials were equivalent at all timepoints (Fig. 6 B). The area percentages of both graft materials did not follow a negative trend with time, which could have indicated material resorption. When combining bone and calcium phosphate graft material (Fig. 6 C), the area percentage for the bone substitutes was greater than for ABG at 3 and 6 weeks. After 12 weeks, area percentage of combined bone and graft material was only higher in BCP<sub>N</sub> (60.3% ± 5.5%) *versus* ABG (44.0% ± 8.5%).

### Fluorochrome label analysis

Intra-animal bone formation dynamics were analyzed by observation of the deposition of sequentially injected calcium-binding fluorochrome labels using fluorescence microscopy (Fig. 7). Presence of the fluorochrome label CN (3 weeks, green) in the majority of BCP<sub>N</sub> and BCP<sub>G</sub> specimens indicated that the onset of new bone formation had occurred by 3 weeks. The calcein label was mostly present in regions near the host bone surfaces (Fig. 7 A,B) but was also observed in isolated sites of osteoinductive bone formation more distant from host bone. However, in the central regions of the implants (Fig. 7 C,D), the labels XO (red, 6 weeks) and OTC (yellow, 9 weeks) were dominant, indicating that osteogenesis had mostly



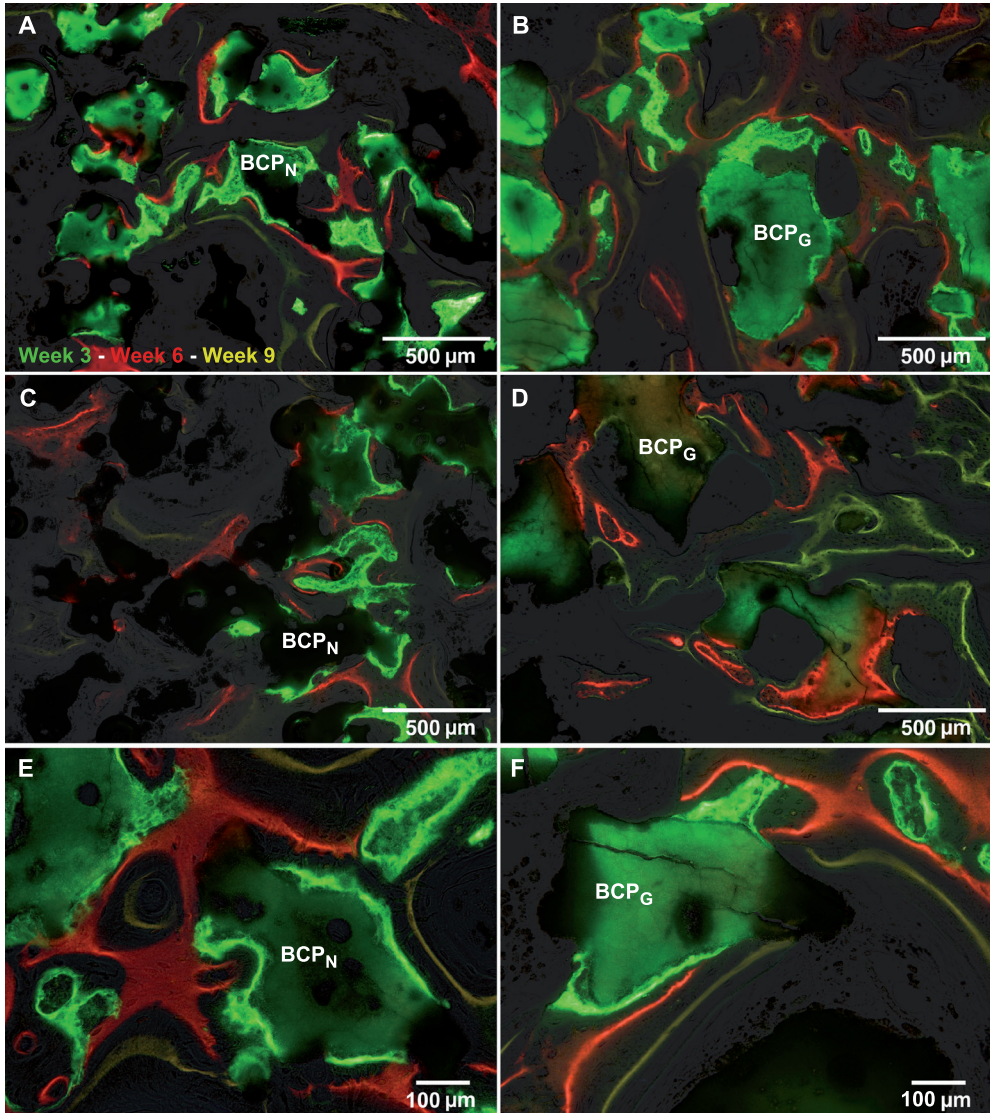


**Figure 7.** Histology of fluorochrome labels. Calcium-binding fluorochrome labels CN (3 weeks, green), XO (red, 6 weeks) and OTC (yellow, 9 weeks) indicate sites of active bone matrix mineralization at the respective time-points. Representative sections of BCP<sub>N</sub> (**A,C,E**) and BCP<sub>G</sub> (**B,D,F**) are shown from regions nearby host bone (**A,B**) and from the center of the grafts (**C,D**). Sequential deposition of the labels shows that bone formation originated against the surface of the graft materials and progressed outwards (**E,F**).

6

started there between week 3 and week 6. Evaluating the sequential deposition of the labels, progression of bone formation with time could be clearly observed. Bone formation was observed to commonly originate at the surface of the calcium phosphate granules, with the fluorochrome label CN, in regions near host bone, and XO, in the core of the implants, being deposited directly against BCP<sub>N</sub> and BCP<sub>G</sub>. OTC was less frequently observed in direct contact with the calcium phosphate surface, indicating that most granules were already incorporated into mineralized bone matrix between 6 and 9 weeks.

## **Clinical MSFA study**

### *Participants, treatment and baseline data*

A total of ten participants were enrolled in the trial, of which five were allocated to the ABG group and five to the BCP<sub>N</sub> group. Sociodemographic and treatment information of the patient cohort are presented in Table 1. Participants in the two treatment arms were not significantly different in age and gender. Likewise, there were no significant differences between treatment characteristics of the cohorts, including unilateral or bilateral MSFA, number of implants per patient and implant dimensions. Residual vertical bone height in the atrophic posterior maxilla was similar for both treatment groups. Except for one participant in the BCP<sub>N</sub> group who missed the final visit at 17 months, all patients completed follow-up.

### *Implant stability*

Results of implant stability measurements are presented in Table 2. Although mean ISQ was higher for BCP<sub>N</sub> in all instances, there were no significant differences between the treatment groups in primary or secondary stability, on either the bucco-lingual and mesio-distal axes. Similarly, no significant differences were determined for  $\Delta$ ISQ. Mean  $\Delta$ ISQ values were close to zero for both treatment groups, indicating a minimal difference between primary and secondary implant stability overall.

### *Bone height*

Bone height was not significantly different between the ABG and BCP<sub>N</sub> groups during the entire study follow-up (Fig. 8). For both treatment groups, bone height after MSFA procedure was significantly greater versus baseline, indicating successful sinus floor augmentation. After MSFA, a trend of decreasing bone height was apparent over time for both groups, albeit only significant for ABG at 17 months.

### *New bone formation*

Histology of trephine core biopsies was used to evaluate new bone formation in the augmented maxillary sinus floor. Low magnification histological overviews (Fig. 9) revealed new bone formation throughout the biopsies for both ABG and BCPN, whereas BCPN specimens presented residual calcium phosphate particles. ABG biopsies appeared to

**Table 1. Participants, treatment and baseline data**

	Total	ABG	BCPN	p-value*
<b>Participants</b> n	10	5	5	
<b>Age (years)</b> Mean (SD), [min-max]	56.7 (11.2) [33-74]	55.8 (14.7) [33-74]	57.6 (9.7) [46-72]	0.794
<b>Gender</b> n (%)				
<b>Female</b>	3 (30)	2 (40)	1 (20)	>0.999
<b>Male</b>	7 (70)	3 (60)	4 (80)	
<b>MSFA procedure</b> n (%)				
<b>Unilateral</b>	4 (40)	1 (20)	3 (60)	>0.999
<b>Bilateral</b>	6 (60)	4 (80)	2 (40)	
<b>Residual bone height (mm)</b> Mean (SD), [min-max]	3.1 (1.1) [2.0-5.8]	3.4 (1.3) [2.0-5.8]	2.6 (0.8) [2.0-4.0]	0.323
<b>Number of implants</b> n (%)	23 (100)	12 (52.2)	11 (47.8)	
<b>Implants per patient</b> Mean (SD), [min-max]	2.4 (1.6) [1-6]	2.4 (1.1) [1-4]	2.2 (2.2) [1-6]	0.476
<b>Implant size (mm)</b> Mean (SD), [min-max]				
<b>Diameter</b>	4.2 (3.7) [3.6-4.8]	4.2 (3.1) [3.6-4.8]	4.4 (4.5) [3.6-4.8]	0.175
<b>Length</b>	10.3 (1.3) [8.0-13.0]	10.4 (1.0) [9.0-11.2]	10.3 (1.7) [8.0-13.0]	0.783

\* Mann-Whitney U test or Fisher's exact test

**Table 2. Implant stability**

	Bucco-lingual			Mesio-Distal		
	ABG	BCPN	p-value*	ABG	BCPN	p-value*
<b>ISQ T0 (Primary stability)</b> Mean (SD), [min-max]	<b>57.0</b> (12.3) [43.0-79.0]	<b>60.2</b> (17.7) [30.0-79.0]	0.820	<b>61.9</b> (12.44) [43.7-79.0]	<b>67.0</b> (13.0) [45.6-80.0]	0.657
<b>ISQ T1 (Secondary stability, 6 months)</b> Mean (SD), [min-max]	<b>56.1</b> (10.4) [43.0-71.0]	<b>65.4</b> (10.7) [53.7-83.0]	0.306	<b>59.6</b> (13.1) [42.3-77.0]	<b>70.7</b> (17.1) [43.0-98.0]	0.2269
<b>Δ ISQ (T1-T0)</b> Mean (SD), [min-max]	<b>-0.8</b> (10.6) [-21.0-16.7]	<b>1.1</b> (12.1) [-21.0-10.7]	0.820	<b>-2.3</b> (12.3) [-30.7-13.0]	<b>-0.8</b> (11.6) [-13.3-18.0]	0.822

\* Two-way ANOVA



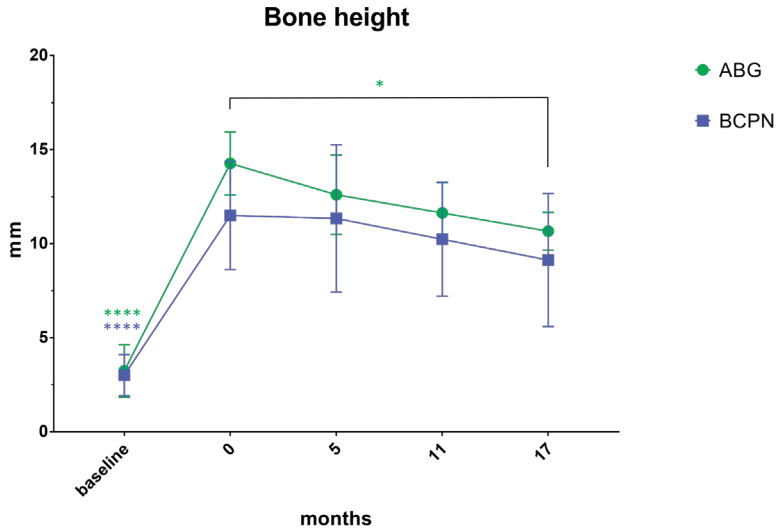
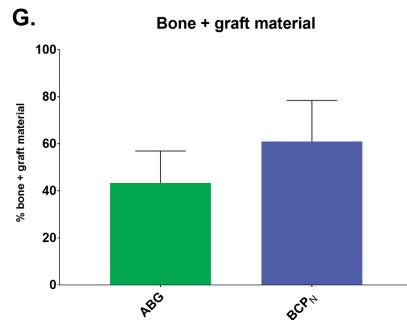
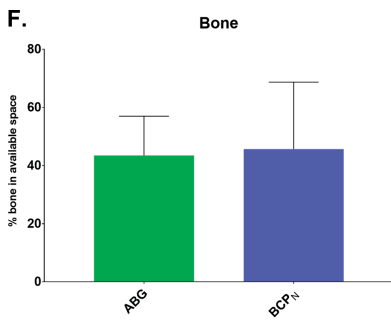
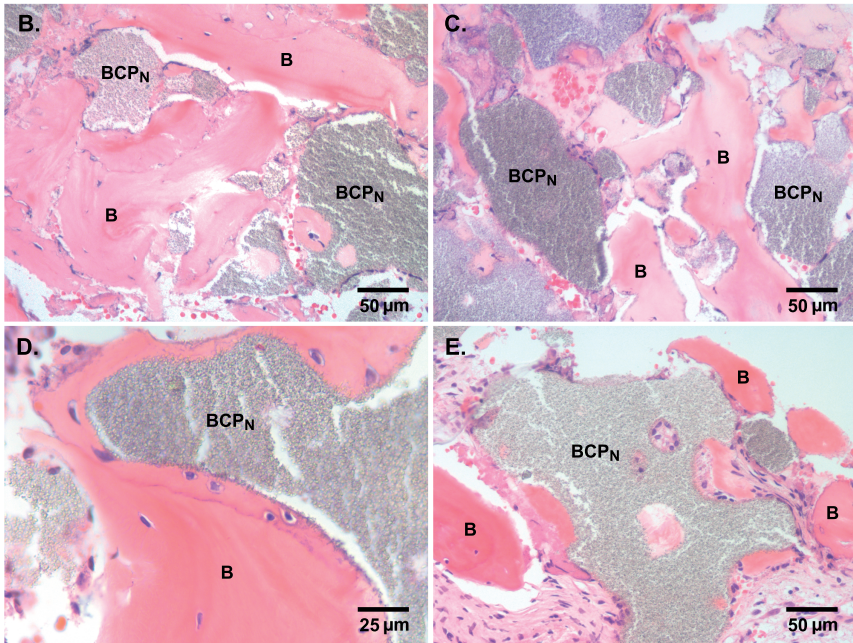
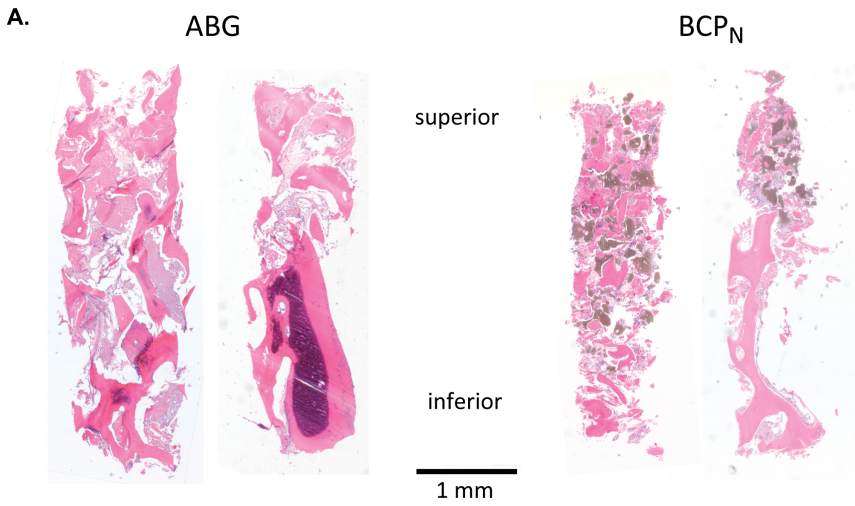


**Figure 8.** Bone height in the posterior maxilla as measured by CT at the location of the implants at baseline, month 5, 11 and 17 months. Green asterisks indicate significance between timepoints for ABG, blue asterisk indicate significance between timepoints for BCP<sub>N</sub>. No significant differences were determined between the treatment groups.

have a slightly greater soft tissue component than BCP<sub>N</sub> biopsies. On higher magnification (Fig. 9), BCP<sub>N</sub> biopsies demonstrated direct apposition of bone tissue against the calcium phosphate particles, and bone tissue was bridging between particles (Fig. 9 A,B). Bone tissue had a normal appearance and presented osteocytes in lacunae (Fig 9. C). New bone formation was occasionally observed originating at the surface of the BCP<sub>N</sub> particles (Fig 9. D).

Histomorphometry of the graft area in the biopsies (Fig 9. F, G) revealed an equivalent area percentage of bone tissue in available space for BCP<sub>N</sub> ( $45.7 \pm 23.0\%$ ) and ABG ( $43.4 \pm 13.6\%$ ) (Fig 9. F). The area percentages of combined bone and residual graft material

**Figure 9 (right).** Histology and histomorphometry of clinical trephine core biopsies. **(A)** Representative histological micrographs of biopsies (hematoxylin-eosin) of ABG and BCP<sub>N</sub>. In the inferior aspect, original dense alveolar bone of the sinus floor can be occasionally observed. The dark granular material in the BCP<sub>N</sub> specimens represents the BCP<sub>N</sub> granules. **(B-E)** High magnification histology of trephine core biopsies of the BCP<sub>N</sub> group (hematoxylin-eosin). Direct bone apposition against BCP<sub>N</sub> granules is apparent, with bone matrix engulfing BCP<sub>N</sub> granules **(B-D)**. New bone formation is occasionally observed originating at the surface and inside pores of the granules **(E)**. **(F-G)** Histomorphometry of clinical trephine core biopsies. **(F)** Percentage of bone matrix in available space for ABG and BCP<sub>N</sub>. **(G)** Percentage of bone and graft material trephine cores. No significant differences were determined between ABG and BCP<sub>N</sub>.



were also equivalent, although the difference between the means of BCP<sub>N</sub> (60.9 ± 17.5%) and ABG (43.4 ± 13.6%) was greater (Fig 9. G).

### *Clinical outcomes*

Table 3 presents the clinical outcomes of participants treated with ABG and BCP<sub>N</sub>. First of all, both treatment groups exhibited 100% implant survival during the study follow-up. Among reported adverse events related to the MSFA procedure were two cases of maxillary sinusitis in the BCP<sub>N</sub> group and one case of vestibular infection in the ABG group. The incidence of adverse events was not significantly different between the treatment groups. Similarly, no significant differences between the treatment groups were detected for the incidence of Schneiderian membrane perforations and implant apex protrusions. With regard to implant health scores, gingival index and plaque index were primarily graded "0" and "1" in both treatment groups, with no significant difference between groups.

**Table 3. Clinical outcomes**

		ABG	BCP <sub>N</sub>	p-value*
<b>Implant survival</b> n/total (%)		12/12 (100)	11/11 (100)	>0.999
<b>Adverse events related to MSFA</b> n (%)				
<b>All</b>		1 (20)	2 (40)	>0.999
<b>Sinusitis maxillaris</b>		0 (0)	2 (40)	0.444
<b>Vestibular infection</b>		1 (20)	0 (0)	>0.999
<b>Schneiderian membrane perforation</b> n/total (%)		4/9 (44.4)	2/7 (28.6)	0.633
<b>Implant apex protrusion</b> n/total (%)		3/12 (25)	3/11 (27.3)	>0.999
<b>Implant health scores</b> n				
<b>Gingival index</b> (0-3)	<b>0</b>	7	3	0.243
	<b>1</b>	3	5	
	<b>2</b>	0	1	
	<b>3</b>	0	0	
<b>Plaque index</b> (0-3)	<b>0</b>	8	5	0.443
	<b>1</b>	2	3	
	<b>2</b>	0	1	
	<b>3</b>	0	0	
<b>Bleeding index</b> (0-2)	<b>0</b>	8	1	0.006
	<b>1</b>	2	8	
<b>Probing depth (mm)</b> Mean (SD), [min-max]		2.2 (0.6) [1.8-3.8]	2.8 (0.8) [1.6-3.8]	0.181

\* Fisher-Freeman-Halton Exact test or Mann-Whitney U test

However, a significant difference was recorded for the bleeding index, with a higher incidence of gingival bleeding in the BCP<sub>N</sub> group compared to ABG. Implant probing depth was equivalent for both treatment groups. Reported pain by visual analog scale (0-10) was equivalent between the treatment groups and was below 1 for >90% of measurements without an apparent trend during time (data not shown).

## **DISCUSSION**

The current study describes the preclinical and clinical evaluation of osteoinductive calcium phosphate with submicron surface topography as bone graft substitute for MSFA. In a preclinical sheep model, two biphasic calcium phosphates with needle-shaped and with grain-shaped submicron surface topography were compared with autograft as control. After MSFA, vertical augmentation height was greater for both synthetic materials versus ABG at all timepoints. Both BCP<sub>N</sub> and BCP<sub>G</sub> were biocompatible, supported bony ingrowth with direct bone apposition against the material, while resorbing at comparable rate. Both BCP<sub>N</sub> and BCP<sub>G</sub> exhibited osteoinductive bone formation as early as 3 weeks post-implantation, but BCP<sub>N</sub> demonstrated significantly more bone formation than BCP<sub>G</sub> at the study endpoint of 12 weeks. Only BCP<sub>N</sub> reached an equivalent amount of bone formation in available space and a greater proportion of calcified material (bone + graft material) beneath the maxillary sinus floor compared to the clinical 'gold standard' ABG after 12 weeks. These results were validated in a clinical study, in which BCP<sub>N</sub> was compared to autograft in a cohort of 10 patients receiving lateral window MSFA with two-stage implant placement. In this study, BCP<sub>N</sub> was found to be equivalent to ABG in implant stability, bone height, new bone formation in trephine core biopsies and in the majority of clinical outcomes.

In recent years, there has been an increasing interest in the effect of biomaterial surface topographies on biological response, with the goal to optimize favorable healing responses following implantation. While relations have been determined between topography and osteogenic differentiation of stem cells [29–31], other research has focused on immunomodulatory effects [32,33]. The osteoinductive potential of calcium phosphates has reproducibly been linked to the presence of a submicron surface topography, *i.e.* a topography of surface crystals smaller than 1 µm in diameter [14–18]. Recent studies have suggested that upregulation of anti-inflammatory M2 macrophages and osteoclastogenesis play an additional role in osteoinduction by calcium phosphate with submicron topography [34–37].

Both bone graft substitutes that were studied in the sheep model, BCP<sub>N</sub> and BCP<sub>G</sub>, have a submicron topography and were previously demonstrated to possess osteoinductive capacity in ectopic implantation models [17–19]. Interestingly, when evaluated in the same canine intramuscular implantation model by our group, osteoinductive bone formation was determined in 100% of implants for both BCP<sub>N</sub> and BCP<sub>G</sub>, but the area percentage of bone as determined by histomorphometry was approximately 10x greater for BCP<sub>N</sub> (24.5% ± 4.3 vs 2.4% ± 1.4%)[17,18]. This suggests that BCP<sub>N</sub> has a higher intrinsic osteoinductive potential than BCP<sub>G</sub>, which may underlie the enhanced bone formation with BCP<sub>N</sub> that we observed in the current study based on higher incidence distant from the host bone and near the Schneiderian membrane.

A potential explanation for the difference in bone forming potential of BCP<sub>N</sub> and BCP<sub>G</sub> in both the current orthotopic model and the ectopic implantation model mentioned above, may lie in their surface crystal morphology. While BCP<sub>N</sub> and BCP<sub>G</sub> overall have similar physicochemical properties (Appendix, Table 1), including granule size, HA/βTCP phase composition and porosity, the materials are different in the morphology of their submicron surface crystals. In a recent study by our group, osteoinduction by calcium phosphates with different morphologies of submicron surface crystals was evaluated [18]. The material with needle-shaped topography showed accelerated osteoinductive bone formation *versus* the material with a grain-shaped topography [18]. These results indicated that, besides the dimension of the surface features (*i.e.* submicron vs micron), the morphology of surface crystals also affects osteoinductive capacity. In the current study, the needle-shaped submicron topography of BCP<sub>N</sub> was similarly associated with a higher bone-forming potential than BCP<sub>G</sub>. Further research is needed to elucidate how surface crystal morphology influences bone regeneration by calcium phosphate bone graft substitutes.

To our knowledge, the observed early bone formation in synthetic implants in the space created after maxillary sinus floor elevation, distant from host bone and near the Schneiderian membrane, has not been previously reported. Although studies have suggested that the Schneiderian membrane itself has osteoinductive potential [38], this concept has been invalidated in later studies [39,40]. However, the Schneiderian membrane has been shown to be osteogenic, since it harbors a niche of mesenchymal osteoprogenitor cells [41–44]. The latter may explain why we often observed early bone formation near the Schneiderian membrane.

The performance of BCP<sub>N</sub> demonstrated in the sheep model was clinically validated in a first clinical study in terms of functionality *i.e.* bone formation, volume augmentation, and implant stability. Bone formation as determined by histomorphometry of trephine core biopsies was equivalent for BCP<sub>N</sub> and the control ABG. Interestingly, the mean



area percentages of bone in available space for BCP<sub>N</sub> and ABG in the sheep study were comparable to the values obtained in the clinical study. The mean area percentages of residual graft material and combined bone and graft material were also similar for BCP<sub>N</sub> between the two studies.

The vertical bone height after MSFA in the preclinical model was greater for the synthetic bone substitutes than ABG at all timepoints, which indicates that ABG had a lower volume stability than the synthetic grafts. However, in the clinical study, bone height was equivalent between ABG and BCP<sub>N</sub> at all follow-up visits. The observation that ABG undergoes greater volume reductions than calcium phosphate-based bone graft substitutes has been reported more often in literature [45–49]. Because of concerns that ABG resorption might compromise MSFA, especially with two-stage implant placement, it has been recommended to use bone graft substitutes as an extender or as substitute to ABG to maintain graft volume [50–52]. Long term graft volume stability is considered a favorable outcome in MSFA, although there is so far no evidence indicating that volume loss negatively affects implant placement or survival [45]. The advantage of using a BCP that has a moderate resorption rate, is that it can provide initial stability to the new bone and allow the tissue to mature, while it is gradually remodeled and replaced by bone tissue during time. Resonance frequency analysis has been used as a tool for the assessment of bone quality and osseointegration. Previous studies have indicated that good primary/mechanical stability, *i.e.* lack of implant micromovement, is a prerequisite for proper peri-implant healing and osseointegration, which leads to secondary/biological stability (Monje et al. 2019). Several studies have positively correlated implant stability to bone quality, although other factors have been found to affect ISQ, including implant location, insertion torque, dimensions and design of the implant (Huang et al. 2020). In our clinical study, resonance frequency analysis of dental implants revealed equivalent primary and secondary implant stability for ABG and BCP<sub>N</sub>, with a negligible difference between primary and secondary stability within groups.

It is challenging to compare the outcomes of the current work directly to results obtained in studies that have used conventional, non-osteoinductive bone graft substitutes. Many pre-clinical studies that have evaluated such materials lack a positive control, used different timepoints and assessment methods or used bone substitutes in combination with autologous bone or other adjuncts (*e.g.* stem cells, platelet rich plasma, composite grafts) [55–64]. However, in studies that evaluated bovine xenograft, porous hydroxyapatite and demineralized freeze-dried bone allografts *versus* ABG in MSFA models, the authors advised against the use of these materials as standalone substitutes for ABG, because they resulted in lower bone-implant contact [65–67]. In other clinical MSFA studies, bone percentage in bone core biopsies was commonly higher for autologous bone graft compared to bone graft substitutes [13,68–71], while results of comparisons between

synthetics, xenografts and allografts have been variable [13,72–75]. Still, questions remain on the relevance of bone substitute selection for MSFA, since clear influence of graft type on clinical outcomes and implant survival has so far not been reported [76–79].

The strengths of this study include the thorough evaluation of bone formation by two similar synthetic bone graft substitutes with different surface crystal morphology, in a clinically-relevant sheep model of MSFA, using the gold standard autograft as control. Moreover, this study is translational because the pre-clinical results were clinically validated in a human trial, which used a full range of assessment methods to compare a bone substitute to the gold standard. A limitation of the sheep MSFA model is that it involved the implantation of bone grafts into the sub-Schneiderian space in non-atrophic maxillae with intact molars, while clinical MSFA cases often involve augmentation of severely resorbed alveolar bone in edentate patients. Furthermore, we have not evaluated placement and osseointegration of dental implants in the sheep model. The clinical study was limited in the relatively low number of patients that was enrolled. A larger sample size would have led to an increase in statistical power that may have resulted in the discovery of significant differences.

In conclusion: the present translational work demonstrated successful maxillary sinus floor augmentation with a novel osteoinductive calcium phosphate with needle-shaped surface topography. In a sheep model of maxillary sinus floor augmentation comparing two osteoinductive calcium phosphate bone substitutes with submicron topography, a material with needle-shaped topography demonstrated enhanced bone formation *versus* a material with a grain-shaped topography. Moreover, it reached an equivalent amount of bone formation (in available space) compared to the 'gold standard' autologous bone graft. These results were validated in a prospective clinical study, in which the same bone substitute reached equivalence to autograft on almost all outcomes. These findings confirm that morphology of submicron surface features on calcium phosphates dictates their *in situ* bone-forming potential. The osteoinductive BCP promoted formation of mature bone in direct contact with the material, facilitating osseointegration and stability of dental implants after 1 year of placement, while avoiding the disadvantages of autograft (i.e. second surgical site, graft resorption). Future investigation of osteoinductive calcium phosphates is recommended to further explore their potential as stand-alone bone graft substitute materials for maxillofacial surgery.

## REFERENCES

- [1] L. Tolstunov, D. Thai, L. Arellano, Implant-guided volumetric analysis of edentulous maxillary bone with cone-beam computerized tomography scan. Maxillary sinus pneumatization classification, *J. Oral Implantol.* 38 (2012) 377–390. <https://doi.org/10.1563/AAID-JOI-D-11-00212>.
- [2] A. Sharan, D. Madjar, Maxillary sinus pneumatization following extractions: a radiographic study., *Int. J. Oral Maxillofac. Implants.* 23 (2008) 48–56. <http://www.ncbi.nlm.nih.gov/pubmed/18416412>.
- [3] S.A. Danesh-Sani, P.M. Loomer, S.S. Wallace, A comprehensive clinical review of maxillary sinus floor elevation: anatomy, techniques, biomaterials and complications, *Br. J. Oral Maxillofac. Surg.* 54 (2016) 724–730. <https://doi.org/10.1016/j.bjoms.2016.05.008>.
- [4] C.O. Tomruk, M.K. Sençift, G.D. Capar, Prevalence of sinus floor elevation procedures and survival rates of implants placed in the posterior maxilla, *Biotechnol. Equip.* 30 (2016) 134–139. <https://doi.org/10.1080/13102818.2015.1102610>.
- [5] G.M. Raghoobar, P. Onclin, G.C. Boven, A. Vissink, H.J.A. Meijer, Long-term effectiveness of maxillary sinus floor augmentation: A systematic review and meta-analysis, *J. Clin. Periodontol.* 46 (2019) 307–318. <https://doi.org/10.1111/jcpe.13055>.
- [6] T.T. Roberts, A.J. Rosenbaum, Bone grafts, bone substitutes and orthobiologics the bridge between basic science and clinical advancements in fracture healing, *Organogenesis.* 8 (2012) 114–124. <https://doi.org/10.4161/org.23306>.
- [7] A. Truedsson, K. Hjalte, B. Sunzel, G. Warfvinge, Maxillary sinus augmentation with iliac autograft—A health-economic analysis, *Clin. Oral Implants Res.* 24 (2013) 1088–1093. <https://doi.org/10.1111/j.1600-0501.2012.02515.x>.
- [8] C.G. Gjerde, S. Shanbhag, E. Neppelberg, K. Mustafa, H. Gjengedal, Patient experience following iliac crest-derived alveolar bone grafting and implant placement, *Int. J. Implant Dent.* 6 (2020) 4. <https://doi.org/10.1186/s40729-019-0200-8>.
- [9] R.J. Klijn, G.J. Meijer, E.M. Bronkhorst, J.A. Jansen, Sinus floor augmentation surgery using autologous bone grafts from various donor sites: A meta-analysis of the total bone volume, *Tissue Eng.—Part B Rev.* 16 (2010) 295–303. <https://doi.org/10.1089/ten.teb.2009.0558>.
- [10] B. Johansson, A. Grepe, K. Wannfors, J.M. Hirsch, A clinical study of changes in the volume of bone grafts in the atrophic maxilla, *Dentomaxillofacial Radiol.* 30 (2001) 157–161. <https://doi.org/10.1038/sj.dmfr.4600601>.
- [11] N. Emeka, F.W. Neukam, Autogenous bone harvesting and grafting in advanced jaw resorption: Morbidity, resorption and implant survival, *Eur. J. Oral Implantol.* 7 (2014) S203–S217. <http://www.ncbi.nlm.nih.gov/pubmed/24977256>.
- [12] H.J. Haugen, S.P. Lyngstadaas, F. Rossi, G. Perale, Bone grafts: which is the ideal biomaterial?, *J. Clin. Periodontol.* 46 (2019) 92–102. <https://doi.org/10.1111/jcpe.13058>.

- [13] S.N. Papageorgiou, P.N. Papageorgiou, J. Deschner, W. Götz, Comparative effectiveness of natural and synthetic bone grafts in oral and maxillofacial surgery prior to insertion of dental implants: Systematic review and network meta-analysis of parallel and cluster randomized controlled trials, *J. Dent.* 48 (2016) 1–8. <https://doi.org/10.1016/j.jdent.2016.03.010>.
- [14] H. Yuan, H. Fernandes, P. Habibovic, J. De Boer, A.M.C. Barradas, A. De Ruiter, W.R. Walsh, C.A. Van Blitterswijk, J.D. De Bruijn, Osteoinductive ceramics as a synthetic alternative to autologous bone grafting, *Proc. Natl. Acad. Sci. U. S. A.* 107 (2010) 13614–13619. <https://doi.org/10.1073/pnas.1003600107>.
- [15] R. Duan, D. Barbieri, X. Luo, J. Weng, J.D. de Bruijn, H. Yuan, Submicron-surface structured tricalcium phosphate ceramic enhances the bone regeneration in canine spine environment, *J. Orthop. Res.* 34 (2016) 1865–1873. <https://doi.org/10.1002/jor.23201>.
- [16] R. Duan, D. Barbieri, F. De Groot, J.D. De Bruijn, H. Yuan, Modulating Bone Regeneration in Rabbit Condyle Defects with Three Surface-Structured Tricalcium Phosphate Ceramics, *ACS Biomater. Sci. Eng.* 4 (2018) 3347–3355. <https://doi.org/10.1021/acsbiomaterials.8b00630>.
- [17] R. Duan, D. Barbieri, X. Luo, J. Weng, C. Bao, J.D. De Bruijn, H. Yuan, Variation of the bone forming ability with the physicochemical properties of calcium phosphate bone substitutes, *Biomater. Sci.* 6 (2018) 136–145. <https://doi.org/10.1039/c7bm00717e>.
- [18] R. Duan, L.A. van Dijk, D. Barbieri, F. de Groot, H. Yuan, J.D. de Bruijn, Accelerated bone formation by biphasic calcium phosphate with a novel sub-micron surface topography, *Eur. Cell. Mater.* 37 (2019) 60–73. <https://doi.org/10.22203/eCM.v037a05>.
- [19] D. Le Nihouannen, G. Daculsi, A. Saffarzadeh, O. Gauthier, S. Delplace, P. Pilet, P. Layrolle, Ectopic bone formation by microporous calcium phosphate ceramic particles in sheep muscles, *Bone.* 36 (2005) 1086–1093. <https://doi.org/10.1016/j.bone.2005.02.017>.
- [20] P. Habibovic, H. Yuan, M. van den Doel, T.M. Sees, C.A. van Blitterswijk, K. de Groot, Relevance of osteoinductive biomaterials in critical-sized orthotopic defect, *J. Orthop. Res.* 24 (2006) 867–876. <https://doi.org/10.1002/jor.20115>.
- [21] L.A. Van Dijk, F. Barrère-De Groot, A.J.W.P. Rosenberg, M. Pelletier, C. Christou, J.D. De Bruijn, W.R. Walsh, MagnetOs, Vitoss, and Novabone in a Multi-endpoint Study of Posterolateral Fusion: A True Fusion or Not?, *Clin. Spine Surg.* 33 (2020) E276–E287. <https://doi.org/10.1097/BSD.0000000000000920>.
- [22] L.A. van Dijk, R. Duan, X. Luo, D. Barbieri, M. Pelletier, C. Christou, A.J.W.P. Rosenberg, H. Yuan, F. Barrère-de Groot, W.R. Walsh, J.D. de Bruijn, Biphasic calcium phosphate with submicron surface topography in an Ovine model of instrumented posterolateral spinal fusion, *JOR Spine.* 1 (2018) e1039. <https://doi.org/10.1002/jsp2.1039>.
- [23] A. De Ruiter, N. Janssen, R. Van Es, M. Frank, G. Meijer, R. Koole, T. Rosenberg, Micro-structured beta-tricalcium phosphate for repair of the alveolar cleft in cleft lip and palate patients: A pilot study, *Cleft Palate-Craniofacial J.* 52 (2015) 336–340. <https://doi.org/10.1597/13-260>.
- [24] N.G. Janssen, R. Schreurs, A.P. de Ruiter, H.C. Sylvester-Jensen, G. Blindheim, G.J. Meijer, R. Koole, H. Vindenes, Microstructured beta-tricalcium phosphate for alveolar cleft repair: a

- two-centre study, *Int. J. Oral Maxillofac. Surg.* 48 (2019) 708–711. <https://doi.org/10.1016/j.ijom.2018.11.009>.
- [25] A. Barroso-Panella, J. Gargallo-Albiol, F. Hernández-Alfaro, Evaluation of Bone Stability and Esthetic Results After Immediate Implant Placement Using a Novel Synthetic Bone Substitute in the Anterior Zone: Results After 12 Months, *Int. J. Periodontics Restorative Dent.* (2018). <https://doi.org/10.11607/prd.2863>.
- [26] J.W.M. Hoekstra, R.J. Klijn, G.J. Meijer, J.J.J.P. van den Beucken, J.A. Jansen, Maxillary sinus floor augmentation with injectable calcium phosphate cements: A pre-clinical study in sheep, *Clin. Oral Implants Res.* 24 (2013) 210–216. <https://doi.org/10.1111/j.1600-0501.2012.02421.x>.
- [27] H. Løe, J. Silness, Periodontal disease in pregnancy I. Prevalence and severity, *Acta Odontol. Scand.* 21 (1963) 533–551. <https://doi.org/10.3109/00016356309011240>.
- [28] J. Silness, H. Løe, Periodontal disease in pregnancy II. Correlation between oral hygiene and periodontal condition, *Acta Odontol. Scand.* 22 (1964) 121–135. <https://doi.org/10.3109/00016356408993968>.
- [29] J. Huang, Y. Chen, C. Tang, Y. Fei, H. Wu, D. Ruan, M.E. Paul, X. Chen, Z. Yin, B.C. Heng, W. Chen, W. Shen, The relationship between substrate topography and stem cell differentiation in the musculoskeletal system, *Cell. Mol. Life Sci.* 76 (2019) 505–521. <https://doi.org/10.1007/s00018-018-2945-2>.
- [30] S. Dobbenga, L.E. Fratila-Apachitei, A.A. Zadpoor, Nanopattern-induced osteogenic differentiation of stem cells – A systematic review, *Acta Biomater.* 46 (2016) 3–14. <https://doi.org/10.1016/j.actbio.2016.09.031>.
- [31] N. Gui, W. Xu, D.E. Myers, R. Shukla, H.P. Tang, M. Qian, The effect of ordered and partially ordered surface topography on bone cell responses: A review, *Biomater. Sci.* 6 (2018) 250–264. <https://doi.org/10.1039/c7bm01016h>.
- [32] T.U. Luu, S.C. Gott, B.W.K. Woo, M.P. Rao, W.F. Liu, Micro- and Nanopatterned Topographical Cues for Regulating Macrophage Cell Shape and Phenotype, *ACS Appl. Mater. Interfaces.* 7 (2015) 28665–28672. <https://doi.org/10.1021/acsami.5b10589>.
- [33] C. Yang, C. Zhao, X. Wang, M. Shi, Y. Zhu, L. Jing, C. Wu, J. Chang, Stimulation of osteogenesis and angiogenesis by micro/nano hierarchical hydroxyapatite: Via macrophage immunomodulation, *Nanoscale.* 11 (2019) 17699–17708. <https://doi.org/10.1039/c9nr05730g>.
- [34] N.L. Davison, A.L. Gamblin, P. Layrolle, H. Yuan, J.D. de Bruijn, F. Barrère-de Groot, Liposomal clodronate inhibition of osteoclastogenesis and osteoinduction by submicrostructured beta-tricalcium phosphate, *Biomaterials.* 35 (2014) 5088–5097. <https://doi.org/10.1016/j.biomaterials.2014.03.013>.
- [35] N.L. Davison, J. Su, H. Yuan, J.J.J.P. van den Beucken, J.D. de Bruijn, F.B. de Groot, Influence of surface microstructure and chemistry on osteoinduction and osteoclastogenesis by biphasic calcium phosphate discs, *Eur. Cells Mater.* 29 (2015) 314–329. <https://doi.org/10.22203/eCM.v029a24>.

- [36] M. Li, X. Guo, W. Qi, Z. Wu, J.D. De Bruijn, Y. Xiao, C. Bao, H. Yuan, Macrophage polarization plays roles in bone formation instructed by calcium phosphate ceramics, *J. Mater. Chem. B* 8 (2020) 1863–1877. <https://doi.org/10.1039/c9tb02932j>.
- [37] X. Chen, M. Wang, F. Chen, J. Wang, X. Li, J. Liang, Y. Fan, Y. Xiao, X. Zhang, Correlations between macrophage polarization and osteoinduction of porous calcium phosphate ceramics, *Acta Biomater.* 103 (2020) 318–332. <https://doi.org/10.1016/j.actbio.2019.12.019>.
- [38] S. Srouji, D. Ben-David, R. Lotan, M. Riminucci, E. Livne, P. Bianco, The innate osteogenic potential of the maxillary sinus (Schneiderian) membrane: An ectopic tissue transplant model simulating sinus lifting, *Int. J. Oral Maxillofac. Surg.* 39 (2010) 793–801. <https://doi.org/10.1016/j.ijom.2010.03.009>.
- [39] A. Scala, D. Botticelli, R.S. Faeda, I. Garcia Rangel, J. Américo de Oliveira, N.P. Lang, Lack of influence of the Schneiderian membrane in forming new bone apical to implants simultaneously installed with sinus floor elevation: An experimental study in monkeys, *Clin. Oral Implants Res.* 23 (2012) 175–181. <https://doi.org/10.1111/j.1600-0501.2011.02227.x>.
- [40] M. Jungner, G. Cricchio, L.A. Salata, L. Sennerby, C. Lundqvist, M. Hultcrantz, S. Lundgren, On the Early Mechanisms of Bone Formation after Maxillary Sinus Membrane Elevation: An Experimental Histological and Immunohistochemical Study, *Clin. Implant Dent. Relat. Res.* 17 (2015) 1092–1102. <https://doi.org/10.1111/cid.12218>.
- [41] X. Li, Q. Rong, S.L. Chen, The innate osteogenic potential of the canine maxillary sinus membrane: An in vitro and in vivo study, *J. Biomater. Tissue Eng.* 5 (2015) 445–451. <https://doi.org/10.1166/jbt.2015.1334>.
- [42] A. Graziano, L. Benedetti, G. Massei, M.G. Cusella de Angelis, F. Ferrarotti, M. Aimetti, Bone production by human maxillary sinus mucosa cells, *J. Cell. Physiol.* 227 (2012) 3278–3281. <https://doi.org/10.1002/jcp.24022>.
- [43] R. Gruber, B. Kandler, G. Fuerst, M.B. Fischer, G. Watzek, Porcine sinus mucosa holds cells that respond to bone morphogenetic protein (BMP)-6 and BMP-7 with increased osteogenic differentiation in vitro, *Clin. Oral Implants Res.* 15 (2004) 575–580. <https://doi.org/10.1111/j.1600-0501.2004.01062.x>.
- [44] A. Berbéri, F. Al-Nemer, E. Hamade, Z. Noujeim, B. Badran, K. Zibara, Mesenchymal stem cells with osteogenic potential in human maxillary sinus membrane: an in vitro study, *Clin. Oral Investig.* 21 (2017) 1599–1609. <https://doi.org/10.1007/s00784-016-1945-6>.
- [45] S. Shanbhag, V. Shanbhag, A. Stavropoulos, Volume Changes of Maxillary Sinus Augmentations over Time: A Systematic Review, *Int. J. Oral Maxillofac. Implants.* 29 (2014) 881–892. <https://doi.org/10.11607/jomi.3472>.
- [46] R. Lutz, S. Berger-Fink, P. Stockmann, F.W. Neukam, K.A. Schlegel, Sinus floor augmentation with autogenous bone vs. a bovine-derived xenograft—a 5-year retrospective study, *Clin. Oral Implants Res.* 26 (2015) 644–648. <https://doi.org/10.1111/clr.12352>.
- [47] T. Jensen, S. Schou, P.A. Svendsen, J.L. Forman, H.J.G. Gundersen, H. Terheyden, P. Holmstrup, Volumetric changes of the graft after maxillary sinus floor augmentation with Bio-Oss and

- autogenous bone in different ratios: A radiographic study in minipigs, *Clin. Oral Implants Res.* 23 (2012) 902–910. <https://doi.org/10.1111/j.1600-0501.2011.02245.x>.
- [48] M.G. Cosso, R.B. De Brito, A. Piattelli, J.A. Shibli, E.G. Zenóbio, Volumetric dimensional changes of autogenous bone and the mixture of hydroxyapatite and autogenous bone graft in humans maxillary sinus augmentation. A multislice tomographic study, *Clin. Oral Implants Res.* 25 (2014) 1251–1256. <https://doi.org/10.1111/clr.12261>.
- [49] K.A. Schlegel, G. Fichtner, S. Schultze-Mosgau, J. Wiltfang, Histologic findings in sinus augmentation with autogenous bone chips versus a bovine bone substitute., *Int. J. Oral Maxillofac. Implants.* 18 (2003) 53–8. <http://www.ncbi.nlm.nih.gov/pubmed/12608669>.
- [50] O. Mardinger, G. Chaushu, S. Sigalov, R. Herzberg, B. Shlomi, D. Schwartz-Arad, Factors affecting changes in sinus graft height between and above the placed implants, *Oral Surgery, Oral Med. Oral Pathol. Oral Radiol. Endodontology.* 111 (2011). <https://doi.org/10.1016/j.tripleo.2010.09.064>.
- [51] T. Jensen, S. Schou, A. Stavropoulos, H. Terheyden, P. Holmstrup, Maxillary sinus floor augmentation\with Bio-Oss or Bio-Oss mixed with autogenous bone as graft: A systematic review, *Clin. Oral Implants Res.* 23 (2012) 263–273. <https://doi.org/10.1111/j.1600-0501.2011.02168.x>.
- [52] S. Kühn, M. Payer, R. Kirmeier, A. Wildburger, W. Wegscheider, N. Jakse, The influence of bone marrow aspirates and concentrates on the early volume stability of maxillary sinus grafts with deproteinized bovine bone mineral—first results of a RCT, *Clin. Oral Implants Res.* 25 (2014) 221–225. <https://doi.org/10.1111/clr.12101>.
- [53] M. A, R. A, W. HL, H. JA, B. JB, Relationship Between Primary/Mechanical and Secondary/Biological Implant Stability, *Int. J. Oral Maxillofac. Implants.* 34 (2019) s7–s23. <https://doi.org/10.11607/JOMI.19SUPPL.G1>.
- [54] H. H, W. G, H. E, The clinical significance of implant stability quotient (ISQ) measurements: A literature review, *J. Oral Biol. Craniofacial Res.* 10 (2020) 629. <https://doi.org/10.1016/J.JOBCR.2020.07.004>.
- [55] S. Sauerbier, K. Stubbe, M. Maglione, J. Haberstroh, J. Kuschnierz, T. Oshima, S.P. Xavier, L. Brunberg, R. Schmelzeisen, R. Gutwald, Mesenchymal stem cells and bovine bone mineral in sinus lift procedures—an experimental study in sheep, *Tissue Eng.—Part C Methods.* 16 (2010) 1033–1039. <https://doi.org/10.1089/ten.tec.2009.0734>.
- [56] S. Sauerbier, A. Stricker, J. Kuschnierz, F. Bühler, T. Oshima, S.P. Xavier, R. Schmelzeisen, R. Gutwald, In vivo comparison of hard tissue regeneration with human mesenchymal stem cells processed with either the ficoll method or the BMAC method, *Tissue Eng.—Part C Methods.* 16 (2010) 215–223. <https://doi.org/10.1089/ten.tec.2009.0269>.
- [57] B. Barboni, C. Mangano, L. Valbonetti, G. Marruchella, P. Berardinelli, A. Martelli, A. Muttini, A. Mauro, R. Bedini, M. Turriani, R. Pecci, D. Nardinocchi, V.L. Zizzari, S. Tetè, A. Piattelli, M. Mattioli, Synthetic Bone Substitute Engineered with Amniotic Epithelial Cells Enhances Bone Regeneration after Maxillary Sinus Augmentation, *PLoS One.* 8 (2013). <https://doi.org/10.1371/journal.pone.0063256>.

- [58] E. Grageda, J.L. Lozada, P.J. Boyne, N. Caplanis, P.J. McMillan, Bone formation in the maxillary sinus by using platelet-rich plasma: an experimental study in sheep., *J. Oral Implantol.* 31 (2005) 2–17. <https://doi.org/10.1563/0-692.1>.
- [59] A. Saffarzadeh, O. Gauthier, M. Bilban, M. Bagot D'Arc, G. Daculsi, Comparison of two bone substitute biomaterials consisting of a mixture of fibrin sealant (Tisseel®) and MBCP™ (TricOs®) with an autograft in sinus lift surgery in sheep, *Clin. Oral Implants Res.* 20 (2009) 1133–1139. <https://doi.org/10.1111/j.1600-0501.2009.01738.x>.
- [60] J. Alayan, C. Vaquette, S. Saifzadeh, D. Hutmacher, S. Ivanovski, A histomorphometric assessment of collagen-stabilized anorganic bovine bone mineral in maxillary sinus augmentation—a randomized controlled trial in sheep, *Clin. Oral Implants Res.* 27 (2016) 734–743. <https://doi.org/10.1111/clr.12652>.
- [61] A. Philipp, W. Duncan, M. Roos, C.H. Hämmerle, T. Attin, P.R. Schmidlin, Comparison of SLA® or SLActive® implants placed in the maxillary sinus with or without synthetic bone graft materials—An animal study in sheep, *Clin. Oral Implants Res.* 25 (2014) 1142–1148. <https://doi.org/10.1111/clr.12255>.
- [62] C. Mangano, B. Barboni, L. Valbonetti, P. Berardinelli, A. Martelli, A. Muttini, R. Bedini, S. Tetè, A. Piattelli, M. Mattioli, In vivo behavior of a custom-made 3D synthetic bone substitute in sinus augmentation procedures in sheep, *J. Oral Implantol.* 41 (2015) 241–251. <https://doi.org/10.1563/AAID-JOI-D-13-00053>.
- [63] R.J. Klijn, J.W.M. Hoekstra, J.J.J.P. Van Den Beucken, G.J. Meijer, J.A. Jansen, Maxillary sinus augmentation with microstructured tricalcium phosphate ceramic in sheep, *Clin. Oral Implants Res.* 23 (2012) 274–280. <https://doi.org/10.1111/j.1600-0501.2011.02190.x>.
- [64] R. Gutwald, J. Haberstroh, J. Kuschnierz, C. Kister, D.A. Lysek, M. Maglione, S.P. Xavier, T. Oshima, R. Schmelzeisen, S. Sauerbier, Mesenchymal stem cells and inorganic bovine bone mineral in sinus augmentation: comparison with augmentation by autologous bone in adult sheep, *Br. J. Oral Maxillofac. Surg.* 48 (2010) 285–290. <https://doi.org/10.1016/j.bjoms.2009.06.226>.
- [65] R. Haas, M. Baron, K. Donath, W. Zechner, G. Watzek, Porous hydroxyapatite for grafting the maxillary sinus: a comparative histomorphometric study in sheep., *Int. J. Oral Maxillofac. Implants.* 17 (2002) 337–46. <http://www.ncbi.nlm.nih.gov/pubmed/12074448>.
- [66] R. Haas, D. Haidvogel, K. Donath, G. Watzek, Freeze-dried homogeneous and heterogeneous bone for sinus augmentation in sheep Part I: Histological findings, *Clin. Oral Implants Res.* 13 (2002) 396–404. <https://doi.org/10.1034/j.1600-0501.2002.130408.x>.
- [67] T. Jensen, S. Schou, H.J.G. Gundersen, J.L. Forman, H. Terheyden, P. Holmstrup, Bone-to-implant contact after maxillary sinus floor augmentation with Bio-Oss and autogenous bone in different ratios in mini pigs, *Clin. Oral Implants Res.* 24 (2013) 635–644. <https://doi.org/10.1111/j.1600-0501.2012.02438.x>.
- [68] A. Stumbras, M.M. Krukis, G. Januzis, G. Juodzbaly, Regenerative bone potential after sinus floor elevation using various bone graft materials: A systematic review, *Quintessence Int. (Berl.)* 50 (2019) 548–558. <https://doi.org/10.3290/j.qi.a42482>.



- [69] J. Handschel, M. Simonowska, C. Naujoks, R.A. Depprich, M.A. Ommerborn, U. Meyer, N.R. Kübler, A histomorphometric meta-analysis of sinus elevation with various grafting materials, *Head Face Med.* 5 (2009). <https://doi.org/10.1186/1746-160X-5-12>.
- [70] S.A. Danesh-Sani, S.P. Engebretson, M.N. Janal, Histomorphometric results of different grafting materials and effect of healing time on bone maturation after sinus floor augmentation: a systematic review and meta-analysis, *J. Periodontol Res.* 52 (2017) 301–312. <https://doi.org/10.1111/jre.12402>.
- [71] R.J. Klijn, G.J. Meijer, E.M. Bronkhorst, J.A. Jansen, A meta-analysis of histomorphometric results and graft healing time of various biomaterials compared to autologous bone used as sinus floor augmentation material in humans, *Tissue Eng.–Part B Rev.* 16 (2010) 493–507. <https://doi.org/10.1089/ten.teb.2010.0035>.
- [72] S. Annibaldi, G. Iezzi, G.L. Sfasciotti, M.P. Cristalli, I. Vozza, C. Mangano, G. La Monaca, A. Polimeni, Histological and histomorphometric human results of HA-Beta-TCP 30/70 compared to three different biomaterials in maxillary sinus augmentation at 6 months: A preliminary report, *Biomed Res. Int.* 2015 (2015). <https://doi.org/10.1155/2015/156850>.
- [73] C.M. Schmitt, H. Doering, T. Schmidt, R. Lutz, F.W. Neukam, K.A. Schlegel, Histological results after maxillary sinus augmentation with Straumann® BoneCeramic, Bio-Oss®, Puros®, and autologous bone. A randomized controlled clinical trial, *Clin. Oral Implants Res.* 24 (2013) 576–585. <https://doi.org/10.1111/j.1600-0501.2012.02431.x>.
- [74] M. Kurkcu, M.E. Benlidayi, B. Cam, Y. Sertdemir, Anorganic bovine-derived hydroxyapatite vs b-tricalcium phosphate in sinus augmentation: A comparative histomorphometric study, *J. Oral Implantol.* 38 (2012) 519–526. <https://doi.org/10.1563/AAID-JOI-D-11-00061>.
- [75] C. Lindgren, L. Sennerby, A. Mordenfeld, M. Hallman, Clinical histology of microimplants placed in two different biomaterials., *Int. J. Oral Maxillofac. Implants.* 24 (2009) 1093–100. <http://www.ncbi.nlm.nih.gov/pubmed/20162114>.
- [76] E. Nkenke, F. Stelzle, Clinical outcomes of sinus floor augmentation for implant placement using autogenous bone or bone substitutes: A systematic review, *Clin. Oral Implants Res.* 20 (2009) 124–133. <https://doi.org/10.1111/j.1600-0501.2009.01776.x>.
- [77] B. Al-Nawas, E. Schiegnitz, Augmentation procedures using bone substitute materials or autogenous bone—a systematic review and meta-analysis, *Eur. J. Oral Implantol.* 7 (2014) S219–S234.
- [78] T. Starch-Jensen, A. Mordenfeld, J.P. Becktor, S.S. Jensen, Maxillary sinus floor augmentation with synthetic bone substitutes compared with other grafting materials: A systematic review and meta-analysis, *Implant Dent.* 27 (2018) 363–374. <https://doi.org/10.1097/ID.0000000000000768>.
- [79] M. Del Fabbro, T. Testori, L. Francetti, R. Weinstein, Systematic review of survival rates for implants placed in the grafted maxillary sinus, *J. Prosthet. Dent.* 94 (2005) 266. <https://doi.org/10.1016/j.prosdent.2005.04.024>.

## APPENDIX

**Supplementary Table 1.** Properties of calcium phosphate bone substitutes

<b>Material</b>	<b>BCP<sub>N</sub></b>	<b>BCP<sub>G</sub></b>
<b>Trade name</b>	MagnetOs Granules™	MBCP™
<b>Supplier</b>	Kuros Biosciences	Biomatlante
<b>Granule size</b>	0.25–1.00 mm	0.50–1.00 mm
<b>Chemistry</b>	30 HA / 70 TCP	40 HA / 60 TCP
<b>Surface crystal structure<sup>a</sup></b>	Needle	Grain
<b>Surface crystal size [<math>\mu\text{m}</math>]<sup>b</sup></b>	0.58 ± 0.20	0.71 ± 0.20
<b>Total porosity<sup>b</sup></b>	80%	73%
<b>Macroporosity<sup>b</sup></b>	69%	55%
<b>Micro-porosity<sup>b</sup></b>	11%	18%
<b>Specific surface area by weight<sup>b</sup> [<math>\text{m}^2 \text{g}^{-1}</math>]</b>	2.77	2.93
<b>Specific surface area by volume<sup>b</sup> [<math>\text{m}^2 \text{ml}^{-1}</math>]</b>	1.78	2.09
<b>Ectopic bone formation<sup>c</sup></b>	<b>Bone incidence</b>	8/8 <sup>1</sup>
	<b>Bone in available space %</b>	24.5 ± 4.3 <sup>1</sup>
		4/4 <sup>2</sup>
		2.1 ± 1.4% <sup>2</sup>

<sup>a</sup> Data from measurements on scanning microscopy images (5000×)

<sup>b</sup> Data from mercury intrusion.

<sup>c</sup> Previously published data in canine intramuscular implantation model, 12 weeks post-implantation.

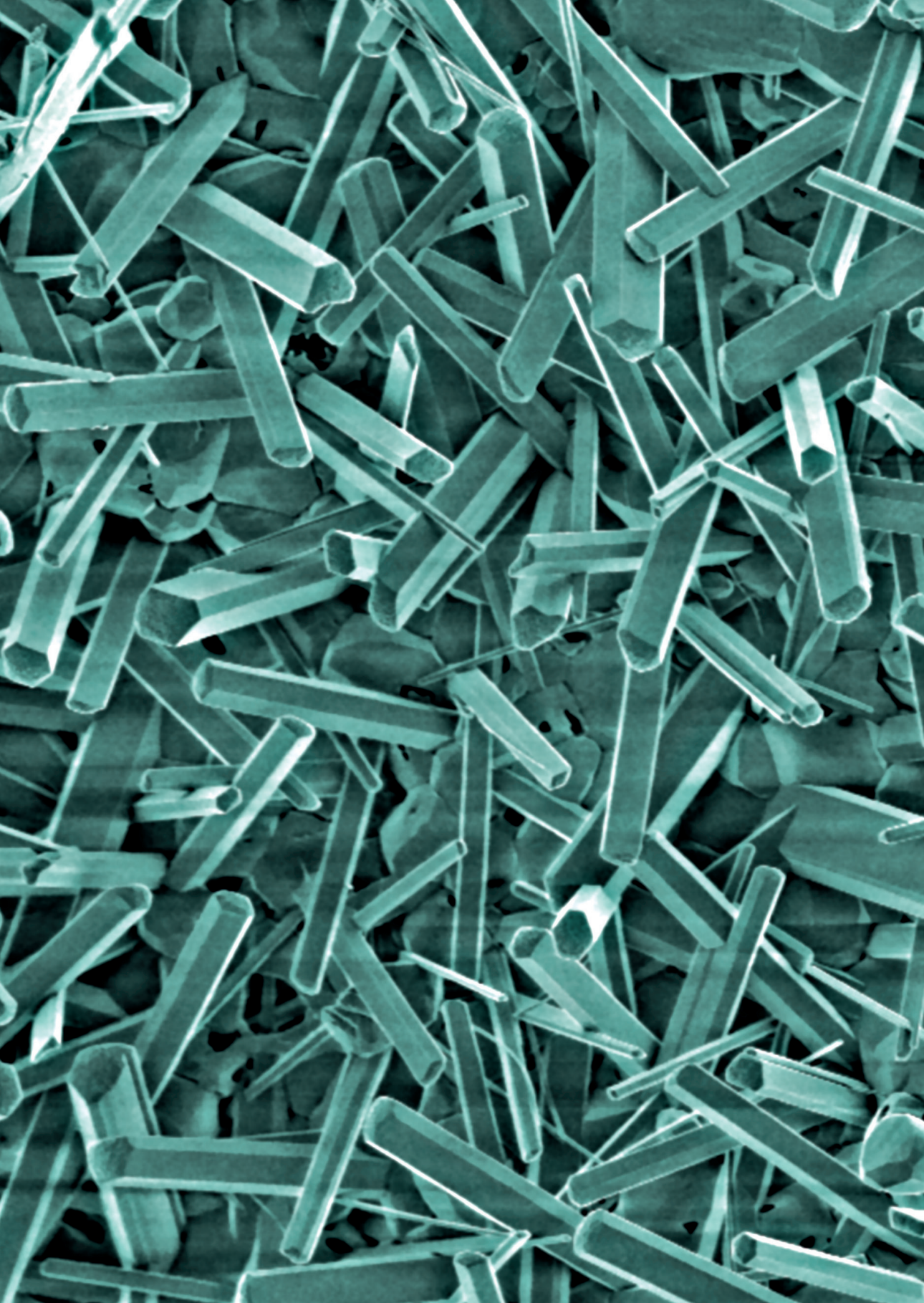
<sup>1</sup> Duan et al. 2019

<sup>2</sup> Duan et al. 2018b

**Supplementary Table 2.** Inclusion and exclusion criteria of clinical study

<b>Inclusion criteria</b>
Male or female patients aged 18-75 years
Patient is willing to give informed consent to participate in the study
Patient qualifies for sinus augmentation surgery
Presence of a unilateral or bilateral (partial) maxillary edentulism involving the premolar/molar areas
Presence of a residual posterior maxillary bone height between 2 and 6 mm
Smoking ≤10 cigarettes per day
<b>Exclusion criteria</b>
Maxillary sinus pathology
Presence of a local or systemic disease or treatment affecting bone formation
Contamination of the (area around the) operative field
Periodontitis
Infectious diseases
Bone metabolic disease
Neurological disorders that could influence mental validity
Smoking >10 cigarettes per day
Pregnant or breast-feeding women
Cancer therapy including immune-suppression, chemotherapy and irradiation
Patients in whom primary stability could not be established
Previous entry into this study or participation in any other clinical trial within 30 days

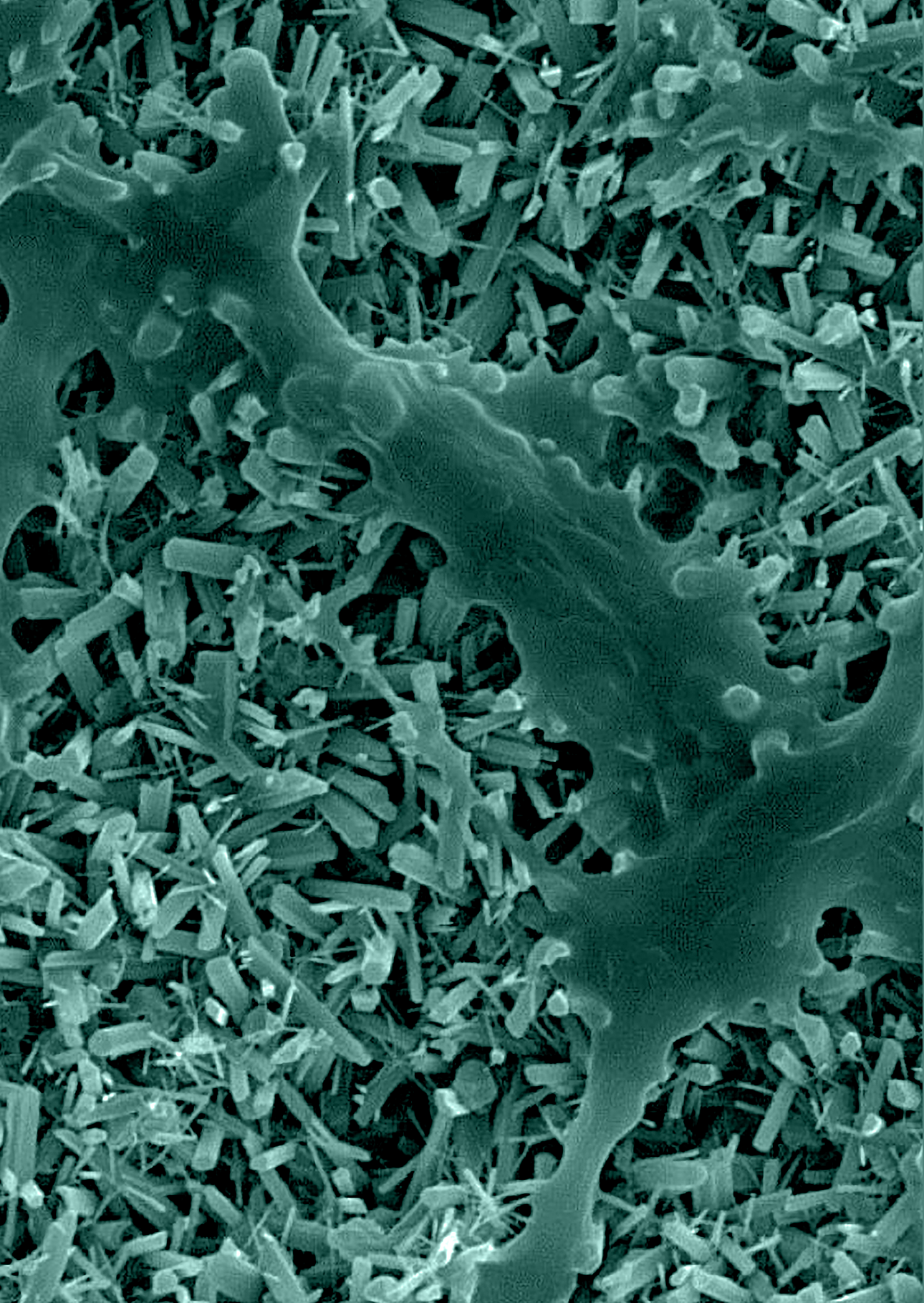






# PART IV

## EVALUATION OF THE MACROPHAGE RESPONSE TO OSTEOINDUCTIVE CALCIUM PHOSPHATE



# CHAPTER 7

## **CALCIUM PHOSPHATE WITH SUBMICRON TOPOGRAPHY INDUCES M2 MACROPHAGE PHENOTYPE IN PRIMARY HUMAN MACROPHAGES, ENHANCING DOWNSTREAM ANGIOGENESIS AND OSTEOGENESIS IN VITRO**

---

Lukas A. van Dijk  
Lizette Utomo  
Huipin Yuan  
Florence Barrère-de Groot  
Debby Gawlitta  
Antoine J.W.P. Rosenberg  
Joost D. de Bruijn

*Submitted*





## INTRODUCTION

---

Calcium phosphate ceramics are among the most well-studied synthetic bone graft substitute materials, due to their excellent biocompatibility, osteoconductive, and bioactive properties[1]. As is common for biomaterials, the efficacy of calcium phosphate bone graft materials has been shown to be correlated with specific physicochemical properties, including phase composition[2-4], micro- and macroporosity [5-7], and surface features[8-10]. Ongoing developments in material engineering, specifically the modification of surface features, have resulted in calcium phosphate bone graft materials that have demonstrated improved efficacy compared to conventional calcium phosphates[8,10-14]. Surface features of calcium phosphates in the submicron scale, *i.e.* pores and crystals < 1  $\mu\text{m}$  in dimension, have been demonstrated to be associated with osteoinductive potential (*i.e.* capacity to induce *de novo* bone formation). They also exhibit an ability to repair critical-sized bone defects that approaches the efficacy of the 'gold standard' bone autograft, without addition of exogenous cells and/or growth factors[8-12,15,16]. The relationship between surface features and bone-inducing potential of calcium phosphates has so far been demonstrated in various animal models, including mouse, rabbit, goat, sheep, canine and baboons[17]. Recently, we have demonstrated accelerated bone formation in soft tissue by calcium phosphate with a topography of submicron needle-shaped crystals compared to calcium phosphate with submicron grain-shaped crystals [9]. This material also exhibited equivalence to autograft and superiority to conventional ceramics in challenging spinal fusion models[12,15,18].

To understand the mechanisms behind the enhanced healing response to submicron surface structured calcium phosphates, it is helpful to consider the biological events that occur after implantation that ultimately lead to bone formation. In the early phases after implantation (hours-days), before interaction of osteogenic cells with the material, initial tissue responses are mostly dictated by cells of the innate immune system[19,20]. A healthy immune response is a prerequisite for the normal healing of tissue injury[21]. Likewise, a favorable innate immune response to a biomaterial is paramount for successful healing and integration after implantation [22,23].

Biomaterial implantation is typically followed by a rapid but short-lived invasion of neutrophils that elicit an acute inflammatory response. Hereafter, circulating monocytes are recruited to the implantation site, become activated, and differentiate into macrophages[19,21]. Macrophages are known to play a central role in the innate immune response to tissue injury and biomaterials. They are the key regulators of the wound healing process, in which they evolve to adopt distinct phenotypes during the different stages of healing[24]. Macrophage phenotypes are broadly categorized into those having



a pro-inflammatory role, better known as the 'classically' activated or 'M1' phenotype, and on the other hand macrophages with an anti-inflammatory function, commonly described as the 'alternatively' activated, 'M2' or 'pro-healing' phenotype[25,26]. M1 macrophages promote inflammation by release of pro-inflammatory cytokines and produce harmful reactive oxygen species to clear pathogens, debris, and foreign materials. M2 macrophages aim to resolve inflammation by secretion of anti-inflammatory factors and facilitate tissue repair and remodeling by signaling to local progenitor cells and stem cells responsible for tissue regeneration[24,27]. Transition between M1 and M2 phenotypes can occur swiftly in response to environmental stimuli, such as cytokines, pathogens, and materials[21,24,25,27,28].

During the normal healing cascade, the macrophage population is dominated by M1 macrophages during the acute inflammatory phase and will then gradually shift towards an M2-dominated population to create the pro-healing environment required for regeneration[24,28]. However, when the transition to M2 macrophages is inhibited, for example due to a bioincompatible implant, the prolonged presence of inflammatory M1 macrophages can exacerbate tissue injury and prevent biomaterial integration[28–30]. The associated chronic inflammatory state can lead to undesirable outcomes, such as granuloma formation, fibrosis and ultimately fibrous encapsulation of the implant, known as the foreign body response[19,23,30,31].

Research in the field of osteoimmunology has established that there exists an intricate relationship between macrophages, and bone tissue formation and homeostasis[30,32,33]. M2-like tissue-resident osteal macrophages, termed OsteoMacs, have been shown to directly regulate osteoblast survival and bone matrix deposition *in vivo*[34,35]. Macrophages have displayed intricate crosstalk with mesenchymal stem cells (MSCs) that leads to osteogenic differentiation[36,37]. Recently, Zhang *et al.* reported a correlation between accelerated fracture healing and greater percentages of M2 macrophages in fracture calluses in human patients [38]. In contrast, upregulated M1 macrophage populations have been associated with destructive bone resorption in bisphosphonate-related osteonecrosis of the jaw [39–41]. Strategies to augment M2 macrophage activation during bone defect repair have demonstrated enhanced bone formation and implant osseointegration associated with greater numbers of M2 macrophages[42–47]. Recently, an M2 macrophage-like cell population has been recognized to have an important role in the process of heterotopic ossification, which is similar to material-induced ectopic bone formation[48,49].

In this context, the macrophage response is deemed highly relevant in bone regeneration utilizing calcium phosphate bone graft substitute materials[33]. Previously, local depletion of monocytes/macrophages has been shown to block *in vivo* ectopic bone formation by calcium phosphate with submicron surface features[50,51]. Moreover, recent results

have indicated murine M2 macrophage upregulation by calcium phosphate materials with osteoinductive capacity [51,52].

In the current study, we set out to assess the *in vitro* response of primary human macrophages to different calcium phosphate bone graft materials. The first material was a biphasic calcium phosphate with a submicron surface topography of needle-shaped crystals ( $\text{BCP}_{<\mu\text{m}}$ ), which exhibits the ability to form bone in soft tissues without added cells or growth factors, and has demonstrated enhanced bone healing compared to conventional ceramics *in vivo* [9,12]. This material was compared to a conventional tricalcium phosphate that had no submicron topography (TCP), was not osteoinductive [53] and has shown low bone healing potential *in vivo* [12,13,54,55]. The goal of this study was to elucidate whether  $\text{BCP}_{<\mu\text{m}}$  with submicron topography induced stronger M2 macrophage activation than the conventional bone graft material TCP. This would suggest a role of pro-healing M2 macrophages in the enhanced bone healing observed with submicron structured calcium phosphates. Additionally, paracrine effects of macrophages on *in vitro* angiogenic tube formation and osteogenic differentiation of mesenchymal stromal cells were assessed using conditioned medium assays.

## MATERIALS AND METHODS

### Materials

Two calcium phosphate bone graft materials were used for the experiments. The first material, a biphasic calcium phosphate ( $\pm 30\%$  HA /  $70\%$   $\beta$ -TCP) with a submicron topography of needle-shaped crystals ( $\text{BCP}_{<\mu\text{m}}$ , MagnetOs Granules™, Kuros Biosciences B.V., Bilthoven, NL) was manufactured by Kuros Biosciences as described previously [9,18]. In brief, porous BCP blocks were produced from calcium orthophosphate powder using foaming agent and porogen, followed by sintering at  $1125^\circ\text{C}$  for 6h. The blocks were crushed and sieved to obtain granules of 1-2 mm. The topography of submicron needle-shaped crystals was obtained by autoclaving the granules at  $135^\circ\text{C}$  for 100 min. The second material was purchased as a porous tricalcium phosphate ( $> 98\%$ – $100\%$   $\beta$ -TCP) with a granule size of 1-2 mm, manufactured by Orthovita Inc. (TCP, Vitoss Morsels, Orthovita Inc., Malvern, PA, USA). The materials were characterized by mercury intrusion porosimetry and measurement of surface crystal size by scanning electron microscopy (SEM, JEOL JSM-5600, JEOL, Akishima, Tokyo, Japan). Both materials were distributed into  $400\ \mu\text{l}$  aliquots and were then subjected to dry heat sterilization (3h at  $200^\circ\text{C}$ ). The material properties of  $\text{BCP}_{<\mu\text{m}}$  and TCP are presented in Table 1.





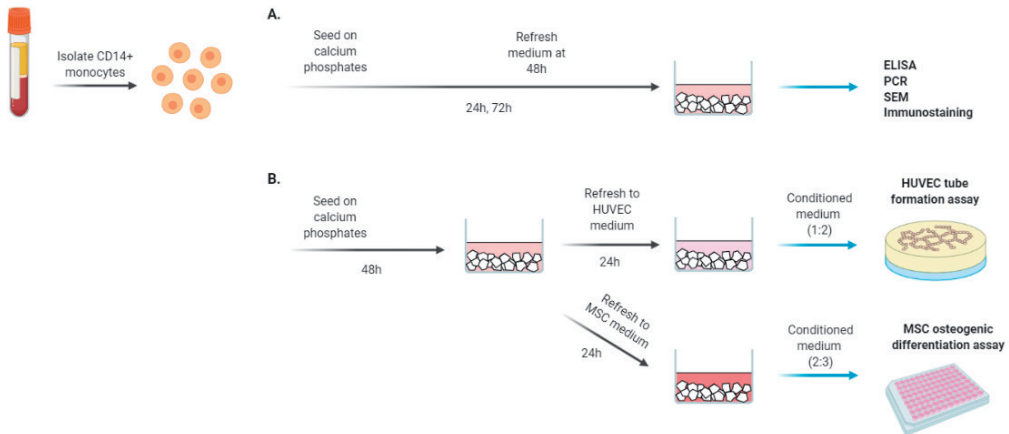


**Figure 1. Schematic overview of the experimental procedures.** After isolation, CD14+ monocytes were seeded on BCP<sub><math>\mu\text{m}</math> and TCP to **(A)** evaluate their response to the materials and **(B)** to generate macrophage-conditioned medium for use in angiogenic and osteogenic assays.</sub>

### Scanning electron microscopy and cell shape quantification

To visualize the material surfaces both before and after macrophage culture, a scanning electron microscope (SEM) was used (JEOL JSM-5600). For cell culture samples (72h), granules were rinsed in phosphate buffered saline (PBS, Gibco), fixed in 2.5% glutaraldehyde (Sigma) for 1.5h, and stored in PBS at 4 °C until further processing. The cells were dehydrated using a graded ethanol series followed by air-drying by evaporation of tetramethylsilane (Sigma, St. Louis, USA). Granules were mounted on specimen mounts and were gold sputter-coated (JEOL JFC 1300) prior to visualization by SEM.

Cell shape quantification was performed on at least 25 different SEM images of macrophages of different donors ( $n=3$ ) by measuring the shortest and longest axis of each cell through the midline using software (AxioVision LE, Carl Zeiss Microscopy, Oberkochen, Germany). An elongation index was calculated for each cell by dividing the length of the long axis by the short axis. Using this elongation index, the percentage of elongated cells was determined, *i.e.* with an elongation index  $\geq 2$ .

### Gene expression analysis

Expression of mRNA by macrophages cultured on BCP<sub><math>\mu\text{m}</math> or TCP was analyzed for different donors ( $n=3$ ) in triplicates. The mRNA was isolated using TRIzol reagent (Thermo Fisher), according to the manufacturer's instructions. Quantification of total extracted RNA was determined using a spectrophotometer (DS-11 series, DeNovix Inc., Wilmington, USA) at 260/280 nm. Subsequently, complementary DNA (cDNA) was synthesized using iScript™ cDNA Synthesis Kit (Bio-Rad, Hercules, USA) following the manufacturer's instructions. Quantitative PCR analysis was performed using a Bio-Rad</sub>

CFX96 Real-Time PCR Detection System using FastStart SYBR Green Master mix (Roche Molecular Systems, Inc., Pleasanton, USA). Expression of cluster of differentiation 206 (*CD206*; Fw: TGGCCGTATGCCGGTCACTGTTA ; Rev: ACTTGTGAGGTCACCGCCTTCCT), *CCL18* (Fw: TTGTGAGTTTCCAAGCCCCA; Rev: GCAGCAGAGCTCTTTGTTGGTA), *CD163* (Fw: GTTGCCATTTTCGTCGCATT; Rev: CTCTCCTCTTGAGGAACTGCAA), C-C motif chemokine ligand 2 (*CCL2*, Fw: AATCACCAGCAGCAAGTGTC; Rev: TCTTCGGAGTTGGGTTTGCT), *CCL5* (Fw: TGCTGCTTTCCTACATTGC; Rev: CACACACTTGGCGGTTCTTT), Interleukin 1 $\beta$  (*IL1 $\beta$* , Fw: AGCTGATGGCCCTAAACAGA; Rev: TGTAGTGGTGGTCGGAGATT) was analyzed, to discriminate between M1 (*CCL2*, *CCL5*, *IL1 $\beta$* ) and M2 (*CD206*, *CCL18*, *CD163*) macrophage phenotypes [57–59]. Glyceraldehyde-3-phosphate dehydrogenase (*GAPDH*, Fw: ATGGGGAAGGTGAAGGTCG; Rev: TAAAAGCAGCCCTGGTGACC) was selected as housekeeping gene for primary human monocyte-derived macrophages based on previous work[60]. The efficiency of all primers was between 0.9 and 1.1 and relative expression was calculated using the formula:  $2^{-\Delta CT}$ .

### Cytokine quantification

After 24h and 72h of culture, cell culture supernatants of different blood donors ( $n=4$ ) were collected for cytokine quantification in triplicates by enzyme-linked immunosorbent assays (ELISA). The supernatants were centrifuged for 10 minutes at 300G, aliquoted, and stored at  $-80^{\circ}\text{C}$  until analysis. Human C-C motif chemokine ligand 18 (*CCL18*; DuoSet ELISA, R&D Systems, Minneapolis, USA), human soluble cluster of differentiation 163 (s*CD163*; DuoSet ELISA, R&D Systems), human C-C motif chemokine ligand 5 (*CCL5*; DuoSet ELISA, R&D Systems), and human interleukin 6 (IL-6; Ready-SET-Go!<sup>®</sup> ELISA, eBioscience, San Diego, USA) were measured with ELISA kits according to the manufacturers' instructions. Absorbance was measured at 450 nm and corrected at 570 nm (Zenyth 3100 Microplate Multimode Detector, Anthos Labtec Instruments, Salzburg, Austria). These cytokines were selected as indicators of M1 (*CCL5*, IL-6) and M2 (*CCL18*, *CD163*) macrophage phenotype based on literature and were confirmed by induction in monolayers (Appendix Figure A.2) [57,61,62]. For each sample, measured cytokine concentrations were divided by DNA concentration to normalize.

### DNA quantification

After the removal of supernatant for cytokine quantitation, calcium phosphate granules were rinsed in PBS followed by treatment with PBS/0.1% Triton X-100 (Sigma) for cell lysis. Lysates were collected after 5 min, vortexed and stored at  $-80^{\circ}\text{C}$  until analysis. Quantification of Double stranded DNA was performed using QuantiFluor<sup>®</sup> dsDNA System (Promega, Madison, USA), according to the manufacturer's instructions. Fluorescence signal was measured with excitation and emission at 504nm and 531nm, respectively (Zenyth 3100 Microplate Multimode Detector, Anthos Labtec Instruments).

## Immunofluorescent staining of macrophages

Immunofluorescent staining of macrophages for cluster of differentiation 68 (CD68 (Kp-1), 10 µg/ml, Cell Marque, Rocklin, USA), CD163 (6.7 µg/ml, ab182422, Abcam, Cambridge, UK) and inducible nitric oxide synthase (iNOS, 1:50, ab15323, Abcam) was performed for visualization by confocal microscopy (SP8x, Leica-microsystems, Mannheim, Germany). These antibodies were selected for use as pan-macrophage marker (CD68), M2 phenotype marker (CD163) and M1 phenotype marker (iNOS), based on literature[63–65]. The cells adherent to calcium phosphate granules were fixed in formalin (10%) and stored in PBS at 4 °C until further processing. After permeabilization using PBS/0.2% Triton X-100, non-specific protein binding was blocked using PBS/5% bovine serum albumin (Sigma) prior to incubation with the primary antibody for 1h. After washing with 0.1% Tween in PBS, cells were incubated for 1h with a biotinylated secondary antibody (1:200, goat anti-rabbit biotinylated, E0432, Dako; or 1:200, sheep anti-mouse biotinylated, RPN1001v1, GE Healthcare). Next, samples were incubated with tertiary antibody streptavidin Alexa Fluor 568 (5 µg/ml, S11226, Invitrogen) and fluorescein isothiocyanate (FITC)-conjugated Phalloidin (0.5 µg/ml, Sigma) to show the F-actin network. Lastly, cell nuclei were stained with 4',6-diamidino-2-phenylindole dihydrochloride (DAPI, 100 ng/mL) for 10 minutes. All incubation steps were performed at room temperature under mild agitation. For image capture, Z-stacks were used to obtain a greater depth of field to capture cells in different focal planes on the uneven material surfaces.

## Angiogenic tube formation assay

To evaluate the effect of macrophage conditioned medium (mCM) on angiogenic tube formation, macrophages of different donors ( $n=3$ ) were cultured in triplicates on BCP<sub><math>\mu\text{m}</math></sub> or TCP for 48h in basic culture medium, supplemented with 10 ng/ml M-CSF, after which the wells were rinsed in PBS and medium was changed to complete endothelial growth medium-2 (EGM-2, Lonza, Basel, Switzerland), containing Endothelial Basic Medium 2 (EBM-2, Lonza) + Singlequots (Lonza), 5% FBS, 2.05 mM L-Glutamine (Gibco) and 100 U/mL penicillin with 100 mg/mL streptomycin (Invitrogen). After 24h, mCM was pooled, centrifuged for 10 minutes at 300G, aliquoted and stored at -80°C until further use. Human umbilical vein-derived endothelial cells (HUVECs) were expanded to 80% confluence on tissue culture polystyrene coated with 0.1% gelatin. For the tube formation assay, µ-slides for angiogenesis (Ibidi, Gräfelfing, Germany) were coated with growth factor reduced Matrigel (1:1 diluted with PBS, 45 min at 37°C, Corning, New York, USA), after which HUVECs were seeded at a density of 48,000 cells/cm<sup>2</sup> in a 1:1 ratio of mCM and EBM-2 supplemented with 1% FBS, using 6 replicates per condition. As positive and negative control, EBM-2 supplemented with 10% and 0% FBS were used, respectively. Slides were incubated for 16h at 37°C under humidified conditions and with 5% CO<sub>2</sub>, followed by observation of tube networks and image capture (full-view of wells) by microscopy (IX53, Olympus, Hamburg, Germany). Images were processed for quantification in graphics



editor software (Adobe Photoshop CS5, Adobe, San Jose, USA) using fixed parameters for cropping, brightness-contrast adjustment and resizing. Tube network images were then quantified using 'Angiogenesis Analyzer for ImageJ'[66] plugin for ImageJ (NIH, Bethesda, USA).

### **Osteogenic differentiation of MSCs**

To assess the indirect effect of macrophages activated by the materials on the osteogenic differentiation of bone marrow-derived MSCs (BMSCs), conditioned medium from the macrophages (mCM) was prepared. Briefly, macrophages of different blood donors ( $n=3$ ) were cultured in triplicates on BCP<sub><math>\mu\text{m}</math> or TCP for 48h in basic culture medium supplemented with 10 ng/ml M-CSF, after which the wells were rinsed in PBS and medium was changed to basic MSC medium: alpha Minimum Essential Medium ( $\alpha$ MEM, 22561, Gibco) supplemented with 10% HI-FBS, 100 U/ mL penicillin, 100 mg/mL streptomycin (15140, Invitrogen), and 0.2 mM L-ascorbic acid-2-phosphate (ASAP, Sigma). After 24h, mCMs from multiple wells were pooled, centrifuged for 10 minutes at 300G, aliquoted, and stored at -80°C until further use. Human BMSCs were isolated and characterized as previously described [67]. For osteogenic differentiation, BMSCs of one donor were seeded in polystyrene well plates at a density of 3,000 cells/cm<sup>2</sup> in basic MSC medium supplemented with 1 ng/mL basic fibroblast growth factor (rh-FGF-2; R&D Systems). After 3 days, medium was refreshed to a 2:3 ratio of, respectively, mCM and osteogenic differentiation medium, containing basic MSC medium supplemented with  $\beta$ -glycerophosphate (BGP, Sigma) to obtain a final concentration of 10 mM BGP. As control conditions, osteogenic differentiation medium and basic culture medium were used. The cells were cultured for 10 days at 37°C under humidified conditions and 5% CO<sub>2</sub>, with media refreshment every 3 days. After 10 days of culture, MSCs were rinsed in PBS and then lysed using PBS/0.2% Triton X-100, prior to storage at -80°C until further use. Additional samples of each condition were fixed using 10% formalin for later osteonectin immunofluorescence staining.</sub>

#### **Quantification of Alkaline Phosphatase Activity**

Quantification of Alkaline Phosphatase (ALP) activity in MSC lysates was performed as previously described[68]. ALP is a relevant marker of osteogenic differentiation[69]. ALP activity was measured after 10 days based on previous work and reports in literature that ALP levels peak after 10-14 days of osteogenic differentiation[70]. ALP activity in cell lysates was measured by conversion of p-nitrophenyl phosphate (pNPP), using the pNPP liquid substrate system (Sigma) according to the manufacturer's instructions. Absorbance was measured at 405 nm and corrected at 655 nm (Bio-Rad, Hercules, CA). A reference curve of serially diluted known activity of calf intestinal ALP (Sigma) in PBS/0.2% Triton X-100 was used to determine ALP activity in lysates. In addition, DNA content in MSC lysates was used for normalization and was quantified as described above, using QuantiFluor® dsDNA System (Promega, Madison, USA).



### ***Osteonectin***

Formalin-fixed MSCs were stained with an antibody against osteonectin (ON, 1:5, AON-1, Developmental Studies Hydromab Bank) as a marker for osteoblast differentiation. The cells were processed for immunofluorescence as described above, using ON as primary antibody, a biotinylated secondary antibody (1:200, sheep anti-mouse biotinylated, RPN1001v1, GE Healthcare) and streptavidin Alexa Fluor 568 (5 µg/ml, Invitrogen) as tertiary antibody. The cell nuclei were stained with DAPI.

### **Statistical analysis**

Statistical analysis was performed using dedicated software tools (MS Excel, Microsoft, Albuquerque, NM, USA; GraphPad Prism, San Diego, CA, USA). Normal distribution of data was assessed by Kolmogorov-Smirnov normality test. Cell shape measurements, protein level, gene expression, tube formation and ALP activity data were analyzed using two-factor analysis of variance with Holm-Sidak's multiple comparisons test with multiplicity adjusted p-values. When protein levels in individual samples were below the detection limit of the standard curves in the assays, they were assigned a value of zero.

## **RESULTS**

### **Macrophages adopt an elongated morphology on submicron needle-shaped topography and mostly a spherical morphology on conventional surface structure**

SEM of the material surfaces confirmed the presence of a topography consisting of submicron needle-shaped crystals on the surface of BCP<sub><µm</sub>, while TCP presented a relatively smooth surface with a globular topography (**Figure 2. A, B**). After seeding, a large proportion of adherent macrophages on the submicron topography of BCP<sub><µm</sub> adopted an elongated, bipolar shape, while on TCP the macrophages remained spherical (**Figure 2. C, D**). Quantification of cell dimensions by measuring the short and long axes of macrophages on SEM images, indicated that the average short axis length was different but in the same order of magnitude for both materials (BCP<sub><µm</sub>: 7.0 ± 3.9 µm; TCP: 5.7 ± 1.7 µm, *p*=0.007), while the average long axis length was substantially greater in macrophages adhering to BCP<sub><µm</sub> versus TCP (BCP<sub><µm</sub>: 26.0 ± 13.5 µm; TCP: 8.4 ± 3.6 µm, *p*<0.001) (**Figure 2. E**). Consequently, the average elongation index was 3.5-fold greater for macrophages on BCP<sub><µm</sub> than those on TCP (BCP<sub><µm</sub>: 5.2 ± 4.8; TCP: 1.5 ± 0.6 µm, *p*<0.001) (**Figure 2. E**). The percentage of elongated macrophages (elongation index ≥ 2) was also higher on BCP<sub><µm</sub> compared to TCP, with 67.5% versus 15.4%, respectively (**Figure 2. E**).



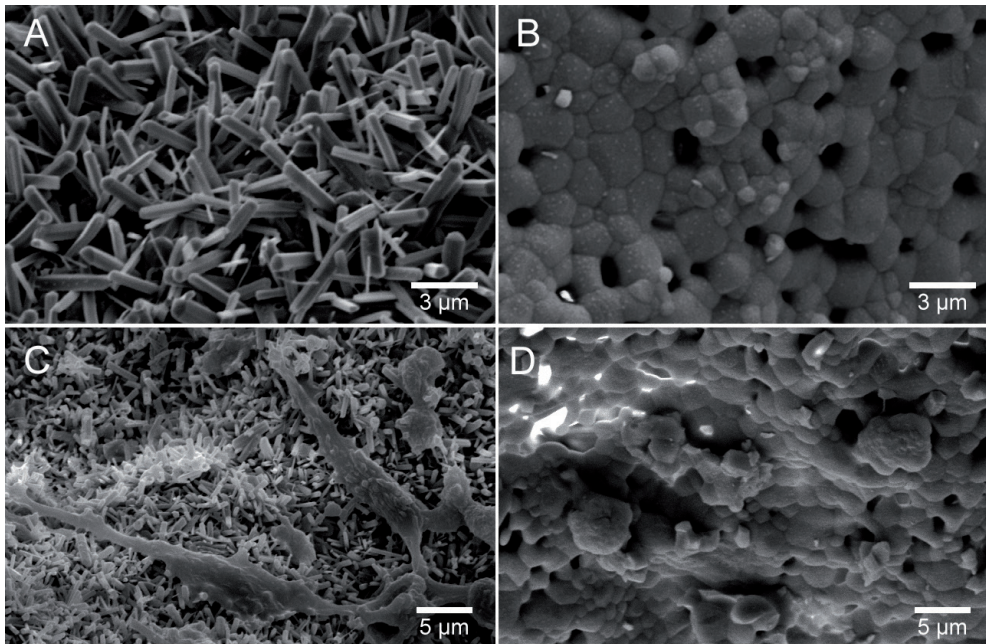
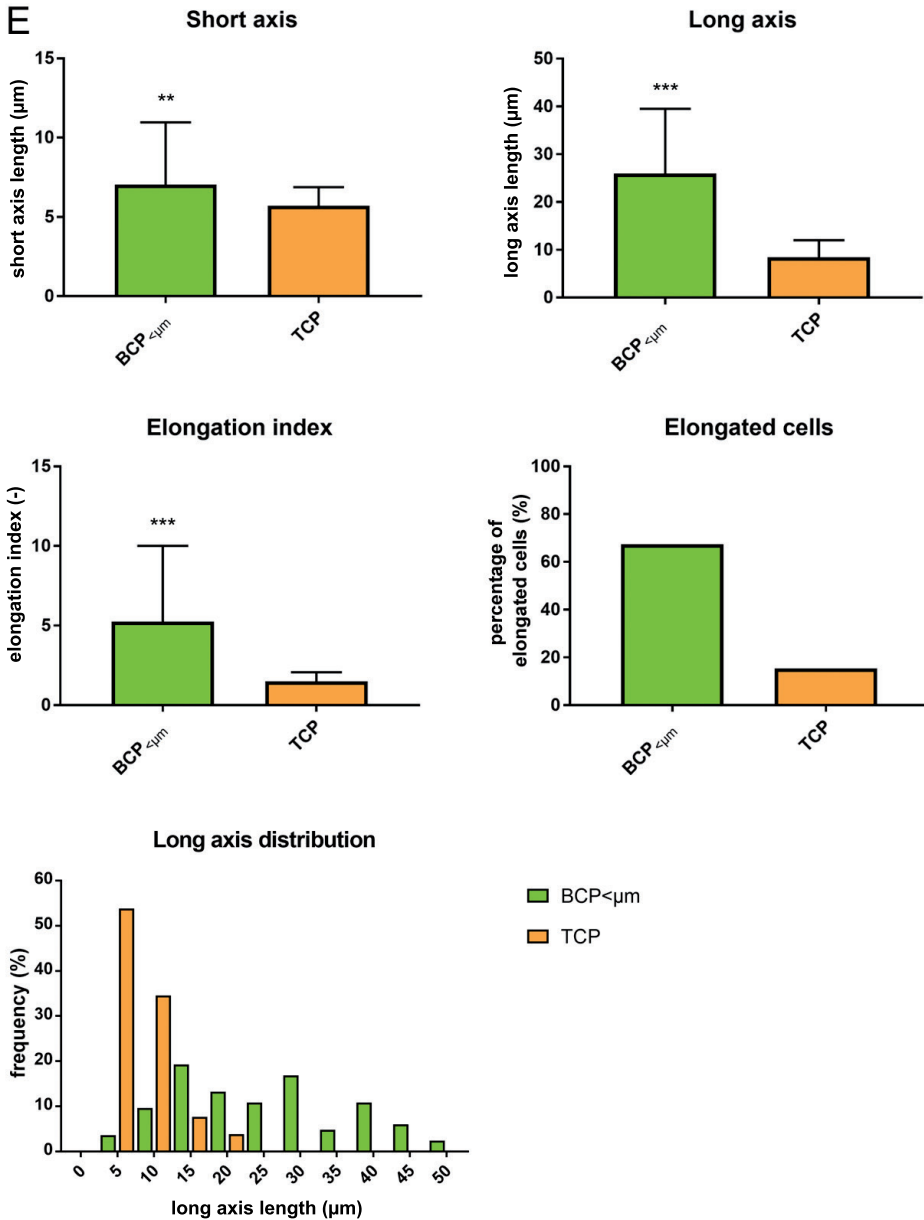


**Figure 2 (above/right). Cell shape of macrophages cultured on calcium phosphates.** SEM images of the surface of **(A)** BCP <sub>$\leq 1\mu\text{m}$</sub>  and **(B)** TCP, prior to macrophage seeding. SEM image of macrophages adhering on the surface of **(C)** BCP <sub>$\leq 1\mu\text{m}$</sub>  and **(D)** TCP after 72h culture. **(E)** Quantification of cell shape analysis of macrophages adherent on BCP <sub>$\leq 1\mu\text{m}$</sub>  and TCP. The length of the short axis and long axis of macrophages was measured and were used to calculate the elongation index. Cells with an elongation index of  $\geq 2$  were considered elongated. Data presented as mean + SD of 3 donors in duplicate. \*\*:  $p < 0.01$ , \*\*\*:  $p < 0.001$

### Gene expression of adherent macrophages is influenced by bone substitute materials

To determine macrophage phenotype, expression of genes encoding for anti-inflammatory (*CD206*, *CD163*, *CCL18*) and for pro-inflammatory proteins (*CCL2*, *CCL5*, *IL1 $\beta$* ) was assessed in macrophages adherent to BCP <sub>$\leq 1\mu\text{m}$</sub>  and TCP (**Figure 3**). These genes were validated as markers for the respective phenotypes (Appendix Figure A.1). Expression of *CD206* was significantly higher in BCP <sub>$\leq 1\mu\text{m}$</sub> -cultured macrophages after 72h. For *CD163* expression, no significant differences between the materials were determined, although average expression at 72h tended to be increased in the BCP <sub>$\leq 1\mu\text{m}$</sub>  condition ( $p=0.053$ ). Likewise, no differences in expression of *CCL18* were found. Expression of *CCL2* was higher in adherent macrophages on BCP <sub>$\leq 1\mu\text{m}$</sub>  at both 24h and 72h, while no differences were found in expression of *CCL5*. For *IL1 $\beta$* , expression was higher in macrophages activated by BCP <sub>$\leq 1\mu\text{m}$</sub>  than by TCP at both time points.



### Protein secretion and expression by macrophages varied between materials with submicron topography and conventional surface

To determine the phenotype of macrophages cultured on the bone graft materials, secretion of specific marker proteins was performed (Figure 4). Based on literature and *in vitro* confirmation (Appendix Figure A.2), production of the proteins CCL18 and sCD163 may be considered an indication for M2 macrophage polarization, while production of IL-6









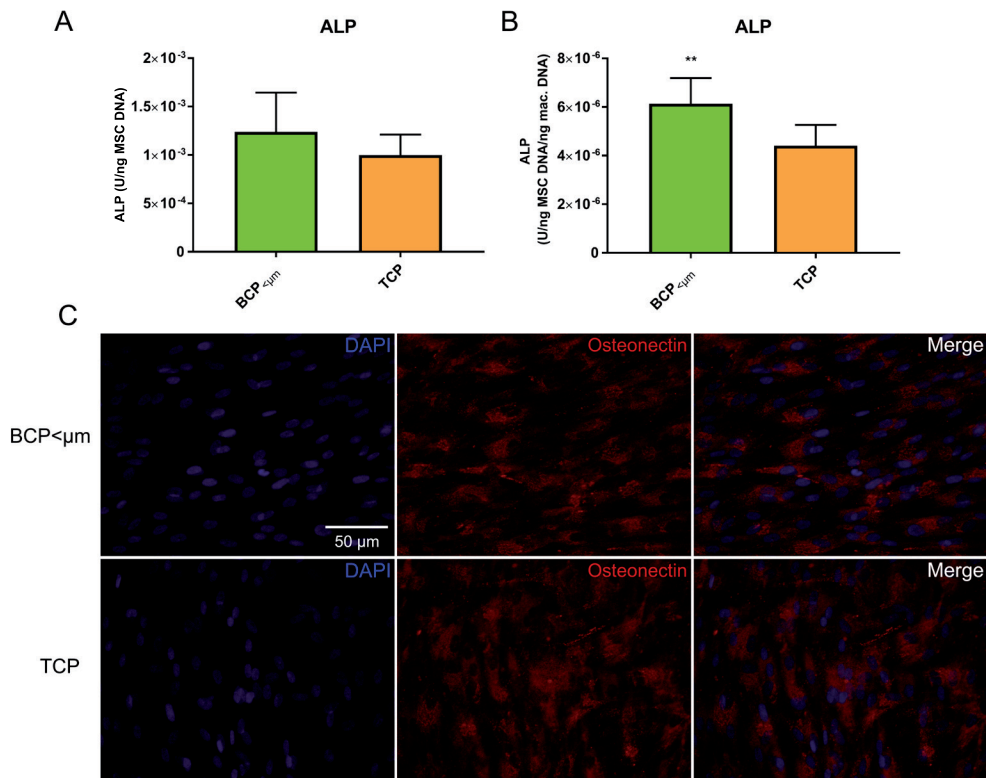


**Figure 7. Osteogenic differentiation of MSCs with medium conditioned by macrophages cultured on calcium phosphates.** (A,B) Quantification of ALP activity in MSCs after 10 days of culture in osteogenic differentiation medium with BCP<sub><μm</sub>-mCM and TCP-mCM. Data are shown as (A) ALP activity normalized to MSC DNA and (B) normalized to MSC DNA and macrophage DNA. Data represent mean + SD of a total of 3 separate monocyte donors. (C) Microscopy images of differentiated MSCs stained for osteonectin and DAPI, which were used for further confirmation of osteogenic differentiation. \*\*:  $p < 0.01$

## DISCUSSION

In this study, we have shown differential responses of primary human macrophages cultured on calcium phosphate materials with different surface topographies. Macrophages cultured on the submicron topography of BCP<sub><μm</sub> were found to have an elongated morphology compared to macrophages cultured on TCP. Protein and gene expression analyses demonstrated higher expression of M1 and M2 markers of macrophages cultured on BCP<sub><μm</sub>, indicating an overall stronger activation of macrophages. The data revealed a phenotypic skewing of macrophages towards the M2 phenotype on BCP<sub><μm</sub> versus TCP after 72h. Lastly, medium conditioned by macrophages cultured on BCP<sub><μm</sub> also enhanced





Interesting questions with the observed macrophage elongation are why and how macrophages take on an elongated shape on BCP<sub><math>\lt; \mu\text{m}</math></sub> and what is its involvement in the observed M2 phenotype skewing. McWhorter *et al.* demonstrated an essential role of the actin cytoskeleton in shape-induced M2 macrophage polarization, as treatment of the cells with various pharmacological inhibitors of the actin cytoskeleton dynamics, *i.e.* actin polymerization and actin/myosin contractility, resulted in loss of M2 phenotype [73]. Likewise, Zhu *et al.* reported that RAW 264.7 macrophage M2 polarization on TiO<sub>2</sub> honeycomb surface topography was associated with upregulation of the Rho family of GTPases, which are regulators of the actin cytoskeleton [80]. Yet another study by Yang *et al.* also reported that M2 macrophage activation by titanium 'micro/nano-net' surface topography was associated with enhanced Rho-associated protein kinase (ROCK) expression and reduced Src expression, which are key up-regulators and down-regulators of actin cytoskeletal tension, respectively [81,82].

These studies demonstrate that topographical features of materials can modulate macrophage shape and induce cytoskeletal rearrangements, which play a role in M2 macrophage phenotype upregulation. It is widely accepted that cell shape can influence downstream signaling and cell behavior through various mechanotransduction pathways [83]. By these means, the submicron needle-shaped topography of BCP<sub><math>\lt; \mu\text{m}</math></sub> may lead to M2 activation through cell shape modulation and mechanotransduction [84]. Further studies are needed to elucidate the precise mechanisms of macrophage elongation on biomaterial topographies and its involvement in macrophage polarization.

The observed concurrent expression of both M1 and M2 protein and gene markers in macrophages cultured on the bone graft materials, especially at 24h, could indicate presence of either a heterogeneous population of polarized M1- and M2-like macrophages, or an intermediate macrophage phenotype. Since immunohistochemistry for M1 (iNOS) and M2 (CD163) markers at 72h revealed presence of both markers in the majority of macrophages, this could indeed suggest that a 'mixed', intermediate macrophage phenotype was observed. It has been long recognized that instead of the reductionist M1/M2 macrophage classification, macrophages probably exist on a spectrum between these phenotypic poles and there are myriad intermediate subtypes [29,85–87]. Nonetheless, it is clear that macrophages cultured on BCP<sub><math>\lt; \mu\text{m}</math></sub> for 72h leaned stronger towards an M2-like phenotype than the macrophages adhering to TCP.

The subsiding M1 marker expression with maintenance of augmented M2 markers after 72h of culture, may be considered to resemble a phenotypic shift towards the M2 phenotype on BCP<sub><math>\lt; \mu\text{m}</math></sub>. Subsidence of M1 markers was also observed in macrophages on TCP (CCL5, IL-1 $\beta$ ), but to an overall lesser extent than on BCP<sub><math>\lt; \mu\text{m}</math></sub>. A gradual phenotypic shift of an M1-dominant to M2-dominant macrophage population has been characterized as an

essential element of the macrophage behavior during normal wound healing [28]. Loi *et al.* demonstrated that a timely transition from primary murine M1 macrophages to M2 macrophages in co-culture with pre-osteoblastic MC3T3 cells, resulted in upregulation of *in vitro* osteogenesis[88]. This suggested that a transient inflammatory, M1-dominant phase (72h) followed by an M2-dominant phase is crucial for enhanced osteogenesis, a finding that has been corroborated in other studies using co-culture models of macrophages with MSCs, including a study using human cells[89,90]. Furthermore, Spiller *et al.* reported a similar augmented effect of macrophage M1-M2 phenotype transition on vascularization of bone scaffolds implanted subcutaneously in mice[91]. Taking these findings into account, the phenotypic switch observed in macrophages on bone graft materials in the current study, which was of greater magnitude on BCP<sub><math>\lt; \mu\text{m}</math></sub> than TCP, may be a potential additional explanation of the enhanced bone healing potential of BCP<sub><math>\lt; \mu\text{m}</math></sub>.

As our results indicate phenotypic skewing of human macrophages towards an M2-like phenotype on BCP<sub><math>\lt; \mu\text{m}</math></sub> *in vitro*, we may speculate on the relevance of these findings to bone regeneration with calcium phosphate bone substitutes *in vivo*. We know from previous studies with animal models that BCP<sub><math>\lt; \mu\text{m}</math></sub> and other submicron surface-structured calcium phosphates, have greater bone regenerative capacity than conventional calcium phosphates without submicron surface structure [9,10,12,13,53]. Recently, in a study similar to the current work, Li *et al.* demonstrated elevated M2-like activation (CD206, *Arg-1*, *VEGF*, *VEGF*, *IGF-1*, *IGF-1*) of murine RAW 264.7 macrophages on osteoinductive  $\beta$ -TCP with submicron surface structure, while  $\beta$ -TCP with micron surface structure induced an M1-like phenotype (*iNOS*, *iNOS*, *TNF- $\alpha$* , *IL6*, *IL-6*, *IL-1 $\beta$* , *IL1B*) [51]. In a similar study using THP-1 macrophages, we have previously also determined M2 activation (CCL18, *TGF- $\beta$* ) on osteoinductive TCP with submicron surface structure and M1-activation (*TNF- $\alpha$* , *IL-1 $\beta$* ) on micron surface structure *in vitro*[92]. Yet another study by Chen *et al.* determined upregulation of M2 markers (*Arg-1*, CD206, *IL-10*, *IGF*) in RAW 264.7 macrophages cultured on BCP with high osteoinductive potential versus HA and  $\beta$ -TCP with lower osteoinductive potential, which exhibited greater M1-like activation (*CCR7*, *iNOS*, *IL-1 $\beta$* , *TNF- $\alpha$* , *CCL2*) [52]. Both studies moved on to evaluate macrophage phenotypes in association with these materials after intramuscular implantation in mice. Both reported a greater population of anti-inflammatory, M2-like macrophages around the osteoinductive materials that induced ectopic bone formation, while more M1-like macrophages were observed around materials that did not induce ectopic bone formation [51,52]. Likewise, we have previously found higher levels of anti-inflammatory factor *IL-10* around osteoinductive versus non-inductive TCP after ectopic implantation in canines, suggesting presence of anti-inflammatory macrophages[92]. Our current *in vitro* findings, together with *in vivo* results previously obtained with BCP<sub><math>\lt; \mu\text{m}</math></sub>, are in agreement with the findings of the aforementioned studies. However, as opposed to the results of these other studies, we did not observe enhanced M1 macrophage activation on the material without submicron surface topography. This



observation may be due to different *in vitro* culture conditions or may be species-related, since to our current knowledge, this study was the first to evaluate macrophage response to calcium phosphate with submicron surface topography using primary macrophages from humans. Naturally, primary macrophages cultured *in vitro* are considered a more representative model of the human immune response as compared to murine macrophages or human monocytic cell lines. While the exact mechanism of M2 macrophage contribution to bone regeneration by calcium phosphates remains to be elucidated, evidence for their involvement has so far been congruent.

Angiogenesis and osteogenic differentiation of stem cells are critical processes during bone healing. Ingrowing blood vessels are needed to provide essential nutrients and are a source of stem cells (i.e. pericytes), while stem cell differentiation provide bone-forming cells. *In vitro* outcomes of angiogenic tube formation by HUVECs and osteogenic differentiation of MSCs have been shown to be predictive of *in vivo* effects[69,93,94]. The enhanced angiogenic tube formation by HUVECs and osteogenic differentiation of MSCs after exposure to BCP<sub><μm</sub>-mCM, suggest an altered or upregulated paracrine signaling by macrophages on BCP<sub><μm</sub> that is indicative of a pro-healing, M2-like functional phenotype. Previous research has demonstrated that macrophages exhibit intricate crosstalk with endothelial cells during angiogenesis and vascularization [58,95,96]. Similarly, macrophages are involved in bone healing through communication with MSCs and pre-osteoblasts by paracrine signaling factors[36,89]. Other studies that have evaluated effects of macrophages in *in vitro* angiogenic tube formation[47,92,97–101] and osteogenic differentiation assays[47,51,52,89,99] have associated upregulated angiogenic and osteogenic responses with anti-inflammatory M2-activated macrophages. These findings further support our observation of pro-healing M2 macrophages on BCP<sub><μm</sub> and suggest involvement of M2 macrophages in the enhanced bone healing observed with calcium phosphates with submicron topography *in vivo*.

The calcium phosphate bone graft materials that we compared in this study were not only different in topographical features but also their chemistry. TCP has a higher solubility than HA, which translates to a higher release of Ca and P ions for TCP than BCP [9,53]. This is a potential confounder for the effect of topography on the results obtained in this study because different concentrations of ionic Ca and P may potentially influence macrophage response. Furthermore, some studies have shown that surface chemistry of calcium phosphate can influence the total amount and type of proteins adsorbed to the material surface, which is dependent on the ratio of available Ca and P sites that have differential affinity for protein adsorption[102]. This could be another means by which chemistry may influence cell-surface interactions and subsequent cell behavior. However, other studies have shown that topography of calcium phosphates has a stronger effect on protein adsorption than chemistry[80,103].

Previous studies have determined an effect of calcium phosphate phase composition on cells *in vitro*, including adhesion, spreading, proliferation and differentiation of osteogenic cells *in vitro*[103–105]. A study by Chen *et al.* claimed that phase composition of calcium phosphates controlled RAW 264.7 macrophage polarization *in vitro*, showing an M2-dominant response on BCP and an M1-dominant response on  $\beta$ -TCP [52]. However, the authors acknowledged that the surface grain size was more than 3-fold greater for  $\beta$ -TCP than BCP and they failed to demonstrate a difference in Ca and P release between these materials *in vitro*. This suggests that topography instead of chemistry of the materials was the main driver of the observed macrophage response. Other studies have already demonstrated a clear effect of material topography on macrophage response by using calcium phosphates with identical chemistry and different topography, or insoluble materials such as titanium and polymers[51,106–108].

Some studies have attempted to isolate chemical and topographical effects of calcium phosphates by coating the surface of materials with metal (i.e. gold, titanium), thereby inhibiting ion dissolution at the surface[103,105,109,110]. Using such an approach, Engel *et al.* concluded that topographical effects are dominant over chemical effects of calcium phosphates on cells *in vitro*[109]. Likewise, Davison *et al.* demonstrated that, compared to uncoated controls, titanium-coated calcium phosphate did not differentially affect *in vitro* osteoclastogenesis of RAW264.7 macrophages *in vitro* or osteoinductive potential of the materials *in vivo*, thereby also indicating a dominant effect of topography[110]. Other studies have previously shown that there is no correlation between *in vitro* ion release by calcium phosphates and *in vivo* osteoinductive potential, whereas this relationship has been clearly established for surface topography[9,53]. Lastly, in the current work, material-only conditioned medium controls of BCP<sub><math>\mu\text{m}</math></sub> and TCP produced no differences in both the tube formation and osteogenic differentiation assays, which indicate that potential differences in ion release did not directly affect the cells in these assays.

Naturally, our findings and conclusions have to be considered within the limitations of this *in vitro* study. Firstly, we have assessed the primary macrophage response to materials using an *in vitro* culture model, with a limited set of assessment techniques and phenotypic markers. *In vivo*, other (immune) cell types will concurrently interact with biomaterials that may potentially influence macrophage response. However, various previous studies have demonstrated correlation between *in vitro* and *in vivo* macrophage phenotype in response to biomaterials and *in vivo* bone healing outcomes[47,51,52,82]. Another limitation is that we only evaluated macrophage response at two chosen time-points (24h and 72h). Additional earlier or later time-points would have provided further insight in macrophage behavior on the different materials. Lastly, in this study, immunofluorescent marker (CD163, iNOS) intensity was difficult to quantify, due to variable cell densities and an uneven surface of the materials. Although the observed cell density at the surface of TCP



was lower than BCP<sub><math>\lt; \mu\text{m}</math></sub>, this was probably the result of cell detachment from TCP during storage and handling before staining, because DNA content was not different between the conditions (data not shown).

## **CONCLUSION**

This *in vitro* study has determined stronger activation of human primary macrophages and phenotypic skewing towards a pro-healing M2 phenotype calcium phosphate with submicron topography, compared to calcium phosphate without submicron topography. This is the first study to confirm this effect using primary human macrophages. Enhanced pro-regenerative paracrine signaling to (stem) cells by these macrophages was determined in angiogenic and osteogenic assays. These findings, in line with findings from other studies, suggest that M2 macrophage polarization has a role in the enhanced bone regeneration capacity of these materials with submicron topography. Immunomodulation through surface topography is indicated as a feasible strategy to improve outcomes in tissue regeneration using biomaterials.

## **ACKNOWLEDGEMENTS**

This study was supported by the European Union's Horizon 2020 research and innovation program (grant agreements no. 674282, no. 874790 and no. 953169).

## REFERENCES

- [1] N. Eliaz, N. Metoki, Calcium phosphate bioceramics: A review of their history, structure, properties, coating technologies and biomedical applications, *Materials (Basel)*. (2017). <https://doi.org/10.3390/ma10040334>.
- [2] N.M. Fariña, F.M. Guzón, M.L. Peña, A.G. Cantalapiedra, In vivo behaviour of two different biphasic ceramic implanted in mandibular bone of dogs, in: *J. Mater. Sci. Mater. Med.*, 2008: pp. 1565–1573. <https://doi.org/10.1007/s10856-008-3400-y>.
- [3] S.S. Jensen, M.M. Bornstein, M. Dard, D.D. Bosshardt, D. Buser, Comparative study of biphasic calcium phosphates with different HA/TCP ratios in mandibular bone defects. A long-term histomorphometric study in minipigs, *J. Biomed. Mater. Res.–Part B Appl. Biomater.* 90 B (2009) 171–181. <https://doi.org/10.1002/jbm.b.31271>.
- [4] H. Yuan, C.A. Van Blitterswijk, K. De Groot, J.D. De Bruijn, A comparison of bone formation in biphasic calcium phosphate (BCP) and hydroxyapatite (HA) implanted in muscle and bone of dogs at different time periods, *J. Biomed. Mater. Res.–Part A*. 78 (2006) 139–147. <https://doi.org/10.1002/jbm.a.30707>.
- [5] O. Gauthier, J.M. Bouler, E. Aguado, P. Pilet, G. Daculsi, Macroporous biphasic calcium phosphate ceramics: Influence of macropore diameter and macroporosity percentage on bone ingrowth, *Biomaterials*. 19 (1998) 133–139. [https://doi.org/10.1016/S0142-9612\(97\)00180-4](https://doi.org/10.1016/S0142-9612(97)00180-4).
- [6] P.S. Egli, W. Muller, R.K. Schenk, Porous hydroxyapatite and tricalcium phosphate cylinders with two different pore size ranges implanted in the cancellous bone of rabbits. A comparative histomorphometric and histologic study of bone ingrowth and implant substitution, *Clin. Orthop. Relat. Res.* (1988) 127–138. <https://doi.org/10.1097/00003086-198807000-00017>.
- [7] L. Galois, D. Mainard, Bone ingrowth into two porous ceramics with different pore sizes: An experimental study, *Acta Orthop. Belg.* 70 (2004) 598–603.
- [8] H. Yuan, H. Fernandes, P. Habibovic, J. De Boer, A.M.C. Barradas, A. De Ruiter, W.R. Walsh, C.A. Van Blitterswijk, J.D. De Bruijn, Osteoinductive ceramics as a synthetic alternative to autologous bone grafting, *Proc. Natl. Acad. Sci. U. S. A.* 107 (2010) 13614–13619. <https://doi.org/10.1073/pnas.1003600107>.
- [9] R. Duan, L.A. van Dijk, D. Barbieri, F. de Groot, H. Yuan, J.D. de Bruijn, Accelerated bone formation by biphasic calcium phosphate with a novel sub-micron surface topography, *Eur. Cell. Mater.* 37 (2019) 60–73. <https://doi.org/10.22203/eCM.v037a05>.
- [10] R. Duan, D. Barbieri, F. De Groot, J.D. De Bruijn, H. Yuan, Modulating Bone Regeneration in Rabbit Condyle Defects with Three Surface-Structured Tricalcium Phosphate Ceramics, *ACS Biomater. Sci. Eng.* 4 (2018) 3347–3355. <https://doi.org/10.1021/acsbomaterials.8b00630>.
- [11] P. Habibovic, H. Yuan, M. van den Doel, T.M. Sees, C.A. van Blitterswijk, K. de Groot, Relevance of osteoinductive biomaterials in critical-sized orthotopic defect, *J. Orthop. Res.* 24 (2006) 867–876. <https://doi.org/10.1002/jor.20115>.



- [12] L.A. Van Dijk, F. Barrère-De Groot, A.J.W.P. Rosenberg, M. Pelletier, C. Christou, J.D. De Bruijn, W.R. Walsh, MagnetOs, Vitoss, and Novabone in a Multi-endpoint Study of Posterolateral Fusion: A True Fusion or Not?, *Clin. Spine Surg.* 33 (2020) E276–E287. <https://doi.org/10.1097/BSD.0000000000000920>.
- [13] D. Barbieri, H. Yuan, A.S. Ismailo lu, J.D. De Bruijn, Comparison of two moldable calcium phosphate-based bone graft materials in a noninstrumented canine interspinous implantation model, *Tissue Eng.–Part A.* 23 (2017) 1310–1320. <https://doi.org/10.1089/ten.tea.2016.0347>.
- [14] R. Duan, D. Barbieri, X. Luo, J. Weng, J.D. de Bruijn, H. Yuan, Submicron-surface structured tricalcium phosphate ceramic enhances the bone regeneration in canine spine environment, *J. Orthop. Res.* 34 (2016) 1865–1873. <https://doi.org/10.1002/jor.23201>.
- [15] L.A. van Dijk, R. Duan, X. Luo, D. Barbieri, M. Pelletier, C. Christou, A.J.W.P. Rosenberg, H. Yuan, F. Barrère-de Groot, W.R. Walsh, J.D. de Bruijn, Biphasic calcium phosphate with submicron surface topography in an Ovine model of instrumented posterolateral spinal fusion, *JOR Spine.* 1 (2018) e1039. <https://doi.org/10.1002/jsp2.1039>.
- [16] P. Habibovic, H. Yuan, C.M. Van Der Valk, G. Meijer, C.A. Van Blitterswijk, K. De Groot, 3D microenvironment as essential element for osteoinduction by biomaterials, *Biomaterials.* 26 (2005) 3565–3575. <https://doi.org/10.1016/j.biomaterials.2004.09.056>.
- [17] A.M.C. Barradas, H. Yuan, C.A. van Blitterswijk, P. Habibovic, Osteoinductive biomaterials: current knowledge of properties, experimental models and biological mechanisms., *Eur. Cell. Mater.* (2011). <https://doi.org/10.22203/eCM.v021a31>.
- [18] L.A. van Dijk, D. Barbieri, F. Barrère-de Groot, H. Yuan, R. Oliver, C. Christou, W.R. Walsh, J.D. de Bruijn, Efficacy of a synthetic calcium phosphate with submicron surface topography as autograft extender in lapine posterolateral spinal fusion, *J. Biomed. Mater. Res.–Part B Appl. Biomater.* 107 (2019) 2080–2090. <https://doi.org/10.1002/jbm.b.34301>.
- [19] J.M. Morais, F. Papadimitrakopoulos, D.J. Burgess, Biomaterials/tissue interactions: Possible solutions to overcome foreign body response, *AAPS J.* (2010). <https://doi.org/10.1208/s12248-010-9175-3>.
- [20] L. Chung, D.R. Maestas, F. Housseau, J.H. Elisseeff, Key players in the immune response to biomaterial scaffolds for regenerative medicine, *Adv. Drug Deliv. Rev.* (2017). <https://doi.org/10.1016/j.addr.2017.07.006>.
- [21] Z. Julier, A.J. Park, P.S. Briquez, M.M. Martino, Promoting tissue regeneration by modulating the immune system, *Acta Biomater.* (2017). <https://doi.org/10.1016/j.actbio.2017.01.056>.
- [22] L. Davenport Huyer, S. Pascual-Gil, Y. Wang, S. Mandla, B. Yee, M. Radisic, Advanced Strategies for Modulation of the Material–Macrophage Interface, *Adv. Funct. Mater.* 30 (2020) 1909331. <https://doi.org/10.1002/adfm.201909331>.
- [23] B.N. Brown, B.D. Ratner, S.B. Goodman, S. Amar, S.F. Badylak, Macrophage polarization: An opportunity for improved outcomes in biomaterials and regenerative medicine, *Biomaterials.* (2012). <https://doi.org/10.1016/j.biomaterials.2012.02.034>.



- [24] A. Mantovani, S.K. Biswas, M.R. Galdiero, A. Sica, M. Locati, Macrophage plasticity and polarization in tissue repair and remodelling, *J. Pathol.* (2013). <https://doi.org/10.1002/path.4133>.
- [25] P.J. Murray, J.E. Allen, S.K. Biswas, E.A. Fisher, D.W. Gilroy, S. Goerdts, S. Gordon, J.A. Hamilton, L.B. Ivashkiv, T. Lawrence, M. Locati, A. Mantovani, F.O. Martinez, J.L. Mege, D.M. Mosser, G. Natoli, J.P. Saeij, J.L. Schultze, K.A. Shirey, A. Sica, J. Suttles, I. Udalova, J.A. vanGinderachter, S.N. Vogel, T.A. Wynn, Macrophage Activation and Polarization: Nomenclature and Experimental Guidelines, *Immunity*. 41 (2014) 14–20. <https://doi.org/10.1016/j.immuni.2014.06.008>.
- [26] D.M. Mosser, J.P. Edwards, Exploring the full spectrum of macrophage activation, *Nat. Rev. Immunol.* (2008). <https://doi.org/10.1038/nri2448>.
- [27] F. Taraballi, M. Sushnitha, C. Tsao, G. Bauza, C. Liverani, A. Shi, E. Tasciotti, Biomimetic Tissue Engineering: Tuning the Immune and Inflammatory Response to Implantable Biomaterials, *Adv. Healthc. Mater.* (2018). <https://doi.org/10.1002/adhm.201800490>.
- [28] T.A. Wynn, K.M. Vannella, Macrophages in Tissue Repair, Regeneration, and Fibrosis, *Immunity*. 44 (2016) 450–462. <https://doi.org/10.1016/j.immuni.2016.02.015>.
- [29] R. Klopffleisch, Macrophage reaction against biomaterials in the mouse model – Phenotypes, functions and markers, *Acta Biomater.* 43 (2016) 3–13. <https://doi.org/10.1016/j.actbio.2016.07.003>.
- [30] Z. Chen, T. Klein, R.Z. Murray, R. Crawford, J. Chang, C. Wu, Y. Xiao, Osteoimmunomodulation for the development of advanced bone biomaterials, *Mater. Today*. (2016). <https://doi.org/10.1016/j.mattod.2015.11.004>.
- [31] R. Klopffleisch, F. Jung, The pathology of the foreign body reaction against biomaterials, *J. Biomed. Mater. Res.–Part A*. (2017). <https://doi.org/10.1002/jbm.a.35958>.
- [32] N.J. Horwood, Macrophage Polarization and Bone Formation: A review, *Clin. Rev. Allergy Immunol.* 51 (2016) 79–86. <https://doi.org/10.1007/s12016-015-8519-2>.
- [33] R.J. Miron, D.D. Bosshardt, OsteoMacs: Key players around bone biomaterials, *Biomaterials*. 82 (2016) 1–19. <https://doi.org/10.1016/j.biomaterials.2015.12.017>.
- [34] K.A. Alexander, M.K. Chang, E.R. Maylin, T. Kohler, R. Müller, A.C. Wu, N. Van Rooijen, M.J. Sweet, D.A. Hume, L.J. Raggatt, A.R. Pettit, Osteal macrophages promote in vivo intramembranous bone healing in a mouse tibial injury model, *J. Bone Miner. Res.* (2011). <https://doi.org/10.1002/jbmr.354>.
- [35] L.J. Raggatt, M.E. Wulschleger, K.A. Alexander, A.C.K. Wu, S.M. Millard, S. Kaur, M.L. Maughan, L.S. Gregory, R. Steck, A.R. Pettit, Fracture healing via periosteal callus formation requires macrophages for both initiation and progression of early endochondral ossification, *Am. J. Pathol.* (2014). <https://doi.org/10.1016/j.ajpath.2014.08.017>.
- [36] J. Pajarinen, T. Lin, E. Gibon, Y. Kohno, M. Maruyama, K. Nathan, L. Lu, Z. Yao, S.B. Goodman, Mesenchymal stem cell-macrophage crosstalk and bone healing, *Biomaterials*. (2019). <https://doi.org/10.1016/j.biomaterials.2017.12.025>.



- [37] P. Humbert, M. Brennan, N. Davison, P. Rosset, V. Trichet, F. Blanchard, P. Layrolle, Immune modulation by transplanted calcium phosphate biomaterials and human mesenchymal stromal cells in bone regeneration, *Front. Immunol.* (2019). <https://doi.org/10.3389/fimmu.2019.00663>.
- [38] R. Zhang, Y. Liang, S. Wei, M2 macrophages are closely associated with accelerated clavicle fracture healing in patients with traumatic brain injury: A retrospective cohort study, *J. Orthop. Surg. Res.* 13 (2018) 213. <https://doi.org/10.1186/s13018-018-0926-7>.
- [39] F. Wehrhan, P. Moebius, K. Amann, J. Ries, R. Preidl, F.W. Neukam, M. Weber, Macrophage and osteoclast polarization in bisphosphonate associated necrosis and osteoradionecrosis, *J. Cranio-Maxillofacial Surg.* 45 (2017) 944–953. <https://doi.org/10.1016/j.jcms.2017.02.023>.
- [40] W. Zhu, R. Xu, J. Du, Y. Fu, S. Li, P. Zhang, L. Liu, H. Jiang, Zoledronic acid promotes TLR-4-mediated M1 macrophage polarization in bisphosphonate-related osteonecrosis of the jaw, *FASEB J.* 33 (2019) 5208–5219. <https://doi.org/10.1096/fj.201801791RR>.
- [41] S. Shi, Q. Zhang, I. Atsuta, S. Liu, C. Chen, S. Shi, A.D. Le, IL-17-mediated M1/M2 macrophage alteration contributes to pathogenesis of bisphosphonate-related osteonecrosis of the jaws, *Clin. Cancer Res.* 19 (2013) 3176–3188. <https://doi.org/10.1158/1078-0432.CCR-13-0042>.
- [42] J. Zhang, H. Shi, N. Zhang, L. Hu, W. Jing, J. Pan, Interleukin-4-loaded hydrogel scaffold regulates macrophages polarization to promote bone mesenchymal stem cells osteogenic differentiation via TGF- $\beta$ 1/Smad pathway for repair of bone defect, *Cell Prolif.* (2020). <https://doi.org/10.1111/cpr.12907>.
- [43] Z. wei Zheng, Y. hong Chen, D. yu Wu, J. bing Wang, M. ming Lv, X. song Wang, J. Sun, Z.Y. Zhang, Development of an accurate and proactive immunomodulatory strategy to improve bone substitute material-mediated osteogenesis and angiogenesis, *Theranostics.* 8 (2018) 5482–5500. <https://doi.org/10.7150/thno.28315>.
- [44] D. Hachim, S.T. LoPresti, C.C. Yates, B.N. Brown, Shifts in macrophage phenotype at the biomaterial interface via IL-4 eluting coatings are associated with improved implant integration, *Biomaterials.* (2017). <https://doi.org/10.1016/j.biomaterials.2016.10.019>.
- [45] D.W. Zhao, K.Q. Zuo, K. Wang, Z.Y. Sun, Y.P. Lu, L. Cheng, G.Y. Xiao, C. Liu, Interleukin-4 assisted calcium-strontium-zinc-phosphate coating induces controllable macrophage polarization and promotes osseointegration on titanium implant, *Mater. Sci. Eng. C.* (2021). <https://doi.org/10.1016/j.msec.2020.111512>.
- [46] I.M. Castaño, R.M. Raftery, G. Chen, B. Cavanagh, B. Quinn, G.P. Duffy, F.J. O'Brien, C.M. Curtin, Rapid bone repair with the recruitment of CD206+M2-like macrophages using non-viral scaffold-mediated miR-133a inhibition of host cells, *Acta Biomater.* (2020). <https://doi.org/10.1016/j.actbio.2020.03.042>.
- [47] O.R. Mahon, D.C. Browe, T. Gonzalez-Fernandez, P. Pitacco, I.T. Whelan, S. Von Euw, C. Hobbs, V. Nicolosi, K.T. Cunningham, K.H.G. Mills, D.J. Kelly, A. Dunne, Nano-particle mediated M2 macrophage polarization enhances bone formation and MSC osteogenesis in an IL-10 dependent manner, *Biomaterials.* 239 (2020) 119833. <https://doi.org/10.1016/j.biomaterials.2020.119833>.

- [48] E. Olmsted-Davis, J. Mejia, E. Salisbury, Z. Gugala, A.R. Davis, A Population of M2 Macrophages Associated With Bone Formation, *Front. Immunol.* 12 (2021) 1. <https://doi.org/10.3389/FIMMU.2021.686769/FULL>.
- [49] M. Bohner, R.J. Miron, A proposed mechanism for material-induced heterotopic ossification, *Mater. Today*. 22 (2019) 132–141. <https://doi.org/10.1016/J.MATTOD.2018.10.036>.
- [50] N.L. Davison, A.L. Gamblin, P. Layrolle, H. Yuan, J.D. de Bruijn, F. Barrère-de Groot, Liposomal clodronate inhibition of osteoclastogenesis and osteoinduction by submicrostructured beta-tricalcium phosphate, *Biomaterials*. 35 (2014) 5088–5097. <https://doi.org/10.1016/j.biomaterials.2014.03.013>.
- [51] M. Li, X. Guo, W. Qi, Z. Wu, J.D. De Bruijn, Y. Xiao, C. Bao, H. Yuan, Macrophage polarization plays roles in bone formation instructed by calcium phosphate ceramics, *J. Mater. Chem. B*. 8 (2020) 1863–1877. <https://doi.org/10.1039/c9tb02932j>.
- [52] X. Chen, M. Wang, F. Chen, J. Wang, X. Li, J. Liang, Y. Fan, Y. Xiao, X. Zhang, Correlations between macrophage polarization and osteoinduction of porous calcium phosphate ceramics, *Acta Biomater.* 103 (2020) 318–332. <https://doi.org/10.1016/j.actbio.2019.12.019>.
- [53] R. Duan, D. Barbieri, X. Luo, J. Weng, C. Bao, J.D. De Bruijn, H. Yuan, Variation of the bone forming ability with the physicochemical properties of calcium phosphate bone substitutes, *Biomater. Sci.* 6 (2018) 136–145. <https://doi.org/10.1039/c7bm00717e>.
- [54] W.R. Walsh, R.A. Oliver, C. Christou, V. Lovric, E.R. Walsh, G.R. Prado, T. Haider, Critical size bone defect healing using collagen-calcium phosphate bone graft materials, *PLoS One*. 12 (2017). <https://doi.org/10.1371/journal.pone.0168883>.
- [55] K.A. Hing, L.F. Wilson, T. Buckland, Comparative performance of three ceramic bone graft substitutes, *Spine J.* 7 (2007) 475–490. <https://doi.org/10.1016/j.spinee.2006.07.017>.
- [56] N. Grotenhuis, Y. Bayon, J.F. Lange, G.J.V.M. Van Osch, Y.M. Bastiaansen-Jenniskens, A culture model to analyze the acute biomaterial-dependent reaction of human primary macrophages, *Biochem. Biophys. Res. Commun.* 433 (2013) 115–120. <https://doi.org/10.1016/j.bbrc.2013.02.054>.
- [57] L. Utomo, G.J.V.M. van Osch, Y. Bayon, J.A.N. Verhaar, Y.M. Bastiaansen-Jenniskens, Guiding synovial inflammation by macrophage phenotype modulation: an in vitro study towards a therapy for osteoarthritis, *Osteoarthr. Cartil.* (2016). <https://doi.org/10.1016/j.joca.2016.04.013>.
- [58] K.L. Spiller, R.R. Anfang, K.J. Spiller, J. Ng, K.R. Nakazawa, J.W. Daulton, G. Vunjak-Novakovic, The role of macrophage phenotype in vascularization of tissue engineering scaffolds, *Biomaterials*. (2014). <https://doi.org/10.1016/j.biomaterials.2014.02.012>.
- [59] B. Buttari, E. Profumo, L. Segoni, D. D’Arcangelo, S. Rossi, F. Facchiano, L. Saso, R. Businaro, L. Iuliano, R. Riganò, Resveratrol counteracts inflammation in human M1 and M2 macrophages upon challenge with 7-oxo-cholesterol: Potential therapeutic implications in atherosclerosis, *Oxid. Med. Cell. Longev.* (2014). <https://doi.org/10.1155/2014/257543>.
- [60] L. Utomo, G.S.A. Boersema, Y. Bayon, J.F. Lange, G.J.V.M. Van Osch, Y.M. Bastiaansen-Jenniskens, In vitro modulation of the behavior of adhering macrophages by medications is biomaterial-dependent, *Biomed. Mater.* 12 (2017). <https://doi.org/10.1088/1748-605X/aa5cbc>.



- [61] L. Utomo, Y.M. Bastiaansen-Jenniskens, J.A.N. Verhaar, G.J.V.M. van Osch, Cartilage inflammation and degeneration is enhanced by pro-inflammatory (M1) macrophages in vitro, but not inhibited directly by anti-inflammatory (M2) macrophages, *Osteoarthr. Cartil.* (2016). <https://doi.org/10.1016/j.joca.2016.07.018>.
- [62] A.A. Tarique, J. Logan, E. Thomas, P.G. Holt, P.D. Sly, E. Fantino, Phenotypic, functional, and plasticity features of classical and alternatively activated human macrophages, *Am. J. Respir. Cell Mol. Biol.* (2015). <https://doi.org/10.1165/rcmb.2015-00120C>.
- [63] M.H.M. Barros, F. Hauck, J.H. Dreyer, B. Kempkes, G. Niedobitek, Macrophage polarisation: An immunohistochemical approach for identifying M1 and M2 macrophages, *PLoS One.* (2013). <https://doi.org/10.1371/journal.pone.0080908>.
- [64] Q. Xue, Y. Yan, R. Zhang, H. Xiong, Regulation of iNOS on immune cells and its role in diseases, *Int. J. Mol. Sci.* (2018). <https://doi.org/10.3390/ijms19123805>.
- [65] F. Raggi, S. Pelassa, D. Pierobon, F. Penco, M. Gattorno, F. Novelli, A. Eva, L. Varesio, M. Giovarelli, M.C. Bosco, Regulation of human Macrophage M1-M2 Polarization Balance by hypoxia and the Triggering receptor expressed on Myeloid cells-1, *Front. Immunol.* (2017). <https://doi.org/10.3389/fimmu.2017.01097>.
- [66] Gilles Carpentier, Contribution: Angiogenesis Analyzer, *ImageJ News.* (2012).
- [67] I. Pennings, L.A. van Dijk, J. van Huuksloot, J.O. Fledderus, K. Schepers, A.K. Braat, E.C. Hsiao, E. Barriet, B.M. Morales, M.C. Verhaar, A.J.W.P. Rosenberg, D. Gawlitta, Effect of donor variation on osteogenesis and vasculogenesis in hydrogel cocultures, *J. Tissue Eng. Regen. Med.* 13 (2019) 433–445. <https://doi.org/10.1002/term.2807>.
- [68] M. Croes, F.C. Öner, D. van Neerven, E. Sabir, M.C. Kruyt, T.J. Blokhuis, W.J.A. Dhert, J. Alblas, Proinflammatory T cells and IL-17 stimulate osteoblast differentiation, *Bone.* 84 (2016) 262–270. <https://doi.org/10.1016/j.bone.2016.01.010>.
- [69] H.J. Prins, A.K. Braat, D. Gawlitta, W.J.A. Dhert, D.A. Egan, E. Tijssen-Slump, H. Yuan, P.J. Coffey, H. Rozemuller, A.C. Martens, In vitro induction of alkaline phosphatase levels predicts in vivo bone forming capacity of human bone marrow stromal cells, *Stem Cell Res.* 12 (2014) 428–440. <https://doi.org/10.1016/j.scr.2013.12.001>.
- [70] M. Eijken, M. Koedam, M. Van Driel, C.J. Buurman, H.A.P. Pols, J.P.T.M. Van Leeuwen, The essential role of glucocorticoids for proper human osteoblast differentiation and matrix mineralization, in: *Mol. Cell. Endocrinol.*, 2006: pp. 87–93. <https://doi.org/10.1016/j.mce.2005.11.034>.
- [71] G. Jundt, K.H. Berghäuser, J.D. Termine, A. Schulz, Osteonectin—a differentiation marker of bone cells, *Cell Tissue Res.* (1987). <https://doi.org/10.1007/BF00218209>.
- [72] T.U. Luu, S.C. Gott, B.W.K. Woo, M.P. Rao, W.F. Liu, Micro- and Nanopatterned Topographical Cues for Regulating Macrophage Cell Shape and Phenotype, *ACS Appl. Mater. Interfaces.* 7 (2015) 28665–28672. <https://doi.org/10.1021/acsami.5b10589>.
- [73] F.Y. McWhorter, T. Wang, P. Nguyen, T. Chung, W.F. Liu, Modulation of macrophage phenotype by cell shape, *Proc. Natl. Acad. Sci. U. S. A.* (2013). <https://doi.org/10.1073/pnas.1308887110>.

- [74] K. Cui, C.L. Ardell, N.P. Podolnikova, V.P. Yakubenko, Distinct migratory properties of M1, M2, and resident macrophages are regulated by  $\alpha\beta 2$  and  $\alpha\beta 2$  integrin-mediated adhesion, *Front. Immunol.* (2018). <https://doi.org/10.3389/fimmu.2018.02650>.
- [75] J. Wosik, W. Chen, K. Qin, R.M. Ghobrial, J.Z. Kubiak, M. Kloc, Magnetic Field Changes Macrophage Phenotype, *Biophys. J.* (2018). <https://doi.org/10.1016/j.bpj.2018.03.002>.
- [76] T. Tylek, C. Blum, A. Hrynevich, K. Schlegelmilch, T. Schilling, P.D. Dalton, J. Groll, Precisely defined fiber scaffolds with 40  $\mu\text{m}$  porosity induce elongation driven M2-like polarization of human macrophages, *Biofabrication.* (2020). <https://doi.org/10.1088/1758-5090/ab5f4e>.
- [77] H. Xiao, Y. Guo, B. Li, X. Li, Y. Wang, S. Han, D. Cheng, X. Shuai, M2-Like Tumor-Associated Macrophage-Targeted Codelivery of STAT6 Inhibitor and IKK $\beta$  siRNA Induces M2-to-M1 Repolarization for Cancer Immunotherapy with Low Immune Side Effects, *ACS Cent. Sci.* (2020). <https://doi.org/10.1021/acscentsci.9b01235>.
- [78] W. Chen, Y. Zhao, X.C. Li, J.Z. Kubiak, R.M. Ghobrial, M. Kloc, Rho-specific Guanine nucleotide exchange factors (Rho-GEFs) inhibition affects macrophage phenotype and disrupts Golgi complex, *Int. J. Biochem. Cell Biol.* (2017). <https://doi.org/10.1016/j.biocel.2017.10.009>.
- [79] S. Gao, Y. Wang, D. Li, Y. Guo, M. Zhu, S. Xu, J. Mao, G. Fan, TanshinoneIIA Alleviates Inflammatory Response and Directs Macrophage Polarization in Lipopolysaccharide-Stimulated RAW264.7 Cells, *Inflammation.* (2019). <https://doi.org/10.1007/s10753-018-0891-7>.
- [80] Y. Zhu, H. Liang, X. Liu, J. Wu, C. Yang, T.M. Wong, K.Y.H. Kwan, K.M.C. Cheung, S. Wu, K.W.K. Yeung, Regulation of macrophage polarization through surface topography design to facilitate implant-to-bone osteointegration, *Sci. Adv.* 7 (2021) eabf6654. <https://doi.org/10.1126/sciadv.abf6654>.
- [81] H.H. Lee, S.C. Tien, T.S. Jou, Y.C. Chang, J.G. Jhong, Z.F. Chang, Src-dependent phosphorylation of ROCK participates in regulation of focal adhesion dynamics, *J. Cell Sci.* 123 (2010) 3368–3377. <https://doi.org/10.1242/jcs.071555>.
- [82] Y. Yang, Y. Lin, Z. Zhang, R. Xu, X. Yu, F. Deng, Micro/nano-net guides M2-pattern macrophage cytoskeleton distribution via Src-ROCK signalling for enhanced angiogenesis, *Biomater. Sci.* (2021). <https://doi.org/10.1039/d1bm00116g>.
- [83] P. Haftbaradaran Esfahani, R. Knöll, Cell shape: effects on gene expression and signaling, *Biophys. Rev.* 12 (2020) 895–901. <https://doi.org/10.1007/s12551-020-00722-4>.
- [84] F.Y. McWhorter, C.T. Davis, W.F. Liu, Physical and mechanical regulation of macrophage phenotype and function, *Cell. Mol. Life Sci.* (2015). <https://doi.org/10.1007/s00018-014-1796-8>.
- [85] F.O. Martinez, S. Gordon, The M1 and M2 paradigm of macrophage activation: Time for reassessment, *F1000Prime Rep.* (2014). <https://doi.org/10.12703/P6-13>.
- [86] J. Xue, S. V. Schmidt, J. Sander, A. Draffehn, W. Krebs, I. Quester, D. DeNardo, T.D. Gohel, M. Emde, L. Schmidleithner, H. Ganesan, A. Nino-Castro, M.R. Mallmann, L. Labzin, H. Theis, M. Kraut, M. Beyer, E. Latz, T.C. Freeman, T. Ulas, J.L. Schultze, Transcriptome-Based Network Analysis Reveals a Spectrum Model of Human Macrophage Activation, *Immunity.* (2014). <https://doi.org/10.1016/j.immuni.2014.01.006>.



- [87] M. Nahrendorf, F.K. Swirski, Abandoning M1/M2 for a network model of macrophage function, *Circ. Res.* (2016). <https://doi.org/10.1161/CIRCRESAHA.116.309194>.
- [88] F. Loi, L.A. Córdova, R. Zhang, J. Pajarinen, T.H. Lin, S.B. Goodman, Z. Yao, The effects of immunomodulation by macrophage subsets on osteogenesis in vitro, *Stem Cell Res. Ther.* 7 (2016) 15. <https://doi.org/10.1186/s13287-016-0276-5>.
- [89] Y. Zhang, T. Böse, R.E. Unger, J.A. Jansen, C.J. Kirkpatrick, J.J.J.P. van den Beucken, Macrophage type modulates osteogenic differentiation of adipose tissue MSCs, *Cell Tissue Res.* (2017). <https://doi.org/10.1007/s00441-017-2598-8>.
- [90] K. Nathan, L.Y. Lu, T. Lin, J. Pajarinen, E. Jämsen, J.F. Huang, M. Romero-Lopez, M. Maruyama, Y. Kohno, Z. Yao, S.B. Goodman, Precise immunomodulation of the M1 to M2 macrophage transition enhances mesenchymal stem cell osteogenesis and differs by sex, *Bone Jt. Res.* (2019). <https://doi.org/10.1302/2046-3758.810.BJR-2018-0231.R2>.
- [91] K.L. Spiller, S. Nassiri, C.E. Witherell, R.R. Anfang, J. Ng, K.R. Nakazawa, T. Yu, G. Vunjak-Novakovic, Sequential delivery of immunomodulatory cytokines to facilitate the M1-to-M2 transition of macrophages and enhance vascularization of bone scaffolds, *Biomaterials.* 37 (2015) 194–207. <https://doi.org/10.1016/j.biomaterials.2014.10.017>.
- [92] R. Duan, Y. Zhang, L. van Dijk, D. Barbieri, J. van den Beucken, H. Yuan, J. de Bruijn, Coupling between macrophage phenotype, angiogenesis and bone formation by calcium phosphates, *Mater. Sci. Eng. C.* 122 (2021) 111948. <https://doi.org/10.1016/j.msec.2021.111948>.
- [93] A. Yuan, Y.J. Hsiao, H.Y. Chen, H.W. Chen, C.C. Ho, Y.Y. Chen, Y.C. Liu, T.H. Hong, S.L. Yu, J.J.W. Chen, P.C. Yang, Opposite Effects of M1 and M2 Macrophage Subtypes on Lung Cancer Progression, *Sci. Rep.* 5 (2015). <https://doi.org/10.1038/srep14273>.
- [94] C. Jaquiéry, S. Schaeren, J. Farhadi, P. Mainil-Varlet, C. Kunz, H.F. Zeilhofer, M. Heberer, I. Martin, Friess, Thorlacius, In vitro osteogenic differentiation and in vivo bone-forming capacity of human isogenic jaw periosteal cells and bone marrow stromal cells, in: *Ann. Surg.*, Lippincott, Williams, and Wilkins, 2005: pp. 859–868. <https://doi.org/10.1097/01.sla.0000189572.02554.2c>.
- [95] C. Du Cheyne, H. Tay, W. De Spiegelaere, The complex TIE between macrophages and angiogenesis, in: *J. Vet. Med. Ser. C Anat. Histol. Embryol.*, 2020. <https://doi.org/10.1111/ahe.12518>.
- [96] C. Baer, M.L. Squadrito, M.L. Iruela-Arispe, M. De Palma, Reciprocal interactions between endothelial cells and macrophages in angiogenic vascular niches, *Exp. Cell Res.* (2013). <https://doi.org/10.1016/j.yexcr.2013.03.026>.
- [97] W.C. Xu, X. Dong, J.L. Ding, J.C. Liu, J.J. Xu, Y.H. Tang, Y.P. Yi, C. Lu, W. Yang, J.S. Yang, Y. Gong, J.L. Zhou, Nanotubular TiO<sub>2</sub> regulates macrophage M2 polarization and increases macrophage secretion of vegf to accelerate endothelialization via the ERK1/2 and PI3K/AKT pathways, *Int. J. Nanomedicine.* 14 (2019) 441–455. <https://doi.org/10.2147/IJN.S188439>.
- [98] N. Jetten, S. Verbruggen, M.J. Gijbels, M.J. Post, M.P.J. De Winther, M.M.P.C. Donners, Anti-inflammatory M2, but not pro-inflammatory M1 macrophages promote angiogenesis in vivo, *Angiogenesis.* (2014). <https://doi.org/10.1007/s10456-013-9381-6>.

- [99] J. Wang, S. Qian, X. Liu, L. Xu, X. Miao, Z. Xu, L. Cao, H. Wang, X. Jiang, M2 macrophages contribute to osteogenesis and angiogenesis on nanotubular TiO<sub>2</sub> surfaces, *J. Mater. Chem. B*. 5 (2017) 3364–3376. <https://doi.org/10.1039/c6tb03364d>.
- [100] M. Sun, S. Qiu, Q. Xiao, T. Wang, X. Tian, C. Chen, X. Wang, J. Han, H. Zheng, Y. Shou, K. Chen, Synergistic effects of multiple myeloma cells and tumor-associated macrophages on vascular endothelial cells in vitro, *Med. Oncol.* 37 (2020) 99. <https://doi.org/10.1007/s12032-020-01426-1>.
- [101] S.E.J. Chambers, C.L. O'Neill, J. Guduric-Fuchs, K.J. McLoughlin, A. Liew, A.M. Egan, T. O'Brien, A.W. Stitt, R.J. Medina, The Vasoreparative Function of Myeloid Angiogenic Cells Is Impaired in Diabetes Through the Induction of IL1 $\beta$ , *Stem Cells*. (2018). <https://doi.org/10.1002/stem.2810>.
- [102] D. Xiao, J. Zhang, C. Zhang, D. Barbieri, H. Yuan, L. Moroni, G. Feng, The role of calcium phosphate surface structure in osteogenesis and the mechanisms involved, *Acta Biomater.* 106 (2020) 22–33. <https://doi.org/10.1016/j.actbio.2019.12.034>.
- [103] E.A. Dos Santos, M. Farina, G.A. Soares, K. Anselme, Surface energy of hydroxyapatite and  $\beta$ -tricalcium phosphate ceramics driving serum protein adsorption and osteoblast adhesion, *J. Mater. Sci. Mater. Med.* 19 (2008) 2307–2316. <https://doi.org/10.1007/s10856-007-3347-4>.
- [104] J.M. Sadowska, J. Guillem-Marti, M. Espanol, C. Stähli, N. Döbelin, M.P. Ginebra, In vitro response of mesenchymal stem cells to biomimetic hydroxyapatite substrates: A new strategy to assess the effect of ion exchange, *Acta Biomater.* 76 (2018) 319–332. <https://doi.org/10.1016/j.actbio.2018.06.025>.
- [105] E.A. Dos Santos, M. Farina, G.A. Soares, K. Anselme, Chemical and topographical influence of hydroxyapatite and  $\beta$ -tricalcium phosphate surfaces on human osteoblastic cell behavior, *J. Biomed. Mater. Res.—Part A*. 89 (2009) 510–520. <https://doi.org/10.1002/jbm.a.31991>.
- [106] K.M. Hotchkiss, G.B. Reddy, S.L. Hyzy, Z. Schwartz, B.D. Boyan, R. Olivares-Navarrete, Titanium surface characteristics, including topography and wettability, alter macrophage activation, *Acta Biomater.* 31 (2016) 425–434. <https://doi.org/10.1016/j.actbio.2015.12.003>.
- [107] J.A. Anderson, S. Lamichhane, G. Mani, Macrophage responses to 316L stainless steel and cobalt chromium alloys with different surface topographies, *J. Biomed. Mater. Res.—Part A*. 104 (2016) 2658–2672. <https://doi.org/10.1002/jbm.a.35808>.
- [108] S. Lamichhane, J.A. Anderson, T. Vierhout, T. Remund, H. Sun, P. Kelly, Polytetrafluoroethylene topographies determine the adhesion, activation, and foreign body giant cell formation of macrophages, *J. Biomed. Mater. Res.—Part A*. 105 (2017) 2441–2450. <https://doi.org/10.1002/jbm.a.36099>.
- [109] E. Engel, S. Del Valle, C. Aparicio, G. Altankov, L. Asin, J.A. Planell, M.P. Ginebra, Discerning the role of topography and ion exchange in cell response of bioactive tissue engineering scaffolds, *Tissue Eng.—Part A*. 14 (2008) 1341–1351. <https://doi.org/10.1089/ten.tea.2007.0287>.
- [110] N.L. Davison, J. Su, H. Yuan, J.J.J.P. van den Beucken, J.D. de Bruijn, F.B. de Groot, Influence of surface microstructure and chemistry on osteoinduction and osteoclastogenesis by biphasic calcium phosphate discs, *Eur. Cells Mater.* 29 (2015) 314–329. <https://doi.org/10.22203/eCM.v029a24>.



## APPENDIX A

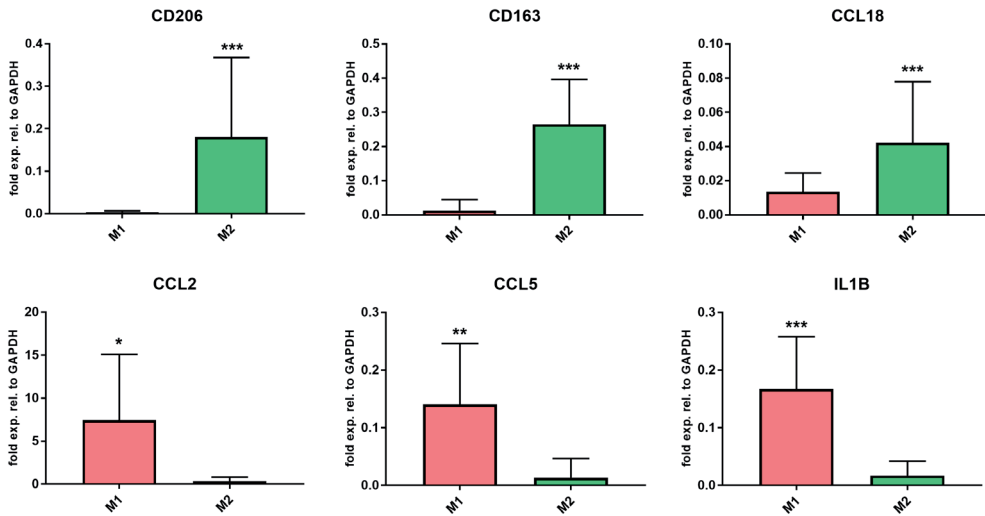


**Figure A.1. Gene expression profiles of *in vitro* induced M1 and M2 macrophages.** M1 and M2 macrophage phenotypes were induced by culturing in basic culture medium supplemented with 10 ng/ml MSCF and for M1: 100 ng/ml interferon-gamma + 100 ng/ml tumor necrosis factor alpha; and for M2: 20 ng/ml interleukin 4. Data show quantification of gene expression of M2 markers CD206, CD163 and CCL18, and M1 markers CCL2, CCL5, IL1 $\beta$  relative to GAPDH expression. Data represent mean + SD of a total of 3 separate donors.



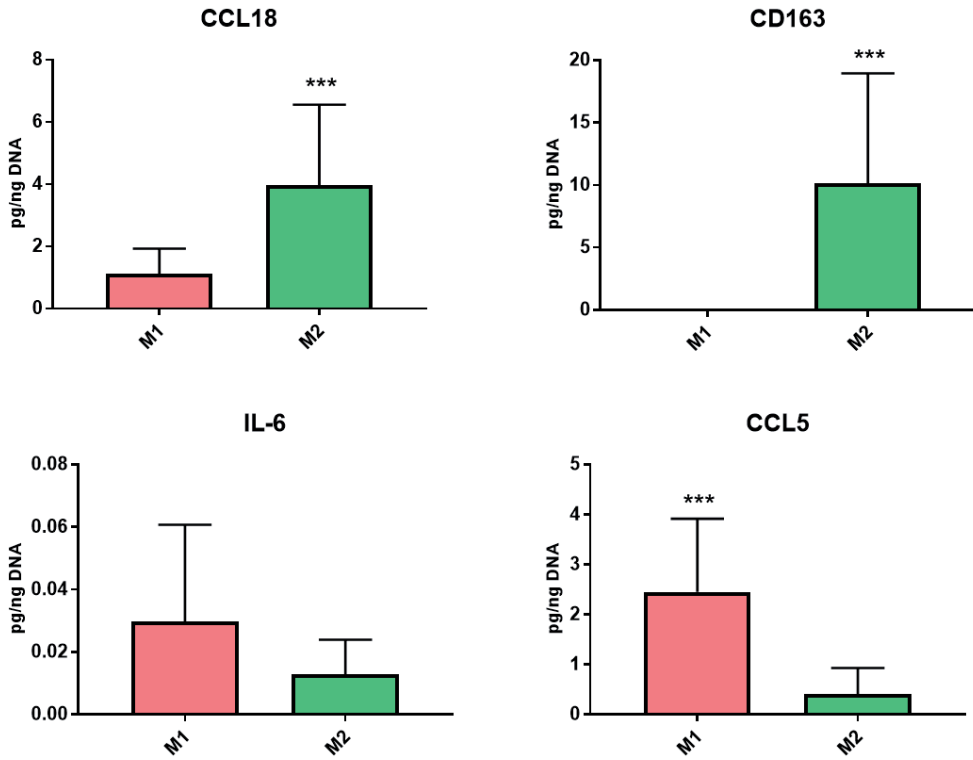
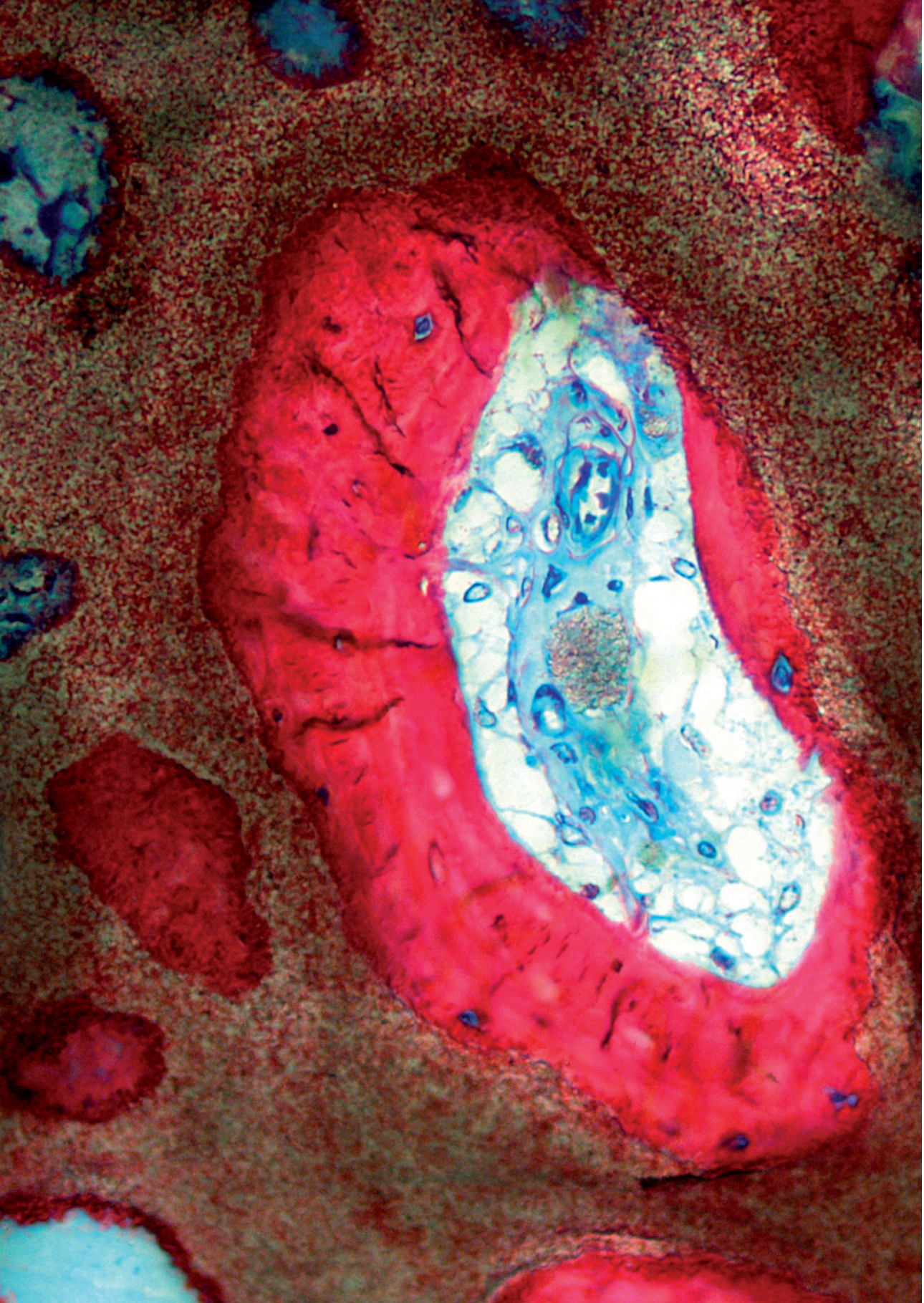


**Figure A.2. Protein marker profiles of *in vitro* induced M1 and M2 macrophages.** M1 and M2 macrophage phenotypes were induced by culturing in basic culture medium supplemented with 10 ng/ml MSCF and for M1: 100 ng/ml interferon-gamma + 100 ng tumor necrosis factor alpha; and for M2: 20 ng/ml interleukin 4. M2 markers CCL18 and CD163, and M1 markers IL-6 and CCL5 were measured in the supernatants after 72h. Protein content was normalized to DNA content for each sample. Data represent mean + SD of a total of 4 separate donors.





# CHAPTER 8

## **FROM BENCHTOP TO CLINIC: A TRANSLATIONAL ANALYSIS OF THE IMMUNE RESPONSE TO SUBMICRON TOPOGRAPHY AND ITS RELEVANCE TO BONE HEALING**

---

Lukas A. van Dijk  
Florence Barrère-de Groot  
Huipin Yuan  
Charlie Champion  
Alpesh Patel  
Kees Poelstra  
Joost D. de Bruijn

*European cells & materials, 2021, 41:756-773*

# A B S T R A C T



The innate immune response to bone graft materials following implantation is pivotal for successful bone healing. Both pro-inflammatory 'M1' and anti-inflammatory 'M2' macrophages have an important role in regulating the healing response to biomaterials. Recently, calcium phosphate bone grafts with submicron needle-shaped surface features have been shown to trigger a 'pro-healing' response through upregulation of M2 polarized macrophages both in vitro and in vivo. This review describes recent research on these materials all the way from benchtop to the clinic, including in vitro and in vivo fundamental studies, evaluation in clinically relevant spinal fusion models, as well as clinical validation in a case series of 77 patients of posterolateral and/or interbody fusion in the lumbar and cervical spine. This research demonstrates the feasibility of enhanced bone regeneration and spinal fusion success by evoking specific innate immune responses to bone grafts through submicron topographical features.

## INTRODUCTION

The annual number of spinal fusions in the US for the treatment of degenerative spine conditions has risen rapidly over the past two decades to more than 770,000[1]. Posterolateral fusion (PLF) is the most commonly used spinal fusion technique (64%), either performed as an individual procedure (19%) or in combination with interbody fusion (45%)[2]. Because of the requirement of large bone graft volumes (12–36 cc)[3], bone graft substitutes are commonly used to reduce or avoid morbidity related to the harvesting of autologous bone[4].

The response of macrophages to bone grafts is pivotal as they are key modulators in tissue healing responses[5,6]. Macrophages, which have a highly plastic nature, can adopt a pro-inflammatory phenotype ('classically activated' or 'M1' macrophage), an anti-inflammatory phenotype ('alternatively activated' or 'M2' macrophage), or exist in an intermediate state in the spectrum between these phenotypes[6,7]. The contribution of M2 macrophages to bone regeneration was clinically demonstrated recently, as M2 macrophage population increased during the first week of bone healing in clavicle fractures (Zhang 2018). Indeed, a correlation between accelerated bone healing and a greater M2 population was found in patients with clavicle fracture and concomitant traumatic brain injury (Zhang, 2018).

For implanted bone graft substitutes, macrophage response is critical because these cells are key regulators of the foreign body response [8]. The surface structure of an implanted biomaterial can impact the phenotype of macrophages [9–11]. An increase in pro-healing macrophages following an initial phase of pro-inflammatory macrophage dominance has been suggested to be important for promotion of bone repair [12,13]. Therefore, directing bone regeneration by promoting the most favorable innate immune response within the first days after bone graft implantation may be the key to successful bone healing. This review describes the current, state-of-the-art research demonstrating how submicron surface structures can direct M2 macrophage polarization and enhance bone regeneration in challenging, non-bony environments without the aid of biological agents or growth factors.

### **Empirical data from ectopic defects suggests that submicron needle-shaped features accelerate osteoinduction by a specific innate immune response**

Since the 1950s, when processed coral was first used as a bone graft, few synthetic materials have demonstrated evidence of osteoinduction when implanted ectopically without any addition of biological agents. However, some researchers have managed to achieve this biological outcome by tuning the physical properties, such as three-dimensional architecture, macropore configuration and surface structure[14–18]. This



incidence (8/8) and bone quantities ( $24.5 \pm 4.3\%$  vs.  $23.9 \pm 6.3$ ). However, the kinetics of bone formation were significantly different, as demonstrated by fluorochrome marker deposition. The Calcein fluorescence marker, indicating bone formed between 3 and 6 weeks, demonstrated a significantly higher incidence in the material with submicron needle-shaped topography ( $\text{BCP}_{<\mu\text{m}}$ ) compared to the material with a submicron grain-shaped topography ( $\text{TCP}_{<\mu\text{m}}$ ). Indeed, on  $\text{BCP}_{<\mu\text{m}}$ , new bone formed between 3 and 6 weeks was identified in 5/8 implants and in a total of 21 independent locations in histological sections. This early bone formation was significantly enhanced compared to  $\text{TCP}_{<\mu\text{m}}$ , where incidence of bone formed between 3 and 6 weeks was 2/8 and was observed in only two locations in histological sections. In other words, the submicron needle-shaped topography led to an accelerated bone formation in a non-bony environment (Figure 1) without the aid of exogenous biological growth factors.

The cellular response events preceding early bone formation are likely to be the key to this accelerated ectopic bone formation. Specifically, the innate immune response involving macrophage recruitment and polarization to pro-healing M2s, as well as macrophage fusion into multinucleated cells, has been shown to play a role in material-directed bone formation. This hypothesis is supported by Davison *et al.*, who demonstrated that the depletion of macrophages in the vicinity of calcium phosphate with submicron surface features directly inhibited ectopic bone formation in vivo [22].

### **An enhanced pro-healing response is observed on needle-shaped features in vitro**

Polarization of macrophages towards the pro-healing M2 phenotype on submicron needle-shaped topography versus conventional surfaces has been demonstrated with human macrophages in vitro using state-of-the-art research methods, i.e. protein quantification by ELISA, gene expression analysis by RT-QPCR, and cell morphology evaluation by SEM. The pro-healing response was qualified and quantified by cytokines specific to either pro-inflammatory M1 macrophages (CCL5, TNF- $\alpha$ , IL-1 $\beta$ , CCL2) or pro-healing M2 macrophages (CCL 18, TGF- $\beta$ 1, CD206, CD163) [23–26]. The morphology of cells cultured on these surfaces was also analyzed at the micron level and compared to typical M1 and M2 macrophage morphology [27–30].

#### ***M2 macrophage polarization on needle-shaped features compared to materials with conventional surfaces***

Human macrophages derived from the monocytic cell line THP-1 were cultured for 4 days in vitro on BCP with submicron needle-shaped topography ( $\text{BCP}_{<\mu\text{m}}$ ), conventional Tricalcium Phosphate ( $\text{TCP}_{\mu\text{m}}$ ) and  $\text{BG}_{\mu\text{m}}$ . The quantification of M2 and M1 cytokines expressed by these cells was analyzed by ELISA and macrophage morphology was analyzed by SEM. M2 macrophage markers TGF- $\beta$  and CCL18 were expressed to a greater extent on  $\text{BCP}_{<\mu\text{m}}$

than on TCP<sub>μm</sub>, while M1 macrophage markers TNF-α and IL-1β were expressed to a greater extent on TCP<sub>μm</sub> than on BCP<sub><μm</sub> (Figure 2). No cytokine signals could be detected in the BG<sub>μm</sub> group, which was in agreement with SEM observations where macrophages were not found attached to the BG<sub>μm</sub> surfaces. This in vitro experiment demonstrated that the submicron topography of BCP<sub><μm</sub> supported an M2-dominant macrophage population after 4 days of culture.

The morphological appearance of the macrophages on the needle-shaped surface texture was prominently large (>20<sub>μm</sub>) and appeared to have fused together, via several cell-cell connections, into a highly networked cell population on BCP<sub><μm</sub> (Figure 3). These large macrophages were only observed on the BCP<sub><μm</sub> material. This spreading and connecting cellular network is indicative of the M2 macrophage phenotype when derived from THP-1 monocytes [27,28]. In contrast, mononuclear cells of 5–10<sub>μm</sub> dispersed on the surface, with no evidence of fusion, were exclusively observed on the standard TCP<sub>μm</sub> material (Figure 3). The morphology of the macrophages and lack of spreading on TCP<sub>μm</sub> is both suggestive of the M1 macrophage phenotype [27,28]. Cells were totally absent on the surface of the BG<sub>μm</sub>. The upregulation of M2 cytokines and interconnected cellular network of macrophages in contact with BCP<sub><μm</sub> suggested a M2 macrophage polarization, in contrast with the other graft materials, confirming a favorable pro-healing response occurred on the submicron needle-shaped topography.

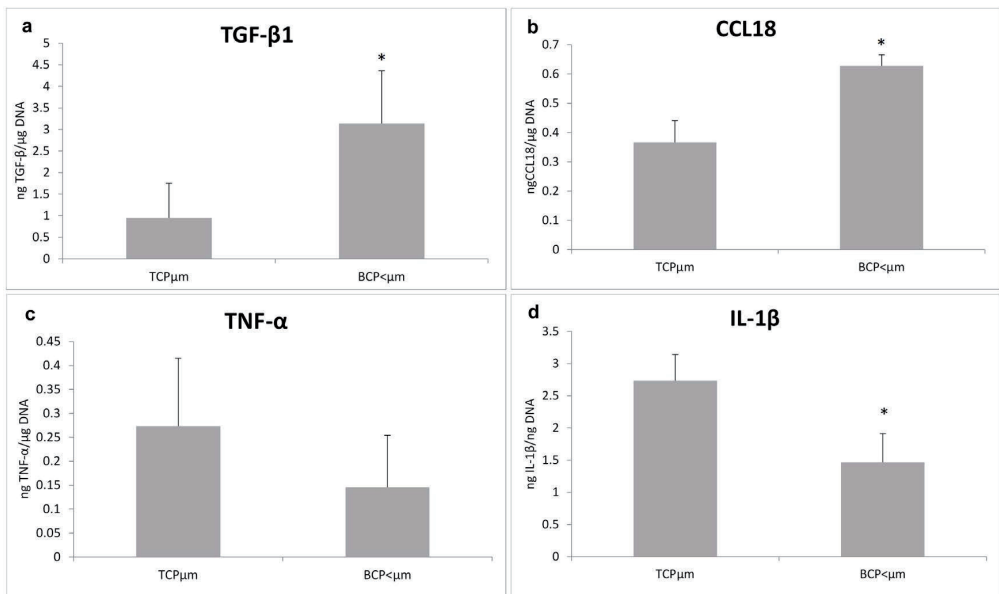


**Figure 2:** ELISA expression of pro-healing M2-markers TGF-β (a) and CCL18 (b) and pro-inflammatory M1-markers TNF-α (c) and IL-1β (d) by human macrophages derived from THP-1 monocytes on needle-shaped surface (BCP<sub><μm</sub>) compared to TCP<sub>μm</sub> at day 4 (n=4, \*: p<0.05).



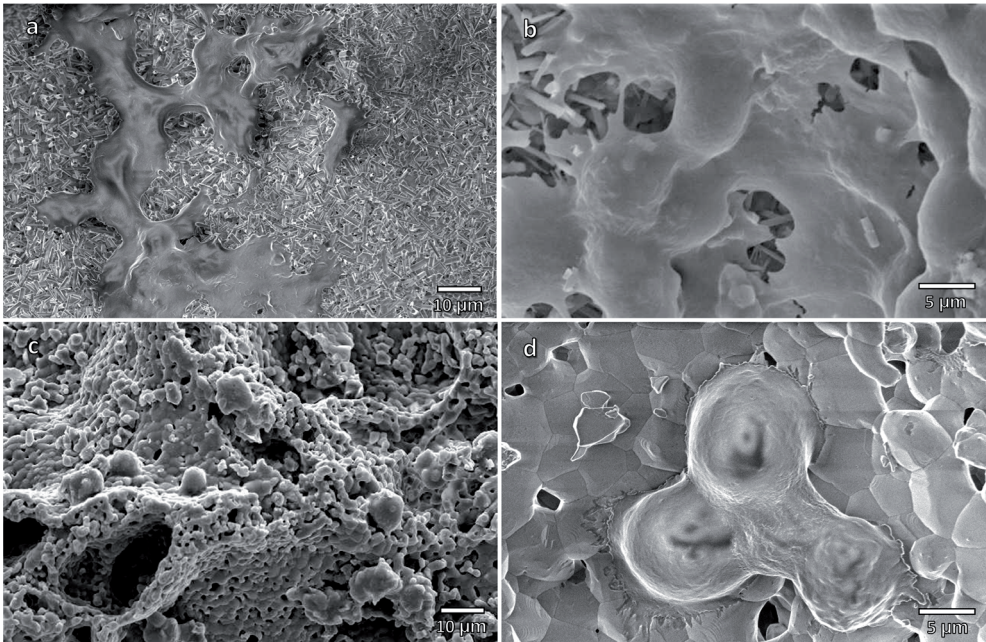


**Figure 3:** SEM of human macrophage derived from THP-1 monocytes at day 4 on needle-shaped surface BCP<sub><math>\le 1\mu\text{m}</math></sub> at low (a) and high magnification (b) and on TCP<sub><math>1\mu\text{m}</math></sub> at low (c) and high magnification (d). No macrophages could be found on bioactive glass in BG<sub><math>1\mu\text{m}</math></sub> (images not shown).

### ***M2 polarization on needle-shaped features: from gene level to cell shape***

Representing a more accurate test of the innate immune system's response, primary human macrophages obtained from three different donors were used to further assess the response to the submicron needle-shaped surface. M0 macrophages derived from primary CD14<sup>+</sup> monocytes isolated from buffy coats were cultured for 4 days. The expression of M1 and M2 markers was compared on BCP<sub><math>\le 1\mu\text{m}</math></sub> discs versus tissue culture plastic (control). Quantification of respective markers was conducted at the protein level by ELISA and at the gene level by RT-QPCR. The resulting cell morphology was analyzed by SEM.

This experiment confirmed our previous findings. On BCP<sub><math>\le 1\mu\text{m}</math></sub>, macrophages secreted high levels of the M2 marker CCL18, while the M1 marker CCL5 could not be detected (Figure 4). At the gene level, the same polarization trend was observed (Figure 5). The M2 gene markers CCL18, CD 206, and CD163 showed a higher expression on BCP<sub><math>\le 1\mu\text{m}</math></sub> compared to the flat surface control. The M2 gene upregulation on BCP<sub><math>\le 1\mu\text{m}</math></sub> was significant for each of the three genes (>1.3) compared to macrophages cultured on flat surfaces, with a maximum upregulation of 27.5 for CD206, followed by 3.9 and 2.3 for CD163 and CCL18, respectively. The M1 gene markers CCL5, CCL2, and IL-1 $\beta$  showed a slightly higher expression on BCP<sub><math>\le 1\mu\text{m}</math></sub> compared to the flat surface control (Figure 5). Nonetheless, downregulation was observed



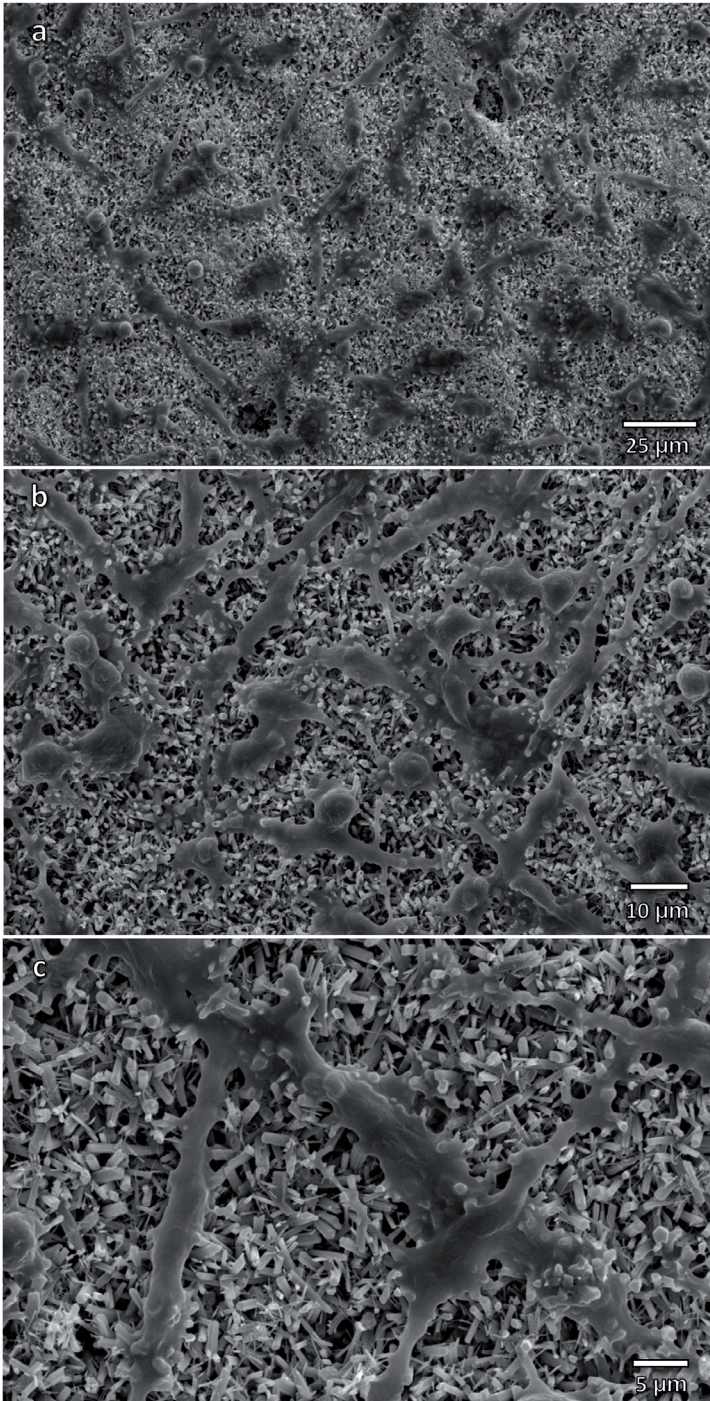


**Figure 6:** SEM images of human primary human macrophages cultured on BCP<sub>50</sub> for 4 days at magnification (a) x500, (b) x1000, (c) x2000.

A limited subset of rounder granular cells of 5–10  $\mu\text{m}$  diameter could also be observed. The elongated morphology and connected cellular network confirmed the M2 macrophage phenotype, as opposed to M1 polarized macrophages, which are less prone to elongation and spreading with high granulation when derived from CD14+ monocytes[29,30]. Based on the quantitative analysis of protein markers, gene expression and SEM observations of cell morphologies, the macrophages present on BCP<sub><math>\mu\text{m}</math></sub> are therefore mostly associated with the M2 macrophage phenotype, again confirming a pro-healing response of macrophages cultured on the submicron needle-shaped surface structure.

### **A pro-healing immune response precedes osteoinduction in vivo**

The M2 polarization on calcium phosphate with submicron needle-shaped topography reported in vitro was also demonstrated in vivo, directly after implantation and preceding ectopic bone formation. Using the same intramuscular implantation model as described above, a kinetic study was conducted on BCP<sub><math>\mu\text{m}</math></sub> compared to conventional TCP<sub><math>\mu\text{m}</math></sub> to elucidate the mechanism and consequence of a pro-healing innate immune reaction submicron surface topography. At 3 days and 1, 3, 6, and 12 weeks after implantation, quantification of immune markers by ELISA (IL10 for the M2 phenotype, TNF- $\alpha$  for the M1 phenotype) and bone markers by biochemical assays (ALP for osteoblasts, TRAP for osteoclasts) was performed after extraction from ex-vivo implants. Histological observations were conducted for all time points using staining to assess bone formation (methylene blue/basic fuchsin), osteoblastic activity by ALP and osteoclastic activity by TRAP and CTSK.

By histology, ectopic bone formation was observed in BCP<sub><math>\mu\text{m}</math></sub> implants from 6 weeks onwards, with increasing amounts of bone up to week 12 (Figure 7). Osteoid was formed in three out of four BCP<sub><math>\mu\text{m}</math></sub> samples at week 6 (< 1% by volume), while mineralized bone was observed in four out of four BCP<sub><math>\mu\text{m}</math></sub> implants at week 12 ( $9.4 \pm 3.7\%$ ). In contrast, mere fibrous tissue formation was observed in the negative control (TCP<sub><math>\mu\text{m}</math></sub>) by histology. These findings confirmed the ability of BCP<sub><math>\mu\text{m}</math></sub> to induce ectopic bone formation.

By histology of bone-related markers, osteoclastic activity was observed from 3 weeks onwards: TRAP-positive multinucleated cells with large cell bodies were detected on the surface of BCP<sub><math>\mu\text{m}</math></sub> at the edge of the implants, and in the entire implant in all samples after 6 weeks. Such cells were also CTSK-positive, supporting the osteoclastic nature of the of these multinucleated cells (Figure 7). Moreover, A strong ALP signal was noted near the newly formed bone in BCP<sub><math>\mu\text{m}</math></sub> at week 6 and week 12.

As for the analysis of immune markers, both M1 and M2 macrophage markers were detected from day 3 onwards in both implants (Figure 8). The pro-healing activity monitored by the M2 marker IL10 showed a consistent increase up to 6 weeks, followed by a slight decrease thereafter. At nearly every time point, IL10 expression was significantly higher





osteoclasts before bone formation occurs. This study also confirmed a pro-inflammatory response immediately after implantation, as shown by the M1 marker TNF- $\alpha$  expression. However, it should be noted that TNF- $\alpha$  expression is also a marker for osteoclasts that are derived from monocytes [23,31,32]. Together with the evident osteoclastic activity on BCP<sub><math>\lt; \mu\text{m}</math></sub> demonstrated by CTSK and TRAP, this elevated TNF- $\alpha$  level may comprise the cumulative expression from both osteoclasts and M1 pro-inflammatory macrophages.

## A pro-healing response leads to reliable spine fusion

### *Spinal fusion equivalent to “gold standard” and superior to conventional graft materials*

The relevance of osteoinductive materials has been repeatedly demonstrated in several challenging preclinical implantation models (van Dijk *et al.* 2018, 2019; van Dijk *et al.* 2020). In the more clinically relevant posterolateral fusion (PLF) indication, the performance of BCP<sub><math>\lt; \mu\text{m}</math></sub> with submicron needle-shaped features was found equivalent to the gold standard autograft as a graft extender in a validated rabbit PLF model [33,36] and as a standalone graft in a sheep PLF model [34]. In sheep, BCP<sub><math>\lt; \mu\text{m}</math></sub> implanted as standalone for 6, 12, and 26 weeks demonstrated rapid and reliable fusion. Only 6 weeks after implantation, new bone was formed in the center of the fusion mass (distant from the host bone) and not solely in the vicinity of host bone. Histology demonstrated bone bridging and 92% to 100% fusion at 12 and 26 weeks, respectively. Fusion masses showed evidence of a pseudo-cortex, bone maturation, and graft integration (Figure 9). Additional assessment methods used to score fusion, that is, manual palpation, mechanical testing, and radiographical examination following the Lenke scale were in agreement with histology, and results were equivalent to the autograft used as a positive control in this study [34,37].

The enhanced fusion performance by BCP<sub><math>\lt; \mu\text{m}</math></sub> was confirmed when compared to conventional bone graft materials, i.e. a BG <sub>material and a TCP <sub>with BG <sub>adjunct (TCP<sub>/BG<sub>), as well as the “gold standard” autograft in the same sheep PLF model (van Dijk *et al.* 2020). By micro-CT, only BCP<sub><math>\lt; \mu\text{m}</math></sub> and autograft maintained an appropriate bilateral fusion mass volume of respectively  $9.6 \pm 0.4 \text{ cm}^3$  and  $5.7 \pm 1.6 \text{ cm}^3$ . Significantly lower fusion</sub></sub></sub></sub></sub>

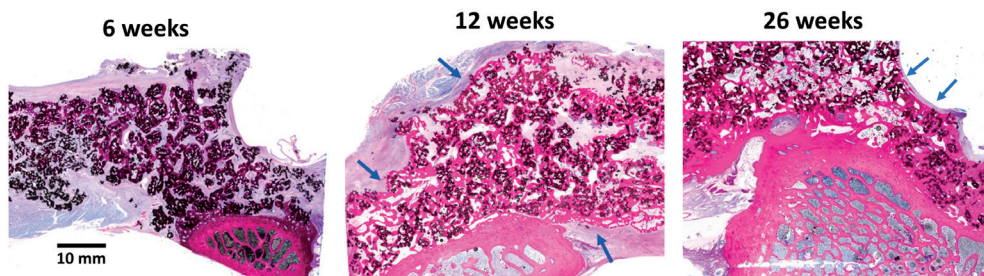


**Figure 9:** Bone formation and neocortex formation (blue arrow) in the fusion mass treated by BCP<sub><math>\lt; \mu\text{m}</math></sub> after 6, 12 and 26 weeks implantation. Adapted from van Dijk *et al.* (2018, 2020).

mass volumes were observed for TCP<sub>μm</sub>/BG<sub>μm</sub> ( $3.0 \pm 1.1 \text{ cm}^3$ ) and TCP<sub>μm</sub> ( $2.4 \pm 1.0 \text{ cm}^3$ ) (Figure 10). Correspondingly, histology revealed abundant bone tissue in direct contact with BCP<sub><μm</sub> throughout the inter-transverse space. A large area of BCP<sub><μm</sub> graft was integrated into newly formed trabecular bone with lamellar morphology and bone marrow spaces (Figure 11, A-C). Osteoblasts lining regions, osteoclasts, and osteocytes were observed throughout the specimens (Figure 11, C). Multinucleated cells were observed resorbing the material on the surface that was not covered by bone (Figure 11, C). Histology on the TCP<sub>μm</sub>/BG<sub>μm</sub> and BG<sub>μm</sub> groups confirmed the absence of bone tissue and significant graft resorption through the implant site. Bone formation was very minimal and limited at the vicinity of host bone (Figure 11, D, G). Throughout the implant site, residual BG<sub>μm</sub> particles were mostly encapsulated in fibrous tissue or granulomatous inflammatory tissue with the presence of lymphocytes and foreign body giant cells in five of six specimens (Figure 11, E, F). Moreover, three of six TCP<sub>μm</sub>/BG<sub>μm</sub> specimens contained dense regions of particles of variable dimensions, which were revealed to be areas of severely fragmented material and evidence of foreign body reaction upon further inspection (Figure 11, F). In the TCP<sub>μm</sub>/BG<sub>μm</sub> implantation sites, TCP<sub>μm</sub> particles were commonly observed in the process of disintegration due to cell-mediated resorption (Figure 11, H). The cellular and tissue reaction on the three different bone grafts showed significant differences, emphasizing the relevance of needle-shaped surface features of BCP<sub><μm</sub>.

The different immune responses for these three graft materials in vivo was evident and led to significantly different fusion performance. On the one hand, the abundant fibrous encapsulation, granulomatous inflammation, and graft resorption observed on the TCP<sub>μm</sub>/BG<sub>μm</sub> and BG<sub>μm</sub> groups is characteristic of pro-inflammatory reaction, which in turn resulted in poor bone formation and did not achieve fusion. On the other hand, material remodeling by multinucleated cells combined with new bone formation in direct contact with the BCP<sub><μm</sub> material suggests a pro-healing reaction resulting in early bone formation throughout the inter-transverse space favorable for fusion. The late endpoints and lack of other histological immunostaining prevent any further insight on the nature of innate immunological reaction in vivo. However, these striking differences in foreign body reaction and bone healing, combined with the above in vitro results on the same materials, suggest a unique pro-healing mechanism orchestrated by the needle-shaped topographical features.

### ***Clinically reliable spine fusion***

The performance of submicron needle-shaped feature bone grafts has been validated clinically in a retrospective cohort study of 77 lumbar and cervical reconstruction patients receiving interbody and posterolateral spinal fusions (Level IV). The bone graft BCP<sub><μm</sub> was mixed with acellular allograft and BMA for the lumbar region, and with local autograft for the cervical region. Radiographic evaluations and clinical outcomes for fusion were assessed at multiple intervals after surgery.



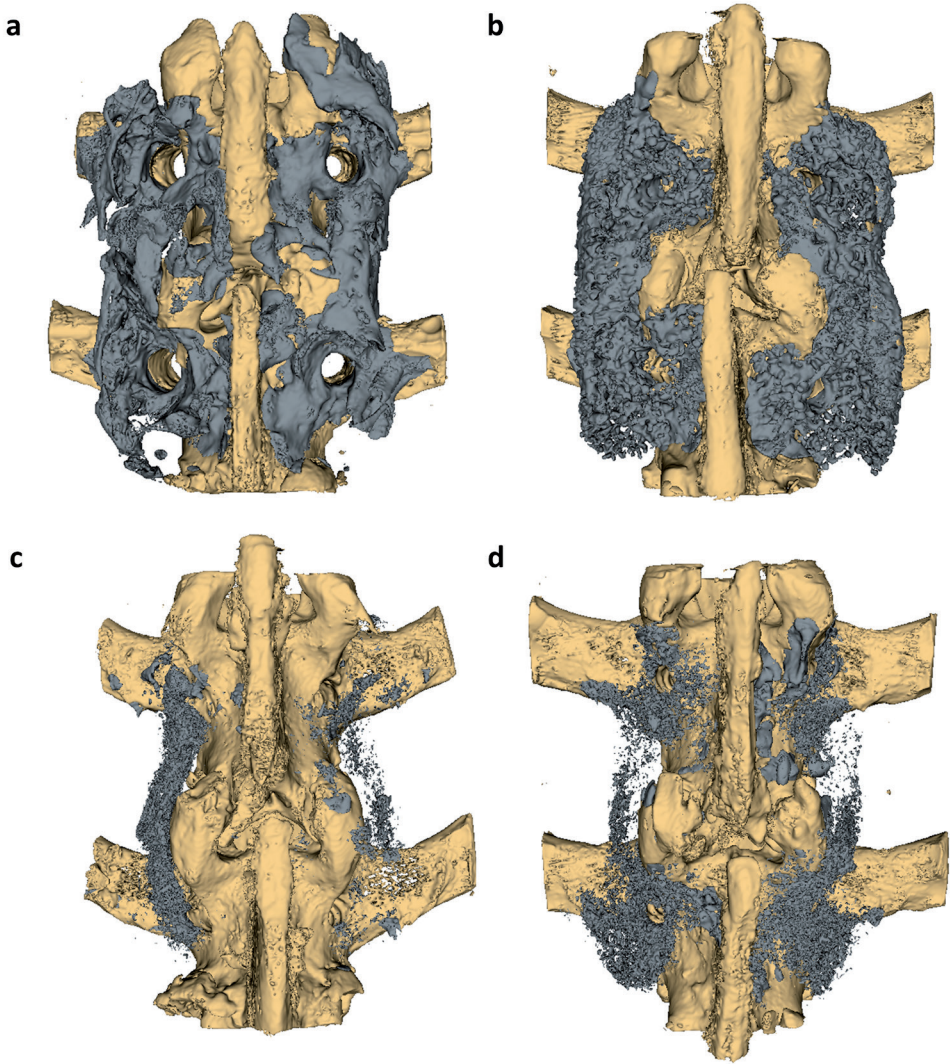


**Figure 10:** Representative examples of 3-dimensional micro-CT reconstructions of spinal levels treated with (a) Autograft, (b)  $\text{BCP}_{\mu\text{m}}$ , (c)  $\text{BG}_{\mu\text{m}}$  and (d)  $\text{BG/TCP}_{\mu\text{m}}$ . The host spinal bone (off-white) and fusion mass (grey) including (new) bone and residual implant material are shown as separate segmentations. Adapted from *van Dijk et al. (2020)*

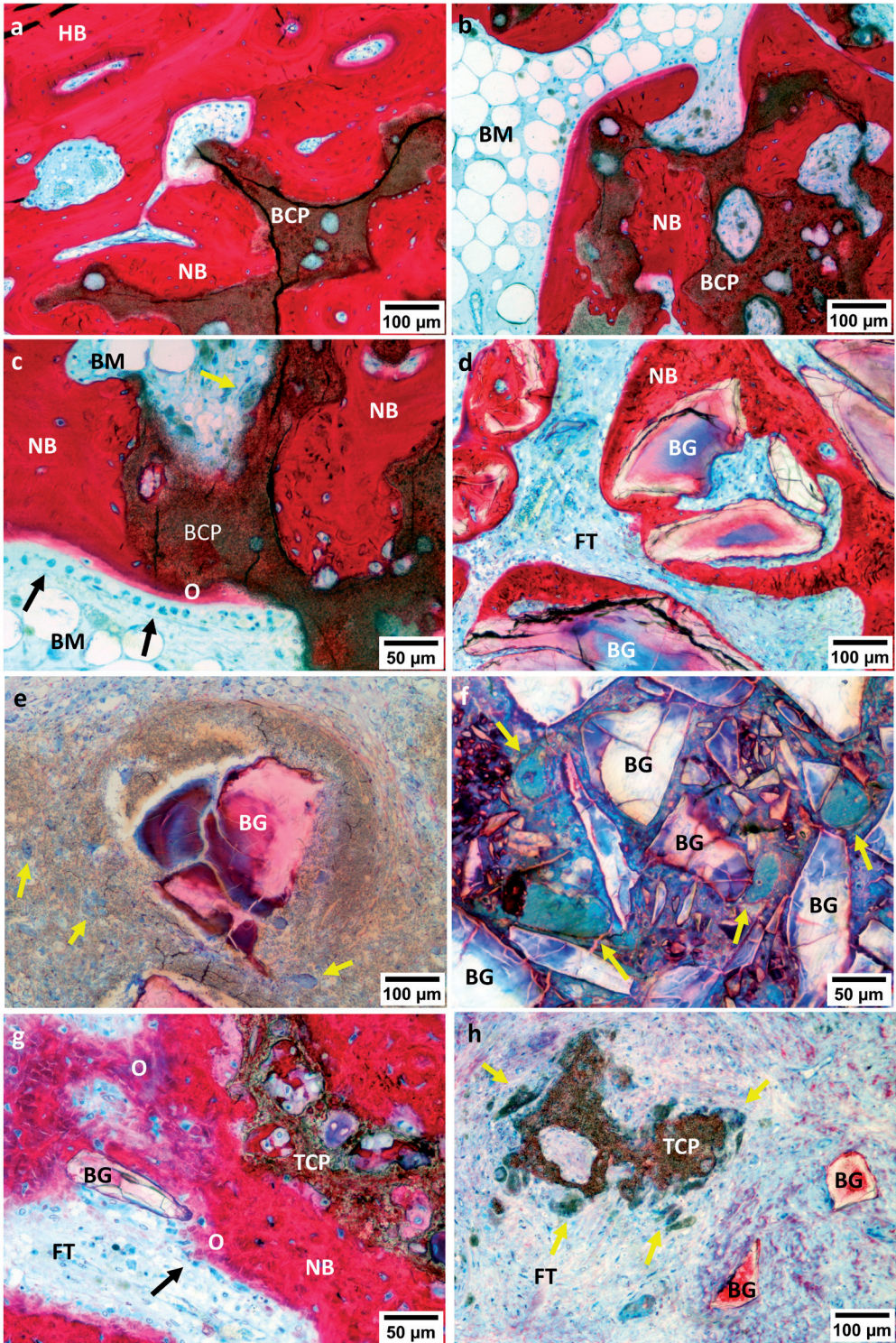
The lumbar group consisted of 24 females and 28 males. This cohort included posterior, lateral, or anterior lumbar interbody fusions with or without posterior instrumented fusions. The bone graft  $\text{BCP}_{\mu\text{m}}$  was mixed with acellular allograft and BMA. The procedures included 22 one-level (42.3%), 19 two-level (36.5%), 7 three-level (13.5%), and 4 four-level (7.7%) procedures for a total of 97 treated levels. The average duration of follow-up was 7.5 months (6.0–11.8 months). The mean age was 60.9 years (28–83), with a mean BMI

of 29.6 (20.6–46.5). The modified Prolo scores (0–20 scale) improved significantly overall from an average of 11.0 preoperatively to 16.1 postoperatively (68.3%) in 51/52 patients. Improvement in pain and function demonstrated successful outcomes following surgery as Prolo scores were reported as excellent (47.1%), good (49.0%), or fair (3.9%), with each reporting  $\geq 3$  points in the post-operative score compared to baseline scores. Successful fusion was confirmed at 6 months postoperatively in 42/52 patients (80.7%), and in 49/52 patients (94.2%) by 12 months postoperatively. Radiographic evidence of successful fusion was seen by 12 months in 94/97 levels (96.9%). A breakdown for this cohort is provided in Table 2. Pseudarthrosis was only observed in 3/97 levels (3.1%). Overall, the lumbar fusion cohort achieved a near 97% (94/97 levels) fusion rate with BCP<sub><math>\lt; \mu\text{m}</math>, which compares favorably to a recent meta-analysis using the same surgical technique[38].</sub>

Likewise, radiographic fusions through 3D-printed titanium cages in the cervical spine were achieved in 75/80 levels (93.8%), of which 31/32 levels (96.9%) fused in 1 to 3-level reconstructions and 20/24 levels (83.3%) fused after 4 level reconstructions, despite multiple comorbidities in the latter cohort. None of these patients required revision surgery within 18 months from the index operation. Overall, cervical fusion was reached in 21/25 patients with excellent clinical outcomes, which compares favorably with recent publications[39].

The cervical group consisted of 9 males and 16 females. The procedures included posterior fusions and anterior-posterior combined reconstructions. The submicron surface BCP<sub><math>\lt; \mu\text{m}</math> bone graft material was mixed with autograft placed either inside of the interbody cages or posterolateral, adjacent to the lateral-mass and pedicle screws. The average length of follow-up for the entire cervical cohort was 6.4 months (3–11). The mean age was 61.2 years (33–80), with a mean BMI of 29.5 (18.7–46.4). Modified Prolo average scores (0–20 scale) improved overall from 10.8 preoperatively to 16.0 postoperatively (68.7%) in 23/25 patients who reported proper follow-up. Prolo scores demonstrated positive outcomes with categories reported as excellent (61%), good (35%), or fair (4%). Each reported at least 3 points post-operative score improvement for pain and function. Fusion status was monitored using flexion/extension films and CT-scan sagittal/coronal reconstructions as early as 3 months and as late as 12 months postoperatively when indicated. Successful</sub>

**Figure 11 (right):** Representative micrographs from histological sections of the spinal levels treated with BCP<sub><math>\lt; \mu\text{m}</math> (a, b, c), BG<sub><math>\mu\text{m}</math> (d, e, f) and BG/TCP<sub><math>\mu\text{m}</math> (g, h). Micrographs were obtained from regions near the host TP (a, d, g) and the intertransverse central region (b-c, e-f, h). High magnification images show cellular processes observed near the graft materials, including osteoblasts (c, g-black arrows) depositing osteoid and cell-mediated resorption of materials by multinucleated cells (c, h - yellow arrows). Inflammatory foreign body reaction was observed in BG<sub><math>\mu\text{m}</math> specimens, as evidenced by encapsulation of material and high numbers of lymphocytes and foreign body giant cells (e, f - yellow arrows). HB: host bone; NB: new bone; BM: bone marrow; O: osteoid; FT: fibrous tissue. Adapted from van Dijk et al. (2020).</sub></sub></sub></sub>



8

fusion was achieved by 6 months in 53/80 levels (66%). At 12 months, the remaining levels fused, except for five proven pseudoarthroses in four patients that all occurred in one 3-level and three 4-level anterior standalone reconstructions fitted with the titanium 3D printed cages and static locking plates. At 12 months, successful fusion was observed in 75/80 levels (93.8%) with radiographic evidence (Table 1). Fusion was achieved in 18/18 PCF levels, 4/4 corpectomy surfaces, and 51/56 ACDF standalone procedure levels (91.1%). All single and two-level ACDF levels fused solid (14/14). In the 3-level cases, 94.5% fused (17/18), whereas 83.3% of the four-level ACDF levels fused without posterior hardware (20/24). All anterior-posterior reconstructions of 5-levels or greater fused solidly. The confirmed pseudarthrosis cases remained clinically asymptomatic more than 12 months after the surgery, and each of these four patients involved one or more comorbidities known to negatively affect fusion success, including two smokers (Table 2). None of them required additional surgical procedures to date (18 months post-op). There

**Table 1: Results from 52 lumbar fusion patients.** Solid arthrodesis was noted in 94/97 levels (96.9%) in 49/52 patients after 12months. Co-morbidities prevalent >30% in this cohort included: Anxiety, Depression, Diabetes, Hyperlipidemia, Gastro-Esophageal Reflux Disease (GERD), Sleep Apnea and Morbid Obesity and Smoking.

Lumbar Group N=52		
Average age (28 - 83)	60.9	
Female	44	46.2%
Male	33	53.8%
Mean BMI (20.6 - 46.5)	29.6	
Procedures		
ALIF + Posterior fusion	23	44.2%
Lateral + Posterior fusion	12	23.1%
ALIF Only	5	9.6%
Lateral Only	9	17.3%
Posterior Only	3	5.8%
Fusion Levels per Procedure		
1 Level	22	42.3%
2 Levels	19	36.5%
3 Levels	7	13.5%
4 Levels	4	7.7%
Fusion Results for all levels		
Fusion Success @ 6mo	82/97	84.5%
Fusion Success @ 12mo	94/97	96.9%
Pseudarthrosis @ 12mo	3/97	3.1%

were no instances of infection, product-related adverse events, or hardware failures in both lumbar and cervical groups.

These data demonstrated that this calcium phosphate bone graft material with submicron surface topography was capable of delivering solid, stable, and reliable fusions in real-world clinical applications, with a pseudo-arthrodesis rate comparable to autograft in both cervical and in lumbar interbody applications [38,40–42]. Future studies with longer-term follow-up and patient-reported outcomes are most certainly indicated, while level I prospective randomized studies (Kruyt, 2018) and additional level IV clinical investigations are currently underway [44].

**Table 2: Results from 25 cervical fusion patients.** Solid arthrodesis was noted in 75/80 levels in 21/25 patients after 12months. 1, 2, and 3 level ACDF cases fused in 31/32 cases (96.8%). Comorbidities prevalent >30% in this cohort included: Hypertension, Gastro-Esophageal Reflux Disease (GERD), Diabetes I or II, Anxiety, Depression, Dyslipidemia, Generalized Osteo Arthritis, Obesity and Smoking.

<b>Cervical Group N=25</b>		
Average age (33–80)	61.2	
Female	16	64.0%
Male	9	36.0%
Mean BMI (18.7–46.4)	29.5	
<b>Procedures</b>		
Anterior only (ACDF = 19 /Corpectomy = 2)	21	84.0%
Posterior only (PCF)	1	4.0%
ACDF + PCF	2	8.0%
<b>Fusion per Surgical Level N=80</b>		
PCF	20/20	100%
Corpectomy Surfaces	4/4	100%
ACDF total	51/56	91.1%
1 + 2 Levels	14/14	100%
3 Levels	17/18	94.4%
4 Levels	20/24	83.3%
Fusion success @ 6 months	53/80	66.3%
Fusion success @ 12 months	75/80	93.8%
Pseudarthrosis @ 12 months	5/80	6.3%

## **CONCLUSION**

---

A submicron surface topography with needle-shaped features on bone grafts is a key modulator in the foreign body response, which leads to accelerated and enhanced bone regeneration. Within the first days following implantation, a unique, innate immune response was induced by these materials, with significant M2 macrophage upregulation and a moderate M1 macrophage population. In vivo, this delicate balance observed on needle-shaped topography favored initial osteoclastic activity, followed by osteoblastic activity leading to bone formation. These studies show the sensitivity of macrophages to material surface features and their crucial role in bone regeneration directly after implantation. The pro-healing immune reaction was translated into reliable spinal fusions induced by submicron surface materials. This result was unambiguously shown by histology in preclinical models and translated to clinical cases. Steering bone regeneration and fusion success by topographical surface features on bone graft materials is feasible, and the innate immune response appears to be a key factor in efficacy of bone graft materials.

## **ACKNOWLEDGEMENTS**

---

We like to thank dr. Ronquan Duan, Devlina Ghosh, dr. Lizette Utomo and dr. ir. Debby Gawlitta for their scientific contribution. This work was supported by Kuros Biosciences BV and the European Union's Horizon 2020 research and innovation program (grant agreements no. 674282 and no. 874790).

## ABBREVIATIONS

$< \mu\text{m}$	Surface features in the submicron range
$\mu\text{m}$	Surface features in the micron range
ACDF	Anterior cervical discectomy and fusion
ALP	Alkaline Phosphatase
BCP	Biphasic Calcium Phosphate
BG	45S5 Bioglass
BMA	Bone Marrow Aspirate
BMI	Body Mass Index
CCL18	C-C Motif Chemokine Ligand 18
CCL2	C-C Motif Chemokine Ligand 2
CCL5	C-C Motif Chemokine Ligand 5
CD14	Cluster of Differentiation 14
CD163	Cluster of Differentiation 163
CD206	Cluster of Differentiation 206
CTSK	Cathepsin K
ELISA	Enzyme-Linked Immunosorbent Assay
IL-10	Interleukin 10
IL-1 $\beta$	Interleukin 1 $\beta$
M0	Non-activated macrophage
M1	Pro-inflammatory macrophage
M2	Anti-inflammatory, pro-healing macrophage
PCF	Posterior Cervical Fusion
PLF	Posterolateral fusion
RT-qPCR	Quantitative Reverse Transcription Polymerase Chain Reaction
SEM	Scanning Electron Microscopy
TCP	Tricalcium Phosphate
TGF- $\beta$ 1	Transforming Growth Factor $\beta$ 1
TNF- $\alpha$	Tumor Necrosis Factor $\alpha$
TRAP	Tartrate-Resistant Acid Phosphatase

## REFERENCES

---

- [1] Millennium Research Group, Orthopedic Biomaterials | Medtech 360 | Market Analysis | US | 2017, Toronto, 2016.
- [2] W.C. Pannell, D.D. Savin, T.P. Scott, J.C. Wang, M.D. Daubs, Trends in the surgical treatment of lumbar spine disease in the United States, *Spine J.* 15 (2015) 1719–1727. <https://doi.org/10.1016/j.spinee.2013.10.014>.
- [3] E.J. Carragee, G.C. Comer, M.W. Smith, Local bone graft harvesting and volumes in posterolateral lumbar fusion: A technical report, *Spine J.* 11 (2011) 540–544. <https://doi.org/10.1016/j.spinee.2011.02.014>.
- [4] K.M. Scheufler, D. Diesing, Einsatz von Knochenersatzmaterialien bei Fusionen der Wirbelsäule, *Orthopade.* 44 (2015) 146–153. <https://doi.org/10.1007/s00132-014-3069-5>.
- [5] P. Italiani, D. Boraschi, From monocytes to M1/M2 macrophages: Phenotypical vs. functional differentiation, *Front. Immunol.* 5 (2014). <https://doi.org/10.3389/fimmu.2014.00514>.
- [6] R. Klopffleisch, Macrophage reaction against biomaterials in the mouse model – Phenotypes, functions and markers, *Acta Biomater.* 43 (2016) 3–13. <https://doi.org/10.1016/j.actbio.2016.07.003>.
- [7] P.J. Murray, J.E. Allen, S.K. Biswas, E.A. Fisher, D.W. Gilroy, S. Goerdt, S. Gordon, J.A. Hamilton, L.B. Ivashkiv, T. Lawrence, M. Locati, A. Mantovani, F.O. Martinez, J.L. Mege, D.M. Mosser, G. Natoli, J.P. Saeij, J.L. Schultze, K.A. Shirey, A. Sica, J. Suttles, I. Udalova, J.A. vanGinderachter, S.N. Vogel, T.A. Wynn, Macrophage Activation and Polarization: Nomenclature and Experimental Guidelines, *Immunity.* 41 (2014) 14–20. <https://doi.org/10.1016/j.immuni.2014.06.008>.
- [8] M.E. Ogle, C.E. Segar, S. Sridhar, E.A. Botchwey, Monocytes and macrophages in tissue repair: Implications for immunoregenerative biomaterial design, *Exp. Biol. Med.* 241 (2016) 1084–1097. <https://doi.org/10.1177/1535370216650293>.
- [9] K.M. Hotchkiss, G.B. Reddy, S.L. Hyzy, Z. Schwartz, B.D. Boyan, R. Olivares-Navarrete, Titanium surface characteristics, including topography and wettability, alter macrophage activation, *Acta Biomater.* 31 (2016) 425–434. <https://doi.org/10.1016/j.actbio.2015.12.003>.
- [10] T.U. Luu, S.C. Gott, B.W.K. Woo, M.P. Rao, W.F. Liu, Micro- and Nanopatterned Topographical Cues for Regulating Macrophage Cell Shape and Phenotype, *ACS Appl. Mater. Interfaces.* 7 (2015) 28665–28672. <https://doi.org/10.1021/acsami.5b10589>.
- [11] P.C.S. Bota, A.M.B. Collie, P. Puolakkainen, R.B. Vernon, E.H. Sage, B.D. Ratner, P.S. Stayton, Biomaterial topography alters healing in vivo and monocyte/macrophage activation in vitro, *J. Biomed. Mater. Res.–Part A.* 95 A (2010) 649–657. <https://doi.org/10.1002/jbm.a.32893>.
- [12] F. Loi, L.A. Córdova, R. Zhang, J. Pajarinen, T.H. Lin, S.B. Goodman, Z. Yao, The effects of immunomodulation by macrophage subsets on osteogenesis in vitro, *Stem Cell Res. Ther.* 7 (2016) 15. <https://doi.org/10.1186/s13287-016-0276-5>.
- [13] K.L. Spiller, S. Nassiri, C.E. Witherel, R.R. Anfang, J. Ng, K.R. Nakazawa, T. Yu, G. Vunjak-Novakovic, Sequential delivery of immunomodulatory cytokines to facilitate the M1-to-M2

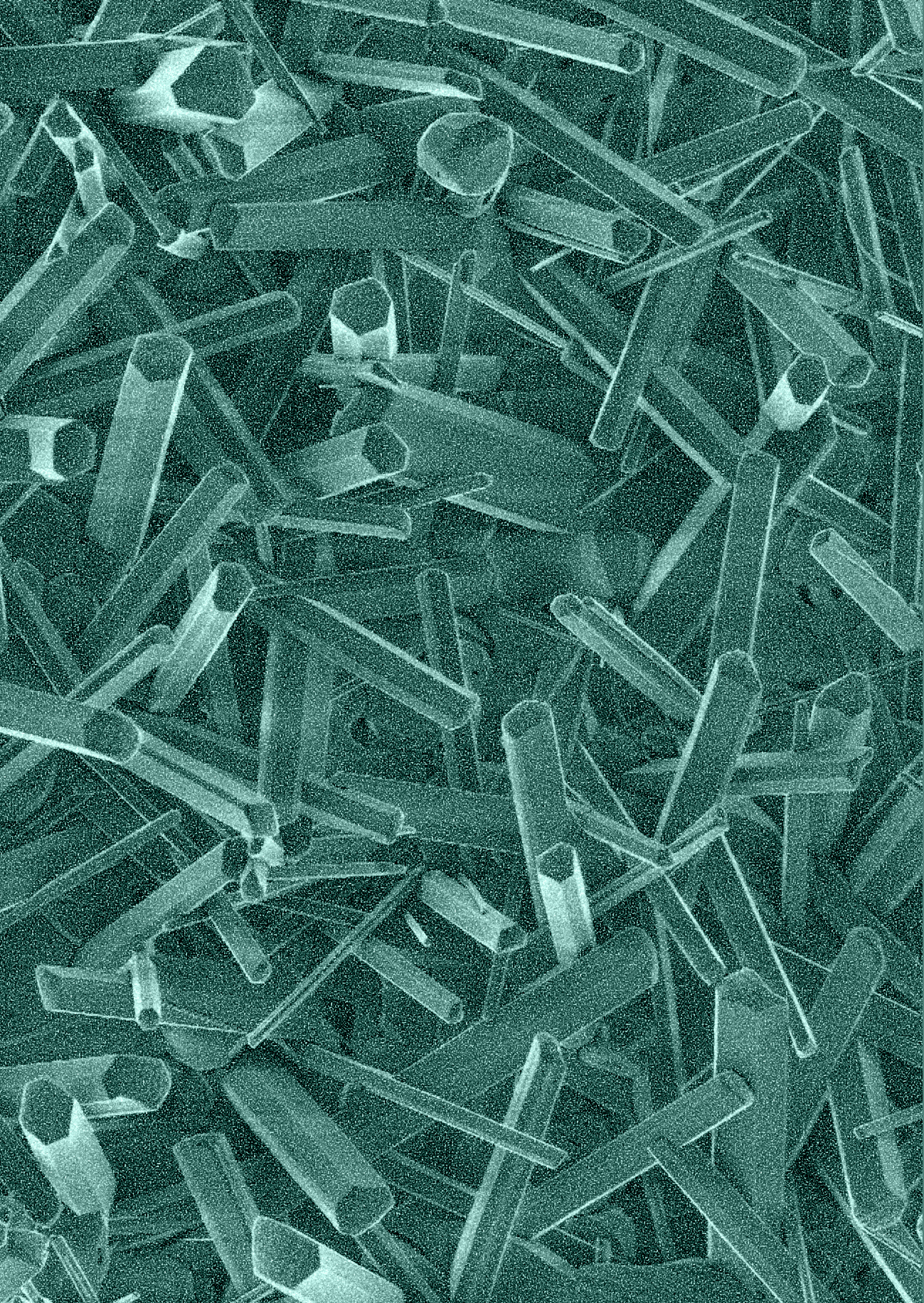


- transition of macrophages and enhance vascularization of bone scaffolds, *Biomaterials*. 37 (2015) 194–207. <https://doi.org/10.1016/j.biomaterials.2014.10.017>.
- [14] M. Heughebaert, R.Z. LeGeros, M. Gineste, A. Guilhem, G. Bonel, Physicochemical characterization of deposits associated with HA ceramics implanted in nonosseous sites, *J. Biomed. Mater. Res.* 22 (1988) 257–268. <https://doi.org/10.1002/jbm.820221406>.
- [15] U. Ripamonti, L.C. Roden, C. Ferretti, R.M. Klar, Biomimetic matrices self-initiating the induction of bone formation, *J. Craniofac. Surg.* 22 (2011) 1859–1870. <https://doi.org/10.1097/SCS.0b013e31822e83fe>.
- [16] H. Yamasaki, H. Sakai, Osteogenic response to porous hydroxyapatite ceramics under the skin of dogs, *Biomaterials*. 13 (1992) 308–312. [https://doi.org/10.1016/0142-9612\(92\)90054-R](https://doi.org/10.1016/0142-9612(92)90054-R).
- [17] C. Klein, K. de Groot, W. Chen, Y. Li, X. Zhang, Osseous substance formation induced in porous calcium phosphate ceramics in soft tissues, *Biomaterials*. 15 (1994) 31–34. [https://doi.org/10.1016/0142-9612\(94\)90193-7](https://doi.org/10.1016/0142-9612(94)90193-7).
- [18] H. Yuan, K. Kurashina, J.D. De Bruijn, Y. Li, K. De Groot, X. Zhang, A preliminary study on osteoinduction of two kinds of calcium phosphate ceramics, *Biomaterials*. 20 (1999) 1799–1806. [https://doi.org/10.1016/S0142-9612\(99\)00075-7](https://doi.org/10.1016/S0142-9612(99)00075-7).
- [19] H. Yuan, H. Fernandes, P. Habibovic, J. De Boer, A.M.C. Barradas, A. De Ruiter, W.R. Walsh, C.A. Van Blitterswijk, J.D. De Bruijn, Osteoinductive ceramics as a synthetic alternative to autologous bone grafting, *Proc. Natl. Acad. Sci. U. S. A.* 107 (2010) 13614–13619. <https://doi.org/10.1073/pnas.1003600107>.
- [20] P. Habibovic, H. Yuan, M. van den Doel, T.M. Sees, C.A. van Blitterswijk, K. de Groot, Relevance of osteoinductive biomaterials in critical-sized orthotopic defect, *J. Orthop. Res.* 24 (2006) 867–876. <https://doi.org/10.1002/jor.20115>.
- [21] R. Duan, L.A. van Dijk, D. Barbieri, F. de Groot, H. Yuan, J.D. de Bruijn, Accelerated bone formation by biphasic calcium phosphate with a novel sub-micron surface topography, *Eur. Cell. Mater.* 37 (2019) 60–73. <https://doi.org/10.22203/eCM.v037a05>.
- [22] N.L. Davison, A.L. Gamblin, P. Layrolle, H. Yuan, J.D. de Bruijn, F. Barrère-de Groot, Liposomal clodronate inhibition of osteoclastogenesis and osteoinduction by submicrostructured beta-tricalcium phosphate, *Biomaterials*. 35 (2014) 5088–5097. <https://doi.org/10.1016/j.biomaterials.2014.03.013>.
- [23] R.J. Miron, D.D. Bosshardt, OsteoMacs: Key players around bone biomaterials, *Biomaterials*. 82 (2016) 1–19. <https://doi.org/10.1016/j.biomaterials.2015.12.017>.
- [24] C.E. Witherel, T. Yu, M. Concannon, W. Dampier, K.L. Spiller, Immunomodulatory Effects of Human Cryopreserved Viable Amniotic Membrane in a Pro-Inflammatory Environment In Vitro, *Cell. Mol. Bioeng.* 10 (2017) 451–462. <https://doi.org/10.1007/s12195-017-0494-7>.
- [25] R. Zhang, Y. Liang, S. Wei, M2 macrophages are closely associated with accelerated clavicle fracture healing in patients with traumatic brain injury: A retrospective cohort study, *J. Orthop. Surg. Res.* 13 (2018) 213. <https://doi.org/10.1186/s13018-018-0926-7>.
- [26] D.T. Ploeger, N.A. Hosper, M. Schipper, J.A. Koerts, S. De Rond, R.A. Bank, Cell plasticity in wound healing: Paracrine factors of M1/ M2 polarized macrophages influence the phenotypical



- state of dermal fibroblasts, *Cell Commun. Signal.* 11 (2013). <https://doi.org/10.1186/1478-811X-11-29>.
- [27] A.R.D. Reeves, K.L. Spiller, D.O. Freytes, G. Vunjak-Novakovic, D.L. Kaplan, Controlled release of cytokines using silk-biomaterials for macrophage polarization, *Biomaterials.* 73 (2015) 272–283. <https://doi.org/10.1016/j.biomaterials.2015.09.027>.
- [28] M. Kumar, J. Coburn, D.L. Kaplan, B.B. Mandal, Immuno-Informed 3D Silk Biomaterials for Tailoring Biological Responses, *ACS Appl. Mater. Interfaces.* 8 (2016) 29310–29322. <https://doi.org/10.1021/acsami.6b09937>.
- [29] T. Buchacher, A. Ohradanova-Repic, H. Stockinger, M.B. Fischer, V. Weber, M2 polarization of human macrophages favors survival of the intracellular pathogen chlamydia pneumoniae, *PLoS One.* 10 (2015) e0143593. <https://doi.org/10.1371/journal.pone.0143593>.
- [30] J.C. Zarif, J.R. Hernandez, J.E. Verdonesi, S.P. Campbell, C.G. Drake, K.J. Pienta, A phased strategy to differentiate human CD14+ monocytes into classically and alternatively activated macrophages and dendritic cells, *Biotechniques.* 61 (2016) 33–41. <https://doi.org/10.2144/000114435>.
- [31] D. Aeschlimann, B. Evans, The vital osteoclast: How is it regulated?, *Cell Death Differ.* 11 (2004) S5–S7. <https://doi.org/10.1038/sj.cdd.4401470>.
- [32] I.E. Adamopoulos, A. Sabokbar, B.P. Wordsworth, A. Carr, D.J. Ferguson, N.A. Athanasou, Synovial fluid macrophages are capable of osteoclast formation and resorption, *J. Pathol.* 208 (2006) 35–43. <https://doi.org/10.1002/path.1891>.
- [33] L.A. van Dijk, D. Barbieri, F. Barrère-de Groot, H. Yuan, R. Oliver, C. Christou, W.R. Walsh, J.D. de Bruijn, Efficacy of a synthetic calcium phosphate with submicron surface topography as autograft extender in lapine posterolateral spinal fusion, *J. Biomed. Mater. Res.–Part B Appl. Biomater.* 107 (2019) 2080–2090. <https://doi.org/10.1002/jbm.b.34301>.
- [34] L.A. van Dijk, R. Duan, X. Luo, D. Barbieri, M. Pelletier, C. Christou, A.J.W.P. Rosenberg, H. Yuan, F. Barrère-de Groot, W.R. Walsh, J.D. de Bruijn, Biphasic calcium phosphate with submicron surface topography in an Ovine model of instrumented posterolateral spinal fusion, *JOR Spine.* 1 (2018) e1039. <https://doi.org/10.1002/jsp2.1039>.
- [35] L.A. Van Dijk, F. Barrère-De Groot, A.J.W.P. Rosenberg, M. Pelletier, C. Christou, J.D. De Bruijn, W.R. Walsh, MagnetOs, Vitoss, and Novabone in a Multi-endpoint Study of Posterolateral Fusion: A True Fusion or Not?, *Clin. Spine Surg.* 33 (2020) E276–E287. <https://doi.org/10.1097/BSD.0000000000000920>.
- [36] S.D. Boden, J.H. Schimandle, W.C. Hutton, An experimental lumbar intertransverse process spinal fusion model: Radiographic, histologic, and biomechanical healing characteristics, *Spine (Phila. Pa. 1976).* 20 (1995) 412–420. <https://doi.org/10.1097/00007632-199502001-00003>.
- [37] L.G. Lenke, K.H. Bridwell, D. Bullis, R.R. Betz, C. Baldus, P.L. Schoenecker, Results of In Situ Fusion for Isthmic Spondylolisthesis, *J. Spinal Disord.* 5 (1992) 433–442. <https://doi.org/10.1097/00002517-199212000-00008>.

- [38] J.X.J. Li, K. Phan, R. Mobbs, Oblique Lumbar Interbody Fusion: Technical Aspects, Operative Outcomes, and Complications, *World Neurosurg.* 98 (2017) 113–123. <https://doi.org/10.1016/j.wneu.2016.10.074>.
- [39] P.M. Arnold, R.C. Sasso, M.E. Janssen, M.G. Fehlings, J.D. Smucker, A.R. Vaccaro, R.F. Heary, A.I. Patel, B. Goulet, I.H. Kalfas, B. Kopjar, Efficacy of i-factor bone graft versus autograft in anterior cervical discectomy and fusion results of the prospective, randomized, single-blinded food and drug administration investigational device exemption study, *Spine (Phila. Pa. 1976)*. 41 (2016) 1075–1083. <https://doi.org/10.1097/BRS.0000000000001466>.
- [40] J.M. Levin, J.E. Tanenbaum, M.P. Steinmetz, T.E. Mroz, S.C. Overley, Posterolateral fusion (PLF) versus transforaminal lumbar interbody fusion (TLIF) for spondylolisthesis: a systematic review and meta-analysis, *Spine J.* 18 (2018) 1088–1098. <https://doi.org/10.1016/j.spinee.2018.01.028>.
- [41] M.-H. Shao, F. Zhang, J. Yin, H.-C. Xu, F.-Z. Lyu, Titanium cages versus autogenous iliac crest bone grafts in anterior cervical discectomy and fusion treatment of patients with cervical degenerative diseases: a systematic review and meta-analysis, *Curr. Med. Res. Opin.* 33 (2017) 803–811. <https://doi.org/10.1080/03007995.2017.1284050>.
- [42] P.C. McAfee, C. Reah, K. Gilder, L. Eisermann, B. Cunningham, A meta-analysis of comparative outcomes following cervical arthroplasty or anterior cervical fusion: Results from 4 prospective multicenter randomized clinical trials and up to 1226 patients, *Spine (Phila. Pa. 1976)*. 37 (2012) 943–952. <https://doi.org/10.1097/BRS.0b013e31823da169>.
- [43] M. Kruyt, MagnetOs™ Granules vs. Autograft in Instrumented Posterolateral Spinal Fusion (MaxA), Identifier: NCT03625544. (n.d.). [www.clinicaltrials.gov](http://www.clinicaltrials.gov).
- [44] Kuros Biosciences, Post Marketing Clinical Follow up Study for MagnetOs Putty in Patients With Degenerative Disc Disease (PROGRESS), Identifier: NCT04128852. (2019). [www.clinicaltrials.gov](http://www.clinicaltrials.gov).



# **C H A P T E R 9**



**SUMMARY, GENERAL DISCUSSION  
AND FUTURE PERSPECTIVES**

## SUMMARY & MAIN FINDINGS

---

The overall aim of this thesis was *to determine if and how topography of calcium phosphates can be improved for increased efficacy as bone graft materials for maxillofacial and orthopedic surgery.*

To achieve this objective, we manufactured calcium phosphate bone grafts with different surface designs, i.e. topographies with different surface crystal morphology (needle-shaped vs. grain-shaped) in the micron- and submicron range, and evaluated their ability to induce ectopic bone formation in a canine intramuscular pouch model. The material with the highest osteoinductive potential, attributed to its needle-shaped submicron topography, was selected for further evaluation in pre-clinical models of orthopedic surgery (i.e. spinal fusion) and maxillofacial surgery (i.e. maxillary sinus floor augmentation). In these studies, the material was compared to the gold standard autograft and/or other synthetic bone graft substitute materials. In addition to these pre-clinical studies, the bone graft material with needle-shaped topography was evaluated in a retrospective cohort study of interbody spinal fusion and a preliminary prospective, randomized controlled trial (RCT) of maxillary sinus floor augmentation. Furthermore, to gain insight into the biological effects of calcium phosphate topography, polarization of primary human macrophages in response to calcium phosphates with submicron needle-shaped topography and conventional topography was assessed *in vitro*, which included an evaluation of downstream regenerative effects of macrophages on osteogenesis and angiogenesis. These findings were placed in perspective of the available literature, in a review of M2 macrophage upregulation by biomaterials with specific structural and topographical features.

The main findings of this thesis are:

### **Part I: Improving the surface topography of calcium phosphates to enhance their osteoinductive potential**

#### **Chapter 2:**

- *By evaluating osteoinduction by calcium phosphates with different surface topographies in a canine intramuscular pouch model, it was determined that the surface design of these materials can be controlled to enhance their osteoinductive potential*
- *Besides submicron size of surface features as a critical factor for osteoinductivity, also the morphology of surface crystals was shown to influence this propensity*
- *Calcium phosphates with a needle-shaped submicron topography demonstrated accelerated osteoinductive bone formation compared to materials with other topographies*

## **Part II: Efficacy of osteoinductive calcium phosphate as bone graft material in spinal fusion**

### **Chapter 3-5:**

- *Used as bone graft extender in a lapine model and as a standalone bone graft in an ovine model of posterolateral spinal fusion, osteoinductive calcium phosphate with improved surface design (i.e. needle-shaped submicron topography) demonstrated equivalent treatment outcomes to the 'gold standard' bone autograft*
- *Compared to other synthetic bone graft materials that are commercially available and in clinical use, the osteoinductive calcium phosphate demonstrated superior efficacy in promoting spinal fusion*
- *Implantation of osteoinductive calcium phosphate particles/granules embedded in a polymeric carrier designed to improve handling properties (i.e. 'putty') was successful and did not reduce the efficacy of the bone graft material*

## **Part III: Efficacy of osteoinductive calcium phosphate in maxillary sinus floor augmentation**

### **Chapter 6:**

- *Comparing calcium phosphates with different surface topographies in a sheep model of maxillary sinus floor augmentation, it was demonstrated that calcium phosphate with improved surface design (i.e. needle-shaped submicron topography) promoted enhanced bone healing compared to calcium phosphate with a grain-shaped submicron topography, while showing equivalence to bone autograft.*
- *Secondly, above pre-clinical results on the efficacy of osteoinductive calcium phosphate with needle-shaped submicron topography were clinically confirmed in a preliminary human study of maxillary sinus floor augmentation, in which equivalence to autograft was determined in implant stability, bone height, new bone formation and in overall clinical outcome, albeit with a small sample size.*

## **Part IV: The response of macrophages to osteoinductive calcium phosphate**

### **Chapter 7-8:**

- *In an in vitro study on immunomodulation by osteoinductive calcium phosphate, it was determined that M2 macrophage upregulation may likely play a role in the enhanced bone regeneration capacity of these materials.*
- *This notion was corroborated by an investigation of the literature on M2 macrophage upregulation by materials with specific structural and topographical features, the underlying biological mechanism, and the role of M2 macrophages in bone healing.*



- *Lastly, in a retrospective cohort study of 77 lumbar and cervical reconstruction patients receiving interbody and posterolateral spinal fusions, osteoinductive calcium phosphate with needle-shaped submicron topography was demonstrated to be an efficacious bone graft material, reaching 12-month fusion rates of 93.8% and 96.9% and favorable clinical outcomes.*



## GENERAL DISCUSSION AND FUTURE PERSPECTIVES

### Requirements for the new gold standard in bone grafting

Since the late 19<sup>th</sup> century, the practice of bone grafting has substantially grown and evolved in the clinics of orthopedic and maxillofacial surgeons. With the ultimate goal to find the new gold standard in bone grafting, developments in biomedical science during the past century have resulted in a wide range of bone graft substitutes that are available today. Due to increasing global numbers of bone graft surgery and a trend towards minimally invasive techniques, the need for an effective alternative to autograft is ever more urgent. To evaluate how far we have come with current available solutions in the development of the new gold standard treatment, we should first define the key criteria that the new gold standard should meet:

- **Efficacy:** At minimum, it should be as efficacious as autograft when used as a standalone solution, thereby eliminating the need to harvest patient-own bone
- **Safety:** It should be safe and have a low risk of complications
- **Level of evidence:** There should be a high level of evidence on its efficacy and safety, from both pre-clinical and clinical (level I-III) studies
- **Ease of use:** It should have 'off-the-shelf' availability and be easy to prepare and handle in the operating room
- **Consistency:** It should have a consistent quality, resulting from a reproducible manufacturing process or sourcing chain
- **Cost-effectiveness:** It should be relatively low cost

Using the above criteria, we can assess for currently available bone graft options which of the requirements are met and which still need to be achieved.

The regenerative potency of bone graft substitutes is often determined based on the bone healing mechanisms that they provide, i.e. the triad of osteoconductivity, osteoinductivity and osteogenicity[1]. Whereas an osteoconductive bone graft can only 'conduct' new bone formation, functioning as a scaffold that guides host bone growth, osteoinductive and osteogenic bone grafts can inherently induce bone formation by inducing an osteogenic response from the host, or by providing the cellular ingredients necessary for bone growth, respectively.

Autograft bone inherently provides all three components required for bone regeneration. In Table 1, the bone graft healing properties, as well as scores for the key criteria for the new gold standard bone graft substitute as defined above, are compared for currently



available bone graft options. Autograft received the highest score (+++) for all criteria apart from safety & complications, ease of use and consistency. Safety and ease of use are suboptimal due to the need to harvest autograft, which may require an extra surgical procedure with associated risks and additional labor. Moreover, for certain procedures, the amount of available autograft bone that can be reasonably harvested may not be sufficient. Furthermore, harvesting of autograft is associated with risks of donor-site morbidity and complications[2]. Lastly, the quality of autograft bone may be lower in compromised or elderly patients, which is why autograft did not receive a full score for consistency [3].

**Table 1. Comparison of bone graft properties and key criteria for most-used treatment options**

	Autograft	Allograft chips, xenograft, synthetics	DBMs	rhBMP-2	BMA	Cellular allograft	Osteoinductive calcium phosphate
<b>Bone graft properties</b>							
Osteoconductive	+++	+++	-	-	-	- / +++ *	+++
Osteoinductive	+++	-	++	+++	-	++	+++
Osteogenic	+++	-	-	-	++	+	-
<b>Key criteria</b>							
Efficacy	+++	+	+	+++	+	+	+++
Safety & complications	+	+++	++	-	+++	++	+++
Level of Evidence	+++	+	+	+++	-	-	+
Ease of use	+	+++	+++	+	++	+	+++
Consistency	++	+++	-	+++	++	-	+++
Cost	+++	++	++	-	+++	-	++
<b>Total criteria score</b>	<b>13</b>	<b>13</b>	<b>9</b>	<b>10</b>	<b>11</b>	<b>4</b>	<b>15</b>
<b>DBM:</b> demineralized bone matrix, <b>rhBMP-2:</b> recombinant human bone morphogenetic protein 2, <b>BMA:</b> bone marrow aspirate (concentrate). <b>Range of scores:</b> - (poor/absent); + (low); ++ (moderate); +++ (high). * Depending on incorporation of allograft chips.							

### **Evaluation of osteoconductive bone graft substitutes**

Typical bone graft substitutes that are considered to be osteoconductive include human cancellous allograft chips, xenograft and most synthetic graft materials. Since these materials cannot stimulate bone formation without the addition of cells or growth factors, this leads to slower and less complete bone growth when used as standalone in critical-sized defects[4]. Favorable outcomes have been reported with the use of osteoconductive bone grafts as extender of autograft, but their efficacy as standalone bone graft in general is much lower than that of the autograft, which is the biggest drawback of this bone graft category [5–10]. In chapter 5 of this thesis, we demonstrated that different osteoconductive synthetic bone grafts used as a standalone were not able to form a functional bony fusion in the posterolateral spine, while a successful outcome was achieved by autograft and a

synthetic bone graft that was osteoinductive and osteoconductive. However, in smaller defects, which are more commonly observed in maxillofacial surgery, i.e. sinus floor augmentation, comparable outcomes to the gold standard have also been reported with standalone use of osteoconductive bone grafts[11–13].

Besides their lower efficacy than autograft, osteoconductive bone grafts are satisfactory in safety, handling, ease of use, consistency and cost. However, the level of evidence for osteoconductive bone grafts and their subcategories is relatively low. The majority of clinical studies consists of uncontrolled case studies (Level IV) with a small sample size and high risk of bias[5,7,10,14,15]. However, even for more well-designed studies (Level I–III), the strength of evidence has been claimed to be low or insufficient for similar reasons[7,15]. Moreover, it should be mentioned that within the category of osteoconductive bone grafts, there is a wide variation in graft characteristics. Performance and efficacy can vary for each unique formulation because this depends on composition and structural properties. Careful consideration of the evidence at individual product-level is therefore important when osteoconductive bone grafts are evaluated for use. However, due to their reproducible manufacturing and/or processing procedures, each individual product is expected to be of consistent quality.

### ***Evaluation of osteoinductive bone graft substitutes***

Traditional osteoinductive bone graft substitutes comprise demineralized bone matrices (DBMs) and rhBMP-2. DBMs are demineralized bone allografts which consist of natural collagen, non-collagenous bone proteins and osteoinductive growth factors[16]. Next to the growth factors, DBMs also provide a scaffold in their collagen matrix. Despite being osteoinductive[17–19], the efficacy of DBMs is low compared to mere osteoconductive bone grafts and they are only supported for use as autograft extender and not as standalone bone graft[6,20–22]. Next to their low efficacy, another disadvantage of DBMs is their poor consistency in biological properties. Various studies have demonstrated that there exists a high product-to-product and lot-to-lot variation in DBM potency, i.e. content of osteoinductive factors and associated healing performance [23–25]. This is believed to be the consequence of donor variability and different processing techniques. Additionally, carrier formulations of DBMs such as polymers and hydrogels have been shown to affect their performance, especially when present in higher ratios[16,23]. Altogether, due to the low consistency in quality of DBMs, they may be considered an unreliable bone graft substitute.

In terms of safety, like other allografts, the main risk of DBMs is disease transmission. However, sterility of DBMs is strictly regulated and preventative measures such as donor screening, microbiological testing and processing techniques are in place[16,26]. Despite risk mitigation, a small risk of disease transmission remains and serious adverse



consequences of allograft products are occasionally reported[27,28]. Interestingly, DBMs are often not terminally sterilized (i.e. gamma-irradiated in their final container) but only aseptically processed as the methods applied for the former can degrade biological components [16]. Similar to the osteoconductive bone graft category, the level of evidence for DBMs is relatively low because of overall poor study quality and lack of level I evidence. Other than the discussed criteria, DBMs have good handling properties, ease of use and cost, but they do not meet the requirements in terms of efficacy, level of evidence, and consistency.

BMPs are a group of cytokines that were first discovered in demineralized bone by Marshall Urist in 1965 and were found to be osteoinductive [ref Urist 65]. After sequencing and cloning of BMPs in the 1990s, recombinant human BMP-2 was introduced into the spinal fusion market following FDA approval in 2003. Since then, rhBMP-2, that is implanted while absorbed in a resorbable collagen sponge, has proven to be an efficacious bone graft for spinal fusion, tibial fractures and maxillofacial surgery. Numerous level I studies, systematic reviews and meta-analyses have indicated that the use of rhBMP-2 in specific indications is highly effective, with at minimum equivalent efficacy to the gold standard autograft [29–31]. However, after the first years of widespread use in spinal fusion in the United States – in up to 60% of lumbar fusion procedures in 2006—it became the subject of great controversy due to reports of life-threatening complications associated with its off-label use in cervical fusion, i.e. swelling, dysphagia and breathing problems[32]. Also, on-label use of rhBMP-2 in lumbar fusion has been associated with serious complications, including inflammation, ectopic bone formation and osteolysis[33]. As a consequence, the North American Spine Society therefore only recommends the use of rhBMP-2 “in cases in which other alternatives are either not available or are not likely to lead to effective fusion”[34]. Therefore, despite the high efficacy, the safety concerns with rhBMP-2 are its greatest drawback.

Other areas in which BMP-2 does not meet the requirements of the new gold standard are its cost-effectiveness and handling characteristics. Compared to other bone graft substitutes, rhBMP-2 is the most expensive option with an average cost of over \$5000 for 10 cc of graft [35]. Economic analyses have indicated that rhBMP-2 in general is unlikely to be a cost-effective alternative to autograft from a payor perspective, although it may be from a societal perspective[31,36,37]. There is no evidence on how this compares to other bone graft substitutes[36]. With regard to handling properties, preparation time of rhBMP-2 in the operating theater takes at least 30 minutes, as the lyophilized protein first needs to be reconstituted, then distributed over a collagen sponge using a syringe, and subsequently is left to incubate for another 15 minutes. Altogether, rhBMP-2 is an effective bone substitute that reaches the efficacy of the gold standard and has a good

level of evidence, but it does not meet the requirements of safety, cost-effectiveness and preparation and handling.

### ***Evaluation of osteogenic bone graft substitutes***

Osteogenic bone grafts contain viable osteogenic cells that may contribute to bone formation after implantation. In bone graft substitutes, these cells may be derived from autologous or allogeneic sources. Strategies to achieve this include combining osteoconductive scaffolds with (concentrated) autologous bone marrow aspirate (BMA) or isolated-expanded bone marrow-derived stem cells, or processing of allograft bone to preserve viable cells from the donor.

The use of BMA is a relatively easy and inexpensive way to add osteogenic cells to a bone graft prior to implantation. Some studies have suggested that adding BMA to osteoconductive bone grafts can improve fusion rates, but recent systematic reviews concluded that the level of evidence is very low due to study design and risk of bias [6,38,39]. Although the latter is also true for the evidence on safety, as autologous material, BMA is likely to be harmless. BMA cannot be used as a standalone graft as it needs to be mixed with an osteoconductive scaffold, therefore it is only useful as a graft enhancer. Similar to the use of BMA, multipotent stem cells from the bone marrow stroma or other tissue sources can be isolated and expanded *ex vivo* to be used as an osteogenic adjunct for bone grafting applications. This strategy is currently in an early investigational stage for both orthopedic and maxillofacial surgery[40–44]. However, isolation and expansion of stem cells is an expensive and time-intensive process and in particular the use of autologous stem cells will be logistically impractical on larger scales. Currently the costs and benefits of the use of autologous or allogeneic cells for bone grafting are not clear.

Cellular allografts are bone allografts that are processed to contain viable osteogenic precursor cells, such as mesenchymal stem cells. Besides cells, these products commonly contain cancellous bone chips and/or DBM, giving them osteoconductive and osteoinductive potential in addition to their osteogenic capacity[45].

As cellular allografts are claimed to provide all three mechanisms of bone healing, they are heavily marketed as bone grafts that mimic the biological profile of autograft. However, pre-clinical studies have challenged the concept that allogeneic cells in these products contribute to bone healing, as no differences in spinal fusion rate were determined between allografts with and without a viable cellular component [46,47]. Systematic reviews of clinical literature have reported the level of evidence for efficacy and safety of cellular allografts to be very low, due to lack of well-designed studies with proper control groups, and a high risk of bias in published studies [45,48,49]. No firm conclusions on their efficacy and safety can be made. However, a recent retrospective multi-institutional study of 326



cervical fusion cases with a cellular allograft reported higher pseudoarthrosis rates than reported for other osteobiologics[50]. Recently, safety concerns of disease transmission for cellular allografts became reality, when a cellular allograft was recalled by the FDA in the United States following reports of post-surgical infection in 7 out of 23 patients that were treated with the product, of which four had tested positive for Tuberculosis [27]. Moreover, similar to DBMs, the consistency of cellular allograft products is low due to donor variability and processing techniques [47,51]. To preserve cell viability, cellular allografts are stored deep frozen (< -70 °C) in cryoprotectant solution [45]. For this reason, preparation of cellular allografts in the operating theater is cumbersome, due to the frozen supply chain and the need to remove cryopreservants. Lastly, cellular allografts are expensive compared to other bone graft substitutes [45]. Taken together, despite having the same mechanistic properties as autograft, cellular allografts are not convincingly an alternative to the current gold standard.

### ***Evaluation of osteoinductive calcium phosphate***

In the current thesis, osteoinductive calcium phosphate with advanced submicron surface topography was evaluated as a bone graft substitute for orthopedic and maxillofacial surgery. The submicron topography on this material endowed it with substantial osteoinductive capacity (**chapter 1**), resulting in the ability to form bridging, lamellar bone in bony voids in the spine and maxillary sinus in both pre-clinical and clinical studies (**chapter 3-6, 8**).

Because osteoinductive calcium phosphates are synthetic bone grafts, they contain all favorable properties of conventional osteoconductive grafts, with the additional benefit of being osteoinductive, resulting in a higher bone forming efficacy. The data in this thesis have shown that osteoinductive calcium phosphate used as standalone bone graft material reached equivalent efficacy to the gold standard autograft in different pre-clinical models, as well as a clinical study. In Table 1, we can see that of all available bone grafting options, the osteoinductive calcium phosphate reached the highest score for the bone graft criteria set out here, compared to all other options. Indeed, it even scored higher than the current gold standard autograft, mainly due to the absence of donor site complications and the improved ease of use.

Does this mean that osteoinductive calcium phosphates qualify as the new gold standard in bone grafting? It is too early to make this claim because the level of evidence, as one of the most important criteria, is currently insufficient. Osteoinductive calcium phosphates are a relatively new option on the bone grafting market, and while there is evidence supporting their efficacy from pre-clinical studies, the number of high-strength clinical studies is still quite low. Currently, there are nine Level IV, three Level III, two Level II and one Level I clinical studies published on osteoinductive calcium phosphates, including chapters 6 and

8 from this thesis [52,53,62–65,54–61]. Although these studies have reported favorable outcomes, additional Level I studies are required to strengthen the level of evidence for this new category of bone grafts. However, at the time of writing, an additional four prospective RCTs are underway for the calcium phosphate with needle-shaped submicron topography that was described in this thesis [66–68]. If the results of these studies are favorable, osteoinductive calcium phosphates may have the potential to surpass autograft as the new gold standard in bone grafting.

### **Osteoinductive versus osteogenic bone graft substitutes**

In theory, a bone graft substitute that, like autograft, provides all three bone graft healing properties is expected to have a higher efficacy than other options that only provide one or two. However, as determined in the above analysis, the bone healing properties of bone graft substitutes do not accurately predict efficacy. For example, whereas DBMs are osteoinductive and slightly osteoconductive, their efficacy as standalone bone graft or autograft extender is not improved compared to mere osteoconductive scaffolds[6,15]. Similarly, cellular allografts are claimed to provide all three mechanism of bone healing, but their efficacy is not improved compared to conventional DBMs[69]. Lastly, osteoinductive rhBMP-2 and osteoinductive calcium phosphate reach equivalent efficacy to autograft as standalone bone grafts, even though they do not contain an osteogenic cellular component. This teaches us that although the principle of bone healing through osteoconductivity, -inductivity and -genicity is theoretically sound, it is a simplified model of reality. This is not surprising, because even though a bone graft may be claimed to have e.g. an osteogenic component, this does not mean that it is effective in a similar way as it is for autograft bone. For cell-based bone grafts, the amount, type and activity of the cells in these grafts may be very critical and can affect the survival and contribution to bone healing. In fact, it has been commonly reported that implanted cells undergo massive apoptotic death within days after implantation, which is probably caused by the hypoxic environment in the core of the grafts due to absence of local circulation [70]. This results in poor survival, low engraftment and ineffective osteogenic differentiation[71,72].

It is interesting that rhBMP-2 and osteoinductive calcium phosphate reach equivalence to autograft without the presence of a cellular component. Through their osteoinductive effect, these bone grafts induce an osteogenic response from the host by recruiting and directly or indirectly activating local osteogenic cells. This demonstrates that if an osteoinductive stimulus is sufficiently strong, there appears to be no need to provide a cellular component. In fact, it was previously shown that adding stem cells to calcium phosphate scaffolds implanted orthotopically resulted in minimally increased bone formation compared to controls without stem cells[73–76]. There is an obvious benefit of using cell-free 'instructive' bone graft materials like osteoinductive calcium phosphate over options that require the presence of cells, because the former option is easier to use,



has a simpler and more reproducible supply chain, is under less regulatory scrutiny and in general is less expensive. As discussed above, osteoinductive calcium phosphates already meet most of the key criteria of the optimal bone graft, and therefore, they may have the potential to become the new standard material in bone grafting. We may hence speculate that the future of bone regeneration might not be in the once so promising field of tissue engineering, which has generated minimal successful therapies since the late 20<sup>th</sup> century, but instead in the field of instructive biomaterials[77].

### **Surface topography, osteoinduction and macrophages**

On the topic of instructive biomaterials, in the current thesis, we have demonstrated that the healing potential and performance of synthetic graft materials can be enhanced by altering their surface topography. Indeed, improving the morphology and size of surface features, i.e. into a submicron needle-shaped topography, was shown to accelerate osteoinduction and enhance bone healing outcomes *in vivo* compared to graft materials with conventional grain-shaped features. The design and optimization of surface topographies to enhance biomaterial efficacy may be expected to become more and more important in biomaterial engineering. In the future, other variations on submicron topographies on synthetic biomaterials may become the topic of investigation, such as topographies with other morphologies than grain-shaped or needle-shaped crystals. For example, current studies have already started to investigate this using high throughput screening experiments with different surface types[78–80]. Also, it may be studied how the size of surface crystals on synthetic bone graft materials can be further reduced towards the nanoscale and how this would affect the healing potential. Also, hierarchical macro/micro/nano surface designs and/or micropatterned surfaces on synthetic bone grafts may be explored to more closely control cellular responses[81,82]. Besides topography, the effects of other surface characteristics such as surface chemistry, charge, and chirality may be investigated as well [83]. Furthermore, we may see a surge in the use of osteoinductive calcium phosphate incorporated in 3D-printed scaffolds for the treatment of complex bone defects [84,85].

As presented in Table 1 in chapter 1 of this thesis, various theories have been proposed to explain the mechanism of osteoinduction by calcium phosphates. All the proposed mechanisms may be influenced by a change in surface topography. For example, a change in surface features can influence the formation of the biological apatite layer, including growth factor incorporation, but also have a direct influence on adherent cells such as stem cells, osteoclasts or macrophages. It is highly likely that these mechanisms are not mutually exclusive and that several theories may be true at the same time. For example, biological apatite formation may play a role in osteoinduction, as well as the response of cells to the direct physical cues from the surface topography.



In this work, we have investigated the effect of submicron topography on the response of macrophages. Modulation of the immune response by controlling macrophage phenotypes through specific material cues is currently researched as a strategy to improve the regenerative potential of implants and tissue grafts. In this thesis, we associated the enhanced healing potential of an osteoinductive calcium phosphate with the upregulation of the 'pro-healing' M2 macrophage phenotype. Various other studies have indicated that M2 macrophage upregulation can have favorable effects on tissue regeneration, although the pathways by which this happens are not yet entirely elucidated. It is known that macrophages and stem cells exert bi-directional crosstalk and have shown synergistic effects on bone healing[86,87]. M2 macrophages were shown to have a critical influence on osteogenic differentiation of MSCs in vitro and in regeneration of bone defects in vivo [88]. Moreover, M2 macrophage upregulation, by osteoinductive calcium phosphate and other strategies, has been associated with enhanced angiogenesis in vitro and in vivo [89]. We may therefore speculate that M2 polarization through direct topographical cues at the surface of osteoinductive materials results in the upregulation of angiogenesis[89], recruitment of MSCs and their subsequent osteogenic differentiation. Alternatively (or additionally), the polarized M2 macrophages might fuse to become multinucleated osteoclast-like giant cells, which form the trigger for osteogenic differentiation [90]. The underlying biological mechanisms will need to be further uncovered in the coming years, for example, by using immunohistochemistry, protein and gene analyses to closely track the behavior of macrophages, recruitment of stem cells and multinucleated cell and osteoclast formation in the very early phases after implantation[91]. Also, to further confirm the role of macrophages, it may be investigated whether delivering immunomodulatory cytokines that upregulate either M1 or M2 macrophages to inductive/non-inductive ceramics can enhance, inhibit or even trigger osteoinductive bone formation by ceramics. Furthermore, the polarization of the M2 phenotype in relation to surface topography may be further characterized, for example by proteomic and transcriptomic analysis of macrophages cultured on different material surfaces[92].

With its wide array of different functions, including clearing of debris and pathogens, regulating the inflammatory response, and recruitment of and communication with (stem) cells, learning how to control the macrophage may have a key role in the future of regenerative medicine and other clinical areas. Perhaps osteoimmunomodulation may one day be included as one of the healing principles of bone graft substitutes, next to the mechanisms of osteoconduction, osteoinduction and osteogenesis.

### **The quality of current evidence**

A returning topic throughout this thesis has been the quality of investigational studies and the associated level of evidence for bone graft substitutes. There is room for improvement of the study quality in both pre-clinical and clinical research of orthobiologics.



As mentioned above, most of the available bone graft options have a relatively low level of evidence due to a lack of well-designed, comparative clinical trials, with proper sample size and procedures to minimize risk of bias. Strikingly, some of the bone graft categories that have been clinically available for over 30 years and are still being used today, such as osteoconductive bone grafts and DBMs, have only been evaluated in a small number of RCTs [6,7]. Literature indicates that only 1 out of 10 clinical studies for orthobiologics is of Level I design and approximately 5 out of 10 contain a comparative control (Level I-III) [5]. Some reviews have determined that most clinical studies, including RCTs, have a high risk of bias [7]. Going forward, the quality of evidence for orthobiologics can be improved by conducting more RCTs and prospective studies with larger sample sizes and appropriate measures to minimize bias, such as blinded or independent assessment of outcomes [7]. Also, a treatment follow-up of more than one or two years could increase the strength of evidence. Besides methodological factors, an additional source of bias that can affect research agendas, clinical study design and conclusions is industry sponsorship [93]. The majority of the clinical studies into commercial products today are sponsored by industry. In the future, an increase in investigator-initiated clinical trials could help to reduce this potential bias in the available evidence.

Besides clinical evidence, also pre-clinical evidence on orthobiologics could be strengthened by improving the quality of research studies. Pre-clinical studies are highly valuable research tools, because they allow for a much more extensive evaluation of healing using different assessment techniques, where clinical studies are usually restricted to radiography and clinical outcomes. In the current thesis, we have evaluated bone graft substitutes in various clinically relevant models in large animals that closely mimic humans in bone structure and metabolism. However, many of the currently available orthobiologics have only been evaluated in lower order animals such as rabbits and rodents, which are more different to humans in biology and anatomy. As an example, spinal fusion by DBMs and cellular allografts have almost exclusively been tested in athymic rats and rarely in larger non-immunocompromised animals. Furthermore, the field could benefit from additional evidence on comparative efficacy between different orthobiologics, generated by studies that compare different commercially available bone grafts in these more relevant models.

## **CONCLUDING REMARKS**

The work in this thesis describes the development and investigation of a synthetic calcium phosphate bone graft substitute with an improved surface topography of submicron needle-shaped crystals. The improved topography resulted in enhanced osteoinductive potential compared to other calcium phosphates and was also shown to upregulate 'pro-healing' macrophages of the M2 phenotype. These effects translated to high efficacy in clinically relevant animal models of spinal fusion and maxillary sinus floor augmentation,

demonstrating equivalence to the current gold standard of autograft and superiority to other synthetic bone grafts that are commercially available. The pre-clinical results were validated in two clinical trials of spinal fusion and sinus floor augmentation. This work is a demonstration of the value of 'bench-to-beside' translational research, using in vitro studies, clinically relevant animal models and clinical studies to evaluate bone graft substitutes. With osteoinductive calcium phosphates, we have come another step closer towards the new gold standard in bone grafting. Further evaluation of this synthetic bone graft material in multiple randomized controlled trials is currently ongoing, which will strengthen the evidence on the efficacy of this unique category of bone graft materials.



## REFERENCES

---

- [1] T.T. Roberts, A.J. Rosenbaum, Bone grafts, bone substitutes and orthobiologics the bridge between basic science and clinical advancements in fracture healing, *Organogenesis*. 8 (2012) 114–124. <https://doi.org/10.4161/org.23306>.
- [2] R. Dimitriou, G.I. Mataliotakis, A.G. Angoules, N.K. Kanakaris, P. V. Giannoudis, Complications following autologous bone graft harvesting from the iliac crest and using the RIA: A systematic review, *Injury*. 42 (2011). <https://doi.org/10.1016/j.injury.2011.06.015>.
- [3] G.C. Berlet, J.F. Baumhauer, M. Glazebrook, S.L. Haddad, A. Younger, J.D. Quiton, D.A. Fitch, T.R. Daniels, C.W. DiGiovanni, The Impact of Patient Age on Foot and Ankle Arthrodesis Supplemented with Autograft or an Autograft Alternative (rhPDGF-BB/ $\beta$ -TCP), *JBJS Open Access*. 5 (2020) e20.00056-e20.00056. <https://doi.org/10.2106/JBJS.OA.20.00056>.
- [4] P. Habibovic, H. Yuan, M. van den Doel, T.M. Sees, C.A. van Blitterswijk, K. de Groot, Relevance of osteoinductive biomaterials in critical-sized orthotopic defect, *J. Orthop. Res*. 24 (2006) 867–876. <https://doi.org/10.1002/jor.20115>.
- [5] M.S. Nickoli, W.K. Hsu, Ceramic-Based Bone Grafts as a Bone Grafts Extender for Lumbar Spine Arthrodesis: A Systematic Review, *Glob. Spine J*. 4 (2014) 211–216. <https://doi.org/10.1055/s-0034-1378141>.
- [6] M.T. Morris, S.P. Tarpada, W. Cho, Bone graft materials for posterolateral fusion made simple: a systematic review, *Eur. Spine J*. 27 (2018) 1856–1867. <https://doi.org/10.1007/s00586-018-5511-6>.
- [7] Z. Buser, D.S. Brodke, J.A. Youssef, H.J. Meisel, S.L. Myhre, R. Hashimoto, J.B. Park, S.T. Yoon, J.C. Wang, Synthetic bone graft versus autograft or allograft for spinal fusion: A systematic review, *J. Neurosurg. Spine*. 25 (2016) 509–516. <https://doi.org/10.3171/2016.1.SPINE151005>.
- [8] J. tao Feng, X. gang Yang, F. Wang, X. He, Y. cheng Hu, Efficacy and safety of bone substitutes in lumbar spinal fusion: a systematic review and network meta-analysis of randomized controlled trials, *Eur. Spine J*. 29 (2020) 1261–1276. <https://doi.org/10.1007/S00586-019-06257-X>.
- [9] T. Floyd, D. Ohnmeiss, A meta-analysis of autograft versus allograft in anterior cervical fusion, *Eur. Spine J*. 9 (2000) 398–403. <https://doi.org/10.1007/S005860000160>.
- [10] E. Cottrill, Z. Pennington, N. Lankipalle, J. Ehresman, C. Valencia, A. Schilling, J. Feghali, A. Perdomo-Pantoja, N. Theodore, D.M. Sciubba, T. Witham, The effect of bioactive glasses on spinal fusion: A cross-disciplinary systematic review and meta-analysis of the preclinical and clinical data, *J. Clin. Neurosci*. 78 (2020) 34–46. <https://doi.org/10.1016/J.JOCN.2020.04.035>.
- [11] E. Nkenke, F. Stelzle, Clinical outcomes of sinus floor augmentation for implant placement using autogenous bone or bone substitutes: A systematic review, *Clin. Oral Implants Res*. 20 (2009) 124–133. <https://doi.org/10.1111/j.1600-0501.2009.01776.x>.
- [12] B. Al-Nawas, E. Schiegnitz, Augmentation procedures using bone substitute materials or autogenous bone—a systematic review and meta-analysis, *Eur. J. Oral Implantol*. 7 (2014) S219–S234.

- [13] T. Starch-Jensen, A. Mordenfeld, J.P. Beckett, S.S. Jensen, Maxillary sinus floor augmentation with synthetic bone substitutes compared with other grafting materials: A systematic review and meta-analysis, *Implant Dent.* 27 (2018) 363–374. <https://doi.org/10.1097/ID.0000000000000768>.
- [14] W.K. Hsu, M.S. Nickoli, J.C. Wang, J.R. Lieberman, H.S. An, S.T. Yoon, J.A. Youssef, D.S. Brodke, C.M. McCullough, Improving the Clinical Evidence of Bone Graft Substitute Technology in Lumbar Spine Surgery, *Glob. Spine J.* 2 (2012) 239–248. <https://doi.org/10.1055/s-0032-1315454>.
- [15] Z. Buser, D.S. Brodke, J.A. Youssef, E. Rometsch, J.B. Park, S.T. Yoon, J.C. Wang, H.J. Meisel, Allograft Versus Demineralized Bone Matrix in Instrumented and Noninstrumented Lumbar Fusion: A Systematic Review, *Glob. Spine J.* 8 (2018) 396–412. <https://doi.org/10.1177/2192568217735342>.
- [16] E. Gruskin, B.A. Doll, F.W. Futrell, J.P. Schmitz, J.O. Hollinger, Demineralized bone matrix in bone repair: History and use, *Adv. Drug Deliv. Rev.* 64 (2012) 1063. <https://doi.org/10.1016/J.ADDR.2012.06.008>.
- [17] Russell, V. Lovric, Oliver, M. Pelletier, Y. Yu, Walsh, The Effect of Processing Conditions of the Osteoinductivity of Sheep Demineralized Bone Matrix in an Ectopic Nude Rat Model: A Pilot Study, in: *Orthop. Res. Soc. Annu. Meet.*, 2012: p. Poster 0629. <https://www.ors.org/Transactions/58/0629.pdf> (accessed December 30, 2021).
- [18] J.T. Kim, H.J. Kang, H.N. Kim, J.Y. Choi, J.M. Lee, E.K. Park, H.I. Shin, Ectopic Osteoinduction by Variously Demineralized Allogenic Cortical Bone Matrix, *Key Eng. Mater.* 342–343 (2007) 105–108. <https://doi.org/10.4028/www.scientific.net/kem.342-343.105>.
- [19] P. Torricelli, M. Fini, M. Rocca, G. Giavaresi, R. Giardino, Xenogenic demineralized bone matrix: Osteoinduction and influence of associated skeletal defects in heterotopic bone formation in rats, *Int. Orthop.* 23 (1999) 178–181. <https://doi.org/10.1007/s002640050341>.
- [20] N.A. SHEPARD, A.J. RUSH, N.L. SCARBOROUGH, A.J. CARTER, F.M. PHILLIPS, Demineralized Bone Matrix in Spine Surgery: A Review of Current Applications and Future Trends, *Int. J. Spine Surg.* 15 (2021) S113–S119. <https://doi.org/10.14444/8059>.
- [21] B. Aghdasi, S.R. Montgomery, M.D. Daubs, J.C. Wang, A review of demineralized bone matrices for spinal fusion: the evidence for efficacy, *Surgeon.* 11 (2013) 39–48. <https://doi.org/10.1016/J.SURGE.2012.08.001>.
- [22] K. Tilkeridis, P. Touzopoulos, A. Ververidis, S. Christodoulou, K. Kazakos, G.I. Drosos, Use of demineralized bone matrix in spinal fusion, *World J. Orthop.* 5 (2014) 30–37. <https://doi.org/10.5312/WJO.V5.I1.30>.
- [23] N. Russell, W.R. Walsh, V. Lovric, P. Kim, J.H. Chen, M.J. Larson, F. Vizesi, In-vivo Performance of Seven Commercially Available Demineralized Bone Matrix Fiber and Putty Products in a Rat Posterolateral Fusion Model, *Front. Surg.* 7 (2020). <https://doi.org/10.3389/fsurg.2020.00010>.
- [24] H. Bae, L. Zhao, D. Zhu, L.E. Kanim, J.C. Wang, R.B. Delamarter, Variability across ten production lots of a single demineralized bone matrix product, *J. Bone Joint Surg. Am.* 92 (2010) 427–435. <https://doi.org/10.2106/JBJS.H.01400>.



- [25] H.W. Bae, L. Zhao, L.E.A. Kanim, P. Wong, R.B. Delamarter, E.G. Dawson, Intervariability and intravariability of bone morphogenetic proteins in commercially available demineralized bone matrix products, *Spine (Phila. Pa. 1976)*. 31 (2006) 1299–1306. <https://doi.org/10.1097/01.brs.0000218581.92992.b7>.
- [26] O. Brink, The choice between allograft or demineralized bone matrix is not unambiguous in trauma surgery, *Injury*. 52 (2021) S23–S28. <https://doi.org/10.1016/J.INJURY.2020.11.013>.
- [27] FDA.gov, Urgent Voluntary Notification: FiberCel Fiber Viable Bone Matrix (“FiberCel”)–Lot Number: NMDS210011, (2021). <https://www.fda.gov/vaccines-blood-biologics/recal>.
- [28] V.Y. Ng, Risk of disease transmission with bone allograft, *Orthopedics*. 35 (2012) 679–681. <https://doi.org/10.3928/01477447-20120725-04>.
- [29] M.C. Simmonds, J.V.E. Brown, M.K. Heirs, J.P.T. Higgins, R.J. Mannion, M.A. Rodgers, L.A. Stewart, Safety and effectiveness of recombinant human bone morphogenetic protein-2 for spinal fusion: a meta-analysis of individual-participant data, *Ann. Intern. Med.* 158 (2013) 877–889. <https://doi.org/10.7326/0003-4819-158-12-201306180-00005>.
- [30] W. lin Xiao, K. ning Jia, G. Yu, N. Zhao, Outcomes of bone morphogenetic protein-2 and iliac cancellous bone transplantation on alveolar cleft bone grafting: A meta-analysis, *J. Plast. Reconstr. Aesthet. Surg.* 73 (2020) 1135–1142. <https://doi.org/10.1016/J.JBJS.2020.01.011>.
- [31] K.R. Garrison, S. Donell, J. Ryder, I. Shemilt, M. Mugford, I. Harvey, F. Song, Clinical effectiveness and cost-effectiveness of bone morphogenetic proteins in the non-healing of fractures and spinal fusion: A systematic review, *Health Technol. Assess. (Rockv)*. 11 (2007). <https://doi.org/10.3310/hta11300>.
- [32] J.W. Hustedt, D.J. Blizzard, The Controversy Surrounding Bone Morphogenetic Proteins in the Spine: A Review of Current Research, *Yale J. Biol. Med.* 87 (2014) 549. [/pmc/articles/PMC4257039/](https://pubmed.ncbi.nlm.nih.gov/24257039/) (accessed December 30, 2021).
- [33] A.W. James, G. LaChaud, J. Shen, G. Asatrian, V. Nguyen, X. Zhang, K. Ting, C. Soo, A Review of the Clinical Side Effects of Bone Morphogenetic Protein-2, *Tissue Eng. Part B. Rev.* 22 (2016) 284. <https://doi.org/10.1089/TEN.TEB.2015.0357>.
- [34] North American Spine Society, Recombinant Human Bone Morphogenetic Protein (rhBMP-2): Defining Appropriate Coverage Positions, (2014) 1–30. <https://www.spine.org/Documents/PolicyPractice/CoverageRecommendations/rhBMP.pdf> (accessed December 31, 2021).
- [35] GlobalData, Bone Grafts and Substitutes–United States–2005-2023, 2018.
- [36] W.K. Hsu, R.E. Hashimoto, S.H. Berven, A. Nassr, Biological Substitutes/Extenders for Spinal Arthrodesis Which Agents Are Cost-effective?, *Assess. VALUE Specif. SPINE Cond. SPINE*. 39 (2014) 86–98. <https://doi.org/10.1097/BRS.0000000000000548>.
- [37] A.P. Lloyd, Counting the Cost of Failed Spinal Fusion for Relief of Low Back Pain: Does Primary Fusion with Bone Morphogenetic Protein Make Economic Sense from a Primary Payer Perspective?, *Clin. Spine Surg.* 30 (2017) E720–E724. <https://doi.org/10.1097/BSD.0000000000000273>.

- [38] Z. Buser, P. Hsieh, H.J. Meisel, A.C. Skelly, E.D. Brodt, D.S. Brodke, J.B. Park, S.T. Yoon, J. Wang, Use of Autologous Stem Cells in Lumbar Spinal Fusion: A Systematic Review of Current Clinical Evidence, *Glob. Spine J.* 11 (2021) 1281–1298. <https://doi.org/10.1177/2192568220973190>.
- [39] P.C. Hsieh, A.S. Chung, D. Brodke, J.B. Park, A.C. Skelly, E.D. Brodt, K. Chang, Z. Buser, H.J. Meisel, S.T. Yoon, J.C. Wang, Autologous Stem Cells in Cervical Spine Fusion, *Glob. Spine J.* 11 (2021) 950–965. <https://doi.org/10.1177/2192568220948479>.
- [40] E. Gómez-Barrena, N. Padilla-Eguiluz, P. Rosset, F. Gebhard, P. Hernigou, N. Baldini, H. Rouard, L. Sensebé, R.M. Gonzalo-Daganzo, R. Giordano, E. García-Rey, J. Cordero-Ampuero, J.C. Rubio-Suárez, M.D. García-Simón, J. Stanovici, C. Ehrnthaller, M. Huber-Lang, C.H. Flouzat-Lachaniette, N. Chevallier, D.M. Donati, B. Spazzoli, G. Ciapetti, S. Fleury, M.N. Fernandez, J.R. Cabrera, C. Avendaño-Solá, T. Montemurro, C. Panaitescu, E. Veronesi, M.T. Rojewski, R. Lotfi, M. Dominici, H. Schrezenmeier, P. Layrolle, Early efficacy evaluation of mesenchymal stromal cells (MSC) combined to biomaterials to treat long bone non-unions, *Injury*. 51 (2020) S63–S73. <https://doi.org/10.1016/j.injury.2020.02.070>.
- [41] P. Šponer, T. Kučera, J. Brtková, K. Urban, Z. Kočí, P. Měřička, A. Bezrouk, Š. Konrádová, A. Filipová, S. Filip, Comparative Study on the Application of Mesenchymal Stromal Cells Combined with Tricalcium Phosphate Scaffold into Femoral Bone Defects, *Cell Transplant.* 27 (2018) 1459–1468. <https://doi.org/10.1177/0963689718794918>.
- [42] N. Sánchez, L. Fierravanti, J. Núñez, F. Vignoletti, M. González-Zamora, S. Santamaría, S. Suárez-Sancho, M.E. Fernández-Santos, E. Figuero, D. Herrera, J.A. García-Sanz, M. Sanz, Periodontal regeneration using a xenogeneic bone substitute seeded with autologous periodontal ligament-derived mesenchymal stem cells: A 12-month quasi-randomized controlled pilot clinical trial, *J. Clin. Periodontol.* 47 (2020) 1391–1402. <https://doi.org/10.1111/jcpe.13368>.
- [43] D.A. Apatzidou, A.A. Bakopoulou, K. Kouzi-Koliakou, V. Karagiannis, A. Konstantinidis, A tissue-engineered biocomplex for periodontal reconstruction. A proof-of-principle randomized clinical study, *J. Clin. Periodontol.* 48 (2021) 1111–1125. <https://doi.org/10.1111/jcpe.13474>.
- [44] A.J. Rahyussalim, A. Nugroho, M.L.L. Zufar, I. Fathurrahman, T. Kurniawati, Integration of Umbilical Cord Mesenchymal Stem Cell Application in Hydroxyapatite-Based Scaffolds in the Treatment of Vertebral Bone Defect due to Spondylitis Tuberculosis: A Translational Study, *Stem Cells Int.* 2021 (2021) 1–14. <https://doi.org/10.1155/2021/9928379>.
- [45] B. Skovrlj, J.Z. Guzman, M. Al Maaieh, S.K. Cho, J.C. Iatridis, S.A. Qureshi, Cellular bone matrices: viable stem cell-containing bone graft substitutes, *Spine J.* 14 (2014) 2763. <https://doi.org/10.1016/J.SPINEE.2014.05.024>.
- [46] A. Abedi, B. Formanek, N. Russell, F. Vizesi, S.D. Boden, J.C. Wang, Z. Buser, Examination of the Role of Cells in Commercially Available Cellular Allografts in Spine Fusion: An in Vivo Animal Study, *J. Bone Joint Surg. Am.* 102 (2020) e135. <https://doi.org/10.2106/JBJS.20.00330>.
- [47] T. Hayashi, E.L. Lord, A. Suzuki, S. Takahashi, T.P. Scott, K. Phan, H. Tian, M.D. Daubs, K. Shiba, J.C. Wang, A comparison of commercially available demineralised bone matrices with and without human mesenchymal stem cells in a rodent spinal fusion model, *J. Neurosurg. Spine.* 25 (2016) 133–137. <https://doi.org/10.3171/2015.12.SPINE15737>.



- [48] S.C. Darveau, O.P. Leary, E.M. Persad-Paisley, E.A. Shaaya, A.A. Oyelese, J.S. Fridley, P. Sampath, J.Q. Camara-Quintana, Z.L. Gokaslan, T. Niu, Existing clinical evidence on the use of cellular bone matrix grafts in spinal fusion: updated systematic review of the literature, *Neurosurg. Focus.* 50 (2021) E12. <https://doi.org/10.3171/2021.3.FOCUS2173>.
- [49] P. Hsieh, Z. Buser, S. AC, B. ED, B. D, M. HJ, P. JB, Y. ST, W. JC, Allogenic Stem Cells in Spinal Fusion: A Systematic Review, *Glob. Spine J.* 9 (2019) 22S-38S. <https://doi.org/10.1177/2192568219833336>.
- [50] B. SM, W. TY, P. C, R. S, G. CR, K. IO, A.-E.-B. MM, S. CI, Y. CK, T. KD, Pseudarthrosis rate following anterior cervical discectomy with fusion using an allograft cellular bone matrix: a multi-institutional analysis, *Neurosurg. Focus.* 50 (2021) 1–8. <https://doi.org/10.3171/2021.3.FOCUS2166>.
- [51] C. Lin, N. Zhang, E.I. Waldorff, P. Punsalan, D. Wang, E. Semler, J.T. Ryaby, J. Yoo, B. Johnstone, Comparing cellular bone matrices for posterolateral spinal fusion in a rat model, *JOR Spine.* 3 (2020) e1084. <https://doi.org/10.1002/JSP2.1084>.
- [52] P. Berjano, F. Langella, M. Damilano, M. Pejrona, J. Buric, M. Ismael, J.H. Villafañe, C. Lamartina, Fusion rate following extreme lateral lumbar interbody fusion, *Eur. Spine J.* 24 (2015) 369–371. <https://doi.org/10.1007/s00586-015-3929-7>.
- [53] R.M. Parker, G.M. Malham, Comparison of a calcium phosphate bone substitute with recombinant human bone morphogenetic protein-2: a prospective study of fusion rates, clinical outcomes and complications with 24-month follow-up, *Eur. Spine J.* 26 (2017) 754–763. <https://doi.org/10.1007/s00586-016-4927-0>.
- [54] M.A. Lehr, C.F. Oner, D. Delawi, R.K. Stellato, E.A. Hoebink, D.H.R. Kempen, J.L.C. Van Susante, R.M. Castelein, M.C. Kruyt, Efficacy of a Standalone Microporous Ceramic Versus Autograft in Instrumented Posterolateral Spinal Fusion: A Multicenter, Randomized, Inpatient Controlled, Noninferiority Trial, *Spine (Phila. Pa. 1976)*. 45 (2020) 944–951. <https://doi.org/10.1097/BRS.0000000000003440>.
- [55] L.A. van Dijk, F. de Groot, H. Yuan, C. Champion, A. Patel, K. Poelstra, J.D. de Bruijn, From benchtop to clinic: a translational analysis of the immune response to submicron topography and its relevance to bone healing, *Eur. Cell. Mater.* 41 (2021) 756–773. <https://doi.org/10.22203/ECM.V041A48>.
- [56] A. Jones, Effective Use of a Novel Biphasic Calcium Phosphate with Submicron Surface Topography in Posterolateral Spine Fusion, *Juniper Online J. Case Stud.* 12 (2021) 01–05. <https://doi.org/10.19080/JOJCS.2021.12.555834>.
- [57] F. Sandhu, Posterior Thoracolumbar Hemivertebra Resection and Fusion with a Biphasic Calcium Phosphate Bone Graft with a Novel Submicron Surface Topography, *Juniper Online J. Case Stud.* 12 (2021) 1–5. <https://doi.org/10.19080/JOJCS.2021.12.555831>.
- [58] A. De Ruiter, E. Dik, R. Van Es, A. Van Der Bilt, N. Janssen, G. Meijer, R. Koole, A. Rosenberg, Micro-structured calcium phosphate ceramic for donor site repair after harvesting chin bone for grafting alveolar clefts in children, *J. Cranio-Maxillofacial Surg.* 42 (2014) 460–468. <https://doi.org/10.1016/j.jcms.2013.05.042>.



- [59] A. De Ruiter, N. Janssen, R. Van Es, M. Frank, G. Meijer, R. Koole, T. Rosenberg, Micro-structured Beta-Tricalcium Phosphate for Repair of the Alveolar Cleft in Cleft Lip and Palate Patients: A Pilot Study, *Cleft Palate. Craniofac. J.* 52 (2015) 336–340. <https://doi.org/10.1597/13-260>.
- [60] N.G. Janssen, R. Schreurs, A.P. de Ruiter, H.C. Sylvester-Jensen, G. Blindheim, G.J. Meijer, R. Koole, H. Vindenes, Microstructured beta-tricalcium phosphate for alveolar cleft repair: a two-centre study, *Int. J. Oral Maxillofac. Surg.* 48 (2019) 708–711. <https://doi.org/10.1016/j.ijom.2018.11.009>.
- [61] A. Barroso-Panella, J. Gargallo-Albiol, F. Hernández-Alfaro, Evaluation of Bone Stability and Esthetic Results After Immediate Implant Placement Using a Novel Synthetic Bone Substitute in the Anterior Zone: Results After 12 Months, *Int. J. Periodontics Restorative Dent.* 38 (2018) 235–243. <https://doi.org/10.11607/PRD.2863>.
- [62] A. Barroso-Panella, O. Ortiz-Puigpelat, P. Altuna-Fistolera, E. Lucas-Taulé, F. Hernández-Alfaro, J. Gargallo-Albiol, Evaluation of Peri-implant Tissue Stability and Patient Satisfaction After Immediate Implant Placement in the Esthetic Area: A 3-Year Follow-up of an Ongoing Prospective Study, *Int. J. Periodontics Restorative Dent.* 40 (2020) 731–739. <https://doi.org/10.11607/PRD.4411>.
- [63] R. Kraus, A. Stricker, D. Thoma, R. Jung, Sinus Floor Elevation with Biphasic Calcium Phosphate or Deproteinized Bovine Bone Mineral: Clinical and Histomorphometric Outcomes of a Randomized Controlled Clinical Trial, *Int. J. Oral Maxillofac. Implants.* 35 (2020) 1005–1012. <https://doi.org/10.11607/JOMI.8211>.
- [64] E. Velasco-Ortega, N.A. Valente, G. Iezzi, M. Petrini, G. Derchi, A. Barone, Maxillary sinus augmentation with three different biomaterials: Histological, histomorphometric, clinical, and patient-reported outcomes from a randomized controlled trial, *Clin. Implant Dent. Relat. Res.* 23 (2021) 86–95. <https://doi.org/10.1111/CID.12964>.
- [65] T. Fusco, K. Sage, S. Rush, F. Blom, K. Colvin, Arthrodesis of the subtalar joint using a novel biphasic calcium phosphate bone graft, (2022). <https://doi.org/10.1016/j.fastrc.2022.100150>.
- [66] Kuros Biosciences, Post Marketing Clinical Follow up Study for MagnetOs Putty in Patients With Degenerative Disc Disease (PROGRESS), Identifier: NCT04128852. (2019). [www.clinicaltrials.gov](http://www.clinicaltrials.gov).
- [67] M. Kruyt, MagnetOs™ Granules vs. Autograft in Instrumented Posterolateral Spinal Fusion (MaxA), Identifier: NCT03625544. (n.d.). [www.clinicaltrials.gov](http://www.clinicaltrials.gov).
- [68] Kuros Biosciences, Post Marketing Study of MagnetOs Putty Compared to Local Autograft in Patients Undergoing Posterolateral Lumbar Fusion—Full Text View—ClinicalTrials.gov, (2020). <https://clinicaltrials.gov/ct2/show/NCT04679844?term=%22magnetOs%22&draw=2&rank=8> (accessed October 3, 2021).
- [69] T. Hayashi, E.L. Lord, A. Suzuki, S. Takahashi, T.P. Scott, K. Phan, H. Tian, M.D. Daubs, K. Shiba, J.C. Wang, A comparison of commercially available demineralized bone matrices with and without human mesenchymal stem cells in a rodent spinal fusion model, *J. Neurosurg. Spine.* 25 (2016) 133–137. <https://doi.org/10.3171/2015.12.SPINE15737>.



- [70] P. Giannoni, S. Scaglione, A. Daga, C. Ilengo, M. Cilli, R. Quarto, Short-time survival and engraftment of bone marrow stromal cells in an ectopic model of bone regeneration, *Tissue Eng.–Part A*. 16 (2010) 489–499. <https://doi.org/10.1089/TEN.TEA.2009.0041/ASSET/IMAGES/LARGE/FIG-7.JPEG>.
- [71] N. Haque, N.H. Abu Kasim, M.T. Rahman, Optimization of Pre-transplantation Conditions to Enhance the Efficacy of Mesenchymal Stem Cells, *Int. J. Biol. Sci.* 11 (2015) 324. <https://doi.org/10.7150/IJBS.10567>.
- [72] D. García-Sánchez, D. Fernández, J.C. Rodríguez-Rey, F.M. Pérez-Campo, Enhancing survival, engraftment, and osteogenic potential of mesenchymal stem cells, *World J. Stem Cells*. 11 (2019) 748. <https://doi.org/10.4252/WJSC.V11.I10.748>.
- [73] M.C. Kruyt, W.J.A. Dhert, H. Yuan, C.E. Wilson, C.A. van Blitterswijk, A.J. Verbout, J.D. de Bruijn, Bone tissue engineering in a critical size defect compared to ectopic implantations in the goat, *J. Orthop. Res.* 22 (2004) 544–551. <https://doi.org/10.1016/J.ORTHRES.2003.10.010>.
- [74] M.C. Kruyt, C.E. Wilson, J.D. de Bruijn, C.A. van Blitterswijk, C.F. Oner, A.J. Verbout, W.J.A. Dhert, The effect of cell-based bone tissue engineering in a goat transverse process model, *Biomaterials*. 27 (2006) 5099–5106. <https://doi.org/10.1016/J.BIOMATERIALS.2006.05.048>.
- [75] M.C. Kruyt, W.J.A. Dhert, F.C. Oner, C.A. van Blitterswijk, A.J. Verbout, J.D. de Bruijn, Analysis of ectopic and orthotopic bone formation in cell-based tissue-engineered constructs in goats, *Biomaterials*. 28 (2007) 1798–1805. <https://doi.org/10.1016/J.BIOMATERIALS.2006.11.038>.
- [76] R.E. Geuze, P.A. Everts, M.C. Kruyt, A.J. Verbout, J. Alblas, W.J.A. Dhert, Orthotopic location has limited benefit from allogeneic or autologous multipotent stromal cells seeded on ceramic scaffolds, *Tissue Eng. Part A*. 15 (2009) 3231–3239. <https://doi.org/10.1089/TEN.TEA.2009.0023>.
- [77] R. Langer, J.P. Vacanti, *Tissue Engineering, Science (80- )*. 260 (1993) 920–926. [www.sciencemag.org](http://www.sciencemag.org) (accessed October 3, 2021).
- [78] M. Nouri-Goushki, A. Isaakidou, B.I.M. Eijkel, M. Minneboo, Q. Liu, P.E. Boukany, M.J. Mirzaali, L.E. Fratila-Apachitei, A.A. Zadpoor, 3D printed submicron patterns orchestrate the response of macrophages, *Nanoscale*. 13 (2021) 14304. <https://doi.org/10.1039/D1NR01557E>.
- [79] M. Nouri-Goushki, L. Angeloni, K. Modaresifar, M. Minneboo, P.E. Boukany, M.J. Mirzaali, M.K. Ghatkesar, L.E. Fratila-Apachitei, A.A. Zadpoor, 3D-Printed Submicron Patterns Reveal the Interrelation between Cell Adhesion, Cell Mechanics, and Osteogenesis, *ACS Appl. Mater. Interfaces*. 13 (2021) 33767. <https://doi.org/10.1021/ACSAMI.1C03687>.
- [80] M.J. Vassey, G.P. Figueredo, D.J. Scurr, A.S. Vasilevich, S. Vermeulen, A. Carlier, J. Lockett, N.R.M. Beijer, P. Williams, D.A. Winkler, J. de Boer, A.M. Ghaemmaghami, M.R. Alexander, Immune Modulation by Design: Using Topography to Control Human Monocyte Attachment and Macrophage Differentiation, *Adv. Sci.* 7 (2020). <https://doi.org/10.1002/ADVS.201903392>.
- [81] Y. Tian, H. Zheng, G. Zheng, P. Hu, Y. Li, Y. Lin, Q. Gao, X. Yao, R. Gao, C. Li, X. Wu, L. Sui, Hierarchical microgroove/nanopore topography regulated cell adhesion to enhance osseointegration around intraosseous implants in vivo, *Biomater. Sci.* (2022). <https://doi.org/10.1039/D1BM01657A>.

- [82] P. Hu, Q. Gao, H. Zheng, Y. Tian, G. Zheng, X. Yao, J. Zhang, X. Wu, L. Sui, The Role and Activation Mechanism of TAZ in Hierarchical Microgroove/Nanopore Topography-Mediated Regulation of Stem Cell Differentiation, *Int. J. Nanomedicine*. 16 (2021) 1021. <https://doi.org/10.2147/IJN.S283406>.
- [83] J. Li, X. Jiang, H. Li, M. Gelinsky, Z. Gu, Tailoring Materials for Modulation of Macrophage Fate, *Adv. Mater.* 33 (2021). <https://doi.org/10.1002/ADMA.202004172>.
- [84] S. V. Murphy, P. De Coppi, A. Atala, Opportunities and challenges of translational 3D bioprinting, *Nat. Biomed. Eng.* 4 (2020) 370–380. <https://doi.org/10.1038/S41551-019-0471-7>.
- [85] R. Detsch, S. Schaefer, U. Deisinger, G. Ziegler, H. Seitz, B. Leukers, In vitro -Osteoclastic Activity Studies on Surfaces of 3D Printed Calcium Phosphate Scaffolds, *J. Biomater. Appl.* 26 (2011) 359–380. <https://doi.org/10.1177/0885328210373285>.
- [86] P. Humbert, M. Brennan, N. Davison, P. Rosset, V. Trichet, F. Blanchard, P. Layrolle, Immune modulation by transplanted calcium phosphate biomaterials and human mesenchymal stromal cells in bone regeneration, *Front. Immunol.* (2019). <https://doi.org/10.3389/fimmu.2019.00663>.
- [87] J. Pajarinen, T. Lin, E. Gibon, Y. Kohno, M. Maruyama, K. Nathan, L. Lu, Z. Yao, S.B. Goodman, Mesenchymal stem cell-macrophage crosstalk and bone healing, *Biomaterials*. 196 (2019) 80–89. <https://doi.org/10.1016/j.biomaterials.2017.12.025>.
- [88] S.S. Jin, D.Q. He, D. Luo, Y. Wang, M. Yu, B. Guan, Y. Fu, Z.X. Li, T. Zhang, Y.H. Zhou, C.Y. Wang, Y. Liu, A Biomimetic Hierarchical Nanointerface Orchestrates Macrophage Polarization and Mesenchymal Stem Cell Recruitment To Promote Endogenous Bone Regeneration, *ACS Nano*. 13 (2019) 6581–6595. <https://doi.org/10.1021/ACS.NANO.9B00489>.
- [89] R. Duan, Y. Zhang, L. van Dijk, D. Barbieri, J. van den Beucken, H. Yuan, J. de Bruijn, Coupling between Macrophage Phenotype, Angiogenesis and Bone Formation by Calcium Phosphates, *Mater. Sci. Eng. C*. 122 (2021) Manuscript submitted for publication. <https://doi.org/10.2139/ssrn.3507484>.
- [90] X. Guo, M. Li, W. Qi, H. Bai, Z. Nie, Z. Hu, Y. Xiao, J.D. de Bruijn, C. Bao, H. Yuan, Serial cellular events in bone formation initiated by calcium phosphate ceramics, *Acta Biomater.* 134 (2021) 730–743. <https://doi.org/10.1016/J.ACTBIO.2021.07.037>.
- [91] R.J. Miron, D.D. Bosshardt, OsteoMacs: Key players around bone biomaterials, *Biomaterials*. 82 (2016) 1–19. <https://doi.org/10.1016/j.biomaterials.2015.12.017>.
- [92] N. Groen, H. Yuan, D.G.A.J. Hebels, G. Koçer, F. Mbuyi, V. LaPointe, R. Truckenmüller, C.A. van Blitterswijk, P. Habibović, J. de Boer, Linking the Transcriptional Landscape of Bone Induction to Biomaterial Design Parameters, *Adv. Mater.* 29 (2017). <https://doi.org/10.1002/ADMA.201603259>.
- [93] A. Fabbri, A. Lai, Q. Grundy, L.A. Bero, The Influence of Industry Sponsorship on the Research Agenda: A Scoping Review, *Am. J. Public Health*. 108 (2018) e9. <https://doi.org/10.2105/AJPH.2018.304677>.



## NEDERLANDSE SAMENVATTING

---

Het algemene doel van dit proefschrift was om te bepalen of en hoe de oppervlakte-topografie van calciumfosfaten verbeterd kan worden zodat het een hogere effectiviteit heeft in het gebruik als botvervanger.

Om dit doel te bereiken, werden calciumfosfaten met verschillende oppervlakteontwerpen vervaardigd, met topografieën van oppervlaktekristallen variërend in vorm (naaldvormig versus korrelvormig) en afmetingen (micron-,  $\geq 1\mu\text{m}$ ; en submicron  $< 1\mu\text{m}$ ;). Vervolgens werd het osteoinductieve potentieel van deze materialen, oftewel het vermogen om ectopische botvorming te induceren, vergeleken bij intramusculaire implantatie in een diermodel. De resultaten toonden aan dat het oppervlakteontwerp van deze materialen een manier is om hun osteoinductieve potentieel te controleren en te verhogen. Naast de submicron afmetingen van oppervlaktestructuren, werd aangetoond dat ook de vorm van oppervlaktekristallen deze eigenschap beïnvloedde, want calcium fosfaten met een naaldvormige submicron topografie lieten een versnelde osteoinductie zien vergeleken met de andere topografieën.

Het materiaal met het hoogste osteoinductieve potentieel, toegeschreven aan zijn naaldvormige submicron topografie, werd geselecteerd voor verdere evaluatie in preklinische modellen van orthopedische chirurgie (spinale fusie) en maxillofaciale chirurgie (maxillaire sinusbodemelevatie). In deze studies werd het betreffende materiaal vergeleken met de gouden standaard autoloog bot, en/of andere synthetische botvervangingsmaterialen. Naast deze preklinische onderzoeken werd het bottransplantaatmateriaal met naaldvormige topografie geëvalueerd in een retrospectieve cohortstudie van interbody spinale fusie en een prospectieve, gerandomiseerde gecontroleerde studie van maxillaire sinusbodemelevatie

In de pre-klinische studies naar de effectiviteit van calciumfosfaat met naaldvormige submicron topografie bij posterolaterale spinale fusie, werden bij gebruik in combinatie met autoloog bot (bone graft extender) in een konijnenmodel en als opzichzelf-staand botvervanger in een schapenmodel, gelijkwaardige resultaten behaald als met de 'gouden standaard', autoloog bot. Daarnaast bleek de implantatie van het materiaal als korrels ingebed in een polymere carrier, met als doel om de verwerkingseigenschappen te verbeteren ('putty'), succesvol en leidde dit niet tot een verminderde werkzaamheid van het materiaal. Tenslotte, in een klinische retrospectieve cohortstudie van 77 lumbale en cervicale reconstructiepatiënten met intervertebrale en posterolaterale spinale fusies, demonstreerde het calciumfosfaat met naaldvormige submicron topografie goede

resultaten, met fusie percentages van respectievelijk 93,8% en 96,9% na 12 maanden, met gunstige klinische uitkomsten.

In de preklinische studie van maxillaire sinusbodemelevatie in een schapenmodel, werd vastgesteld dat het calciumfosfaat met naaldvormige submicron topografie leidde tot betere botgenezing in vergelijking met calciumfosfaat met korrelvormige submicron topografie. Daarnaast was het resultaat van het calciumfosfaat met naaldvormige submicron topografie gelijkwaardig aan dat van autoloog bot. Daarnaast werd de werkzaamheid van dit materiaal bevestigd in een preliminaire klinische studie van maxillaire sinusbodemelevatie, waarin gelijkwaardigheid met autoloog bot werd vastgesteld in implantaatstabiliteit, bothoogte, nieuwe botvorming en in algehele klinische uitkomsten, zij het met een kleine steekproefomvang van 10 patiënten.

Verder werd, om inzicht te krijgen in de biologische effecten van calciumfosfaattopografie, polarisatie van primaire menselijke macrofagen in reactie op calciumfosfaten met naaldvormige submicron topografie en conventionele topografie in vitro onderzocht, inclusief de stroomafwaartse regeneratieve effecten van deze macrofagen op osteogenese en angiogenese. In dit in vitro-onderzoek werd vastgesteld dat de opregulatie van M2-macrofagen waarschijnlijk een rol speelt in het verhoogde botregeneratievermogen van materialen met submicron topografie. Tenslotte werd door middel van een literatuurreview vastgesteld dat deze conclusie wordt ondersteund door de beschikbare literatuur over M2-macropaag-opregulatie door biomaterialen met specifieke structurele en topografische kenmerken.



## **DANKWOORD**

---

En dan nu nog het dankwoord. Dit is zo ongeveer het allerlaatste gedeelte dat ik voor mijn proefschrift heb geschreven, maar het is zeker niet het onbelangrijkst. In de afgelopen jaren heb ik met heel veel mensen samengewerkt om dit proefschrift tot stand te brengen. Daarnaast heb ik ook van mijn familie, vrienden en collega's heel veel steun en gezelligheid ervaren. Een bedankje is daarom dus zeker op zijn plaats.

### **Mijn promotieteam**

Beste **Florence**, ik begin graag met jou. Als mijn co-promotor en direct leidinggevende bij het R&D team bij Kuros (eerst Xpand) heb ik heel veel gehad aan jouw begeleiding. Ik heb altijd genoten van onze wekelijkse, diepgaande discussies over study designs, statistiek, cell culture, en ga zo maar door. Je hebt me geleerd het hoofd koel te houden en rustig de alternatieve opties te overwegen wanneer dingen niet zo lopen als verwacht. Verder ben je een hele warme en gezellige collega waar je altijd een leuk gesprek mee kan voeren. Het was ook indrukwekkend om te zien hoe goed jij bent in het managen van je grote projecten met hele strakke deadlines (510K, CE, new product development, etc.). Ik twijfelde of ik deze tekst in het Nederlands of Engels moest schrijven, maar ik herinner me dat je ooit zei dat ik de eerste PhD student was waarmee je Nederlands kon praten. Ook al zijn we daarna vrij snel op het Engels overgestapt, is dit wellicht weer eens een goede oefening ;-). Florence, ontzettend bedankt. Je bent tijdens mijn PhD een echte steun voor mij geweest, als altijd luisterend en meedenkende supervisor.

Beste **Joost**, Bedankt voor het mogelijk maken van mijn PhD en je begeleiding en vertrouwen in mij gedurende de jaren. Ik heb veel bewondering voor jouw vakkundigheid als wetenschapper en ondernemer. Toen ik begon bij Xpand Biotechnology in 2015 waren we nog met een klein team van ongeveer 12 mensen in het ceramics team, maar inmiddels is dit uitgegroeid tot een globaal team van meer dan 60 mensen. Ik heb veel geleerd van het werken bij Xpand/Kuros, ook door deze grote verandering te hebben mogen meemaken. Ik kon het erg waarderen hoe jij ondanks je drukke agenda toch de tijd nam een paper of hoofdstuk van mijn proefschrift kritisch te lezen en te voorzien van heel goed en constructief commentaar, waardoor de stukken echt verbeterden. Ik herinner me ook de gezellige avonden die we hebben gehad in New Orleans, Austin en Chicago. Dankjewel, Joost.

Beste **Debby**, In 2012 leerden wij elkaar kennen bij het masterprogramma Regenerative Medicine & Technology, en niet lang daarna begon ik bij jou aan mijn onderzoeksstage naar tissue engineering van botweefsel. In die 9 maanden leerde ik heel veel van jou over het doen van wetenschappelijk onderzoek, wat er mede toe heeft geleid dat ik overwoog

aan een PhD te beginnen. Ik ben je dankbaar dat je aan het einde van mijn Master traject, mij de kans hebt gegeven om aan dit PhD project bij de Kaak en Xpand te beginnen. Samen waagden we ons aan het opzetten van een klinische studie, wat nieuw terrein voor ons beiden was, en een enorme papiermolen... Ook al was ik lang niet elke dag in het UMC te vinden, heb ik altijd veel gezelligheid ervaren met jou en de meiden in de groep. Later kregen we allebei kleintjes en hadden we opeens hele andere onderwerpen om te bespreken. Debby, dankjewel voor je begeleiding de afgelopen jaren, ik heb veel van je geleerd. Ik zal zeker nog eens bij je langskomen voor een praatje en een bak koffie.

Beste **Toine**, ook jou wil ik natuurlijk hartelijk bedanken voor je supervisie tijdens mijn PhD. Ik heb veel gehad aan je begeleiding. Je hebt mij, waarschijnlijk meer dan je denkt, echt geholpen met het afronden van projecten en mijn proefschrift als geheel, door me regelmatig te motiveren en te blijven vragen over de voortgang. Zeker in het laatste jaar, toen ik al aan een nieuwe functie bij Kuros was begonnen, heeft dit mij geholpen om gefocust te blijven op het eindresultaat. Onze gesprekken op je kamer waren altijd erg waardevol en constructief, waardoor ik steeds weer met een concreet actieplan wegging. Bedankt ook voor de gesprekken over carrière na mijn PhD. Heel erg bedankt, professor.

### **Mijn colleagues at Kuros/Xpand**

To all my dear colleagues and ex-colleagues at Kuros, thank you so much for the past 7 years. Since the day I walked into the office at the Berg and Bosch premises, the atmosphere has always been so very warm and friendly. This has surely made my PhD journey a lot more enjoyable. **Vincent, Georgios, Davide, Duan, Shaun, Alice**: although most of you have already left Kuros, I have really enjoyed the time with you as my colleagues in Bilthoven. Thank you for the fun times we had during the bootcamps, BBQs and other company events. Special thanks to **Vincent** and **Georgios**, who were a comedic duo in the lab and always busy with pranks, jokes, funny memes, and a lot of yellow movies. Gogogogo! **Davide and Alice**, the Italians in the group. You have always been great company, and thanks for the lessons about good coffee and Italian food. **Viola**, jij bent persoonlijk een hele grote factor in het creëren van de goede sfeer bij Kuros. Bedankt voor de vele gezellige praatjes die we hebben gehad, in het begin nog in het krappe kantoor, maar nu nog steeds in de wandelgangen. Dankjewel! **Yuan**, thank you for teaching me a lot in the lab, and in general about preclinical studies. It has been amazing to experience how passionate and knowledgeable you are about science, ceramics, osteoinduction and since recently, the innate immune response to biomaterials. **Charlie**, thank you for seeing potential in me and asking me to join your team, you are a great, kind and fun manager. And last but not least, my current team: **Joerg, Berdine, Kate, Fred, Carly**; thanks for being such an awesome team, I'm having a blast. There are a many people that I have not mentioned, but I want to thank all of my Kuros (ex-)colleagues for the good times I have had in Bilthoven—and for the good times to come!



## Mijn collega's bij de kaakchirurgie

Natuurlijk wil ik ook mijn collega's bij de kaakchirurgie van het UMC bedanken. First of all, my dear all-female PhD-team in the Gawlitta research group. **Barbara, Alessia, Iris** and **Leanne**, thank you for the comradery as my fellow PhD students at the UMC/RMCU. Even though I was the only guy in the team, and not as much into pink, unicorns and alpaca's, I have truly appreciated you being there to share the struggles of PhD life. **Barbara**, it has been quite some time since I have last seen you, but I remember you as such a calm, kind and friendly colleague. Thank you for that. **Alessia**, thank you for your kindness and generosity and for helping me with the sheep surgeries—it was a real experience (especially the harvesting, I will never forget the smell...). **Iris**, dankjewel. Het was fijn om naast de vele internationals in het lab ook een nuchtere mede-Nederlander en tegelijk gezellige Brabander in het team te hebben. **Leanne**, thanks for being such a fun person to be around, you have a great sense of humor and always look at the bright side of life. Pity that we didn't get to work together more. **Lizette**, ontzettend bedankt voor je hulp en goede samenwerking op mijn in vitro project. Ik heb deze samenwerking enorm gewaardeerd, zonder jou was het me niet gelukt.

En dan nog de mensen van de staf kaakchirurgie met wie ik heb samengewerkt. **Nard**, enorm bedankt voor je medewerking aan de schapen studie, waar je veel tijd in hebt geïnvesteerd. **Silke** en **Marvick**, ik wil jullie beide bedanken voor het mogelijk maken van klinische sinus lift studie, door patiënten te includeren, behandelen, biopten te nemen, en de vele follow-up formulieren in te vullen. Als laatste wil ik ook alle stafleden, assistenten en medewerkers bij de kaakchirurgie, en daarnaast alle onderzoekers bij de orthopedie hartelijk bedanken voor de afgelopen jaren.

## Familie en vrienden

En als laatste dan de mensen die voor van mij van het allergrootste belang zijn geweest bij het werk aan mijn PhD en het schrijven van mijn proefschrift. De steun die ik aan jullie heb gehad was hoewel niet in collegiale of academische vorm, eigenlijk nog veel belangrijker dan dat. Jullie hebben met mij de momenten gedeeld die het maken dat het leven ertoe doet, waar het allemaal om draait.

Lieve, mooie **Marit** en kleine **Liv**, ik kan niet in woorden uitdrukken hoe belangrijk jullie voor mij zijn. Lieve **Marit**, samen maken wij al heel lang elke week, maand en jaar de mooiste nieuwe herinneringen. Super bedankt hoe je mij de ruimte hebt gegeven, en met de situatie hebt gedeeld, toen ik het afgelopen jaar heel, heel veel vrije avonden aan mijn proefschrift heb moeten besteden. Bedankt ook voor je begrip en het zijn van een goede gesprekspartner als het soms even tegenzat. Lieve **Liv**, je bent zo'n lief en vrolijk meisje, en maakt mij elke dag wel minstens 10 keer aan het lachen. Ik vind het echt geweldig om te zien hoe jij een steeds groter en ondeugender meisje wordt, en ben blij om jou nog heel



mijn leven te mogen zien opgroeien. Jullie twee zijn verreweg mijn trouwste supporters langs de zijlijn geweest, en mijn allergrootste steun bij het tot stand brengen van dit boekje. Ik hou oneindig veel van jullie, en kan niet wachten om te zien wat het leven nog voor ons in petto heeft.

Lieve **Mam** en **Pap**, ontzettend bedankt dat jullie mij altijd hebben gesteund om het beste uit mezelf te halen. Alles begint bij een goed voorbeeld en een goede opvoeding, en dat hebben jullie mij zeker gegeven. Pas wanneer je zelf een kleintje krijgt hebt ga je beseffen hoeveel tijd, energie en aandacht je ouders voor je over hebben gehad. Bedankt voor alles wat jullie voor me hebben gedaan. Lieve zusjes, **Renée** en **Sanne**, wij hebben onze hele jeugd samen doorgebracht, maar met het ouder worden wordt dat vanzelf helaas steeds minder. Daarom vind ik het extra mooi om mijn verdediging en promotie met jullie als mijn paranimfen aan mijn zijde te mogen meemaken. Bedankt dat jullie er altijd voor me waren, en weet dat ik er ook altijd voor jullie zal zijn. Ook bedankt aan **Folkert**, **Karlen** en natuurlijk mijn kleine nichtje **Lotte**. Last but not least wil ik mijn lieve schoonfamilie Evers: **René**, **Ingrid** en al mijn schoonzusjes en zwagers, heel hartelijk bedanken voor de gastvrijheid, gezelligheid, en de vele mooie momenten die we hebben gedeeld de afgelopen jaren.

Als laatste mijn maten, m'n homies, waarmee ik ontelbaar veel mooie avonden, feestjes, weekendjes, vakanties, festivals, chilldaagjes, etentjes, boottochtjes, into-the-wild-avonturen, grappen, grollen, nummertjes, biosjes, warzone potjes, fifa potjes, biertjes, mixjes, kapsalons en döner kebab heb gedeeld. Deze momenten hebben voor de oh zo belangrijke afleiding gezorgd, zodat ik de volgende ochtend, of na het weekend, weer fris en vol energie (maar soms ook iets minder fris) op de werkvloer verscheen. Het is niet nodig om hier namen te noemen want jullie weten zelf wel dat het om jullie het gaat. Thanks boys!!



## LIST OF PUBLICATIONS

---

1. **L.A. van Dijk**, N.G. Janssen, S.J. Nurmohamed, M.S.M. Muradin, A. Longoni, R.C. Bakker, F. Barrère-de Groot, J.D. de Bruijn, D. Gawlitta, A.J.W.P. Rosenberg. *Osteoinductive Calcium Phosphate with Submicron Topography as Bone Graft Substitute for Maxillary Sinus Floor Augmentation: A Translational Study*. Submitted.
2. **L.A. van Dijk**, L. Utomo, H. Yuan, F. Barrère-de Groot, D. Gawlitta, A.J.W.P. Rosenberg, J.D. de Bruijn. *Calcium phosphate with submicron topography induces M2 phenotype in primary human macrophages, enhancing downstream angiogenesis and osteogenesis in vitro*. Submitted.
3. **L.A. van Dijk**, F. Barrère-de Groot, H. Yuan, C. Champion, A. Patel, K. Poelstra, J.D. de Bruijn. *From benchtop to clinic: a translational analysis of the immune response to submicron topography and its relevance to bone healing*. *European Cells and Materials*. 2021 Jun 18;41:756-773. doi: 10.22203/eCM.v041a48. PMID: 34151417.
4. R. Duan, Y. Zhang, **L.A. van Dijk**, D. Barbieri, J.J.J.P. van den Beucken, H. Yuan, J.D. de Bruijn. *Coupling between macrophage phenotype, angiogenesis and bone formation by calcium phosphates*. *Materials Science & Engineering: C-Materials for Biological Applications*. 2021 Mar;122:111948. doi: 10.1016/j.msec.2021.111948. Epub 2021 Feb 6 PMID: 33641931.
5. **L.A. van Dijk**, F. Barrère-de Groot, A.J.W.P. Rosenberg, M. Pelletier, C. Christou, J.D. de Bruijn, W.R. Walsh. *MagnetOs, Vitoss, and Novabone in a Multi-endpoint Study of Posterolateral Fusion: A True Fusion or Not?* *Clinical Spine Surgery*. 2020 Jul;33(6):E276-E287. doi: 10.1097/BSD.0000000000000920. PMID: 31977334; PMCID: PMC7337107.
6. **L.A. van Dijk**, D. Barbieri, F. Barrère-de Groot, H. Yuan, R. Oliver, C. Christou, W.R. Walsh, J.D. de Bruijn. *Efficacy of a synthetic calcium phosphate with submicron surface topography as autograft extender in lapine posterolateral spinal fusion*. *Journal of Biomedical Materials Research Part B: Applied Biomaterials*. 2019 Aug;107(6):2080-2090. doi: 10.1002/jbm.b.34301. Epub 2019 Jan 7. PMID: 30614621; PMCID: PMC6690075.
7. R. Duan, **L.A. van Dijk**, D. Barbieri, F. Barrère-de Groot, H. Yuan, J.D. de Bruijn. *Accelerated bone formation by biphasic calcium phosphate with a novel sub-micron surface topography*. *European Cells and Materials*. 2019 Jan 28;37:60-73. doi: 10.22203/eCM.v037a05. PMID: 30687909.
8. I. Pennings, **L.A. van Dijk**, J. van Huuksloot, J.O. Fledderus, K. Schepers, A.K. Braat, E.C. Hsiao, E. Barruet, B.M. Morales, M.C. Verhaar, A.J.W.P. Rosenberg, D. Gawlitta. *Effect of donor variation on osteogenesis and vasculogenesis in hydrogel cocultures*. *Journal of Tissue Engineering and Regenerative Medicine*. 2019 Mar;13(3):433-445. doi: 10.1002/term.2807. Epub 2019 Feb 8. PMID: 30650247; PMCID: PMC6593839.

9. **L.A. van Dijk**, R. Duan, X. Luo, D. Barbieri, M. Pelletier, C. Christou, A.J.W.P. Rosenberg, H. Yuan, F. Barrère-de Groot, W.R. Walsh, J.D. de Bruijn. *Biphasic calcium phosphate with submicron surface topography in an Ovine model of instrumented posterolateral spinal fusion*. JOR Spine. 2018 Nov 28;1(4):e1039. doi: 10.1002/jsp2.1039. PMID: 31463454; PMCID: PMC6686792.





Lukas (Luuk) A. van Dijk was born in 1989 in Woerden, the Netherlands. Starting in 2001, he attended secondary school with a 'Science and Health' pre-university education (VWO) profile, at the Kalsbeek College in Woerden. After graduating in 2007, Luuk started a Bachelor's programme in Biology at Utrecht University and moved to Utrecht shortly thereafter. During his undergraduate, he learned about all the facets of biology, including molecular and cellular biology. Luuk obtained his Bachelor of Science degree in 2011, with a Bachelor's thesis, titled: "*The hair follicle: A complex mini-organ with many faces*". This thesis included a chapter on the therapeutic potential of hair follicle-derived stem cells, which sparked his interest in the field of regenerative medicine. This led him to apply for the Master's programme in Regenerative Medicine and Technology, a collaborative programme between Utrecht University, the University Medical Center Utrecht (UMCU) and the Faculty of Biomedical Engineering at Eindhoven University of Technology (TU/e). During this postgraduate programme, Luuk completed a nine-month research internship focusing on tissue engineering of pre-vascularized bone tissue analogs at the Orthopedics department of the UMCU. For his second internship, Luuk moved to Leuven, Belgium for a project on stem cell encapsulation in hydrogels at ReGenesys BV, a subsidiary of the publicly held biotechnology company Athersys Inc., focusing on the development of potential new applications for their proprietary stem cell product. In 2015, Luuk obtained his Master of Science degree in Regenerative Medicine and Technology. Soon after, he got the opportunity to start a PhD project to investigate osteoinductive calcium phosphate ceramics for bone regeneration at the department of Oral and Maxillofacial Surgery of the UMCU and Xpand Biotechnology BV. The results of his PhD research are presented in this thesis. As of January 2021, Luuk is working as Scientific Affairs Manager at Kuros Biosciences B.V.



